A Cell Panel to Characterise Tau Aggregation

Dissertation

zur

Erlangung des Doktorgrades (Dr. rer. nat.)

der

Mathematisch-Naturwissenschaftlichen Fakultät

der

Rheinischen Friedrich-Wilhelms-Universität Bonn

vorgelegt von

Alina Siobhan Hebestreit

aus

Leverkusen

Bonn Oktober, 2024

Angefertigt mit Genehmigung der Mathematisch-Naturwissenschaftlichen Fakultät

der Rheinischen Friedrich-Wilhelms-Universität Bonn

Gutachterin/Betreuerin: Professor Dr. Ina Maja Vorberg

Gutachter: Professor Dr. Jörg Höhfeld

Tag der Promotion: 19.12.2024

Erscheinungsjahr: 2025

Summary

Tauopathies are neurodegenerative diseases characterised by the pathological folding of Tau into highly ordered, β-sheet rich fibrils (so-called amyloid), which progressively spread through the central nervous system in a prion-like manner. Despite extensive research, inter- and intracellular prion-like Tau aggregate formation and transmission mechanisms remain unresolved. Tauopathies can be classified based on the aggregating Tau isoforms, which differ in the number of amino-terminal inserts (1N, 2N) and the number of repeats (3R or 4R). Cryogenic electron microscopy (cryoEM) revealed distinct Tau amyloid core structures associated with different Tauopathies. The clinical presentation and progression of these diseases are highly variable, potentially related to the accumulation of disease-specific Tau aggregates with amyloid cores that comprise shorter or longer stretches of the repeat region. However, the impact of these distinct amyloid folds on the prion-like spreading of Tau aggregates remains to be fully understood. This project had two aims. First, we used a semi-automated high-throughput screen to identify Tau aggregation inhibitors. A previously established HEK cell line expressing the P301L/V337M Tau 4R repeat domain was used for the screen. Two hits were identified in a library of 144 compounds that effectively inhibited Tau aggregation. Second, a cell panel expressing different Tau fragments based on the cryoEM Tau amyloid cores was established. The commonly used Tau repeat domain fragments might not represent the most suitable model to study Tau aggregation as the length of the Tau variants might affect its fibril conformation. The exact regions that form the core of the amyloid fibril might allow only selective intramolecular interactions, potentially enabling disease-specific seeding. Therefore, we established cell lines expressing the short cryoEM Tau core fragments associated with different Tauopathies (AD, CBD, PSP and PiD). Our data showed that highly expressed cryoEM Tau core fragments spontaneously aggregate. Cells with weak stable expression and no spontaneous aggregation were generated to investigate fibril-induced seeding. We demonstrated that the length and number of repeats of our Tau fragments influence the efficiency by which they are misfolded by exogenous Tau 3R or 4R fibrils. Tau fragments were seeded best by patient-derived Tau fibrils with an amyloid core of identical length and repeat number. The length of the expressed cryoEM Tau core fragments likely allows only the assembly of specific core conformations due to possibly fewer and more selective intramolecular interactions. In summary, our cell panel can discriminate between 3R, 4R and mixed 3R/4R Tauopathies. The inter- and intracellular mechanisms involved in Tau aggregation and propagation can be investigated using our cell panel assay. Our data can help to develop new therapeutic strategies to inhibit or reduce the aggregation of Tau by compounds.

Table of Contents

List of Figures

List of Tables

List of Abbreviations

aa	Amino acid
ACE2	Angiotensin-converting enzyme 2
AD	Alzheimer's disease
ALP	Autophagy-lysosomal pathway
ALS	Amyotrophic lateral sclerosis
APP	Amyloid precursor protein
ASO	Antisense oligonucleotides
Aβ	Amyloid-β
BBB	Blood-brain barrier
BH	Brain homogenate
C	Control
CBD	Corticobasal degeneration
CFP	Cyan fluorescence protein
CMA	Chaperone-mediated autophagy
Cryo-EM	Cryogenic electron microscopy
CTE	Chronic traumatic encephalopathy
CV	Cell Voyager
ddH_2O	Double distilled H_2O
dNTP	Deoxynucleotide triphosphate
E. coli	*Escherichia coli*
EDTA	Ethylenediaminetetraacetic acid
EM	Electron microscopy
ERAD	Endoplasmic reticulum-associated degradation
ERP	Endoplasmic reticulum pathway
ESC	Embryonic stem cell
EV	Extracellular vesicle
FCS	Fetal calf serum
FR	Fusion red
FTA	Filter trap assay
FTD	Frontotemporal dementia
FTDL	Frontotemporal lobar degeneration
FTDP-17	Frontotemporal dementia and Parkinsonism (chromosome 17)
FUS	Fused in sarcoma protein
GFP	Green fluorescent protein

GGT	Globular glial Tauopathy
HMW	High molecular weight
HSPG	Heparan sulfate proteoglycan
IC_{50}	Half maximal inhibitory concentration
IF	Immunofluorescence
iPSCs	Induced pluripotent stem cells
kDa	Kilodalton
LDL	Low-density lipoprotein receptor
LLPS	Liqui-liquid phase separation
LRP1	Low-density lipoprotein receptor-related protein 1
mAChR	Muscarinic acetylcholine receptor
MAP	Microtubule-associated protein
MAPT	Microtubule-associated protein Tau
mGFP	monomeric GFP
MVB	Multivesicular body
N	Amino
NEB	New England Biolabs
NFT	Neurofibrillary tangle
NPF	Narrow PiD filament
NM	N-terminal (N) and middle (M) domains of Sup35
OGA	O-GlcNAcase
P	Pellet
PAGE	Polyacrylamide gel electrophoresis
PBS	Phosphate-buffered saline
PD	Parkinson’s disease
PFA	Paraformaldehyde
PFFs	Pre-formed fibrils
PHF	Paired helical filament
PI	Protease inhibitor
PiD	Pick’s disease
PQC	Protein quality control system
PRD	Proline-rich domain
PrP^{C}	Cellular prion protein
PrP^{Sc}	Scrapie-associated, pathological prion protein
PSEN	Presenilin
PSP	Progressive supranuclear palsy

PTM	Posttranslational modification
PVDF	Polyvinylidene difluoride
R	Repeat
RD	Repeat domain
RT	Room temperature
RT-QuIC	Real-time quaking-induced conversion
SARS-CoV-2	Severe acute respiratory syndrome coronavirus type 2
SD	Standard deviation
SDS	Sodium dodecyl sulfate
SF	Straight filament
SN	Supernatant
ssNMR	Solid-state nuclear magnetic resonance
SORL-1	Sortilin-related receptor-1
SORLA	Sortilin-related receptor
TDP-43	TAR DNA-binding protein of 43 kDa
TNT	Tunnelling nanotube
UPR	Unfolded protein response
UPS	Ubiquitin-proteasome system
VCP	Valosin-containing protein
VSV-G	Vesicular stomatitis virus glycoprotein
WPF	Wide PiD filament
WT	Wild type
x g	Times gravitational acceleration
YFP	Yellow fluorescent protein

1 Introduction

1.1 Physiological function of Tau

Tauopathies are characterised by the pathological misfolding of the microtubule-associated protein Tau (MAPT) into highly ordered fibrils in neurons and glial cells (Eisenberg and Jucker, 2012). Tau is a microtubule-associated protein (MAP) primarily expressed in the nervous system. It was discovered in 1975 (Weingarten et al., 1975). Microtubules are composed of tubulin polymers, which are essential for the structure and function of cells. Tau plays a role in regulating the assembly and dissociation of microtubules and their dynamic behaviour. This enables axonal transport and supports the spatial organisation of the cytoskeleton (Weingarten et al., 1975). The MAPT gene on chromosome 17q2.1 encodes Tau (Neve et al., 1986). Tau is a highly soluble intrinsically disordered protein and consists of an amino-terminus (N-terminus), followed by a proline-rich domain (PRD). The microtubule-binding domain, also termed repeat domain (RD), is located within the carboxy-terminus (C-terminus) (Figure 1). The MAPT gene allows for the translation of six distinct Tau isoforms, which are the result of alternative mRNA splicing. The promoter is located in exon 0. Alternative splicing of the second and third exons results in the insertion of either zero (0N), one (1N), or two (2N) 29-residue-long sequences in the N-terminus. Additionally, Tau can be classified into two distinct groups: Tau 3R and Tau 4R, which contain three or four repeats within the RD, respectively (Lee et al., 1988; Goedert et al., 1989). The alternative splicing of the 10^{th} exon results in the loss of the second repeat (R2) in Tau 3R isoforms (R1, R3-R4), while Tau 4R isoforms have all four repeats (R1-R4). These repeats play an important role in regulating microtubule assembly and axonal transport. The expression of Tau isoforms is regulated during development (Goedert and Jakes, 1990). Fetal Tau ($0N3R^{(0-352)}$) is highly phosphorylated and more dynamic, playing a crucial role in synaptogenesis and neural network formation (Kenessey and Yen, 1993; Brion et al., 1994; Yu et al., 2009). It is most abundant during the fetal stages. As individuals age, Tau 4R isoforms increase, promoting microtubule assembly at a rate of 2.5 to 3.0 times faster than Tau 3R isoforms (Goedert and Jakes, 1990). The discrepancy may be attributed to the elevated phosphorylation of fetal Tau, which diminishes its capacity to promote microtubule assembly (Lindwall and Cole, 1984). The Tau 4R isoforms have a higher binding affinity to microtubules due to the second repeat (R2) (Aswathy et al., 2010; Goedert and Spillantini, 2011). The Tau 3R and 4R isoforms are expressed almost equally in the human cerebral cortex (Goedert and Jakes, 1990). In pathological conditions, there is an imbalance between the Tau 3R and 4R isoforms.

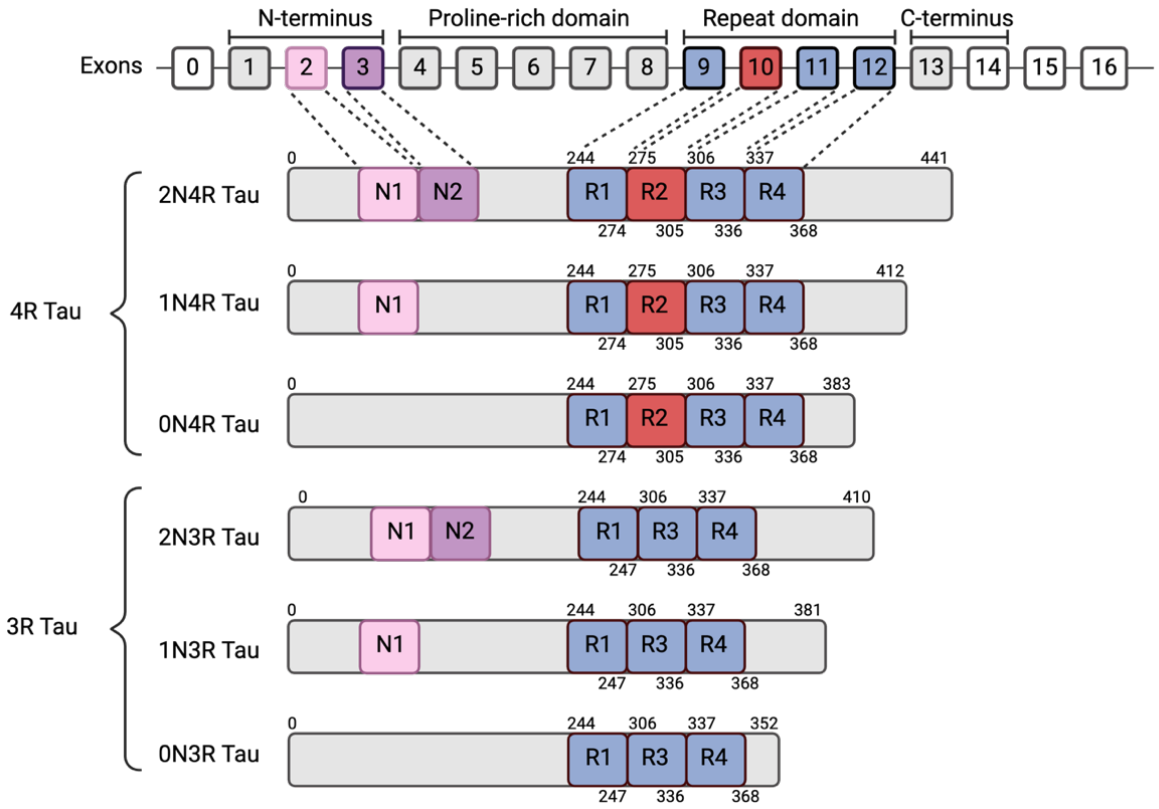

Figure 1 Tau 4R and 3R isoforms. The MAPT gene comprises 16 exons. By alternative splicing of exons 2,3 and 10, the formation of 6 isoforms is possible. Exon 0 is part of the promotor region. Exons 2 and 3 encode the N-inserts (N1, N2) near the N-terminus, followed by the proline-rich domain. Exons 9-12 comprise the repeat domain (R1-R4), followed by the C-terminus. Created with BioRender.com.

1.2 Tauopathies

More than 20 Tauopathies have been described, displaying a wide range of clinical and phenotypic heterogeneity. Tauopathies are characterised by the ordered assembly of soluble Tau into insoluble aggregated assemblies, termed amyloids (Eisenberg and Jucker, 2012). Amyloids are defined as unbranched protein fibrils with a cross-β rich structure that can be stained with Congo red, Thioflavin S and T, and Amylo Glo (Puchtler and Sweat, 1965; Westermark et al., 2005; Schmued et al., 2012; Ow and Dustan, 2014). The accumulation of potentially toxic Tau aggregates in the brain results in neurodegeneration, including the breakdown of the cytoskeleton, loss of synapses and neuroinflammation (Ross and Poirier, 2004). Tauopathies can be distinguished by the predominant aggregated Tau isoform, aggregate morphology, affected cell types and brain regions (Chung et al., 2021) (Table 1). Furthermore, they can be classified as primary or secondary Tauopathies. Primary Tauopathies are defined by Tau as the primary protein pathology, whereas in secondary Tauopathies, Tau aggregates result from other pathological events that drive the disease. For

example, in Alzheimer's disease (AD), the misfolding of amyloid-β (Aβ) is the central pathology, and Tau aggregation is considered to be a secondary event (Hardy, 2006). Further, Tauopathies can be caused by a combination of genetic and environmental factors, including repetitive (sub)concussions in chronic traumatic encephalopathy (CTE) (McKee et al., 2009). According to the primary isoform within the Tau deposits, Tauopathies can be categorised into three distinct subtypes: 3R, 4R and 3R/4R Tauopathies (Kovacs, 2017). For instance, in Pick's disease (PiD), the predominant Tau isoforms within the aggregates are 3R. In corticobasal degeneration (CBD) and progressive supranuclear palsy (PSP), the Tau isoforms are 4R, while in AD and CTE, the aggregates are made of Tau 3R and 4R. The heterogeneity and overlap of affected cell types, brain regions and symptoms present a significant challenge for accurate clinical diagnosis (Beach et al., 2012). A definite diagnosis is often only possible post-mortem.

Table 1 Pathological heterogeneity of primary and secondary Tauopathies.

Tauopathy	Predominant Tau isoform	Morphology	Brain region	Clinical features
FTDP-17 (primary)	3R/4R	Pick bodies and AD-like NFT	Cortical and subcortical grey and white matter	Behaviour and personality change, cognitive dysfunction, atypical Parkinsonism
PiD (primary)	3R	Pick bodies and ballooned neurons	Neocortex, Hippocampus	Deterioration of language, personality, memory, social disinhibition, judgement
PSP (primary)	4R	NFTs and Pretangles	Striatum, Globus pallidus, Subthalamic nucleus, midbrain tectum/tegmentum, Substantia nigra, Basis pontis, Cerebellar dentate nucleus, Cerebellar peduncles	L-DOPA non-responsive parkinsonism, oculomotor dysfunction, gait failure, postural instability
CBD (primary)	4R	Pretangles and ballooned neurons	Substantia nigra, Globus pallidus, cerebral cortex	Bradykinesia, rigidity, dystonia, apraxia, cortical sensory signs, alien limb phenomenon
AD (secondary)	3R/4R	NFTs	Transentorhinal cortex, Limbic regions, Isocortex	Cognitive dysfunction, memory loss, judgement, personality
CTE (secondary)	3R/4R	NFTs	Neocortex, Sulci, Cortical grey matter, Penumbra	Memory deficits, personality changes

1.2.1 Alzheimer's disease

AD is a secondary Tauopathy first described by Alois Alzheimer in 1907 (Alzheimer, 1907). The patient, a 51-year-old woman, exhibited impaired cognition, and post-mortem analysis revealed the presence of senile plaques. Today, AD is the most prevalent form of dementia, comprising between 50 and 80 % of dementia cases (Long et al., 2023). AD cases are projected to increase from 55 million in 2019 to 139 million in 2050 (Alzheimer's Association, 2024). A definitive clinical diagnosis of AD dementia is currently only possible through post-mortem neuropathological evaluation (Caselli et al., 2017). The most common form of AD is sporadic and typically occurs after age 60. High-risk factors for sporadic AD include old age, female gender, cardiovascular risk factors, and the apolipoprotein E allele 4 (Verghese et al., 2011; Scheltens et al., 2021). In contrast, rare familial cases (5 %) account for early onset of the disease in the twenties (Devi et al., 2000). The most common cause of familial AD is associated with mutations in the amyloid precursor protein (APP) and the presenilin 1 and 2 (PSEN1 and PPSEN2) genes on chromosome 14 and 1, respectively (Bateman et al., 2011). These mutations result in the accumulation of extracellular senile plaques composed of Aβ, which leads to neuronal and synaptic loss (Masters et al., 1985; Hardy and Allsop, 1991; Selkoe, 1991). However, the presence of Aβ plaques alone is insufficient for clinical diagnosis. The presence of neurofibrillary lesions (NFTs), which contain β-sheet-rich Tau aggregates and neuropil threads, is essential for the diagnosis (Wilcock and Esiri, 1982). It is crucial to emphasise that Aβ and Tau are closely associated with the disease progression, highlighting their critical role in AD pathology (Roberson et al., 2007; Felice et al., 2008). AD is a mixed (3R/4R) Tauopathy, given that the Tau aggregates observed within the inclusions comprise Tau 3R and 4R (Yagishita et al., 1981; Goedert, 1993). While Aβ accumulation begins 10-20 years before cognitive symptoms manifest, Tau accumulation correlates with disease progression (Knopman et al., 2021). The Braak staging scheme is based on the progression of tangles in the brain (Braak and Braak, 1991). Braak stage I encompasses the earliest stage of NFT accumulation in the transentorhinal cortex. When NFT pathology becomes more robust in the transentorhinal cortex, it is defined as Braak stage II. In Braak stages III and IV, NFTs intrude the limbic regions, including the thalamus, hippocampus, amygdala and putamen. In Braak stage V, the pathology becomes more pronounced in the affected areas, with the involvement of the isocortex. Braak stage VI affects all associated areas, and profound NFT pathology is observed. Currently, there are no disease-modifying therapies for AD. The only available treatment for patients is symptomatic, with anti-Aβ antibodies Lecanemab or Aducanumab being used to slow cognitive decline (Budd Haeberlein et al., 2022; van Dyck et al., 2023).

1.2.2 Frontotemporal dementia and Parkinsonism (chromosome 17)

Frontotemporal dementia and Parkinsonism (chromosome 17) (FTDP-17) is an autosomal-dominant inherited Tauopathy traced back to over 67 mutations in the MAPT gene (Smith, 2023). These mutations result in abundant filamentous hyperphosphorylated Tau deposits in nerve and glial cells in cortical and subcortical grey and white matter (Spillantini et al., 1998a). Approximately 10 % of FTD cases are familial (Currens et al., 2023). Despite the absence of MAPT gene mutations in AD, FTDP-17 cases have demonstrated that Tau pathology can cause neurodegeneration even in the absence of Aβ (Ghetti et al., 2015). Mutations are located in exons 1, 9-13 or the introns following exon 10, resulting in missense mutations or deletions. Exonic mutations (S305N) have been demonstrated to induce more neuronal inclusions accompanied by dementia (Iijima et al., 1999; Kobayashi et al., 2002). Intronic mutations (N279K) can disrupt alternative mRNA splicing, resulting in an imbalanced Tau 3R to 4R ratio. This imbalance increases the relative amount of Tau 4R, which is associated with neuronal and glial pathology (Wszolek et al., 1992; Hutton et al., 1998). The substitution of proline for serine at position 301 (P301S) in exon ten has been demonstrated to disrupt the ability of Tau to promote microtubule assembly (Bugiani et al., 1999; Anne D. Sperfeld et al., 2001; Lossos et al., 2003; Kundel et al., 2018). In contrast, substituting proline for leucine at position 301 (P301L) has been observed to promote β-sheet formation and accelerate paired helical filament (PHF) formation (Hutton et al., 1998; Clark et al., 1998; Dumanchin et al., 1998; Spillantini et al., 1998b; Chen et al., 2019). Furthermore, the formation of Tau fibrils is accelerated when valine is substituted with methionine at position 337 (V337M) (Sumi et al., 1992; Poorkaj et al., 1998).

1.2.3 Pick's disease

PiD is classified as a 3R Tauopathy and is associated with a range of clinical symptoms, including language deterioration, social disinhibition, personality changes, impaired judgement, and memory loss. However, no motor deficits are observed in PiD (Piguet et al., 2011). The incidence of PiD is 2.7 to 4.1 per 100,000 person-years (Pippin and Gupta, 2023). While most PiD cases are sporadic, a few familial cases have been linked to missense mutations in the MAPT gene (Neumann et al., 2001; Tacik et al., 2015). The principal histological characteristics of this condition include severe neuronal loss, swollen neurons, and pathognomonic large spherical argyrophilic neuronal inclusions, commonly referred to as Pick bodies. The Pick bodies are primarily composed of Tau 3R isoforms and are found mainly in the neocortical cortex and the hippocampus, which parallels brain atrophy (Lee et al., 2001; Kovacs et al., 2013).

1.2.4 Progressive supranuclear palsy

PSP is a sporadic 4R Tauopathy characterised by neuronal and glial Tau pathology, neuronal loss and fibrillary astrogliosis. Reported incidence rates for PSP ranged from 0.3-2.6 per 100.000 person-years (Lyons et al., 2023). PSP is frequently misdiagnosed as Parkinson's disease (PD) due to the presence of similar symptoms. The subcortical regions affected by PSP include the striatum, globus pallidus, subthalamic nucleus, midbrain tectum/tegmentum, substantia nigra, basis pontis, cerebellar dentate nucleus, and cerebellar peduncles (Dickson et al., 2007). In comparison to non-demented PSP patients, dementia in PSP is associated with severe cerebral cortical degeneration (Bigio et al., 1999). Neuropathological features include spherical, globose, and flame-shaped NFTs and diffuse granular "pre-tangles." Tufted astrocytes are a distinctive feature of PSP, characterised by a complex branching pattern of proximal and medial cell processes.

1.2.5 Corticobasal degeneration

CBD is a sporadic 4R Tauopathy that shares histopathological features with PSP (Dickson et al., 2002). Reported incidence rates range between 0.03-0.8 per 100.000 person-years (Lyons et al., 2023). CBD is characterised by the following pathological features: depigmentation of the substantia nigra, atrophy of the globus pallidus, and cerebral cortical atrophy. A diagnosis of CBD is based on the presence of cortical and striatal Tau-positive neuronal and glial lesions in both white and grey matter (Dickson et al., 2002). Furthermore, CBD is characterised by the presence of 'astrocytic plaques', which are circular or ring-shaped formations resulting from the pathological accumulation of Tau in the distal processes of a single astrocyte.

1.2.6 Chronic traumatic encephalopathy

CTE is a specific form of Tauopathy that develops subsequently into traumatic brain injury. Neuronal Tau inclusions contain Tau 3R and 4R isoforms (McKee et al., 2015). Traumatic brain injury can occur as a consequence of a variety of sporting activities, including boxing and American football, as well as in accidents (McKee et al., 2009). Attention deficits, memory impairments, and progressive personality changes characterise the clinical presentation of CTE (McKee et al., 2009). It is hypothesised that Tau pathology commences at the depths of the sulci, manifesting as perivascular neuronal and glial Tau lesions (McKee et al., 2013). Currently, the diagnosis of CTE is only possible post-mortem, according to specific criteria.

1.3 Tau amyloid fibrils: Seeded polymerisation and prion-like spreading

Amyloid fibrils are highly ordered, insoluble protein aggregates studied for over fifty years. One of the initial discoveries was that amyloids are rich in β-sheets that run perpendicular to the fibril axis (protofilament) (Eanes and Glenner, 1968; Sunde et al., 1997). These β-sheets form through extensive hydrogen bonding between β-strands of individual or multi-layered monomeric subunits, with an interstrand distance of 4.7 Å (Cohen and Calkins, 1959; Nelson et al., 2005; Sawaya et al., 2007; Eisenberg and Sawaya, 2017). The polypeptide chains are stacked in extended β-strands that form in-register parallel or antiparallel β-sheets (Sawaya et al., 2007; Wiltzius et al., 2009; Berryman et al., 2011). Polar and non-polar side chains from nearby β-sheets interlock to create a "steric zipper," further stabilised by van der Waals forces (Schmidt et al., 2016). Intramolecular covalent, hydrogen and ionic bonds stabilise the multi-layered monomeric subunits (Liberta et al., 2019; Swuec et al., 2019; Radamaker et al., 2019). These individually stacked cross-β-sheets result in insoluble, protease-resistant, helical protofilaments that vary by degrees of symmetry and pitch (Rambaran and Serpell, 2008). Amyloid fibrils have one or more protofilaments associated via their protofilament-protofilament interfaces, enabling ultrastructural polymorphs (Seidler et al., 2018).

Soluble Tau is assembled into amyloid fibrils by a seeded polymerisation mechanism. Tau begins to self-aggregate spontaneously (primary nucleation) in a slow, rate-determining step (Figure 2). Amyloid motifs suggested to be essential for Tau nucleation are ^{275}VQIINK^{250} (PHF6*) in R2 and ^{306}VQIVYK^{311} (PHF6) in R3 (Bergen et al., 2000; Li and Lee, 2006). The mechanism of primary nucleation is unknown, but it is suggested that the nucleation step may be followed by a liquid-liquid phase separation (LLPS) (Wallace et al., 2013). Thereby, liquid droplets of a dense liquid phase are formed, enabling the formation of solid nuclei (Ambadipudi et al., 2017; Hughes et al., 2018; Wegmann et al., 2018). Transient oligomeric species represent intermediates that evolve into amyloid fibrils. These recruit monomeric Tau into the cross-β-sheet-rich amyloid fold, rapidly increasing the fibril concentration (Padrick and Miranker, 2002; Lee et al., 2007). The formation of large, highly-ordered amyloid fibrils is initiated by the recruitment of Tau monomers to the fibril ends, a process known as elongation. The newly evolved shorter Tau seeds continue to recruit and convert soluble Tau into amyloid fibrils (secondary nucleation). Alternatively, Tau monomers or clusters of monomers are suggested to be directly recruited to the fibril surface, followed by nucleation on the surface and detachment (Törnquist et al., 2018). The seeded polymerisation process enables Tau propagation *in vivo*, *in vitro* and *in cellula* (Friedhoff et al., 1998; Clavaguera et al., 2009; Frost et al., 2009). The transmission and propagation of Tau aggregates between cells is reminiscent of prion propagation (Kaufman and Diamond, 2013; Prusiner, 2013;

Kaufman et al., 2016; Woerman et al., 2016). The cellular prion protein (PrP^{C}) is converted into the pathological and infectious prion (PrP^{Sc}), which can spread throughout the brain, leading to a progressive pathology (Weissmann et al., 2002; Aguzzi and Calella, 2009; Prusiner, 2013; Kaufman and Diamond, 2013). PrP^{C} is converted on the cell surface, while Tau is converted in the cytoplasm. However, once converted, they share the same amyloid cross-β-sheet structure despite differences in primary structure, localisation, and function.

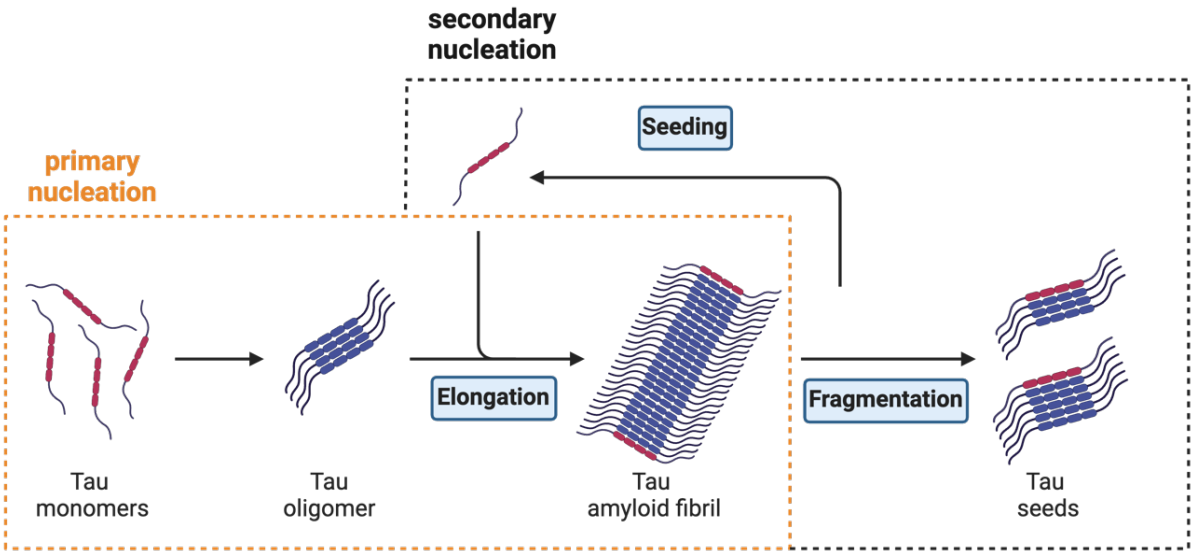

Figure 2 Model of seeded polymerisation of Tau fibrils. Native Tau can form oligomers, an intermediate state that evolves into highly ordered Tau amyloid fibrils (primary nucleation). Secondary nucleation of the β-sheet-rich Tau amyloid fibrils generates seeds with new active ends that recruit more Tau monomers into Tau seeds. Created with BioRender.com

1.4 Cryo-EM of Tau amyloid cores

In 1960, electron microscopy (EM) first identified and pictured PHFs of Tau (KIDD, 1963, 1964). These filaments consist of an ordered core and a 'fuzzy coat', the unstructured part of the protein outside the ordered core (Wischik et al., 1988). In 1991, straight filaments (SF) of Tau were discovered. Subsequently, the protofilaments' internal cross-section morphology, orientation, and dimeric structures were determined for both PHFs and SFs (Crowther, 1991). The initial atomic structures of *in vitro*-generated amyloids were obtained using solid-state nuclear magnetic resonance (ssNMR) spectroscopy (Petkova et al., 2002; Lu et al., 2013; Tuttle et al., 2016). It was not until 2017 that the structure of Tau filaments of an AD patient could be identified (Fitzpatrick et al., 2017). This was possible by developing improved electron detectors, imaging techniques, software, and image processing (Kühlbrandt, 2014; He and Scheres, 2017). Since then, several three-dimensional amyloid structures have been reported for Tau fibrils associated with distinct Tauopathies. All share an ordered core of β-

strands, loops, and turns with different organisations and molecular interactions. Within patients with the same Tauopathy, fibril cores are preserved, supporting the hypothesis that distinct conformations might be linked to defined local motifs. These are exposed during aggregation and kinetically drive the fibril formation process into Tau conformers (Chen et al., 2019; Mullapudi et al., 2023). The unique folds of the cryoEM Tau cores arise from the individual proteins that build protein-specific protofilaments (Creekmore et al., 2021). In detail, Tauopathies like AD, CTE PiD, PSP and CBD have distinct protofilament structures (Table 2). All Tau amyloid cores comprise R3 and R4, along with 10-12 amino acids C-terminally of the RD region, that build the monomeric subunits of the parallel, in-register cross-β-structure. They differ in the number of protofilaments (1-2), the number of residues included before R3, the core fold and their inter- and intramolecular forces. Intermolecular forces stabilising the core are hydrogen bonds and van der Waals forces. Intramolecular interactions include, among others, covalent (peptide bonds, disulfide bridges) or ionic bonds. The monomeric subunit folds result in cores that can be 2-4 layered. Differences within the protein's core constitution may explain Tau aggregation and propagation variability, resulting in clinical and pathological heterogeneity.

Table 2 CryoEM Tau amyloid cores.

Tauopathy	Isoform*	Core fold	Protofilaments	Protofilament-Protofilament interface
AD	$3R^{(273-380)}$ $4R^{(304-380)}$	2-layered	2	PHFs: symmetrically back-to-back, hydrogen bonds SFs: asymmetrically, additional densities
PiD	$3R^{(254-378)}$	2-layered	1-2	End-to-end, van der Waals interactions
PSP	$4R^{(272-381)}$	3-layered	1	-
CBD	$4R^{(274-380)}$	4-layered	1-2	Symmetrically, van der Waals interactions
CTE	$3R^{(274-379)}$ $4R^{(305-379)}$	2-layered	2	Type I: symmetrically, anti-parallel steric zipper Type II: asymmetrically, hydrogen bonds

*numbering according to Tau $2N4R^{(0-441)}$

Despite clinical and phenotypic heterogeneity, the amyloid core is retained in AD cases (Falcon et al., 2018c) (Figure 3 A). The amyloid structure of PHFs and SFs from AD patients was resolved by cryoEM, demonstrating a helical symmetry of 4.7 Å. The two-layered C-shaped core of the symmetrically packed protofilaments is composed of R3 and R4, along with ten additional residues from the adjacent C-terminal region, which include residues

306-378 (Fitzpatrick et al., 2017; Falcon et al., 2018c). A second study demonstrated with higher-resolution images that two additional residues from R1 (273-274) or R2 (304-305) plus two residues from the C-terminus (379-380) are present within the ordered core of AD (304-380) (Falcon et al., 2018c). If residues from R1 are included within the cores, they are representative of Tau 3R isoforms, and if residues of R2 are included, they represent Tau 4R

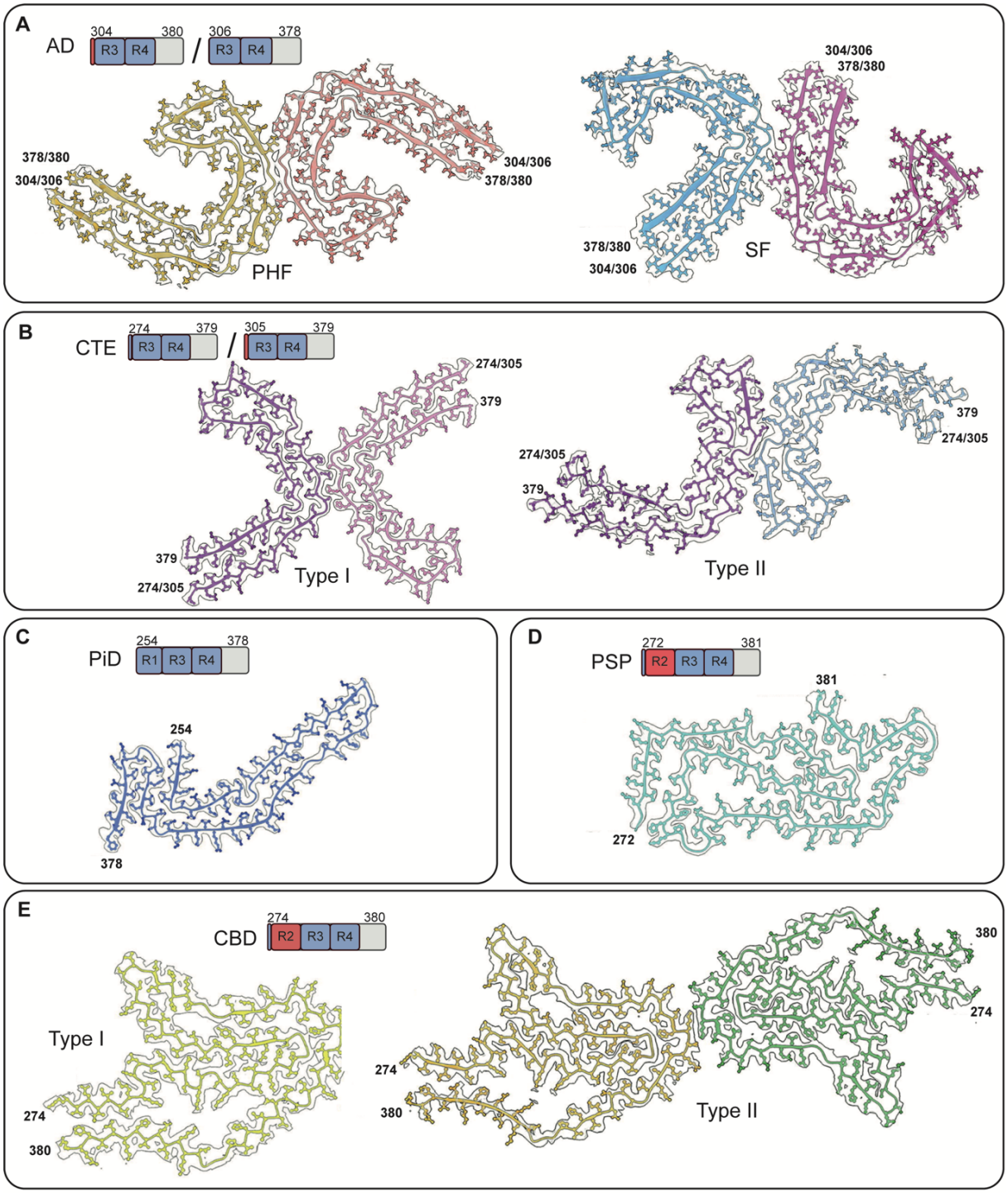

Figure 3 CryoEM cores of Tau fibril folds from Tauopathy patients. CryoEM Tau fibril core folds from (A) AD (PHF/SF), (B) CTE (Type I/II), (C) PiD, (D) PSP and (E) CBD (Type I/II), patients. The figure was adapted from Mishra, 2023.

isoforms. PHFs and SFs are fibril polymorphs that consist of two identical protofilaments but differ in their protofilament-protofilament interface (Fitzpatrick et al., 2017). The two protofilaments in PHFs are packed symmetrically back-to-back via hydrogen bonds. The protofilaments of SFs are packed asymmetrically and are stabilised by additional densities (Falcon et al., 2018c). The protofilament structure in AD is characterised by monomers stacked on top of each other in register and parallel, forming β-sheets. The interaction of mainly R3 and the C-terminus and another PGGG motif at the end of R4 generates the C-shaped protofilaments. Intramolecular hydrophobic clusters, hydrogen bonds, and aliphatic and aromatic stacking stabilise the core. The fuzzy coat comprises disordered residues from the N- and C-terminus, which leads to less well-defined densities and probably adopts random conformations. AD is a mixed Tauopathy because Tau 3R and 4R isoforms can be found within the Tau deposits.

Like the AD core, CTE-ordered cores can consist of Tau 3R and 4R isoforms. The C-shape of the CTE fold reminds of the AD fold but is less tightly packed, resulting in a hydrophobic cavity at the C-shape's tip. This hydrophobic cavity contains an unidentified non-proteinaceous density, contributing to a more open fold than AD. The topology and secondary structure of the CTE fold are analogous to that of the AD fold. The cryoEM 3R CTE core comprises residues 274-379, according to the numbering of Tau 2N4R$^{(0\text{-}441)}$, but missing R2 (Figure 3 B). The cryoEM 3R CTE core includes one amino acid, K274 from R1, the complete R3-R4, and eleven amino acids from the C-terminus (Falcon et al., 2019) (Figure 3 B). The cryoEM 4R CTE core is similar to the 3R-ordered core but comprises residues 305-379 based on 2N4R$^{(0\text{-}441)}$, with the last residue, S305, from R2. R3-R4 and eleven C-terminal residues follow R2. Cryo-EM 3R CTE cores exhibit a typical protofilament architecture. CTE type I (20-25 nm, 75 %) and type II (15-30 nm) filaments are ultrastructural polymorphs with different protofilament-protofilament interfaces. CTE type I protofilaments interact via an anti-parallel steric zipper. CTE type II protofilaments form hydrogen bonds between the PGGG motifs.

The cryoEM PiD core contains only Tau 3R isoforms. It comprises a singlet or doublet two-layered protofilament consisting of 254-378 residues representing parts of R1, all of R3, and R4, and an additional ten amino acids following the RD (Falcon et al., 2018b) (Figure 3 C). While the AD and CTE protofilament cores are C-shaped, the PiD core is more elongated. The β-sheets in the AD and PiD cores mostly align locally in regions 306-354 but differ in the core fold. In contrast to cryoEM AD filament cores, cryoEM PiD cores comprise four cross-packed stacks of β-strands, which end in a three-layer sandwich. Entirely hydrophobic regions are in the middle of the core, whereas the other cross-β packing interfaces possess non-polar and polar side chains. Within cryoEM PiD cores, one can distinguish between narrow 5-15 nm PiD filaments (NPFs), which account for 93 % of the filaments, while wide 5-30 nm PiD filaments

(WPFs) comprise the remainder. The single-folded NPFs consist of one elongated protofilament, while WPFs comprise two NPFs that are arranged end-to-end. The tips of the NPFs within the WPFs are intermolecularly connected via van der Waals interactions. Due to the elongated conformation of the PiD core, it is incompatible with Tau 4R isoforms, explaining the existence of mainly Tau 3R aggregates.

PSP is a 4R Tauopathy. The core is composed of a single protofilament with a unique three-layered fold, which includes R2, R3, and R4 (272-381) of Tau 4R (Shi et al., 2021; Mishra, 2023) (Figure 3 D). After each repeat, the protein backbone turns back and forth, with R3 being between R2 and R4. In line with CTE, additional densities can be observed within two small cavities situated along the R2-R3 interfaces of PSP and a larger cavity at the R3-R4 interface. The remainder of the R3-R4 interface is intramolecularly connected via hydrophobic interactions and salt bridges. The conserved PGGG motifs at the end of each repeat support the three-layer fold, which facilitates the formation of hairpin turns. Outside the PSP core, a minimum of six extra densities were identified. The origins and functions of the additional densities remain unknown.

The ordered cryoEM core of CBD a 4R Tauopathy contains residues 274-380, which correspond to R2, R3, and R4, and 12 amino acids after R4 (Zhang et al., 2020) (Figure 3 E). Singlet and doublet polymorphs of CBD have been identified, exhibiting varying ratios between patients. The type I CBD fold comprises a single protofilament, whereas the type II fold consists of two protofilaments that adopt a four-layer fold. Despite the different overall shape of the CBD fold, the four-layered fold retained a secondary structure similar to AD and CTE. Like in CTE and PSP, a hydrophilic cavity is constructed between R2 and R4. The interfaces include polar and hydrophilic groups. The two protofilaments of CBD fold type II are symmetrical, and their interfaces are connected by antiparallel stacking and via van der Waals interactions and hydrogen bonds. The hydrophilic cavity contains an unidentified non-proteinaceous polyanionic density not associated with Tau. It is postulated that these unidentified densities serve to stabilise the CBD fold.

1.5 Posttranslational modifications of Tau

In Tauopathies, post-translational modifications (PTMs) contribute to the structural and phenotypic diversity of amyloids. PTMs such as phosphorylation, ubiquitination, acetylation, methylation, and truncation modify protein structure, stability, localisation, and activity in different brain regions and cell types (Alquezar et al., 2020). In pathological stages, dysregulation of PTMs could influence fibril formation and disease pathology, contributing to

the heterogeneity of clinical symptoms and pathogenesis (Malbica and Monson, 1975; Mahul-Mellier et al., 2014; Morris et al., 2015; Hu et al., 2019; Levine et al., 2019; Zhao et al., 2020). Hyperphosphorylation is the most studied PTM in soluble Tau and Tau aggregates (Martin et al., 2011). In healthy human brains, Tau is typically decorated with 2-3 moles of phosphate, which is essential for the normal physiological function of Tau in microtubule stabilisation (Cleveland et al., 1977; Iqbal et al., 2005). In contrast, Tau phosphorylation levels are approximately two to three times higher in Tauopathies (Iqbal et al., 2016). Over 85 phosphorylation sites have been identified, of which approximately 50 can be modified (Martin et al., 2011; Phipson et al., 2016). The phosphorylation sites are primarily located in the RD of Tau and the adjacent C-terminus, while the N-terminus contains the non-modified sites. The alteration of net change caused by the phosphorylation of Tau results in altered molecular interactions, which can lead to the loss of microtubule association (Biernat et al., 1993; Bramblett et al., 1993). The phosphorylation of Tau near and within the RD has been shown to reduce the affinity of Tau for microtubules (Drewes et al., 1995; Sengupta et al., 1998; Liu et al., 2007). The phosphorylation of specific serines has been demonstrated to promote self-aggregation, while the phosphorylation of certain asparagines has been shown to inhibit Tau truncation (Haase et al., 2004; Guillozet-Bongaarts et al., 2006). Truncation of Tau can lead to enhanced fibril formation (Canu et al., 1998; Gamblin et al., 2003). CryoEM, mass spectrometry (MS) and immunohistochemistry have significantly contributed to determining PTM profiles on Tau aggregates (Ebru Ercan et al., 2017; Arakhamia et al., 2020). Intriguingly, fetal Tau is highly phosphorylated during neuronal development but does not aggregate in the brain (Kenessey and Yen, 1993; Brion et al., 1994; Yu et al., 2009). One challenge is that patient-derived Tau is dephosphorylated due to a post-mortem delay before analysis. Further, decreased body temperature and anaesthesia can lead to dephosphorylation of mainly soluble Tau, as phospho-sites in Tau aggregates might be protected from dephosphorylation (Matsuo et al., 1994; Whittington et al., 2013; Wang et al., 2015). As a result, the precise phosphorylation status of Tau in the human brain remains to be determined. It remains unclear whether hyperphosphorylation of Tau is a cause or a consequence of the formation of potentially toxic Tau aggregates. Moreover, acetylation and ubiquitination share PTM sites, primarily located within the RD of Tau, suggesting a competitive role in PTMs (Morris et al., 2015; Mair et al., 2016). Acetylation of Tau can enhance its aggregation *in vitro* and reverse LLPS separation (Cohen et al., 2011; Ukmar-Godec et al., 2019). Acetylation of specific lysines in R3 enhanced fibril formation (Li et al., 2023). In contrast, the acetylation of multiple lysine residues in R2 of Tau 2N4R$^{(0\text{-}441)}$ can block Tau 4R aggregation, possibly by preventing the CBD- or PSP-fold formation. In contrast, the acetylation of these residues has been shown to accelerate the aggregation of Tau 0N3R$^{(0\text{-}352)}$ (Chakraborty et al., 2023). Acetylation of

specific lysine residues in the proximity of the amyloid motifs increased the aggregation of the Tau fragments (Li et al., 2023). All other PTMs occur less frequently within the Tau sequence.

1.6 Tau secretion and uptake

Different mechanisms have been proposed for the secretion and uptake of oligomeric and fibrillar Tau to spread from a donor to a recipient cell. Initially, it was suggested that NFTs in the CSF of AD patients were a result of dying neurons. However, the presence of Tau at both the pre- and post-synapse in humans and mice has demonstrated that Tau secretion is an active process (Hampel et al., 2004; Ittner et al., 2010; Tai et al., 2012). The transmission of Tau aggregates from cell to cell involves three basic steps: (1) secretion of pathological Tau aggregates from donor cells, (2) uptake of secreted Tau aggregates by recipient cells, and (3) seeded polymerisation of Tau in the recipient cell (Gibbons et al., 2019; Brunello et al., 2020) (Figure 4).

Secretion steps involve extracellular vesicles (EVs) associated with Tau. EVs play a role in the exchange of cellular agents, such as proteins or lipids, between remote cells (Cocucci and Meldolesi, 2015). EVs include exosomes (30-150 nm) and ectosomes (100-1000 nm) that have been shown to contribute to Tau transmission (DeLeo and Ikezu, 2018). Exosomes are intraluminal vesicles that can take up Tau and enter endosomal multivesicular bodies (MVB). MVBs fuse with the donor cell membrane and release the exosomes into the extracellular space (Rajendran et al., 2014; Rabouille, 2017). Exosomes containing Tau were detected in the CSF and blood of AD patients (Saman et al., 2012; Jia et al., 2019). Ectosomes are directly released from the plasma membrane by ectosome shedding (Barteneva et al., 2013; Kalra et al., 2016). Cytosolic proteins like Tau can be taken up during the formation of ectosomes, which are subsequently released in the extracellular space (Dujardin et al., 2014; Spitzer et al., 2019). Besides the secretion of Tau in vesicles, Tau can also be directly translocated through the plasma membrane (Kfoury et al., 2012; Katsinelos et al., 2018). It was shown that the secretion of Tau associated with EVs from rat cortical neurons was relatively low (3 %) (Wang et al., 2017) and that most of Tau must be secreted freely. Heparan sulfate proteoglycans (HSPG) are ubiquitously expressed transmembrane receptors that recruit and cluster molecules, mediating their translocation (Condomitti and Wit, 2018). It is suggested that HSPGs anchor Tau, enabling a bi-directional translocation through the plasma membrane (Xu and Esko, 2014).

For the efficient transmission of Tau, the recipient cell needs to take Tau up. EVs either directly fuse with the membrane of the recipient cell via receptor-ligand interactions, or they are

internalised by endocytosis (Morelli et al., 2004; Del Conde et al., 2005; Parolini et al., 2009; Montecalvo et al., 2012; Tian et al., 2013; Svensson et al., 2013). Our group showed that viral glycoproteins on the cell surface of the donor cell can enhance the intercellular spreading of Tau associated with EVs if the corresponding receptor is expressed on the cell surface of the recipient cell (receptor-ligand interaction) (Liu et al., 2021). HSPGs on the membrane of the recipient cell can take up extracellular Tau (Holmes et al., 2013). Macropinocytosis (bulk-endocytosis) involves the non-specific internalisation of extracellular fluid, including large, insoluble Tau aggregates (Wu et al., 2013; Evans et al., 2018). Macropinosomes are formed once Tau aggregates bind to the HSPGs on the cell surface (Holmes et al., 2013; Rauch et al., 2018; Annadurai et al., 2021). Subsequently, macropinosomes traffic their cargo to lysosomes for degradation and recycling (Donaldson, 2019). Receptor-dependent clathrin-mediated endocytosis mediates the recruitment of cargo molecules by different transmembrane receptors, followed by their internalisation via the clathrin-coated pit (Doherty and McMahon, 2009). It has been shown that Tau internalisation is mediated by the endocytic lipoprotein receptor-related protein 1 (LRP1) (Lane-Donovan et al., 2014; Rauch et al., 2020), muscarinic acetylcholine receptors (mAChR) (Morozova et al., 2019), and sortilin protein-related receptors (SORLA) (Bok et al., 2021). LRP1 regulates the uptake of Tau monomers, oligomers and fibrils (Rauch et al., 2020). Once inside the recipient cell, Tau aggregates must be released from the endosome or lysosome to initiate seeded polymerisation in the cytosol. Membrane rupture is one mechanism for Tau to escape the vesicles (Calafate et al., 2016; Flavin et al., 2017; Falcon et al., 2018a; Rose et al., 2024). It is suggested that Tau aggregates and other amyloids can disrupt vesicle membranes, but the mechanism is unknown. In cell culture, Lipofectamine is used to enhance the seeding of Tau as it is known to facilitate the entry of Tau into cells and to rupture vesicle membranes, resulting in the release of Tau in the cytosol (Dalby et al., 2004; Wittrup et al., 2015; Joshi et al., 2020; Kolay et al., 2022, 2022).

Besides secretion and uptake, Tau transmission can occur via cell-cell contact through tunnelling nanotubes (TNT) directly entering the cytosol of the recipient cell. TNTs are filamentous-actin-containing membranous tubes that connect adjacent cells and can be used by prions and viruses to infect neighbouring cells (Sowinski et al., 2008; Gousset et al., 2009). It has been shown that exogenous Tau fibrils can increase the formation of TNTs and facilitate the intercellular transfer of Tau aggregates from cell to cell (Tardivel et al., 2016). *In vivo*, microglia and astrocytes are also involved in Tau aggregate spreading. This hypothesis is supported by a recent study, which demonstrated that primary microglia from Tauopathy patient brains can secrete seeding-competent Tau into the media (Hopp et al., 2018). The minimal Tau species required for seeding is still under debate, but oligomers are considered

the most seeding-prone Tau species (Lasagna-Reeves et al., 2012a; Lasagna-Reeves et al., 2012b; Takeda et al., 2015).

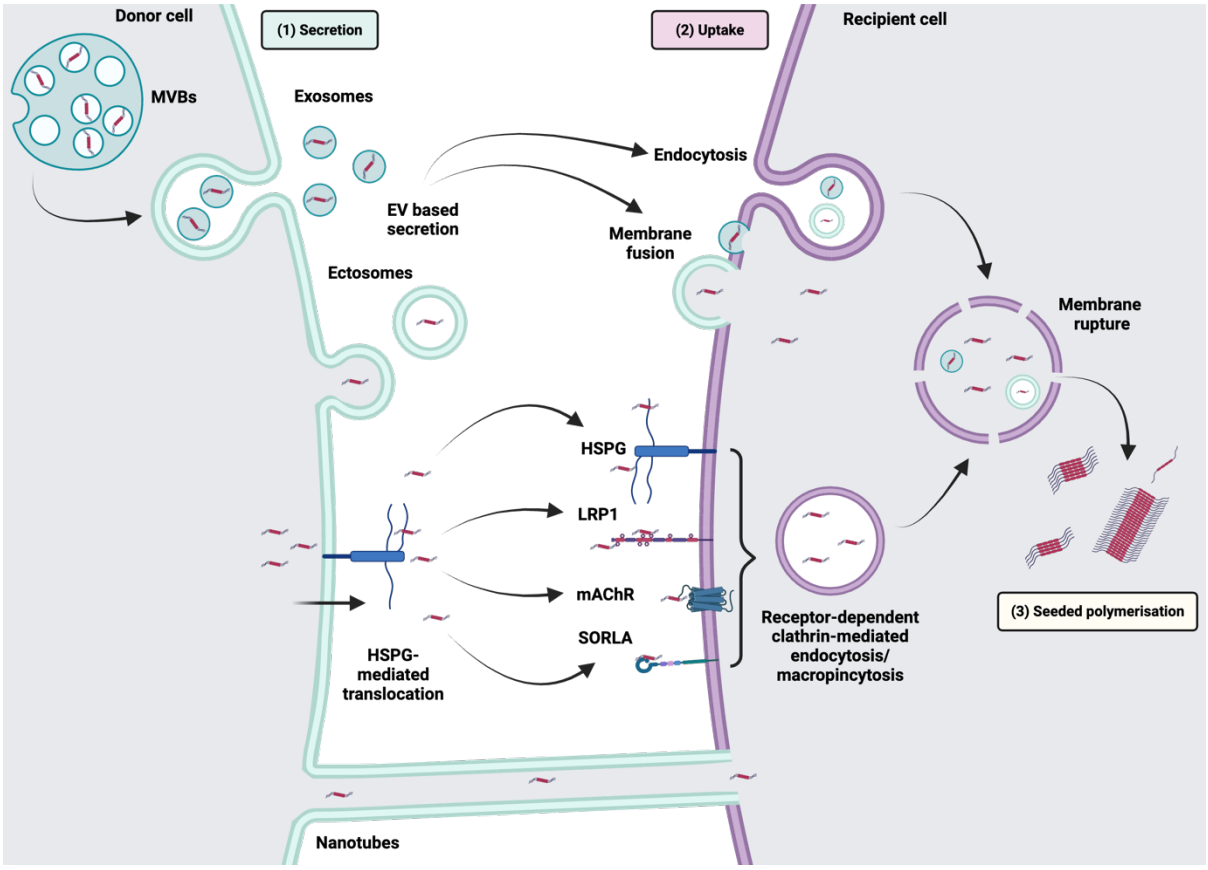

Figure 4 Possible mechanisms of Tau secretion and uptake. (1) Tau secretion involves EVs (exosomes and ectosomes) and HSPG-mediated translocation through the plasma membrane. **(2)** Tau uptake is mediated by endocytosis, fusion of EVs with the recipient cell membrane, or receptor-dependent clathrin-mediated endocytosis or macropinocytosis. Tau enters the cytoplasm of recipient cells directly via nanotubes or through membrane rupture, followed by seeded Tau polymerisation. MVB: Multivesicular body. HSPG: Heparan Sulfate Proteoglycans, LRP1: Low-Density Lipoprotein Receptor-related Protein 1, mAChR: muscarinic acetylcholine receptors, SORLA: sortilin protein-related receptors. Created with BioRender.com

1.7 The cellular protein quality control system

The cellular protein quality control system (PQC) comprises the endoplasmic reticulum pathway (ERP), autophagy-lysosome pathway (ALP), and the ubiquitin-proteasome system (UPS). These pathways recognise damaged proteins and regulate their turnover (Gestwicki and Garza, 2012). In AD, the PQC plays a critical role in maintaining the regular state of the cell to prevent protein dysfunction that could contribute to both physiological and pathophysiological processes (Chaari, 2019). Once an unfolded protein response (UPR) is triggered as an adaptive response of the ERP, the expression of molecular chaperones is upregulated. In contrast, total protein synthesis is downregulated to reduce the accumulation of misfolded proteins (Uddin et al., 2020). In the event of a failure of the ERP to refold the

proteins, chaperones will mediate the misfolded proteins to the ALP or UPS (Chaari, 2019). Abnormal protein expression and dysregulation of key components in the pathways can result in an overload of protein deposits in the PQC, leading to neurodegeneration (Douglas and Dillin, 2010).

The UPS and ALP mainly regulate the degradation of misfolded proteins. The UPS is responsible for the degradation of short-lived proteins (Lee et al., 2013; Cao et al., 2019), whereas the ALP, including macroautophagy, is involved in the degradation of long-lived organelles and large protein aggregates (Cheung and Ip, 2011; Orr and Oddo, 2013; Zhu et al., 2013). Macroautophagy involves the formation of a double-membrane autophagosome that sequesters protein inclusions, eventually fusing with lysosomes, leading to enzymatic digestion of its content (Ciechanover, 2006). Tau can be degraded by macroautophagy but is also known to impair ALP by disrupting the fusion of the autophagosome with the lysosome and triggering lysosomal dysfunction in AD (Hamano et al., 2008; Khurana et al., 2010; Li et al., 2010). The UPS requires ubiquitination at Lysine residues for degradation. Substrates with poly-ubiquitin chains are then transported to the 26S proteasome for further degradation (Campello et al., 2013; Dikic, 2017). The dysfunction of the UPS and overexpression of phosphorylated Tau appear to be correlated (Tai et al., 2012; Gadhave et al., 2016), playing an important role in the pathogenesis of AD.

1.8 Therapeutic strategies

Therapeutic strategies targeting Tau have shown promising results in preclinical studies and early clinical trials. Still, despite extensive research, many Tau-targeting therapies have failed in later-stage clinical trials (Cummings et al., 2024). Aβ was the primary target for drug discovery, but over time, Tau became the major drug target as it correlates with the degree of cognitive impairment and neurodegeneration (Arriagada et al., 1992; Murray et al., 2011; Nelson et al., 2012; Ossenkoppele et al., 2016). The heterogeneity of Tauopathies is a major challenge for developing Tau-targeting drugs as well as the effective transfer of drugs across the blood-brain barrier. Further, the precise mechanism of Tau aggregation and toxicity remains to be solved, complicating the development of drugs. Nevertheless, there are several ways to target Tau aggregation. Possible therapeutic strategies include downregulating Tau expression by antisense therapies, enhanced extracellular Tau clearance via active or passive immunotherapy, modifying or inhibiting PTMs, aggregation, and intercellular spreading by small molecules.

By downregulating Tau expression, the source of toxic aggregates might be reduced, which could mitigate neuronal damage. One approach is antisense therapies that use single-

stranded, short antisense oligonucleotides (ASOs) to modulate protein translation by preventing or restoring it (Havens et al., 2013). One challenge is the uptake of ASOs due to their small size, highly charged nature, stability, susceptibility to nuclease degradation and passage through the blood-brain barrier. Currently, two ASOs are tested in early clinical trials as they inhibit the translation of Tau mRNAs into protein, reducing toxin-induced seizures, neuronal loss, and NFT pathology in transgenic mice (DeVos et al., 2013; DeVos et al., 2017). Additionally, the behavioural phenotypes in transgenic mice were normalised, and the survival rate was prolonged (DeVos et al. 2013; DeVos et al. 2017). However, it is essential to consider the physiological roles of Tau, such as stabilising microtubules. If the translation of soluble Tau is downregulated too much, it could disrupt normal cellular functions. Therefore, it is critical to find the balance between eliminating pathological Tau without affecting the normal function of Tau.

Tau passive immunotherapies were applied to target Tau epitopes or specific Tau conformations to neutralise extracellular Tau and facilitate its clearance (Pedersen and Sigurdsson, 2015). In addition, several antibodies were identified that prevented seeding, propagation, and uptake of Tau (Boutajangout et al., 2011; Chai et al., 2011; Yanamandra et al., 2013; Nicholls et al., 2017; Nobuhara et al., 2017). Antibodies targeted either the N-terminus, the PRD, the RD, or the C-terminus of the Tau isoforms (Castillo-Carranza et al., 2014; Walls et al., 2014; Dai et al., 2015; Ittner et al., 2015; Yanamandra et al., 2015; Agadjanyan et al., 2017). A monoclonal antibody is being tested for AD in a phase 3 clinical trial (Cummings et al., 2024). The antibody binds to the RD of Tau, thereby preventing the cell-to-cell propagation of pathological Tau species and enhancing Tau clearance by microglia in transgenic mice (Roberts et al., 2020). Another monoclonal antibody potently blocks the seeding of human AD and PSP-derived Tau aggregates in the brains of transgenic mice (Courade et al., 2018; Albert et al., 2019). The disadvantages of passive immunotherapies are inflammatory responses and off-target effects. The selectivity of the antibody to pathological Tau must be given to prevent the elimination of endogenous soluble Tau.

PTMs are crucial in pathological Tau aggregation, seeding, and propagation. Therefore, a potential treatment strategy is modulating or inhibiting hyperphosphorylation and phosphorylation, as Tau is hyperphosphorylated or abnormally phosphorylated in AD. The glycogen synthase kinase 3β (GSK-3β) has an increased activity in AD patients and phosphorylates numerous residues on Tau (Pei et al., 1997; Rippin and Eldar-Finkelman, 2021). Clinical trials inhibiting GSK-3β function have produced inconsistent results or have not shown clinical efficacy (Medina et al., 2011; Forlenza et al., 2011; Tolosa et al., 2014; Lovestone et al., 2015). An inhibitor of the (protein)-3-O-(N-acetyl-D-glucosaminyl)-L-

serine/threonine N-acetylglucosaminyl hydrolase (OGA) was shown to reduce Tau phosphorylation, aggregation, and neuronal loss in transgenic mice and is currently being tested in phase III clinical trial (Yuzwa et al., 2012; Graham et al., 2014; Hastings et al., 2017; Cummings et al., 2024). It is critical not to disrupt normal phosphorylation processes, which could affect cognitive functions and synaptic plasticity.

Small molecules that inhibit Tau aggregation and intercellular spreading of Tau are another approach to reducing Tau pathology. Small molecules have the advantage of an enhanced ability to penetrate the blood-brain barrier. High-content screens *in vitro* or cell-based assays are frequently used to identify small molecules that inhibit Tau aggregation (Pickhardt et al., 2005a; Pickhardt et al., 2005b; Crowe et al., 2007; Crowe et al., 2009; Bulic et al., 2010; Hebestreit, 2020; Cheng et al., 2021; Antoniou et al., 2022; Bahnassawy et al., 2024). Methylene blue was found to block Tau aggregation and induce autophagy, thereby preventing Tau propagation *in vitro* and transgenic mice (Wischik et al., 1988; Congdon et al., 2012; Hosokawa et al., 2012). Due to strong side effects, Methylene blue did not pass the early clinical trials. Another small-molecule inhibitor (clinical trial phase I) inhibits Tau self-association, preventing the nucleation of Tau and, consequently, the formation of toxic oligomers, NFTs and their propagation through the brain (Moe et al., 2016; Moe et al., 2017). Our group also employed a semi-automated high-throughput screen to identify Tau aggregation inhibitors (Hebestreit, 2020). C22 inhibited Tau aggregation with an IC_{50} of 0.15-1.5 µM, but its target remains unknown. Small molecules that reduce or inhibit Tau aggregation could help resolve Tau uptake, aggregation, propagation and transmission mechanisms by identifying their targets within the cells.

1.9 Tau cell models

Cell models, also known as biosensor cell lines, are widely used to detect Tau seeding activity and to investigate intra- and intercellular Tau aggregation and propagation. The advantages of cell-based reporter systems over animal models include short time periods (24-96 hours) and the possibility of using high-throughput assays (Holmes and Diamond, 2017). Cell models played an instrumental role in the discovery that Tau fibrils can propagate from the outside to the inside of a cell (Frost et al., 2009). Strategies for the stable expression of Tau in cells include Tau-inducible cell lines that overexpressed Tau via a doxycycline-inducible system (Khlistunova et al., 2006) or cell lines that permanently stably express Tau detected by antibodies (Vogelsberg-Ragaglia et al., 2000; Ferrari et al., 2003; Choi et al., 2014) or tagged to fluorophores, like green (GFP), yellow (YFP) or cyan fluorescent protein (CFP) (Lu and Kosik 2001; Woerman et al. 2016). In addition, fluorescent protein technologies such as

fluorescence resonance energy transfer (FRET) have been used to study the Tau-Tau interaction in living cells. In the FRET system, Tau is tagged to CFP or YFP. The incubation of cells with exogenous Tau seeds results in the initiation of Tau aggregation, evidenced by a FRET signal that can be quantitatively assessed (Holmes et al., 2014; Furman et al., 2015; Furman and Diamond, 2017). Either full-length Tau or Tau RD fragments are used in the cell models. As the Tau RD fragments demonstrated an enhanced seeding efficacy, most cell models are based on Tau 3R or 4R RD fragments with (P301S/P301L/V337M) or without mutations (Kfoury et al., 2012; Holmes et al., 2014; Woerman et al., 2016; Liu et al., 2021).

Tau fibrils are added to the cells as naked exogenous recombinant fibrils or as seeds derived from transgenic mice or patient brains. Due to low numbers of aggregate-bearing cells, exogenous Tau seeds are mixed with lipid-based transfection reagents like Lipofectamine to increase the seeding efficacy (Guo and Lee, 2011; Holmes and Diamond, 2017). Lipofectamine facilitates Tau uptake and potentially enables Tau release by membrane rupture, leading to enhanced Tau seeding (Cardarelli et al., 2016; Holmes and Diamond, 2017; Pemberton et al., 2024). Based on this system, LRP1 and HSPG have been identified as cell-surface receptors involved in vesicle-free Tau uptake (Holmes et al., 2013; Rauch et al., 2018; Rauch et al., 2020). Further, it was shown that individual Tau conformers can be stably propagated within cell clones, and their transmission into naïve cell clones resulted in identical Tau conformations (Sanders et al., 2014). The same Tau conformers were injected into transgenic mice and re-introduced into mice, creating the earlier seeding patterns. Tau strain patterns in PS19 mice expressing the P301S mutated Tau 1N4R (Tau $1N4R^{S\ (0\text{-}412)}$) can be correlated with specific cell types, brain regions, distinct aggregation rates and dissemination routes (Kaufman et al., 2016). Additionally, biosensor cell lines have been used to detect Tau seeding activity in the brains of transgenic mice and the brains of patients with AD and other Tauopathies (Holmes et al., 2014; Bennett et al., 2017; DeVos et al., 2018; Polanco et al., 2021; Lathuiliere et al., 2023).

Co-culture of aggregate-bearing cell lines (donor cells) with cell lines expressing soluble Tau (recipient cells) is used to investigate mechanisms of cell-to-cell transmission of prion-like proteins such as Tau (Liu et al., 2021; Liu et al., 2023). The Vorberg lab used a cell model based on the expression of the soluble GFP-tagged, P301L/V337M mutated Tau RD (recipient cells) and the same cell line stably propagating Tau RD aggregates (donor cells) to investigate the intercellular spreading of Tau aggregates (Liu et al. 2021). The transmission of aggregates between the donor and the recipient cells was poor. Interestingly, when the viral glycoprotein vesicular stomatitis virus G (VSV-G) or the spike protein of the severe acute respiratory syndrome coronavirus 2 (SARS-CoV-2) was transfected into donor cells, the efficacy of aggregate transmission between donor and recipient cells was increased given that the

recipient cells expressed the corresponding low-density lipoprotein (LDL) or angiotensin-converting enzyme 2 (ACE2) receptor. The same results were obtained when the secretion of Tau-associated EVs was investigated as a possible mechanism for intercellular Tau spreading (Liu et al., 2021). EVs obtained from the donor cells transfected with VSV-G or SARS-CoV-2 efficiently dock and fuse via ligand-receptor interaction with the recipient cells expressing the LDL or ACE2 receptor. This interaction indicates that viral infections may facilitate the propagation of Tau *in vivo* (Liu et al., 2021).

Studies using cell-based assays expressing Tau demonstrated that cellular systems can be used to investigate spatial and temporal resolution of Tau aggregation and enable the study of mechanisms of pathological Tau aggregation, propagation and transmission. Since the residues within the Tau amyloid core were identified by cryoEM (Scheres et al., 2023), it is intriguing to investigate if these residues associated with the Tau amyloid core might be a better and more efficient substrate when seeded by Tau amyloid fibrils derived from the corresponding disease compared to the established Tau RD fragments.

2 Aim

Tauopathies are devastating diseases characterised by the assembly of Tau into highly ordered, β-sheet rich fibrils, termed amyloid. Tau pathology spreads in a prion-like manner between cells and connected brain regions. Despite extensive research, the mechanisms of inter- and intracellular prion-like Tau aggregate propagation and transmission remain unresolved. Tauopathies can be distinguished by the isoforms found within the Tau deposits in the brain. Isoforms differ in the number of their N-terminal inserts (1N, 2N) and their repeats, namely three (3R) or four (4R). CryoEM has shown that Tauopathies are associated with different Tau amyloid core folds. Tauopathies show heterogeneous clinical symptoms and pathogenesis, possibly due to the accumulation of Tau aggregates with specific amyloid cores comprising certain polypeptide regions of the Tau 3R and 4R isoforms. However, how the different Tau amyloid folds affect the prion-like spreading of Tau aggregates remains to be elucidated. If Tau aggregation can be inhibited by compounds, this might alleviate neuronal pathology and correlating symptoms, laying the cornerstone for a mechanism-based treatment.

The aims of this project were twofold. First, we used a semi-automated high-throughput screen to identify Tau aggregation inhibitors. A previously established cell line expressing the soluble P301L/V337M mutated Tau 4R repeat domain was used for the high-throughput screen. A library of 144 compounds was screened for Tau inhibitors that reduce the number of cells with aggregates without being toxic to the cells. Second, since cryoEM revealed that Tau can fold into different amyloid conformers associated with distinct Tauopathies, the commonly used Tau RD fragments might not be the most suited for studying intracellular Tau spreading and propagation. Therefore, we established HEK cell lines expressing the protein regions spanning the cryoEM cores of Tau fibrils associated with different Tauopathies. Using the cryoEM Tau core fragments, we hypothesised that they might exhibit the same intramolecular interactions upon aggregation, enforcing a core structure similar to the Tau amyloid core of fibrils derived from patients. In addition, we used full-length and Tau RD fragments to reveal the potential differences between the Tau variants. Using transient and stable expression, we investigated their tendency to aggregate spontaneously. Next, cell lines that stably expressed Tau variants were exposed to Tau fibrils from different sources. In this context, we tested whether Tau variants in the newly generated cell lines could be specifically induced to aggregate by 3R, 4R and 3R/4R Tau amyloid fibrils and if seeding barriers between 3R and 4R isoforms existed. Further, our aim was to use the cell panel and the respective aggregate seeding patterns associated with different patient-derived Tau fibrils to discriminate between 3R, 4R and 3R/4R Tauopathies. In the future, the new cell panel could

be used to identify drugs that inhibit the induction of disease-specific Tau aggregation. Further, it could be used to study the intra- and intercellular mechanisms of Tau propagation and transmission. Findings from our study might help to develop new therapeutic strategies to inhibit or reduce the aggregation of Tau by compounds.

3 Material

3.1 Antibodies

Table 3 Primary antibodies

Primary Antibody	Host	Application	Dilution	Supplier
Actin	Rabbit	WB	1:5.000	Abcam (ab8227)
GFP	Rabbit	WB	1:5.000	Abcam (ab183734)
HT7	Mouse	WB	1:1.000	Thermo Fisher (MN100)
MBD	Rabbit	WB	1:1.000	Abcam (ab308439)
p-Tau (AT8)	Mouse	WB	1:1.000	Thermo Fisher (MN1020)
p-Tau (AT180)	Mouse	WB	1:1.000	Thermo Fisher (MNB1040)
p-Tau (Thr231)	Rabbit	WB	1:1.000	Invitrogen (44-746G)
Tau	Rabbit	WB	1:1.000	Abcam (ab64193)
Tau-5	Mouse	WB	1:1.000	Invitrogen (#AHB0042)

GFP: Green fluorescent protein, MBD: Microtubule binding domain, p: phosphorylated

Table 4 Secondary antibodies

Secondary Antibody	Species	Application	Dilution	Supplier
Mouse IgG, HRP-conjugated	Goat	WB	1:10.000	Dianova
Rabbit IgG, HRP-conjugated	Goat	WB	1:10.000	Dianova
Rat IgG, HRP-conjugated	Goat	WB	1:10.000	Dianova

IgG: Immunoglobulin G, HRP: Horseradish peroxidase, WB: Western blot

3.2 Plasmids

Table 5 Plasmids

Construct	Isoform	aa Sequence	Mutations	Tag	Backbone
Tau 2N4R$^{(0\text{-}441)}$	2N4R	0-441	No	mGFP	pHR-CAG_3C_Twin-Strep
Tau 2N4R$^{LM\ (0\text{-}441)}$	2N4R	0-441	P301L, V337M	mGFP	pHR-CAG_3C_Twin-Strep

Tau 2N4R$^{S\ (0\text{-}441)}$	2N4R	0-441	P301S	mGFP	pHR-CAG_3C_Twin-Strep
Tau 0N3R$^{(0\text{-}352)}$	0N3R	0-352	No	mGFP	pHR-CAG_3C_Twin-Strep
Tau 4R$^{LM\ (243\text{-}375)}$	4R	243-375	P301L, V337M	mGFP	pHR-CAG_3C_Twin-Strep
Tau 4R$^{S\ (246\text{-}378)}$	4R	246-378	No	mGFP	pHR-CAG_3C_Twin-Strep
Tau 3R$^{M\ (244\text{-}400)}$	3R	244-400	V337M	mGFP	pHR-CAG_3C_Twin-Strep
Tau 4R$^{(CBD\ 274\text{-}380)}$	4R	274-380	No	mGFP	pHR-CAG_3C_Twin-Strep
Tau 4R$^{(CTE\ 305\text{-}379)}$	4R	305-379	No	mGFP	pHR-CAG_3C_Twin-Strep
Tau 4R$^{(CTE\ 274\text{-}379)}$	3R	305-379	No	mGFP	pHR-CAG_3C_Twin-Strep
Tau 3R$^{(PiD\ 254\text{-}378)}$	3R	254-378	No	mGFP	pHR-CAG_3C_Twin-Strep

mGFP: monomeric GFP

3.3 Fibrils

Table 6 Recombinant Tau fibrils

Fibril	Supplier
Recombinant Tau 2N4R$^{L\ (0\text{-}441)}$	Professor Markus Zweckstetter
Recombinant 0N3R$^{(0\text{-}352)}$	Professor Markus Zweckstetter

3.4 Cell extract

Table 7 Cell extract

Cell extract	Seed
HEK Tau 2N4R$^{L\ (0\text{-}441),\ agg}$ GFP	Recombinant Tau 2N4R$^{L\ (0\text{-}441)}$ fibrils
HEK Tau 3R$^{(PiD254\text{-}378),\ \textit{agg}}$ GFP	PiD brain homogenate #67
HEK Tau 3R$^{(PiD254\text{-}378),\ \textit{sol}}$ GFP	None

3.5 Patient brain samples and ethics statement

Frozen post-mortem brain tissue samples from neuropathologically confirmed AD, PSP, CBD, PiD and control cases were provided by the Brain Bank associated with the Biobanc-Hospital Clinic-IDIBAPS and the Netherland Brain Bank. In these Brain Banks, material and data are sampled and collected from donors upon written informed consent for brain autopsy and the use of the material and clinical information for research purposes obtained by the probands or their legal representative according to the approval of the responsible ethic committee. The study was conducted following the Declaration of Helsinki, and the protocol was approved by the Ethics Committee of the Medical Faculty of the University of Bonn, Germany (380/17; 236/18).

Table 8 Patient brain samples

No.	Age	Sex	Neuropathological-Diagnosis	Clinical Diagnosis	Braak stage	Brain region
C	70	M	Control	Control	NA	Pons
C2	82	M	AD	Control	IV	Hippocampus
C3	31	M	No histological changes (Control)	Control	NA	Pons
C4	64	M	LBD + possible PART, AD	Control	I-II	Pons
C5	83	F	Definite PART, AD + lacunar infarcts	Control	II	Pons
1	41	F	FTLD, PiD	FTD	NA	Hippocampus
2	74	M	FTLD, PiD	AD	NA	Hippocampus
3	75	F	FTLD, PiD + AD + acute infarcts	AD	III	Hippocampus
4	66	F	FTLD, PiD	AD	NA	Hippocampus
5	69	F	FTRL, PiD + diffuse beta amyloid plaques + acute microinfarct	Early-onset AD	NA	Hippocampus
6	73	M	FTLD, PiD + AD + SVD + lacunar infarcts	AD frontal symptoms	III	Hippocampus
7	70	M	CBD + AD + LBD	Lewy bodies disease	IV	Hippocampus

8	64	M	CBD + diffuse amyloid plaques	FTD - PiD	NA	Hippocampus
9	72	M	CBD + multiple lacumar infarcts + AD	AD	NA	Pons
10	65	F	CBD	FTD/AD	NA	SFG
11	66	F	CBD	FTD with primary progressive aphasia	III	SFG
12	63	F	Tauopathy with neuronal and glial affection + CBD	FTD	NA	Hippocampus
13	83	F	PSP	FTD	IV	SFG
14	80	M	PSP	PD	III	SFG
15	59	M	PSP + AD	PSP	III	Hippocampus
16	77	M	PSP	PSP	NA	Hippocampus
17	64	M	PSP + AD + PD	PSP	I-II	Pons
18	60	F	PSP + AD + SVD	PSP	II	Pons
19	84	F	AD	AD	VI	Hippocampus
20	80	F	AD	AD	VI	Hippocampus
21	86	M	AD	AD	V	Hippocampus
22	81	F	AD + cerebral infarcts	AD	VI	Hippocampus
23	62	M	AD	AD	VI	SFG
24	82	M	AD	AD	VI	SFG
25	64	M	VD	Pre-senile dementia	NA	SFG
26	50	M	VD	Amyloid angiopathy	NA	SFG
27	62	M	VD	AD	NA	SFG

3.6 Buffer and solutions

All buffers and solutions are mentioned in the respective method section.

3.7 Cell lines

Table 9 Cell lines

Cell lines	Isoform	Mutation	References
HEK293T	x	x	ATCC, Manassas, Virginia
HEK Tau$^{(0-441)}$ mGFP	2N4R	x	A. S. Hebestreit, AG Vorberg
HEK Tau$^{LM\ (0-441)}$ mGFP	2N4R	P301L, V337M	A. S. Hebestreit, AG Vorberg
HEK Tau$^{S\ (0-441)}$ mGFP	2N4R	P301S	A. S. Hebestreit, AG Vorberg
HEK Tau 0N3R$^{(0-352)}$ mGFP	0N3R	x	A. S. Hebestreit, AG Vorberg
HEK Tau 4R$^{LM\ (243-375)}$ mGFP	4R	P301L, V337M	A. S. Hebestreit, AG Vorberg
HEK Tau 4R$^{S\ (246-378)}$ mGFP	4R	P301S	A. S. Hebestreit, AG Vorberg
HEK Tau 3R$^{M\ (244-400)}$ mGFP	3R	V337M	A. S. Hebestreit, AG Vorberg
HEK Tau 4R$^{(CBD\ 274-380)}$ mGFP	4R	x	A. S. Hebestreit, AG Vorberg
HEK Tau 3R$^{(CTE\ 274-379)}$ mGFP	4R	x	A. S. Hebestreit, AG Vorberg
HEK Tau 4R$^{(CTE\ 305-379)}$ mGFP	3R	x	A. S. Hebestreit, AG Vorberg
HEK Tau 3R$^{(PiD\ 254-378)}$ mGFP	3R	x	A. S. Hebestreit, AG Vorberg
HEK Tau 4R$^{(AD\ 304-380)}$ mGFP	4R	x	A. S. Hebestreit, AG Vorberg
HEK Tau$^{(AD\ 306-378)}$ GFP	x	x	A. S. Hebestreit, AG Vorberg
HEK NM GFP	x	x	S. Liu et al., 2017

3.8 Chemicals, reagents, enzymes

Table 10 Chemicals, reagents, enzymes

Item	Company
Acrylamid 30 % (Protogel)	Bio-Rad
Agarose	Biozym
Ampicillin	Life Technologies
Amylo Glo	Biosensis
Aqua Poly Mount Solution	Polysciences
Bradford Dye Reagent	Bio-Rad
Benzonase	Merck
Bromphenol blue	Merck
ChemiBLOCKER™	Merck
Complete ULTRA Tablets, EDTA free	Roche
Dextran blue 2000	Sigma-Aldrich
ddH_2O	Merck

Dimethyl Sulfoxide (DMSO)	Honeywell
DMEM® I (1X) + GlutaMAX™ -I	Life Technologies
DRAQ5™ Fluorescent Probe Solution	Thermo Fisher Scientific
100 bp DNA Ladder	New England Biolabs
100 mM dNTP Mix	Agilent
Dulbecco's Phosphate Buffered Saline (PBS)	Life Technologies
Ethanol	Roth
Ethylenediaminetetraacetate acid (EDTA)	Roth
Fetal Bovine Serum (FBS)	Pan Biotech GmbH
Formaldehyde solution	Sigma Aldrich
Gel Loading Dye 6x	New England Biolabs
GelRed Nucleic Acid Stain 10.000X in water (0.5 ml)	VWR
Glycerin	Sigma-Aldrich
Glycin	Roth,
Hoechst 33342 solution	Thermo Fisher Scientific
Isopropanol	Roth
Lipofectamine 2000	Thermo Fisher Scientific
Lysogenic broth (LB) medium	Roth
2-Mercaptoethanol	Sigma-Aldrich
MG132	Cell Signaling Technology
Methanol	Roth
Nonident® P-40 (NP-40)	Thermo Fisher Scientific
Opti-MEM® I (1 x) + GlutaMAX™	Life Technologies
Page Ruler Pre-Stained Protein Ladder	Thermo Fisher Scientific
Paraformaldehyde 16 % (w/v)	Thermo Fisher Scientific
Penicillin-Streptomycin (PS)	Thermo Fisher Scientific
Pfu DNA Polymerase	Promega
Phosphate buffered saline (PBS)	Life Technologies
Poly-L-Lysine	Sigma-Aldrich
Proteinase K	Roche
Re-Bot Plus Strong Solution	Merck
Roti®-Stock 20 % (w/v) Sodium dodecyl sulfate (SDS)	Roth
Skim milk powder	Roth
Sodium Chloride (NaCl)	Roth
SuperHotTaq DNA Polymerase	Geyer

SuperSignal West Femto	Thermo Fisher Scientific
SuperSignal West Pico	Thermo Fisher Scientific
T4 DNA Ligase	NEB
Trans-IT	Mirius
Tris	Roth
Triton-X-100	Roth
Trypan Blue Stain (0.4 %)	Life Technologies
Top10 Competent cells	Thermo Fisher Scientific
0.25 % Trypsin-EDTA	Life Technologies
Tween 20	Roth

3.9 Consumables

Table 11 Consumables

Consumables	Company
Bacteria Culture Tubes	Roth
BRAND 96-well plates	Brand
Cell counting slides	Bio-Rad
Cell culture dishes	Corning
Cell culture flasks	Neolab
Cell culture multiwells	Thermofisher Scientific
Coverslips	Paul Marienfeld
Cryotubes	Corning
Eppendorf tubes	Eppendorf
Falcon tubes	BD Biosciences
Filter tips	Biozym
Glasware	Schott
Microplates 96-well	Geyer
Microplates 384-well	Geyer
Microscope slides, SuperFrost Plus	Thermo Scientific
NuPAGE™ 4-12 % Bis Tris Protein Gels	Life Technologies
Parafilm	VWR
Pipettes	Eppendorf
Precellys Ceramic kit	VWR
Protein Low-Bind Tubes	Eppendorf

PVDF Membrane	Geyer
Reagent Reservoir	Thermo Fisher
Stripettes	Comin International
SuperFrost® Plus Slides	Thermo Fisher Scientific
UZ Tube Polypropylene	Beckman Coulter
Whatman paper	Roth

3.10 Instruments

Table 12 Instruments

Instrument	Company
Agarose Gel system	VWR
Automated cell counter TC20	Bio-Rad
Cell Voyager 6000/8000	Yokogawa Inc.
CO_2 Incubator HERAcell 240i	Heraeus
Criterion™ Blotter	Bio-Rad
Echo 650 Series	Beckman Coulter
Eppendorf Centrifuge 5417R	Eppendorf
Fluostar OMEGA BMG	BMG Labtech
Fusion FX Imaging System	Vilber Lourmat
Laser scanning microscope (LSM) 900	Carl Zeiss
Leica DM IL LED microscope	Leica Microsystems
Magnetic stirrer RCT Bacic	IKA Labortechnik
Maxisafe 2020 Class II Biological Safety Cabinet	Thermo Fisher Scientific
Mini Fold-1 Dot-Blot System	Whatman
Mini-PROTEAN Gel System	Bio-Rad
Minisee Sawrocker SSM4	Stuart
Minitron Shaker	Infors HT
Mr. Frosty Freezing container	Thermo Fisher Scientific
Multifuge X3R Hereus	Thermo Fisher Scientific
NanoDrop™ 2000	Thermo Fischer Scientific
pH-Meter Seven Easy	Mettler-Toledo
Pipette controller	BrandTech Scientific
PowerPac™	Bio-Rad

Scale ABT320-4M analytical balance	Kern & Sohn
Scale EMS balance	Kern & Sohn
Sonopuls HD 2070 Sonicaor	Bandelin
Sonopuls HD 3200 Sonicator	Bandelin
StepOnePlus Real-Time PCR System	Thermo Fisher Scientific
T100 Thermocycler	Bio-Rad
Thermomixer compact	Eppendorf
Ultra-Low – 80 °C freezer	Panasonic Healthcare
Vacuum Pump	KNF Beuberger
Vortex Genie 2	Scientific Industries
Water bath	G.F.L.
XCell4 SureLock™ Midi-Cell Electrophoresis System	Thermo Fisher Scientific

3.11 Kits

Table 13 Kits

Product	Company
Plasmid Maxi Kit	Qiagen
Q5® Site-Directed Mutagenesis Kit	NEB
QIAprep Spin Miniprep Kit	Qiagen
QIAquick Gel Extraction Kit	Qiagen
Quick Start Bovine γ-Globulin Standard Set	Bio-Rad

3.12 Software

Table 14 Software

Software	Company
Adobe Illustrator 2022	Adobe
Adobe Photoshop 2022	Adobe
CV7000 Analysis Software	Yokogawa Inc.
Fiji (ImageJ)	http://rsbweb.nih.gov/ij/
Fluostar Software	BMG Labtech
Fusion FX	Vilber Lourmat

Graph Pad Prism 9	Graph Pad Software
Lalign	https://embnet.vital-it.ch/software/LALIGN_form.html
MARS Data Analysis Software	BMG Labtech
NEBase Changer™	NEB
Snapgene	https://www.snapgene.com/
ZenBlue	Carl Zeiss
DeepL write	https://www.deepl.com/write/write-mobile

4 Methods

4.1 Molecular Biochemical Methods

4.1.1 Biological safety

All work with genetically modified organisms was conducted under biosafety containment level 1 or 2 according to the current guidelines of the German Act on Genetic Engineering (*Gentechnikgesetz*). All materials, solutions, and biologically contaminated material were collected, inactivated, and disposed of according to the official rules. Genetic engineering was approved by genetic engineering authorities.

4.1.2 Gene synthesis

All Tau constructs were designed based on the numbering of full-length Tau 2N4R$^{(0\text{-}441)}$ (Uniprot ID: P10636-8). Gene synthesis was done by Biocat. Codon usage optimisation was performed for Homo sapiens.

4.1.3 Transformation

To amplify the desired plasmid DNA, Top10 competent cells were thawed on ice. 10-50 ng plasmid DNA or 5 µl of the ligation mixture was incubated with the bacteria on ice for 30 minutes. This was followed by a heat shock at 42 °C for 55 seconds. Transformed bacteria were incubated on ice for 5 minutes. 500 µl of super optimal broth with catabolic repressor (SOC) medium was added, and samples were incubated at 300 rpm (Thermomixer F1.5, Eppendorf) for 30 minutes at 37 °C. 100 µl of the bacterial solution was plated onto Luria broth (LB) agar plates supplemented with 100 µg/ml ampicillin. LB plates were incubated overnight at 37 °C and stored at 4 °C for further experiments.

4.1.4 Cultivation of bacteria and DNA preparation

To culture bacteria containing the desired plasmid after transformation, a single colony was picked and inoculated for a Miniprep in 5 ml LB medium (20 g/l) and a Maxiprep in 200 ml LB medium, supplemented with 100 µg/ml Ampicillin. The bacteria culture was grown overnight at 180 rpm (Minitron, Infors HT) for 12-18 hours at 37 °C. The isolation of plasmids was performed with a QIAprep Spin Miniprep Kit (3.11), and isolated plasmids were sent to Eurofins for sequencing (4.1.6). Subsequently, a QIAgen Maxi Kit was used to isolate the desired plasmid according to the manufacturer's instructions. The isolated plasmid was resuspended for a Miniprep in 50 µl and for a Maxiprep in 100-200 µl of the supplied buffer,

depending on the size of the pellet. The concentration was measured, DNA quality was confirmed using the Nanodrop, and plasmid DNA was stored at -20 °C.

4.1.5 Enzymatic digestion and ligation of plasmid DNA

Enzymatic digestion of plasmid DNA was performed using restriction enzymes and buffers from New England Biolabs (NEB). Approximately 0.5-1 µg of DNA was digested for each reaction. Buffers and enzymes were selected according to the manufacturer's instructions. Enzymatic digestion was performed for 2 hours at 37 °C. Enzymatic DNA ligation was performed by mixing plasmid DNA and insert DNA at a 1:3 molar ratio. DNA, ligase, and buffer were mixed according to the manufacturer's instructions (NEB) and incubated for 1 hour at room temperature (RT) or overnight at 16 °C.

4.1.6 DNA sequence analysis

GATC Eurofins sequencing service performed DNA sequencing to validate the correct sequence of the DNA construct of interest. Snapgene Viewer and Lalign (3.12) were used to analyse sequence information.

4.2 Cell Biological Methods

4.2.1 Cell culture

All cell culture work was performed under sterile conditions. Cells (3.7) were grown on 10 cm plates at 37 °C and 5 % CO_2 in DMEM + GlutaMax medium supplemented with 10 % fetal calf serum (FCS) and 5 % Penicillin-Streptomycin (PS) (referred to as DMEM culture medium). During the cell culture routine, the medium was removed, and cells were washed with 5 ml PBS. Cells were detached from the flask with 0.5 ml of 0.05 % trypsin-EDTA solution for 3-5 minutes at RT. Proteolysis was stopped by adding 6 ml of pre-warmed complete medium, and cells were counted using an automated cell counter (Bio-Rad). The appropriate number of cells was seeded on a fresh 10 cm plate, flask or multi-well for 3 to 4 days. Cells were cultured at 37 °C in 5 % CO_2 for further experiments.

4.2.2 Thawing and freezing of cells

Cells were removed from the liquid nitrogen tank and thawed in a water bath at 37 °C for approximately 1-2 minutes. Cells were transferred to 10 ml culture medium and centrifuged at 300 x g for 5 minutes to remove DMSO. After centrifugation, the cells were resuspended in 10 ml culture medium and grown on a 10 cm plate as described in 4.2.1. For cryopreservation, the cells were washed with 5 ml PBS and detached as described above (4.2.1). The cell

suspension was centrifuged at 300 x g for 5 minutes, and the cell pellet was resuspended in FCS containing 10 % DMSO as a cryoprotectant. Cells were aliquoted into cryogenic vials and frozen at a controlled cooling rate of -1 °C/minute in freezing containers and short-term stored at -80 °C. For long-term storage, cells were transferred to liquid nitrogen.

4.2.3 Transient transfection

To validate the expression of the desired protein, 1 x 10^6 cells per construct were plated on a 6-well plate in 2 ml culture medium. Cells were cultured at 37 °C and 5 % CO_2 for 18-24 hours. The next day, the transfection mixture containing OptiMEM medium, Trans-IT and the desired DNA (3.2) was prepared and incubated at RT for 30 minutes.

Transient transfection medium	4.0 µg DNA
	7.5 µl Trans-IT
	in 250 µl OptiMEM

The transfection mixture was added dropwise to the cells. The cells were incubated with the transfection medium for 18-24 hours at 37 °C and 5 % CO_2. Cells were further used for immunofluorescence and quantification (4.2.5, 4.3.7).

4.2.4 Proteasomal inhibition

The clearance of Tau variants was investigated by inhibiting the proteasome with 1.5 µM MG132. The culture medium was removed, and the cells were treated with culture medium mixed with MG132. Cells were either fixed for microscopic analysis (4.2.5) or pelleted for sedimentation assay (4.3.5) after 4, 8 and 24 hours.

4.2.5 Immunofluorescence

For immunofluorescence, 5 x 10^4 cells were incubated overnight in 500 µl culture medium on poly-L-lysine-coated coverslips in a 24-well plate. Coverslips were coated with poly-L-lysine (250 µg/ml) in sterile ultrapure water for 2 hours at 37 °C, followed by two washes with Milli-Q water. Cells were treated according to the individual experiment and fixed with 4 % paraformaldehyde (PFA) (2 % final concentration) and DRAQ-5 (1:3.500) or Hoechst (1:4.000) for 20 minutes at RT, followed by two washes for 1 minute with PBS. For Amylo Glo staining, cells were permeabilised with 0.5 % Triton in PBS for 10 minutes at RT and washed twice with PBS. Cells were incubated with Amylo Glo in PBS (1:200) for 10 minutes at RT on a shaker and washed twice with PBS. Coverslips were mounted onto microscope slides using

Aqua Polymount and dried at RT overnight. Slides were stored at 4 °C and then imaged with the confocal microscope LSM900.

Blocking buffer Amylo Glo staining	0.5 % Triton in PBS

For HA Alexa 647 staining, cells were plated on 384-well plates and treated according to the individual experiment. Cells were permeabilised and blocked with 0.5 % Triton in PBS plus 5 % Chemiblock solution in PBS for 30 minutes at RT. HA staining was performed with the appropriate HA 647 coupled antibody (3.1) diluted in blocking solution for 1 hour at RT. The cells were washed twice with PBS and scanned with the CV600 or CV8000.

Blocking buffer HA 647 staining	5.0 % Chemiblock solution 0.5 % Triton in PBS

4.2.6 Lentivirus production

Lentiviral transfer vectors were used to produce lentiviral particles (3.2). The third-generation system was employed to prevent replication-competent viruses. In this system, the HIV-1 genome is modified and split into four different plasmids, which allows for the incorporation of the provirus into the host cell genome.

DNA [µg]	Plasmid	Function
2.03	pMDl.g/pRRE	Packaging plasmid
1.02	pRSV-Rev	Rev encoding plasmid
1.36	pMD2.VSVG	Envelop plasmid
6.78	pHR-CAG_3C_Twin-Strep containing the desired construct	Transfer vector

HEK293T cells were used as packaging cell line to transfect lentiviral plasmids. 8.3 x 10^5 cells per construct were plated in 2 ml complete medium on a 6-well plate and incubated at 37 °C and 5 % CO_2 overnight. The lentiviral plasmids, including the transfer vector, were mixed with 14 µl Lipofectamine in 1 ml OptiMEM and incubated for 20 minutes at RT in a 1.5 ml tube. To perform the transfection, 1 ml of medium was removed from the 6-well plate, and the transfection mixture was added dropwise. After 5 hours, the medium was removed, and 2 ml of fresh culture medium was added to the cells. The virus particle-containing medium was

harvested 24 and 48 hours after transfection and was collected in 50 ml tubes. To eliminate any remaining cells, the virus particle suspension was centrifuged at 2.000 x g for 5 minutes. The resulting supernatant was mixed with 5x PEG (resulting in a final concentration of 1x PEG) and incubated overnight at 4 °C.

5x Polyethylene glycol	25 mM Polyethylene glycol
	0.2 M NaCl
	2 mM Tris/HCL, pH 7.5
	in H_2O bidest.

Following the second harvest, HEK293T cells were discarded. The virus particles were precipitated by centrifugation at 1.500 x g for 30 minutes at 4 °C, followed by an additional 15 minutes of centrifugation at 4 °C to remove the supernatant. The lentiviral particles were resuspended in 100-200 µl of culture medium, depending on the pellet size, and stored at -80 °C.

4.2.7 Lentiviral transduction of HEK293T Cells

For stable expression of the desired transgene, 5 x 10^4 cells were plated on a 24-well plate and cultured for 16-24 hours. For transduction, the culture medium was replaced with a culture medium containing Polybrene (1:1.250), and 50-100 µl of virus was added to each well. 24-72 hours later, aliquots of the stable bulk cell populations were frozen in liquid nitrogen, as previously described (4.2.2), or used directly for further experiments.

Transduction	5 % FCS
	8 µg/ml Polybrene
	in DMEM culture medium

4.2.8 Single-cell cloning

To generate single-cell clones that homogeneously express the desired protein, the bulk population was diluted to a final concentration of 10 cells/ml in culture medium. Next, 100 µl per well was plated onto a 96-well plate. Cells were grown for 7-14 days, depending on the growth rate of the clones. The clones were then cultured from 96- to 24- and 6-well plates, as described before (4.2.1). The clones were frozen in liquid nitrogen, as described in 4.2.2, or directly used for further experiments.

4.2.9 Cell extract

Cell extracts were generated to seed Tau variants by plating HEK cells that stably propagate the aggregated Tau protein of interest on a 5-layer flask in 100 ml culture medium (3.4). After 4 days, the cells were washed with 80-100 ml of PBS. Subsequently, the cells were detached by adding 8 ml of 0.25 % Trypsin for 5 minutes at 37 °C. To remove the cells from the flask, 90 ml of culture medium was added, and the resulting cell suspension was transferred to two 50 ml falcon tubes. 10-20 ml of cell suspension was used to continue culturing cells in a 5-layer flask. The cell suspension was centrifuged at 300 x g for 5 minutes at 4 °C. Pellets were either used directly or stored at -20 °C. 1.25 ml ice-cold OptiMEM + 1x protease inhibitor (PI) was used to resuspend the cell pellet for homogenisation. When the cell suspension was split into two 50 ml tubes, the cell pellets were combined in the 1.25 ml ice-cold OptiMEM + 1x PI. 500 µl of cell suspension was added per Precellys tube, and samples were homogenised by Precellys (Precellys® 24, VWR) at 5500 rpm, 30 seconds on, 5 seconds off, for 2 minutes at 4 °C. The Precellys tubes were centrifuged at 842 x g for 10 seconds at 4 °C to reduce foam. The cell suspension was transferred and combined in new 1.5 ml Eppendorf tubes. The tubes were sonicated in a water bath at 50 % amplitude for 6 minutes constantly. Next, all 1.5 ml Eppendorf tubes were combined in a 5 ml Eppendorf tube and centrifuged at 842 x g for 5 minutes at 4 °C to remove cell debris. The supernatant was transferred to fresh 1.5 ml Eppendorf tubes and stored at -20 °C. The amount of cell extract with the highest seeding efficiency was determined by titrating for aggregate induction.

4.2.10 Patient and mouse brain homogenates

The number of the patient brain samples and ethics statement can be found in section 26. PS19 mice expressing P301S mutated 1N4R$^{(0\text{-}412)}$ human Tau (Tau 1N4R$^{S\ (0\text{-}412)}$) under the murine prion protein promoter were used (Yoshiyama et. al., 2007). PS19 mice were purchased from the Jackson Laboratory. Mice were housed in individually ventilated cages with 12 hour light/dark cycle at 22 °C and 60 % humidity. Animals had free access to autoclaved food and water. All animal experiments performed in this study were approved by the animal protection committee of the North Rhine-Westphalia State Environment Agency (LANUV), animal protocol 81-02.04.2021.A037. Non-transgenic WT C57Bl/6NCrl control animals were purchased from Charles River Laboratories and were continuously bred in the animal facility of the DZNE.

The patient's brain samples were divided into 200-400 mg pieces and transferred to Precellys tubes. 500 µl of ice-cold OptiMEM, freshly supplemented with 1x PI, was added. The samples were homogenised with the Precellys at 5500 pm for 2 minutes at 4 °C, with 30 seconds on and 5 seconds off intervals. The tubes were centrifuged at 842 x g for 10 seconds at 4 °C to

reduce foam. Brain homogenates were transferred to fresh tubes and sonicated in a water bath for 6 minutes at 50 % amplitude. Tubes containing the same patient's brain were combined and topped up to 10 % brain homogenate with OptiMEM plus 1x PI. The tubes were centrifuged at 842 x g for 5 minutes at 4 °C to remove cell debris. The supernatant was transferred to fresh 1.5 ml Eppendorf tubes and stored at -80 °C. The amount of brain homogenate with the highest seeding efficiency was determined by titrating for best aggregate induction.

4.2.11 Seeding of Tau variants

Tau aggregates were induced using recombinant Tau fibrils (3.3), cell extract (4.2.9), and PS19 Tau 1N4R$^{S\ (0\text{-}412)}$ mouse (2.2.10) or human brain homogenate from PiD, CBD, PSP and AD patients (3.5). Two different recombinant Tau fibrils, Tau 2N4R$^{L\ (0\text{-}441)}$ and 0N3R$^{(0\text{-}352)}$, were kindly provided by Prof. Dr. Markus Zweckstetter. Recombinant Tau fibrils were stored at RT and were sonicated once using 30 % amplitude for 2 minutes with a pulse on for 10 seconds and a pulse off for 20 seconds. Cell extract and brain homogenate were centrifuged at 5.200 x g for 5 minutes to remove any cell debris or tissue before use. The optimal seeding efficiency was determined by titration. For aggregate induction, 3 x 10^3 cells per well were plated on a 384-well plate and were cultured for 1 hour. Then, cells were treated with 0.8-1.5 µM recombinant Tau fibrils, 0.5-1.5 µl cell extract, or 1.5-3.0 µl patient brain homogenate diluted in 10 µl OptiMEM plus 0.07 µl Lipofectamine. For 24-well plates, 5 x 10^4 cells were plated, and aggregation was initiated with 0.8-1.5 µM recombinant Tau fibrils, 6-10 µl cell extract or 10 µl patient brain homogenate in 100 µl OptiMEM. After 24-96 hours, depending on the experiment, the cells were fixed with a final concentration of 2 % PFA for 20 minutes at 37 °C. Fixed cells were stored at RT if imaged with the Cell Voyager (CV) the following day or at 4 °C if imaged later.

4.2.12 Semi-automated high-throughput screen

Compounds of varying concentrations (0.025-40 µM) were spotted by the Echo 650 (3.10) to create a dose-response curve and were stored at -20 °C. To identify compounds that affect Tau aggregation, 3 x 10^3 cells were seeded onto a 384-well plate and incubated overnight at 37 °C and 5 % CO_2. Compounds were diluted in 25 µl culture medium, and 10 µl of each concentration was added to the respective well. After 1 hour, 0.5-1.5 µl of cell extract was diluted in 10 µl of OptiMEM plus 0.07 µl of Lipofectamine. To induce aggregation, 10 µl of cell extract mix was added per well. The plate was centrifuged at 300 x g for 10 seconds at RT. After 24 hours at 37 °C and 5 % CO_2, the cells were fixed and imaged using the CV.

4.2.13 Compound kinetics

To assess whether compounds could inhibit Tau aggregation when seeds were first added to cells, 3 x 10^3 cells were seeded onto a 384-well plate and incubated ON at 37 °C and 5 % CO_2. Cell extract (0.1-1.5 µl) diluted in 10 µl of OptiMEM plus 0.07 µl of Lipofectamine was added for 1 hour. Compounds (0.025-40 µM) diluted in culture medium were added, with seeds at the same time (0 hours) and 1-22 hours after seed addition. Cells pre-incubated (-1 hour) with the compound and then treated with seeds, as described for the high content screen, served as a positive control. Cells were fixed 24 hours after seed addition and imaged using the CV.

4.3 Biochemical Methods

4.3.1 Cell lysis

NP-40 lysis buffer	10 mM Tris/HCL, pH 7.5
	100 mM NaCl
	10 mM EDTA
	0.5 % NP-40
	1x Protease inhibitor (complete, EDTA free)
	in ddH_2O

For cell lysis, cells were detached using 0.05 % Trypsin (4.2.1). The cells were resuspended 1 ml of PBS and pelleted by centrifugation at 300 x g for 10 minutes at 4 °C. The washing step was repeated twice with PBS, followed by resuspending the pellet in an appropriate amount of lysis buffer containing freshly supplemented 1x PI (24-well: 500 µl, 6-well: 1 ml). Cell lysis was carried out for 30 minutes on ice. To remove cell debris, the samples were centrifuged at 2.300 x g for 3 minutes at 4 °C. The supernatant was transferred to a fresh 1.5 ml Eppendorf tube. The cell lysates were either used immediately or stored at -20 °C.

4.3.2 Bradford

Protein concentration was determined using the Bradford protein assay. Lysates were diluted 1:20 in nuclease-free water, and 5 µl of the diluent was added in duplicates to a 96-well plate. A BSA standard dilution series ranging from 62.5-2.000 µg/ml and three H_2O blank controls were also added. After 5 minutes, the absorbance was measured at 595 nm using an Omega plate reader (3.10). The protein concentration was calculated by generating a standard curve from the measured absorbance of the standard concentration using the MARS data analysis software.

4.3.3 Sodium dodecyl sulfate-polyacrylamide gel electrophoresis

3x Sample buffer	90 mM Tris/HCL, pH 6.8
	7 % SDS
	30 % Glycerol
	20 % β-mercaptoethanol
	0.003 % Bromphenol blue
	in ddH_2O
20x NuPAGE MOPS SDS Running buffer	50 mM MOPS
	50 mM Tris/HCL pH 7.7
	0.1 % SDS
	1 mM EDTA
	in ddH_2O

Discontinuous sodium dodecyl sulfate-polyacrylamide gel electrophoresis (SDS-PAGE) was performed to separate proteins by size. 30-100 µg total protein of each sample with 3x sample buffer was mixed and heated for 10 minutes at 95 °C. All of the samples and 8 µl page ruler protein ladder were loaded onto 4-12% Bis-Tris gels and ran at 100-150 V for 60-90 minutes. Proteins were transferred to PVDF membranes via Western blot (WB) (4.3.4).

4.3.4 Western Blot

1x Blotting buffer	20 % Methanol
	250 mM Tris
	1.92 M Glycine
	0.1 % SDS
	in dd H_2O
10x TBS-T	100 mM Tris/HCL, pH 7.6
	1.5 M NaCl
	0.5 % Tween-20
	in dd H_2O

Blocking buffer	5 % Milk powder in TBS-T

Immunochemical detection was carried out using WB analysis. PVDF membranes were activated in methanol for 10-20 seconds and equilibrated in blotting buffer for 20 seconds. The blotting sandwich was placed in a wet blot chamber filled with blotting buffer. The protein transfer from the gel onto the membrane was run at 100 V for 45 minutes. Subsequently, the membrane was blocked with milk for 60 minutes. Incubation was performed either overnight at 4 °C or for 2 hours at RT at 20 oscillations per minute. The primary antibody (3.1) was diluted (1:1.000) in blocking buffer and added to the membrane. The membrane was washed thrice for 5 minutes in TBS-T, and the secondary antibody was diluted (1:10.000) in blocking buffer. This was followed by three washing steps for 10 minutes with TBS-T. Subsequently, the membrane was incubated in ECL solution according to the manufacturer's instructions. The light reaction was detected using Fusion FX (3.10). To detect an additional protein, the membrane was stripped using 1x ReBlot Plus Strong Antibody Stripping Solution (1:10 in ddH_2O) for 20 minutes. After removing the stripping solution, the membrane was washed with ddH_2O and blocked again for 30 minutes, followed by the previously described steps.

4.3.5 Sedimentation assay

To confirm protein aggregation, 1x10^6 cells were plated on a 6-well plate. The cells were detached and lysed in NP-40 lysis buffer, as described in section 4.3.1. Next, 100 µg of total protein was diluted in 200 µl NP-40 lysis buffer, plus 10 µl blue dextran in ddH_2O was centrifuged at 100.000 x g for 1:05 hour at 4 °C. The supernatant was transferred to a fresh tube. To precipitate soluble protein, 800 µl of methanol was added, and the sample was stored at -20°C overnight. The pellet was washed with 500 µl of PBS and centrifuged 100.000 x g for 35 minutes at 4 °C. The pellet was stored at -20 °C overnight.

NP-40 lysis buffer + SDS	10 mM Tris/HCL, pH 7.5
	100 mM NaCl
	10 mM EDTA
	0.5 % Triton X-100
	0.5 % Protease inhibitor (complete, EDTA-free)
	4 % SDS

The next day, the supernatant was centrifuged at 2.300 x g for 25 minutes at 4 °C. The methanol was removed, and the precipitated proteins were air-dried for 10 minutes. The

pellets and the precipitated soluble proteins were dissolved in NP-40 lysis buffer containing 4 % SDS and 3x SEB buffer. The samples were heated for 10 minutes at 95 °C and stored at -20 °C for WB (4.3.3, 4.3.4).

4.3.6 Filter trap assay

To detect Tau aggregates, a filter trap assay (FTA) was performed. The filter trap module was set up following the manufacturer's instructions. A single Whatman paper, followed by a nitrocellulose membrane, was placed between the vacuum manifold and the sealing gasket. The sample plate was screwed in place, and the vacuum pump connected.

NP-40 lysis buffer + SDS	10 mM Tris/HCL, pH 7.5
	150 mM NaCl
	10 mM EDTA
	0.5 % Triton X-100
	0.5 % Protease inhibitor (complete, EDTA-free)
	4 % SDS

200 µl SDS-washing buffer was added to wells. To prevent bubbles, SDS-washing buffer was added to all wells, including those not used for samples. Vacuum was applied until all SDS-washing buffer was removed from the wells. This step was repeated twice. Cell lysates and patient brain homogenates were diluted to 20-25 µg total protein and adjusted to 200 µl with NP40-lysis buffer supplemented with 4 % SDS.

SDS-washing buffer	10 mM Tris/HCL, pH 8.0
	150 mM NaCl
	0.1 % SDS
	in ddH_2O

Samples were loaded and incubated at RT for 10 minutes. Vacuum was applied, and SDS-washing buffer was added to all wells twice. The membrane was removed and washed once more in SDS-washing buffer for 5 minutes. The membrane was blocked in 5 % milk in TBS-T for 30 minutes at RT. Corresponding primary antibodies were diluted in blocking buffer (5 % milk in TBS-T) and either incubated for 2 hours at RT or overnight at 4 °C. The membrane was washed twice with TBS-T for 5 minutes to remove primary antibodies. The membrane was incubated with secondary antibodies in blocking buffer for 45 minutes at RT. Subsequently, it was developed using the ECL solution following the manufacturer's instructions.

4.3.7 Aggregate quantification with automated image analysis software

The automated confocal microscopes CV6000 or CV8000 of the laboratory automation technologies (LAT) were used to image fixed and stained cells with a 20x water immersion objective scanning 9-36 positions within one well. CV7000 analysis, an automated imaging analysis software, was used. To quantify cells with aggregates, an image segmentation pipeline based on signal intensities of nuclei stained with DRAQ-5 (excitation 647 nm) or Hoechst (excitation 350 nm) and soluble and aggregated Tau protein tagged to GFP (excitation 488), FR (excitation 576), and HA (excitation 647) was applied. The percentage of cells with aggregates was calculated as a ratio to the total number of cells.

4.3.8 Analysis and statistics

Confocal images acquired with the LSM 900 were processed using ZEN 2010 image sets (light microscope facility (LMF)). For statistical analysis, images were acquired using the Cell Voyager 6000 and 8000 automated confocal microscopes (Yokogawa Inc.) with a 20x water objective. Maximum intensity projections were generated from Z-stacks, and 9-36 fields per well were imaged. Image analysis was performed using the Cell Voyager Analysis support software (CV7000 analysis). An image analysis routine was developed for single-cell segmentation and identification of aggregates (Liu et al., 2020). Total cell numbers were determined by Hoechst or DRAQ-5 signals, and recipient cells were identified by their GFP signal. Green aggregates were identified by fluorescence intensities. The percentage of cells with aggregates (strong GFP signal) was calculated as the number of aggregate-positive cells per total cells, set to 100 %. Adjustment for false positive recipient cells due to heterogeneity in GFP expression was made by subtracting the mean percentage of false positives in control recipient cells from all samples. Therefore, negative values were occasionally observed when no induction was detected. Graphical data are presented as mean values ±SD. Three to four biological replicates were used for statistical analysis. A minimum of 9 fields per well were imaged. One-way ANOVA and Two-way ANOVA with Bonferroni's multiple comparison or t-test were used for statistical analysis (Graph Pad Prism 9 software). The significance level was set at $p \leq 0.05$. Dose-response graphs were generated by interpolating a 4PL sigmoidal standard curve, where x represents concentration, using Graph Pad Prism 9 software.

5 Results

5.1 High-throughput screen identified Tau 4R$^{LM\ (243-375)}$ aggregation inhibitors

Tau aggregation inhibitors are a promising therapeutic strategy to treat Tauopathies. Our group has previously developed a semi-automated cell-based assay to identify Tau aggregation inhibitors in high-content screens (Hebestreit, 2020). This assay is based on HEK cells expressing the soluble repeat domain with mutations P301L (L)/V337M (M) (Tau 4R$^{LM\ (243-375)}$) tagged to GFP. Tau 4R$^{LM\ (243-375)}$ GFP aggregation can be initiated with recombinant full-length Tau fibrils. Here, we used Tau fibrils composed of recombinant full-

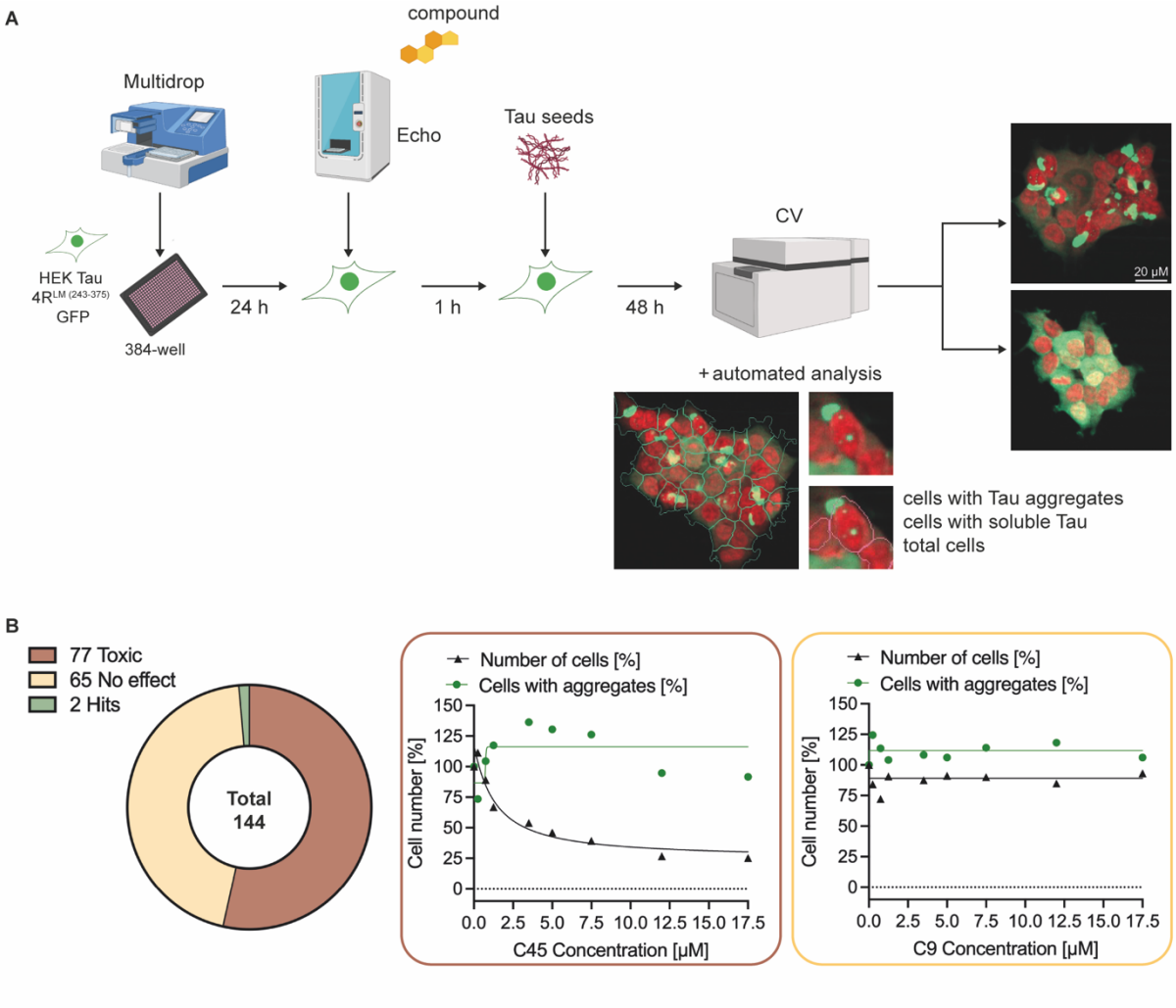

Figure 5 Semi-automated high-throughput screen workflow. (A) HEK Tau 4R$^{LM\ (243-375)}$ GFP cells were plated on a 384-well and incubated for 24 h. Compounds were spotted in a dose-response curve and were added to the cells. Tau seeds were added 1 hour later. Cells were fixed after 48 hours, and images were captured with the Cell Voyager (CV). Automated image analysis determined the number of cells with soluble or aggregated Tau and the total number of cells. Scale bar: 20 µM. **(B)** Summary of tested compounds. Two hits were identified and were used for further experiments. Examples of toxic compounds (brown) and compounds with no effect (yellow). The cartoon was created with BioRender.com.

length wildtype Tau with the mutation P301L (Tau 2N4R$^{L\ (0\text{-}441)}$), kindly provided by Prof. Dr. Zweckstetter. The fibril was assembled co-factor-free, as these Tau fibrils have been shown to have a rigid core similar to fibrils isolated from CBD patients (Chakraborty et al., 2021). To identify compounds that inhibit Tau aggregation, HEK Tau 4R$^{LM\ (243\text{-}375)}$ GFP cells were plated on a 384-well plate (Figure 5 A). Compounds (0-40 µM) were added to the cells, and after 1 hour, recombinant Tau 2N4R$^{L\ (0\text{-}441)}$ fibrils were used to initiate Tau aggregation. Lipofectamine was used to enhance the uptake of the fibrils into the cells. A total of 144 compounds were screened (Figure 5 B). Prof. The Zweckstetter lab provided the compounds blindly. Of 144 compounds, 77 had a toxic effect on the cells, like C45, while 65 compounds did not affect Tau aggregation, such as C9. Ultimately, two hits were identified: compound 22 and 57 (C22, C57). One of the hits, C22, was already identified by our group in collaboration with the Zweckstetter lab in 2020 (Hebestreit, 2020). In previous experiments, C22 (IC_{50}: 0.15-1.5 µM) efficiently reduced the number of cells with Tau 4R$^{LM\ (243\text{-}375)}$ aggregates from 100 % to ~ 2 % when seeded with Tau 2N4R$^{L\ (0\text{-}441)}$ fibrils without causing cell toxicity. The IC_{50} is the half-maximal inhibitory concentration of the compound at which 50 % fewer cells with aggregates are detected. In this project, the effects of C22 on Tau aggregation were further investigated by studying different Tau seeds and the kinetics of aggregate induction in the presence of C22. Further, we tested its effect on other amyloids. Similarly, the impact of C57 and its kinetics on Tau aggregation was assessed.

5.1.1 C22 inhibits amyloid formation independent of the Tau seed

C22 was identified as a potent Tau aggregation inhibitor in 2020 when cells were exposed to recombinant Tau fibrils (Hebestreit, 2020). Here, we investigated if C22 also inhibits the induction of Tau aggregates with Tau seeds from other sources. Different exogenous Tau seeds were used, including cell extract from cells producing aggregated Tau_{40}^{L} (Tau 2N4R$^{L\ (0\text{-}441),\ agg}$) and Tau from transgenic mouse brain homogenate. PS19 mice express human P301S (S) mutated 1N4R Tau (Tau 1N4R$^{S\ (0\text{-}412)}$) (Yoshiyama et al., 2007). It was previously shown that PS19 Tau 1N4R$^{S\ (0\text{-}412)}$ mice exhibit prion-like spreading of Tau and that PS19 Tau 1N4R$^{S\ (0\text{-}412)}$ brain homogenate can be used for proteopathic Tau seeding (Holmes et al., 2014). Further, extracellular vesicles (EVs) from HEK cells that stably propagate Tau GFP^{AD} aggregates and express the vesicular stomatitis virus glycoprotein (VSV-G) were used (Liu et al., 2021) (Figure 6). VSV-G mediates the binding of the virus to the low-density lipoprotein (LDL) receptor (Finkelshtein et al., 2013; Kim et al., 2017). Our group has shown that VSV-G-coated EVs obtained from HEK cells expressing Tau GFP^{AD} increased aggregate induction in recipient cells by an efficient fusion of the EVs with the membrane of the recipient cells (Liu et al., 2021). C22 reduced the number of cells with Tau 4R$^{LM\ (243\text{-}375)}$ aggregates with an IC_{50} of

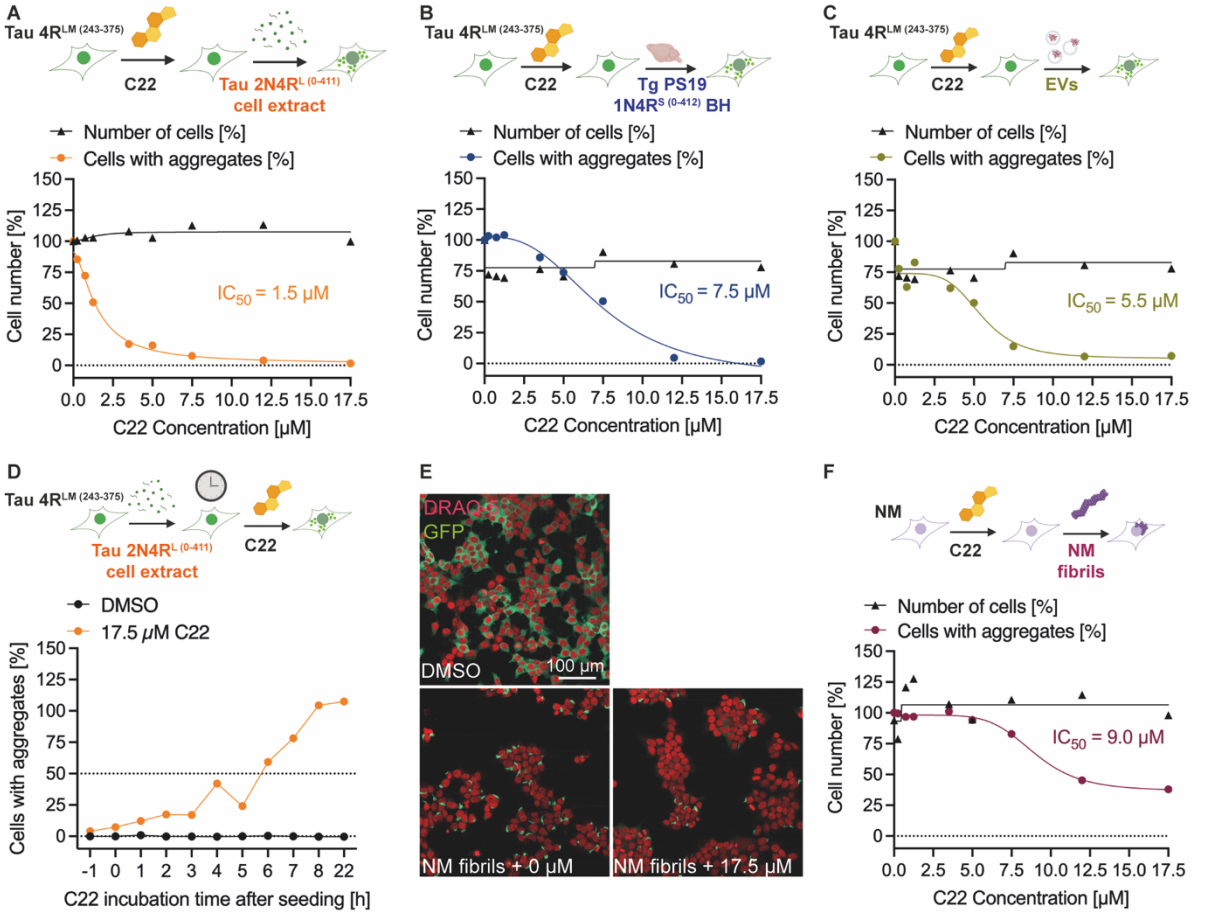

Figure 6 C22 significantly inhibits seed-induced Tau and NM aggregation. (A-C) HEK Tau 4R$^{LM\ (243-375)}$ GFP cells were plated 24 hours before compound 22 (C22) treatment. Seeds were added after 1 hour of pre-incubation of the cells with the compound (0-17.5 µM). Cells were fixed 24-48 hours later. Representative dose-response curves of C22. Tau aggregates were induced with **(A)** Tau 2N4R$^{L\ (0-441),\ agg}$ cell extract, **(B)** PS19 1N4R$^{S\ (0-412)}$ brain homogenate, and **(C)** EVs. **(D)** C22 was added with Tau 2N4R$^{L\ (0-441),\ agg}$ cell extract (0 hours) and 1-22 hours after seeding. -1 hour served as control: C22 was added 1 hour before seeding. DMSO served as a negative control. **(E)** Representative confocal images of HEK NM GFP cells with NM fibril-induced aggregates treated with compound 22. As negative control served DMSO. **(F)** Dose-response curve of C22 in HEK cells expressing GFP-tagged NM. NM aggregates were induced by NM fibrils. **(A-F)** Automated image analysis using fluorescence intensities determined the percentage of cells with aggregated Tau variants. To determine the $IC_{50,}$ a sigmoidal fit was interpolated, where x is concentration. The percentage of cells with aggregated Tau 4R$^{LM\ (243-375)}$ GFP/NM GFP was calculated as the number of aggregate-positive cells per total cells, set to 100 %. Toxicity was assessed by determining the total number of cells. The number of cells that received DMSO was set to 100 %. h: hour. BH: Brain homogenate. Tg: Transgene. EV: Extracellular vesicles.

1.5 µM when cells had been exposed to Tau 2N4R$^{L\ (0-441),\ agg}$ cell extract (Figure 6 A). The IC_{50} of C22 was 7.5 µM when cells were exposed to PS19 1N4R$^{S\ (0-412)}$ brain homogenate (Figure 6 B). Cells treated with C22 and EVs had an IC_{50} of 5.5 µM (Figure 6 C). C22 was the most effective in inhibiting Tau 4R$^{LM\ (243-375)}$ aggregates induced by Tau 2N4R$^{L\ (0-441),\ agg}$ cell extract (IC_{50}: 1.5 µM), followed by EVs (IC_{50}: 5.5 µM) and lastly by PS19 1N4R$^{S\ (0-412)}$ brain homogenate (IC_{50}: 7.5 µM). Concentrations of up to 17.5 µM of C22, in combination with Tau seeds, were non-toxic. Differences in the number of cells with aggregates were only observed between 1 and 12.5 µM. At 17.5 µM, C22 effectively inhibited Tau 4R$^{LM\ (243-375)}$ aggregation by all three

seed types, indicating that C22 inhibited Tau aggregation independent of the Tau seed. DMSO-treated cells were used as a control and did not affect Tau aggregation (data not shown). As the concentration and conformation of the Tau seeds used are unknown, this may affect the IC_{50}.

Next, we determined if C22 also inhibits already initiated Tau aggregation. To investigate this, cells expressing GFP-tagged Tau $4R^{LM\ (243\text{-}375)}$ were plated, and 17.5 µM of C22 was added the following day along with Tau $2N4R^{L\ (0\text{-}441),\ agg}$ cell extract (0 hours). Alternatively, C22 was added 1-22 hours after seeding with Tau $2N4R^{L\ (0\text{-}441),\ agg}$ cell extract (Figure 6 D). As a positive control, cells were pre-incubated with the drug as before, followed by aggregate induction (-1 hours). Pre-incubation of C22, followed by aggregate induction with Tau $2N4R^{L\ (0\text{-}441),\ agg}$ cell extract, most effectively inhibited Tau $4R^{LM\ (243\text{-}375)}$ aggregation. C22 reduced the number of cells with aggregates up to 50 %. However, this inhibitory effect was only observed when the drug was added within the first 5-6 hours after seeding. After 7 hours, C22 had little to no effect. We conclude that C22 can only reduce the number of cells with aggregates before a certain threshold of Tau seeds enters the cytosol of the HEK cells and Tau aggregates start to propagate.

We then investigated whether C22 also inhibits the aggregation of other amyloidogenic proteins. To this end, HEK cells expressing the GFP-tagged yeast Sup35 prion domain NM (hereafter NM) were used. NM is a model for studying amyloid formation and spreading in cells (Krammer et al., 2009; Hofmann et al., 2013; Liu et al., 2017). C22 also decreased NM aggregate formation in HEK NM GFP cells exposed to recombinant NM fibrils (IC_{50} = 9.0 µM) (Figure 6 E-F). Low concentrations of C22 (0.25-5.0 µM) poorly inhibited aggregate formation. We conclude that C22 can also prevent the aggregation of other amyloid proteins like NM. Overall, C22 inhibited protein aggregation regardless of the seed type and the amyloidogenic protein expressed by the cells without being toxic to the cells. However, C22 was only effective during the initial stages of aggregate induction. C22 most efficiently inhibited protein aggregation when cells had been pre-incubated with C22 prior to aggregate induction. It is known that C22 binds to Tau aggregates (Prof. Dr. Zweckstetter, personal communication). However, it is necessary to investigate whether it also affects cellular mechanisms involved in Tau aggregation. Due to its size, C22 cannot cross the blood-brain barrier (BBB) and is therefore unsuitable for animal studies. Hence, semi-automated high-content screening was continued to identify other compounds that can inhibit Tau aggregation.

5.1.2 C57 inhibits Tau aggregation when pre-incubated with cells

High-content screening was continued to identify more compounds that inhibit Tau aggregation. One of the hits was C57, with an IC_{50} of 1.7 µM when pre-incubated for 1 hour

with the HEK Tau $4R^{LM\ (243\text{-}375)}$ GFP cells and then seeded with Tau $2N4R^{L\ (0\text{-}441),\ agg}$ cell extract (Figure 7 A). C57 showed low toxicity up to 3.5 µM and slight toxicity at 4 µM. The kinetics of C57 were analysed similarly to those of C22. Plated HEK Tau $4R^{LM\ (243\text{-}375)}$ GFP cells were directly incubated with Tau $2N4R^{L\ (0\text{-}441),\ agg}$ cell extract and C57 (0 hours) (Figure 7 B). In addition, cells were first seeded with Tau $2N4R^{L\ (0\text{-}441),\ agg}$ cell extract, and C57 was added 1-22 hours later. Importantly, aggregate formation was inhibited by C57 only when cells were pre-incubated with the drug prior to aggregate induction. The exposure of cells to combined seeds and C57 (0 hours) has already increased the number of cells with aggregates by 30 %. Although the inhibitory effect of C57 on Tau aggregation was not as potent as that of C22 at higher concentrations, the C57 IC_{50} (1.7 µM) is comparable to the C22 IC_{50} (1.5 µM). Once a certain amount of Tau seeds entered the cells, the aggregation of the Tau $4R^{LM\ (243\text{-}375)}$ could not be inhibited by C57. This shows the importance of an early intervention in Tau aggregation. Derivatives of C57 are currently being tested to enhance the overall inhibitory effect without increasing toxicity.

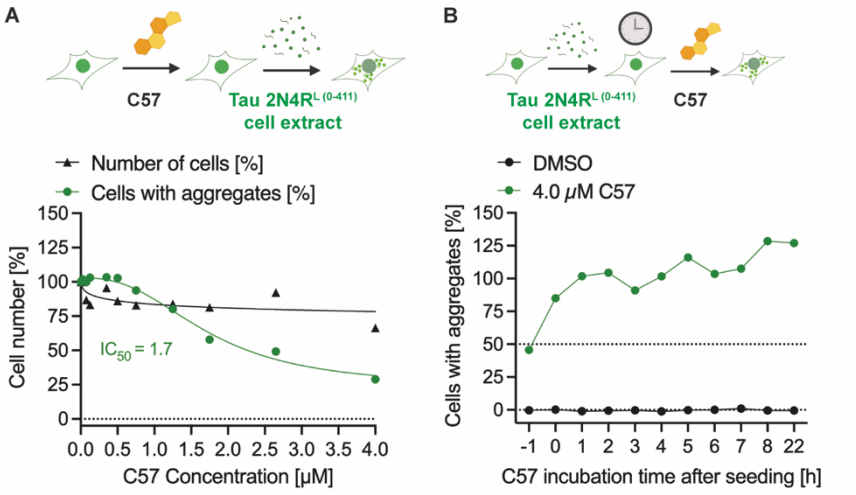

Figure 7 Pre-incubation of C57 with HEK Tau $4R^{LM\ (243\text{-}375)}$ cells inhibits seed-induced Tau aggregation. (A) Dose-response curve of C57, Tau aggregates were induced with Tau $2N4R^{L\ (0\text{-}441),\ agg}$ cell extract. **(B)** C57 was added 1-22 hours after seeding with Tau $2N4R^{L\ (0\text{-}441),\ agg}$ cell extract. Compound addition at -1 hours served as control. **(B)** Automated image analysis measuring fluorescence intensities determined the percentage of cells with aggregated Tau $4R^{LM\ (243\text{-}375)}$. To determine the IC_{50}, a sigmoidal fit was interpolated, where x is concentration. The percentage of cells with aggregated Tau $4R^{LM\ (243\text{-}375)}$ GFP/NM GFP was calculated as the number of aggregate-positive cells per total cells, set to 100 %. Toxicity was assessed by determining the total number of cells. The number of cells with aggregates exposed to DMSO only was set to 100 %. h: hour.

5.2 Generation of cell lines expressing full-length Tau, Tau RD fragments or Tau fragments corresponding to Tau amyloid cores

Cell-based assays are widely used to investigate Tau seeding activity and cellular mechanisms of intra- and intercellular prion-like Tau aggregation (Frost et al., 2009, 2009; Holmes et al., 2014; Sanders et al., 2014; Kaufman et al., 2016; Furman and Diamond, 2017). In addition, cell-based assays expressing Tau have been valuable tools for high-throughput compound screens to identify small molecules that inhibit Tau aggregation (Pickhardt et al., 2005b; Pickhardt et al., 2005a; Bulic et al., 2010; Hebestreit, 2020; Cheng et al., 2021; Antoniou et al., 2022; Bahnassawy et al., 2024). Most cell lines expressed Tau $3R^{(243\text{-}375,\ \Delta R2)}$ or Tau $4R^{(243\text{-}375)}$ RD fragments tagged with fluorescent proteins like GFP, CFP or YFP (Lu and Kosik, 2001; Woerman et al., 2016). The addition of exogenous Tau seeds like pre-formed recombinant Tau fibrils or Tau fibrils derived from mouse or patient brains induces the aggregation of the fluorescent protein-tagged Tau, which can be used as a readout for Tau aggregate induction (Furman and Diamond, 2017; Liu et al., 2021). However, the residues of the Tau amyloid cores of PiD, CBD, PSP, AD and CTE were recently identified (Scheres et al., 2023). It was shown that the cryoEM Tau amyloid cores differ in length and comprise fewer residues of the respective Tau 3R or 4R isoforms than the Tau RD fragments expressed previously in cell-based assays. Various intramolecular interactions within monomers and intermolecular interactions between monomeric subunits stabilise the cores. Consequently, the Tau amyloid core folds can differ between the respective Tauopathies. We hypothesised that the expression of the cryoEM Tau fragments that comprise the exact regions that form the core in the amyloid might facilitate the formation of disease-specific Tau aggregates. This could allow the discrimination of different Tauopathies based on the respective, seeding activity of isolated Tau fibrils in different cell lines expressing the Tau fragments related to Tau cryoEM cores.

Therefore, we generated a cell panel for this project based on the Tau fragments corresponding to the cryoEM Tau amyloid cores of PiD, CBD, PSP, CTE, and AD. By expressing only fragments corresponding to the cryoEM Tau amyloid cores, we hypothesised that the fragments may adopt the intramolecular interactions of the specific Tau amyloid cores obtained from patient brains. In addition, cell lines expressing full-length Tau and Tau RD fragments were generated. The length differences of the fragments corresponding to the cryoEM Tau amyloid cores might affect their tendency to aggregate spontaneously compared to the longer Tau RD fragments and full-length Tau. In addition, the length and the number of repeats included might also affect the kinetics and efficacy of fibril-induced aggregation. Flanking regions at the N- and C-terminus are suggested to protect from aggregation (Berry

et al., 2003; Jeganathan et al., 2006; Mukrasch et al., 2009). The missing N- and truncated C-terminus could render the fragments corresponding to the cryoEM Tau amyloid cores more prone to aggregation. Furthermore, only specific parts of the RD and the C-terminal are part of the cryoEM Tau amyloid cores. Therefore, it may be that the highest seeding activity is achieved when the expressed Tau fragments comprise the same amino acid residues as the amyloid cores of Tau fibrils derived from patients. The number of repeats within the Tau amyloid cores could result in a bilateral seeding barrier between Tau 3R and 4R isoforms. This may allow for the differentiation between 3R, 4R, and 3R/4R Tauopathies based on specific 3R, 4R and 3R/4R seeding patterns.

Within the cell panel, we included the soluble full-length wildtype (WT) 2N4R Tau (Tau 2N4R$^{(0\text{-}441)}$) 2N4R Tau with mutations P301L/V337M, or P301S (Tau 2N4R$^{LM\ (0\text{-}441)}$, Tau 2N4R$^{S\ (0\text{-}441)}$) and 0N3R Tau (Tau 0N3R$^{(0\text{-}352)}$) (Figure 8 A). Additionally, the well-established Tau 4R RD fragment with mutations P301L/V337M or P301S (Tau 4R$^{LM\ (243\text{-}375)}$, Tau 4R$^{S\ (246\text{-}378)}$) and a Tau 3R variant harbouring mutation V337M (Tau 3R$^{M\ (244\text{-}400)}$) were used, commonly referred to as Tau RD fragments (Figure 8 B). Tau 3R$^{M\ (244\text{-}400)}$ was chosen as it was shown to be preferentially seeded by Tau 3R seeds (Metrick et al., 2020). For the Tau fragments corresponding to the cryoEM Tau amyloid cores, we chose the AD cores representative for Tau 4R (Tau 4R$^{(AD\ 304\text{-}380)}$) and the shorter AD core representative of Tau 3R and 4R isoforms (Tau$^{(AD\ 306\text{-}378)}$) (Figure 8 C). Tau$^{(AD\ 306\text{-}378)}$ was included as it was the first cryoEM structure of AD missing two residues at the beginning and the end of the core, which might affect its aggregation into the AD amyloid fold. Tau constructs comprising the residues of the cryoEM core associated with CBD (Tau 4R$^{(CBD\ 274\text{-}380)}$) and PiD (Tau 3R$^{(PiD\ 254\text{-}378)}$), and two CTE fragments based on Tau 3R (Tau 3R$^{(CTE\ 274\text{-}379)}$) or Tau 4R (Tau 4R$^{(CTE\ 305\text{-}379)}$), were also included. The constructs based on the cryoEM Tau cores are generally referred to as cryoEM Tau core fragments. The residue numbering is according to full-length Tau 2N4R$^{(0\text{-}441)}$. All Tau 3R variants lack R2. All fragments corresponding to the cryoEM Tau amyloid cores comprise R3 and R4, along with ten to twelve residues C-terminally of the RD region. Tau 4R$^{(AD\ 304\text{-}380)}$ comprises the first two amino acids of R2 and twelve residues carboxyterminal to R4. Tau$^{(AD\ 306\text{-}378)}$ includes only R3 and R4 plus ten residues after R4. Tau 4R$^{(AD\ 304\text{-}380)}$ consists of one residue of R1, and twelve additional residues follow R4. Tau 3R$^{(PiD\ 254\text{-}378)}$ encompasses only the last 20 residues of R1 plus, and ten residues follow R4. Tau 3R$^{(CTE\ 274\text{-}379)}$ and Tau 4R$^{(CTE\ 305\text{-}379)}$ comprise one residues of R1 (3R) or R2 (4R) and eleven residues follow R4. All Tau constructs were tagged via a linker with monomeric GFP to prevent sterically impairing amyloid folds.

5.2.1 Spontaneous amyloid formation of cryoEM Tau core fragments

To investigate if our Tau fragments that correspond to cryoEM Tau cores spontaneously aggregate, we transiently overexpressed them in HEK cells and analysed cells by immunofluorescence (Figure 8 A-C). Interestingly, all truncated Tau variants exhibited nuclear Tau expression, while full-length Tau variants were mainly distributed in the cytoplasm (Figure 8 D-F). Tau lacks nuclear localisation signals, but it was suggested that it could interact with nuclear core complexes that enable the entry of smaller macromolecules via transport receptors or diffusion (Lemke, 2016; Fallini et al., 2020). Full-length Tau does not spontaneously aggregate *in vitro* and *cellula* (Frost et al., 2009; Ingham et al., 2022). It can only be induced *in vitro* with polyanionic factors like heparin or cofactor-free by double orbital shaking and polytetrafluoroethylene beads (Goedert et al., 1996; Chakraborty et al., 2021). In line with this, our full-length Tau fragments did not spontaneously aggregate when expressed in cells (Figure 8 D). Further, no spontaneous aggregation was observed for Tau RD fragments (Figure 8 E). In contrast, all cryoEM Tau fragments spontaneously formed puncta in some cells (Figure 8 F). Tau puncta were mainly present in the cytosol, except for Tau $4R^{(CBD\ 274\text{-}380)}$ aggregates, which primarily localised to the nucleus. Co-staining with the amyloid dye, Amylo Glo (Schmued et al., 2012; Saha et al., 2023) suggested that Tau puncta were of an amyloid nature. Quantitative analysis of the cells transiently transfected with Tau constructs confirmed that full-length Tau and Tau RD fragments did not spontaneously aggregate (Figure 8 G-H). Tau fragments corresponding to cryoEM Tau cores differed in their spontaneous aggregation propensity (Figure 8 I). $Tau^{AD\ (306\text{-}380)}$, the shortest cryoEM Tau core fragment, exhibited the highest level of spontaneously forming amyloid. Tau $3R^{(PiD\ 254\text{-}378)}$, the most extended cryoEM Tau core fragment, demonstrated the lowest. Despite being the second most extended variant, Tau $4R^{(CBD\ 274\text{-}380)}$ was the second fastest to aggregate spontaneously. One potential explanation for the high aggregation propensity of Tau $4R^{(CBD\ 274\text{-}380)}$ could be the presence of both amyloid motifs, PHF6* and PHF6, that drive Tau aggregation and two neighbouring cysteines in R2 and R3 that establish intermolecular disulphide bonds promoting aggregation (Gerson et al., 2014; Petri et al., 2022). Thus, we conclude that Tau fragments corresponding to Tau amyloid cores are prone to aggregate spontaneously. The length of the core, as well as the number of amyloid motifs included and intermolecular interactions, might affect its propensity to aggregate spontaneously. At the same time, full-length and Tau RD fragments may be protected due to the additional residues at the N- and C-terminus and, therefore, do not spontaneously self-assemble.

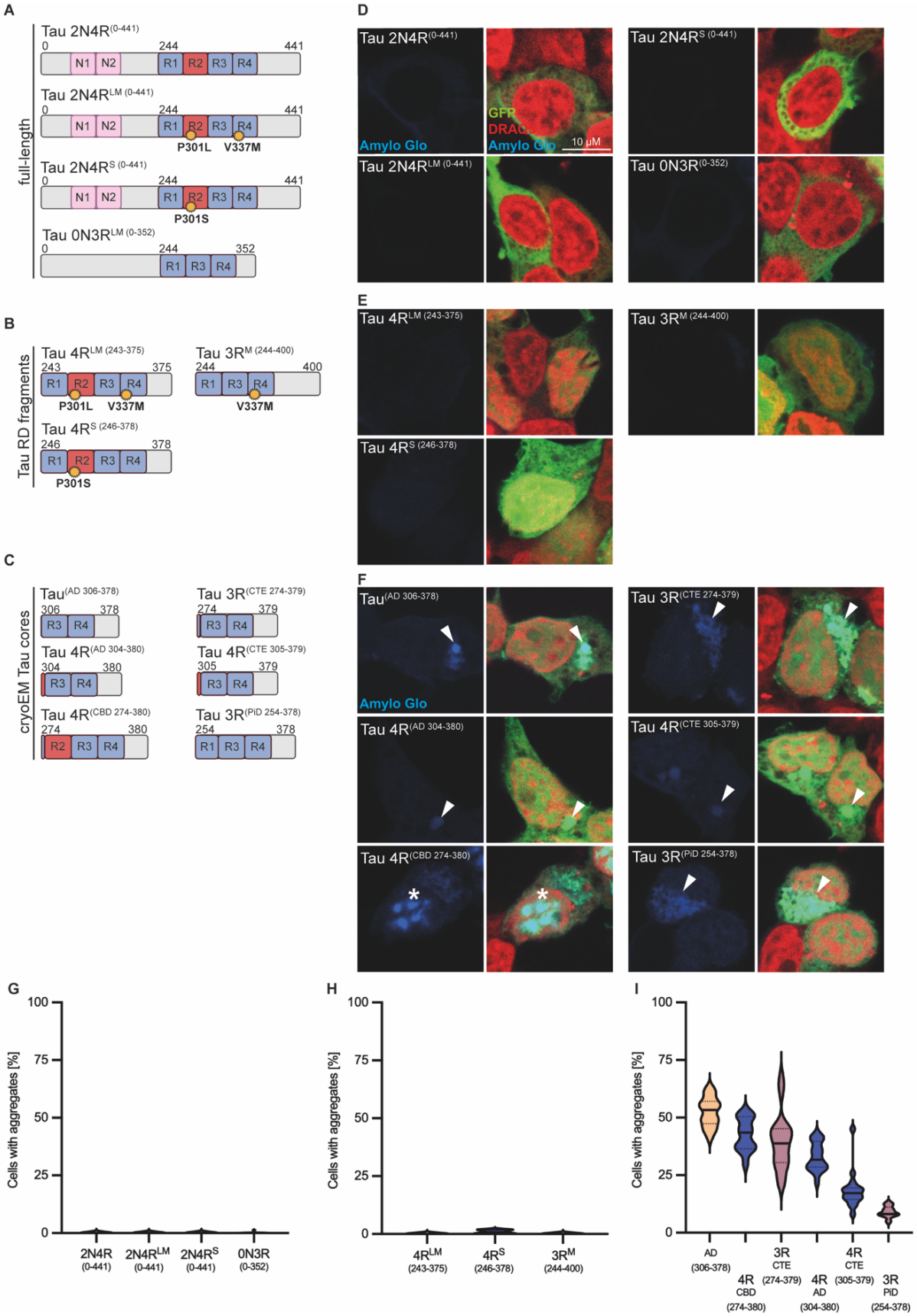

Figure 8 Tau fragments comprising cryoEM Tau cores spontaneously aggregate. (A) Full-length Tau constructs: Tau 2N4R$^{(0-441)}$, mutant (P301L/V337M, P301S) 2N4R Tau$^{(0-441)}$, referred to as Tau 2N4R$^{LM\ (0-441)}$ and Tau 2N4R$^{S\ (0-441)}$ and Tau 0N3R$^{(0-352)}$. **(B)** RD fragments: Mutant (P301L/V337M; P301S) repeat domain (RD), termed Tau 4R$^{LM\ (243-375)}$ and Tau 4R$^{S\ (246-378)}$, as well as a mutated (V337M) 3R RD, referred to as Tau 3R$^{M\ (244-400)}$ (Metrick et al.,

2020). **(C)** Tau fragments comprising Tau cryoEM cores: Constructs were designed to code for Tau amyloid cores previously determined by cryo-EM: Alzheimer's disease (Tau $4R^{(AD\ 306\text{-}378)}$, Tau $4R^{(AD\ 304\text{-}380)}$), Corticobasal degeneration (Tau $4R^{(CBD\ 274\text{-}380)}$), Chronic traumatic encephalopathy (Tau $3R^{(CTE\ 274\text{-}379)}$, Tau $4R^{(CTE\ 305\text{-}379)}$), and Pick's disease (Tau $3R^{(PiD254\text{-}378)}$). **(D-F)** Tau variants tagged with GFP were transiently overexpressed. Cells were stained with Amylo Glo to detect amyloid formation. Representative confocal images are shown. Arrowheads indicate spontaneous cytoplasmic amyloid inclusions. Asterisks indicate spontaneous nuclear aggregation. **(D)** Confocal images of full-length Tau and **(E)** Tau RD fragments. **(F)** Confocal images of spontaneously aggregating cryoEM Tau cores. **(G-I)** Quantification of spontaneous Tau aggregation. Tau aggregates were manually quantified using Fiji. Two hundred cells were counted per well. Data are shown as violin plots, the mean is indicated as a straight line, and dotted lines represent quartiles (n=2). Scalebar: 10 µm.

5.2.2 Proteasomal clearance of stably expressed Tau variants, which are prone to spontaneous aggregation

Some cryoEM Tau fragments spontaneously aggregated when expressed transiently in HEK cells. High transient expression levels can cause spontaneous aggregation (Seidler et al., 2019), so we investigated whether the cryoEM Tau core fragments could be stably expressed without spontaneous aggregation to study fibril-induced aggregation. Lentiviral transduction typically results in few integration events and lower protein expression levels. Therefore, cell lines stably expressing full-length Tau, Tau RD fragments and cryoEM Tau core fragments were generated. Single-cell clones with a stable homogenous expression of soluble Tau were selected. This prevented false positive aggregate detection due to heterogeneous expression levels during automated image analysis. The resulting cell clones were analysed for Tau expression levels and spontaneous aggregation using WB and confocal microscopy (Figure 9). HEK cells stably expressed full-length Tau and Tau RD fragments. For cryoEM Tau core fragments, only Tau $4R^{(CTE\ 305\text{-}379)}$, Tau $4R^{(AD\ 304\text{-}380)}$, and Tau $3R^{(PiD\ 254\text{-}378)}$ showed easily detectable protein levels (Figure 9 A). In contrast, $Tau^{(AD\ 306\text{-}378)}$ showed weak detectable WB bands, while no bands were detected for Tau $4R^{(CBD\ 274\text{-}380)}$ and Tau $3R^{(CTE\ 274\text{-}379)}$ (Figure 9 B). Also, IF showed weak GFP intensities for cryoEM $Tau^{(AD\ 306\text{-}378)}$, Tau $4R^{(CBD\ 274\text{-}380)}$, and Tau $3R^{(CTE\ 274\text{-}379)}$ core fragments (Figure 9 C). No spontaneous aggregation was observed for any of the Tau variants when stably expressed. The decreased protein levels of the core fragments comprising cryoEM $Tau^{(AD\ 306\text{-}378)}$, Tau $3R^{(CTE\ 274\text{-}379)}$, and Tau $4R^{(CBD\ 274\text{-}380)}$ suggested that these variants, which were highly prone to spontaneous aggregation when transiently expressed, might be cleared by the cells when stably expressed. Spontaneous aggregation could enhance the UPS and the ALP activity, which regulate the refolding and degradation of misfolded proteins (Morley et al., 2002; Taylor and Dillin, 2011). To determine if the proteasome is involved in Tau degradation in cells expressing the core fragments of cryoEM $Tau^{(AD\ 306\text{-}378)}$, Tau $4R^{(CBD\ 274\text{-}380)}$, and Tau $3R^{(CTE\ 274\text{-}379)}$, we inhibited proteasomal clearance for 4, 8, and 24 hours using the proteasome inhibitor MG132 (Figure 9 C). HEK cells stably expressing Tau $4R^{S\ (246\text{-}378)}$ RD fragments were used as a control because this variant does not

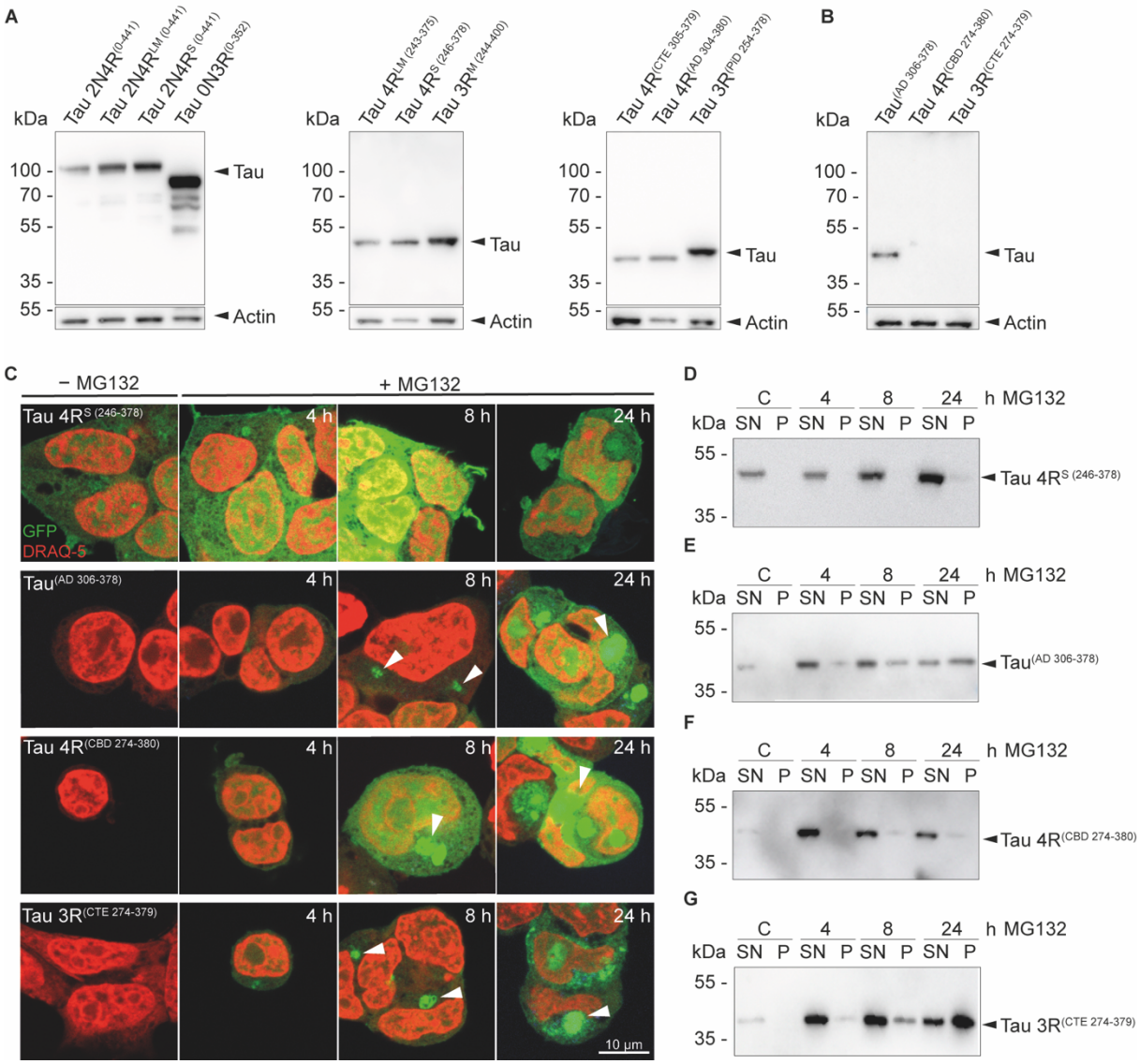

Figure 9 Clearance of CryoEM Tau$^{(AD\ 306-378)}$, Tau 4R$^{(CBD\ 274-380)}$, and Tau 3R$^{(CTE\ 274-379)}$ core fragments by the proteasome prevents spontaneous aggregation. Western blot (WB) of **(A)** full-length Tau (Tau 2N4R$^{(0-441)}$, Tau 2N4R$^{LM\ (0-441)}$, Tau 2N4R$^{S\ (0-441)}$, Tau 0N3R$^{(0-352)}$), Tau RD fragments (Tau 4R$^{LM\ (243-375)}$, Tau 4R$^{S\ (246-378)}$, Tau 3R$^{M\ (244-400)}$), cryoEM Tau core fragments (Tau 4R$^{(CTE\ 305-379)}$, Tau$^{(AD\ 306-378)}$, Tau 3R$^{(PiD\ 254\ 378)}$) and **(B)** weakly expressed cryoEM Tau$^{(AD\ 306-378)}$, Tau 4R$^{(CBD\ 274-380)}$ and Tau 3R$^{(CTE\ 274-379)}$ core fragments. Tau variants were detected with anti-Tau antibody (MBD). 30 µg total protein was loaded. WB was reprobed for β-Actin as a loading control. **(B)** Blots displaying cryoEM Tau 3R$^{(CTE\ 274-379)}$, Tau$^{(AD\ 306-378)}$ and Tau 4R$^{(CBD\ 274-380)}$ core fragments were developed with ECL Femto for a minimum of 5 minutes for signal detection. **(C)** Cells with weak protein levels of cryoEM Tau 3R$^{(CTE\ 274-379)}$, Tau$^{(AD\ 306-378)}$ and Tau 4R$^{(CBD\ 274-380)}$ core fragments were treated with MG132 for 4, 8, and 24 hours to inhibit proteasomal clearance. Tau 4R$^{S\ (246-378)}$ was used as a control. Representative confocal images are shown. Nuclei were stained with DRAQ-5. Arrowheads indicate Tau aggregates. **(D-G)** Cells were lysed and used for sedimentation assays. 100 µg total protein was used. Anti-Tau antibody (MBD) was used for band detection. h: hour. C: Control. SN: Supernatant. P: Pellet. kDa: kilodalton. Scalebar: 10 µm.

spontaneously aggregate at high concentrations during transient transfection. Confocal imaging revealed that untreated GFP-tagged cryoEM Tau$^{(AD\ 306-378)}$, Tau 4R$^{(CBD\ 274-380)}$, and Tau 3R$^{(CTE\ 274-379)}$ core fragments expressed in HEK cells showed almost no GFP signal. In contrast, cells expressing Tau 4R$^{S\ (246-378)}$ RD fragments showed a clear GFP signal. Upon incubation with MG132 for 4 hours, the Tau protein levels of all Tau variants increased. After 8 hours in

the presence of MG132, spontaneously forming aggregate-like puncta appeared in HEK cells expressing cryoEM Tau$^{(AD\ 306-378)}$, Tau 4R$^{(CBD\ 274-380)}$, and Tau 3R$^{(CTE\ 274-379)}$ core fragments, and nuclei became deranged. The inclusions continued to grow, and by 24 hours, the cells became apoptotic. Tau 4R$^{S\ (246-378)}$ RD fragments did not aggregate but underwent apoptosis after 24 hours (Figure 9 C). We conclude that the increased protein levels of cryoEM Tau$^{(AD\ 306-378)}$, Tau 4R$^{(CBD\ 274-380)}$, and Tau 3R$^{(CTE\ 274-379)}$ core fragments in HEK cells by MG132 lead to their spontaneous aggregation. The missing N- and truncated C-terminus could make the cryoEM Tau amyloid cores more prone to aggregation. To prevent spontaneous aggregation, protein levels of cryoEM Tau$^{(AD\ 306-378)}$, Tau 4R$^{(CBD\ 274-380)}$, and Tau 3R$^{(CTE\ 274-379)}$ fragments are decreased by proteasomal degradation.

To validate the increase in Tau expression levels and the formation of aggregates, MG132-treated cells were lysed after 4-24 hours and used for sedimentation assays (Figure 9 D-G). In line with the confocal images, the expression level of soluble cryoEM Tau$^{(AD\ 306-378)}$, Tau 4R$^{(CBD\ 274-380)}$, and Tau 3R$^{(CTE\ 274-379)}$ core fragments represented in the supernatant, as well as the Tau aggregates in the pellet fraction, increased gradually over the 24-hour treatment. To rule out that MG132 treatment leads to the general formation of spontaneous Tau aggregates, we treated HEK cells stably expressing Tau 4R$^{S\ (246-378)}$ RD fragments with MG132. Notably, these cells did not show spontaneous aggregation when the variant was transiently over-expressed. We found no detectable aggregation in cells stably expressing Tau 4R$^{S\ (246-378)}$ RD fragments exposed to MG132, except at the 24-hour time point. This was expected, as MG132 inhibits the proteasome, leading to protein accumulation after a certain time. Combined, these findings suggest that cryoEM Tau$^{(AD\ 306-378)}$, Tau 4R$^{(CBD\ 274-380)}$, and Tau 3R$^{(CTE\ 274-379)}$ core fragments are degraded by the proteasome. This might be due to enhanced proteasomal clearance to prevent spontaneous aggregation and a natural selection process that possibly favours cells without detrimental spontaneous Tau aggregation. However, it is currently unclear whether the loss of cells with high Tau protein levels and spontaneous aggregation is due to cell death. This requires further investigation. Cells expressing the cryoEM Tau$^{(AD\ 306-378)}$, Tau 4R$^{(CBD\ 274-380)}$, and Tau 3R$^{(CTE\ 274-379)}$ core fragments were excluded from further experiments due to their weak expression in HEK cells. HEK cells stably expressing GFP-tagged full-length Tau 2N4R$^{(0-441)}$, full-length Tau 2N4R$^{LM\ (0-441)}$, full-length Tau 2N4R$^{S\ (0-441)}$, full-length Tau 0N3R$^{(0-352)}$, Tau 4R$^{LM\ (243-375)}$ RD, Tau 4R$^{S\ (246-378)}$ RD, Tau 3R$^{M\ (244-400)}$ RD fragments, cryoEM Tau 4R$^{(CTE\ 305-379)}$, cryoEM Tau 4R$^{(AD\ 304-380)}$ and cryoEM Tau 3R$^{(PiD\ 254-378)}$ core fragments were successfully established and were further used to investigate fibril-induced Tau aggregation.

5.3 Seeding barriers between Tau 4R recombinant fibrils and Tau 3R and Tau 4R variants that have only parts of R2

Previous studies have shown that Tau seeds, such as recombinant Tau fibrils, can induce Tau aggregation *in vitro* and *in cellula* (Frost et al., 2009; Guo and Lee, 2011; Tanaka et al., 2019; Longhini et al., 2024). It was shown that seeding barriers exist *in vitro* between recombinant Tau $4R^{(244\text{-}372)}$ fibrils (template) and recombinant Tau $3R^{(244\text{-}372)}$ monomers (substrates) (Dinkel et al., 2011; Yu et al., 2012; Weismiller et al., 2018). Recently, this 4R:3R seeding barrier was confirmed in cells that expressed Tau $1N3R^{(0\text{-}381)}$ and were exposed to patient-derived Tau fibrils. The Tau fibrils were obtained from 4R CBD or 4R PSP patient brain homogenate (Tarutani et al., 2021). The same 4R:3R seeding barrier was detected in cells expressing Tau $3R^{(255\text{-}441)}$ exposed to fibrillised Tau $4R^{(295\text{-}313)}$ peptides comprising R2 and R3 (Longhini et al., 2024). In our cell model, we studied whether a 4R:3R seeding barrier exists and whether exogenous Tau 4R seeds can induce aggregation of Tau 4R variants. To this end, we exposed HEK cells that stably expressed full-length Tau, Tau RD fragments, and the core fragments of cryoEM Tau $4R^{(CTE\ 305\text{-}379)}$, Tau $4R^{(AD\ 304\text{-}380)}$ and Tau $3R^{(PiD\ 254\text{-}378)}$ to recombinant Tau $2N4R^{L\ (0\text{-}441)}$ fibrils provided by Prof. Dr. Markus Zweckstetter. Recombinant Tau $2N4R^{L\ (0\text{-}441)}$ monomers were used as a control. Cells exposed to 1.5 µM recombinant Tau $2N4R^{L\ (0\text{-}441)}$ fibrils or monomers were assessed for Tau aggregate induction by automated image acquisition and analysis (Figure 10 A-C). Full-length Tau $2N4R^{(0\text{-}441)}$ did not aggregate when recombinant Tau $2N4R^{L\ (0\text{-}441)}$ fibrils were added, confirming earlier work (Aoyagi et al., 2007). By contrast, in a few cells, mutated full-length Tau $2N4R^{LM\ (0\text{-}441)}$ and Tau $2N4R^{S\ (0\text{-}441)}$ accumulated as cytosolic aggregates (Figure 10 A). Full-length Tau $0N3R^{(0\text{-}352)}$ did also not aggregate when cells were exposed to recombinant Tau $2N4R^{L\ (0\text{-}441)}$ fibrils. The Tau $4R^{LM\ (243\text{-}375)}$ RD and Tau $4R^{S\ (246\text{-}378)}$ RD fragments were seeded, while Tau $3R^{M\ (244\text{-}400)}$ RD fragments did not aggregate (Figure 10 B). None of the cryoEM Tau core fragments aggregated when exposed to recombinant Tau $2N4R^{L\ (0\text{-}441)}$ fibrils, including cryoEM Tau $4R^{(CTE\ 305\text{-}379)}$ and Tau $4R^{(AD\ 304\text{-}380)}$ core fragments, which contain 1-2 aa residues from R2 of Tau 4R (Figure 10 C).

Automated image analysis revealed that hardly any cells expressing the full-length Tau variants contained Tau aggregates (Figure 10 D). No cells were found to contain aggregates when exposed to the recombinant Tau $2N4R^{L\ (0\text{-}441)}$ monomer. The automated image analysis uses a fluorescence threshold to detect GFP-tagged aggregates. Cells expressing soluble Tau variants may have diffuse green dots with low GFP intensity, which are not considered aggregates but the background and are, therefore, not counted. Although aggregates were visible in the IF images for full-length Tau variants, the percentage of cells with aggregates in cells expressing mutated full-length Tau $2N4R^{LM\ (0\text{-}441)}$ or Tau $2N4R^{S\ (0\text{-}441)}$ was less than 1 %.

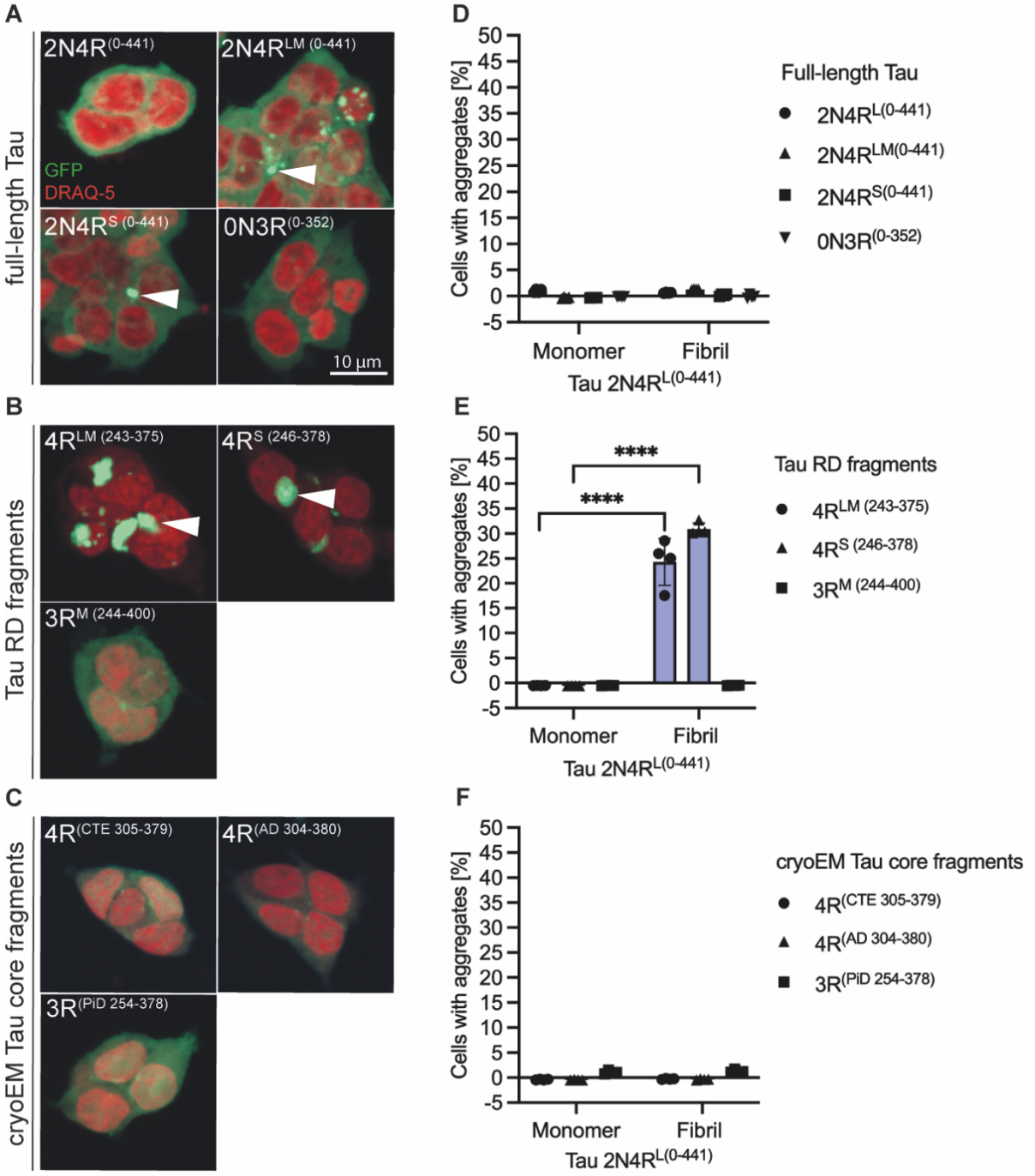

Figure 10 Recombinant Tau 2N4R$^{L\ (0\text{-}441)}$ fibrils induce mainly Tau 4R$^{LM\ 243\text{-}375)}$ RD and Tau 4R$^{S\ (246\text{-}378)}$ RD fragment aggregates. (A-C) Representative confocal images of GFP-tagged **(A)** full-length Tau, **(B)** Tau RD fragments, and **(C)** cryoEM Tau core fragments stably expressed in HEK cells and exposed to 1.5 µM recombinant Tau 2N4R$^{L\ (0\text{-}441)}$ fibrils. Cells were fixed after 24 hours. Nuclei were stained with DRAQ-5. Arrowheads indicate cytosolic aggregates of the corresponding Tau variant. **(D-F)** Tau aggregate quantification. Cells treated with Tau 2N4R$^{L\ (0\text{-}441)}$ monomers served as a control. The percentage of cells with aggregated Tau was calculated as the number of aggregate-positive cells per total cells, set to 100 %. Data are presented as mean ± SD (n=4). Two-way ANOVA was used for statistical analysis. The mean was compared to the control (P: **** >0.0001). Three **(D-F)** independent experiments with four technical replicates were carried out with similar results. Scalebar: 10 µm.

When exposed to Tau 2N4R$^{L\ (0\text{-}441)}$ fibrils, cells expressing Tau 4R$^{LM\ (243\text{-}375)}$ RD and Tau 4R$^{S\ (246\text{-}378)}$ RD fragments showed the highest seeding efficiency with 24 % and 31 % of cells with

aggregates, respectively (Figure 10 E). This confirms that cells expressing Tau 4R$^{LM\ (243-375)}$ RD and Tau 4R$^{S\ (246-378)}$ RD fragments are sensitive cells for homotypic seeding by Tau 2N4R$^{L\ (0-441)}$ fibrils. In contrast, aggregation of cryoEM Tau 4R$^{(CTE\ 305-379)}$ and Tau 4R$^{(AD\ 304-380)}$ core fragments could not be seeded by recombinant Tau 2N4R$^{L\ (0-441)}$ fibrils (Figure 10 F). Similarly, the Tau 3R isoforms full-length Tau 0N3R$^{(0-352)}$, Tau 3R$^{M\ (244-400)}$ RD fragments, and the cryoEM Tau 3R$^{(PiD\ 254-378)}$ core fragments could not be induced by recombinant Tau 2N4R$^{L\ (0-441)}$ fibrils in our model (Figure 10 D-F). We conclude that Tau 4R RD fragments are efficiently seeded by recombinant Tau 2N4R$^{L\ (0-441)}$ fibrils and that a 4R:3R seeding barrier exists between recombinant Tau 4R fibrils and Tau 3R variants expressed in cells. This confirms the *in vitro* and *in cellula* data of previous experiments in the Tau field. Surprisingly, the aggregation of the cryoEM Tau 4R$^{(CTE\ 305-379)}$ and Tau 4R$^{(AD\ 304-380)}$ core fragments was not induced by recombinant Tau 2N4R$^{L\ (0-441)}$ fibrils, despite covering parts of the residues of the Tau 4R isoform. This may be because the sequence of the core fragments of cryoEM Tau 4R$^{(CTE\ 305-379)}$ and Tau 4R$^{(AD\ 304-380)}$ starts with only the last 1-2 residues of R2 followed by R3-R4 of the repeat domain. By contrast, the recombinant Tau 2N4R$^{L\ (0-441)}$ fibrils and the Tau 4R RD fragments include all of the RD (R1-R4). The shorter sequence length of the cryoEM core fragment and the missing parts of R2 might lead to a seeding barrier similar to Tau 3R variants that completely lack R2. In addition, altered intramolecular interactions between the cryoEM Tau core fragment residues may further contribute to the seeding barrier by allowing only specific core conformations. This might lead to a general conformational incompatibility between cryoEM Tau 4R core fragments that lack most of R2 and recombinant Tau 2N4R$^{L\ (0-441)}$ fibrils that include all four repeats.

To confirm the induction of Tau aggregates by recombinant Tau 2N4R$^{L\ (0-441)}$ fibrils, soluble and insoluble protein fractions were analysed via sedimentation assay (Figure 11 A-C). Therefore, cells expressing full-length Tau 2N4R$^{(0-441)}$, Tau 2N4R$^{LM\ (0-441)}$, and Tau 2N4R$^{S\ (0-441)}$ exposed to recombinant Tau 2N4R$^{L\ (0-441)}$ fibrils were cultured over several passages. In addition, they were re-exposed to recombinant Tau 2N4R$^{L\ (0-441)}$ fibrils to ensure Tau aggregation. This was done because full-length Tau aggregation is slow, and aggregation rates are poor. All Tau variants showed a clear signal in the soluble fraction, confirming stable expression of the corresponding soluble Tau variant. Signals in the pellet fraction of cells propagating aggregated mutated full-length Tau, Tau 4R$^{LM\ (243-375)}$ RD, and Tau 4R$^{S\ (246-378)}$ RD fragments confirmed Tau 2N4R$^{L\ (0-441)}$ fibril-induced aggregation of Tau 4R variants (Figure 11 A-B). Only one band corresponding to the expected protein size was detected for full-length Tau 2N4R$^{(0-441)}$, full-length Tau 2N4R$^{LM\ (0-441)}$, full-length Tau 2N4R$^{S\ (0-441)}$, Tau 4R$^{LM\ (243-375)}$ RD fragments, cryoEM Tau 4R$^{(AD\ 304-380)}$ and cryoEM Tau 3R$^{(PiD\ 254-378)}$ core fragments. Yet, two fragments were detected for full-length Tau 0N3R$^{(0-352)}$, Tau 3R$^{M\ (244-400)}$ RD fragments, and

cryoEM Tau 4R$^{(CTE\ 305\text{-}379)}$ core fragments, and three bands were detected for Tau 4R$^{S\ (246\text{-}378)}$ RD fragments (Figure 11 A-C). The difference in banding patterns may be due to the protease cleavage of Tau variants, resulting in both GFP-tagged and untagged Tau fragments. However, the sedimentation assay confirmed the aggregation of full-length Tau 2N4R$^{LM\ (0\text{-}441)}$, Tau 2N4R$^{S\ (0\text{-}441)}$, and Tau 4R$^{LM\ (243\text{-}375)}$, and Tau 4R$^{S\ (246\text{-}378)}$ RD fragments by recombinant Tau 2N4R$^{L\ (0\text{-}441)}$ fibrils. Our cell-based assay proved the 4R:3R seeding barrier between recombinant Tau 2N4R$^{L\ (0\text{-}441)}$ fibrils and cells expressing Tau 3R variants as substrates. As cryoEM Tau 4R$^{(CTE\ 305\text{-}379)}$ and cryoEM Tau 4R$^{(AD\ 304\text{-}380)}$ core fragments could not be induced by full-length Tau 2N4R$^{L\ (0\text{-}441)}$ recombinant fibrils, we conclude that the residues of R2 play a crucial role in 4R:4R homotypic seeding. The truncation of R2 in Tau 4R variants and the lack of R2 in Tau 3R variants may lead to conformational incompatibility with Tau 4R seeds. Hence, cryoEM Tau 4R$^{(CTE\ 305\text{-}379)}$ and cryoEM Tau 4R$^{(AD\ 304\text{-}380)}$ core fragments may be only seeded by Tau seeds that incorporate the same or a similar sequence within the amyloid core.

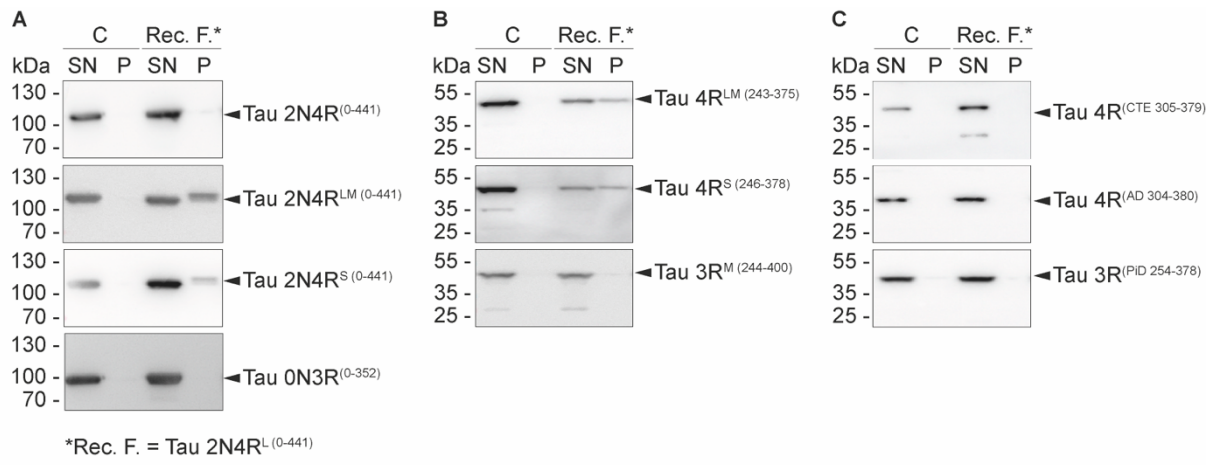

Figure 11 Sedimentation assay confirms aggregation of full-length Tau 2N4R$^{LM\ (0\text{-}441)}$, full-length Tau 2N4R$^{S\ (0\text{-}441)}$, Tau 4R$^{LM\ (243\text{-}375)}$ RD, and Tau 4R$^{S\ (246\text{-}378)}$ RD fragments induced by recombinant Tau 2N4R$^{L\ (0\text{-}441)}$ fibrils. (A-C) Sedimentation assays with extracts of HEK cells expressing full-length Tau, Tau RD fragments and cryoEM Tau core fragments. 1.5 µM recombinant Tau 2N4R$^{L\ (0\text{-}441)}$ fibrils were added to induce aggregation. Cells were re-exposed twice and cultured over 4-6 passages before cells were lysed. Tau was detected using **(A)** anti-Tau-5 #AHB0042 antibody, **(B)** anti-Tau ab64193 (Tau 4R$^{LM\ (243\text{-}375)}$, Tau 4R$^{S\ (246\text{-}378)}$), anti-GFP (Tau 3R$^{M\ (244\text{-}400)}$), and **(C)** anti-GFP antibody. P: Pellet. SN: Supernatant. C: Control, non-treated cells. Rec.: Recombinant, F: Fibril. kDa: kilodalton. Three independent experiments were carried out with similar results.

5.4 PS19 Tau 1N4R$^{S\ (0\text{-}412)}$ brain homogenate confirms seeding barrier between Tau 3R variants and Tau 4R variants that lack parts of R2

To assess the seeding activity of different Tau 4R seeds in our cells panel, we used, aside from the recombinant Tau 2N4R$^{L\ (0\text{-}441)}$ fibrils, PS19 brain homogenate (Figure 12). PS19 mice overexpress the mutant P301S human Tau 1N4R (PS19 Tau 1N4R$^{S\ (0\text{-}412)}$) and are widely used

as a Tauopathy mouse model (Yoshiyama et al., 2007). While the cryoEM core of recombinant Tau 2N4R$^{L\ (0\text{-}441)}$ fibrils is not resolved yet, the hydrophobic core of PS19 Tau 1N4R$^{S\ (0\text{-}412)}$ fibrils was recently determined by cryoEM (Schweighauser et al., 2023). The PS19 Tau 1N4R$^{S\ (0\text{-}412)}$ fibril core resembles an intermediate core length of heparin-induced recombinant Tau fibrils and Tau fibrils isolated from patients with AD. In our cells expressing full-length Tau 4R variants, only the mutated Tau 2N4R$^{LM\ (0\text{-}441)}$ and Tau 2N4R$^{S\ (0\text{-}441)}$ formed inclusions upon exposure to PS19 Tau 1N4R$^{S\ (0\text{-}412)}$ brain homogenate. In contrast, full-length Tau 2N4R$^{(0\text{-}441)}$ and Tau 0N3R$^{(0\text{-}352)}$ remained soluble (Figure 12 A). Additionally, only the Tau 4R$^{LM\ (243\text{-}375)}$ RD and Tau 4R$^{S\ (246\text{-}378)}$ RD fragments aggregated, while the Tau 3R$^{M\ (244\text{-}400)}$ RD fragments did not (Figure 12 B). None of the cells expressing cryoEM Tau core fragments showed Tau inclusions (Figure 12 C). This aligns with the results of the recombinant Tau 2N4R$^{L\ (0\text{-}441)}$ fibrils and shows that only the cells expressing the mutated full-length Tau 4R and Tau 4R RD fragments can be used to detect Tau 4R seeds.

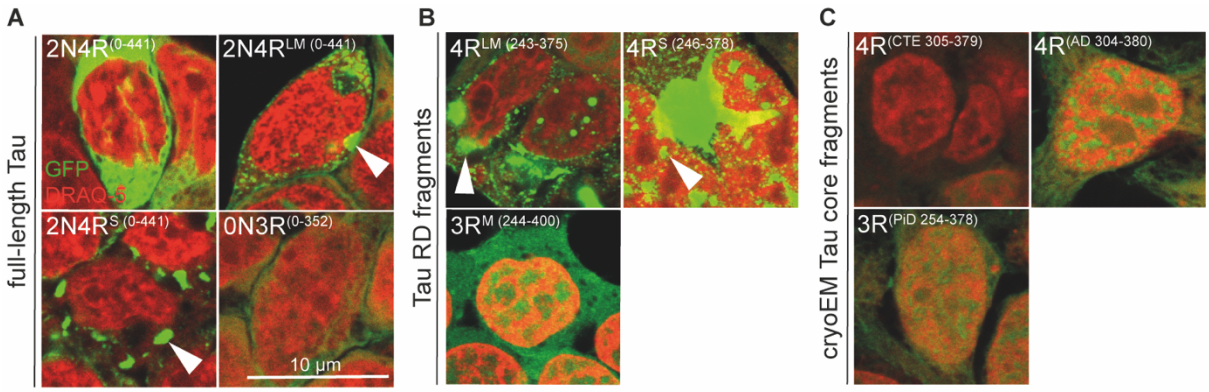

Figure 12 PS19 Tau 1N4R$^{S\ (0\text{-}441)}$ brain homogenate confirms seeding barrier with Tau 3R variants and cryoEM Tau 4R core fragments. (A-C) Representative confocal images of GFP-tagged **(A)** full-length Tau, **(B)** Tau RD fragments, and **(C)** cryoEM Tau core fragments stably expressed in HEK cells and exposed to 1.5 µl PS19 1N4R$^{S\ (0\text{-}441)}$ brain homogenate. Cells were fixed after 48 hours. Nuclei were stained with DRAQ-5. Arrowheads indicate cytosolic aggregates of the corresponding Tau variant. Scalebar: 10 µm.

The sedimentation assay confirmed that PS19 Tau 1N4R$^{S\ (0\text{-}412)}$ brain homogenate-treated cells expressing mutated full-length Tau 2N4R$^{LM\ (0\text{-}441)}$, full-length Tau 2N4R$^{S\ (0\text{-}441)}$, Tau 4R$^{LM\ (243\text{-}375)}$ RD, and Tau 4R$^{S\ (246\text{-}378)}$ RD fragments contained aggregates, as signals were detected in the insoluble pellet fraction (Figure 13 A-C). Together, we show that both Tau 4R seeds, recombinant Tau 2N4R$^{L\ (0\text{-}441)}$ fibrils and PS19 Tau 1N4R$^{S\ (0\text{-}412)}$ fibrils, induce aggregation of mutated full-length Tau 2N4R$^{LM\ (0\text{-}441)}$, full-length Tau 2N4R$^{S\ (0\text{-}441)}$, Tau 4R$^{LM\ (243\text{-}375)}$ RD and Tau 4R$^{S\ (246\text{-}378)}$ RD fragments. Recombinant Tau 4R seeds cannot induce cryoEM Tau 4R$^{(CTE\ 305\text{-}379)}$ and Tau 4R$^{(AD\ 304\text{-}380)}$ core fragments. This may be because cryoEM Tau 4R$^{(CTE\ 305\text{-}379)}$ and Tau 4R$^{(AD\ 304\text{-}380)}$ core fragments may have a different conformation than the amyloid core of the Tau 4R seeds. This is likely due to the shorter sequence length of the

cryoEM Tau core fragments and the missing parts of R2 at the beginning of the cryoEM Tau core fragment sequence. Conversely, the recombinant Tau 2N4R$^{L\ (0\text{-}441)}$ fibrils and PS19 1N4R$^{S\ (0\text{-}412)}$ Tau fibrils include more residues, including all of R1-R4 in their sequence. Heterotypic seeding of full-length Tau 0N3R$^{(0\text{-}352)}$, Tau 3R$^{M\ (244\text{-}400)}$ RD fragments and cryoEM Tau 3R$^{(PiD\ 254\text{-}378)}$ core fragments by the Tau 4R seeds was impossible, proving the 4R:3R seeding barrier. Hence, the specificity of the cells expressing mutated full-length Tau 4R and Tau 4R RD fragments to Tau 4R seeds is confirmed. At the same time, a seeding barrier exists between Tau 4R seeds and cryoEM Tau core fragments with a truncated R2.

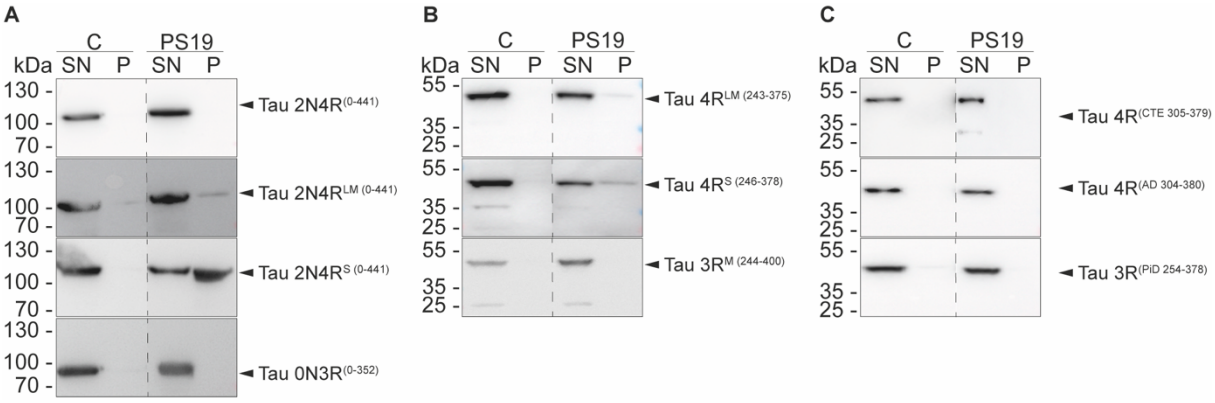

Figure 13 Sedimentation assay confirms the aggregation of full-length Tau 2N4R$^{LM\ (0\text{-}441)}$, full-length Tau 2N4R$^{S\ (0\text{-}441)}$, Tau 4R$^{LM\ (243\text{-}375)}$ RD, and Tau 4R$^{S\ (246\text{-}378)}$ RD fragments induced by PS19 Tau 1N4R$^{S\ (0\text{-}441)}$ brain homogenate. (A-C) Sedimentation assay with cell extract of HEK cells expressing full-length Tau, Tau RD fragments and cryoEM Tau cire fragments. PS19 1N4R$^{S\ (0\text{-}441)}$ brain homogenate was added to induce aggregation. Cells were 1-2x re-induced and were cultured over 4-6 passages. Tau was detected using **(A)** anti-Tau-5 #AHB0042 antibody, **(B)** anti-Tau ab64193 (Tau 4R$^{LM\ (243\text{-}375)}$, Tau 4R$^{S\ (246\text{-}378)}$), anti-GFP (Tau 3R$^{M\ (244\text{-}400)}$), and **(C)** anti-GFP antibody. P: Pellet. SN: Supernatant. kDa: kilodalton. Three **(A-C)** independent experiments were carried out with similar results.

5.5 Homo- and heterotypic seeding of Tau variants by recombinant 0N3R$^{(0\text{-}352)}$ fibrils

The previous experiments revealed that Tau 4R seeds could not seed Tau 3R variants in our cell model, confirming the 4R:3R seeding barrier observed *in vitro* and *in cellula* (Yu et al., 2012; Tarutani et al., 2021; Longhini et al., 2024). In contrast, former studies have demonstrated that recombinant Tau 3R$^{(244\text{-}372,\ \Delta R2)}$ fibrils seed Tau 3R$^{(244\text{-}372,\ \Delta R2)}$ and Tau 4R$^{(244\text{-}372)}$ without a 3R:4R seeding barrier *in vitro* (Dinkel et al., 2011; Yu et al., 2012; Weismiller et al., 2018). To test if recombinant Tau 3R seeds could induce Tau 3R and 4R aggregates in our cell panel, cells were exposed to 1.5 µM recombinant Tau 0N3R$^{(0\text{-}352)}$ fibrils, kindly provided by the Zweckstetter lab. The cryoEM structure for the cofactor-free assembled recombinant

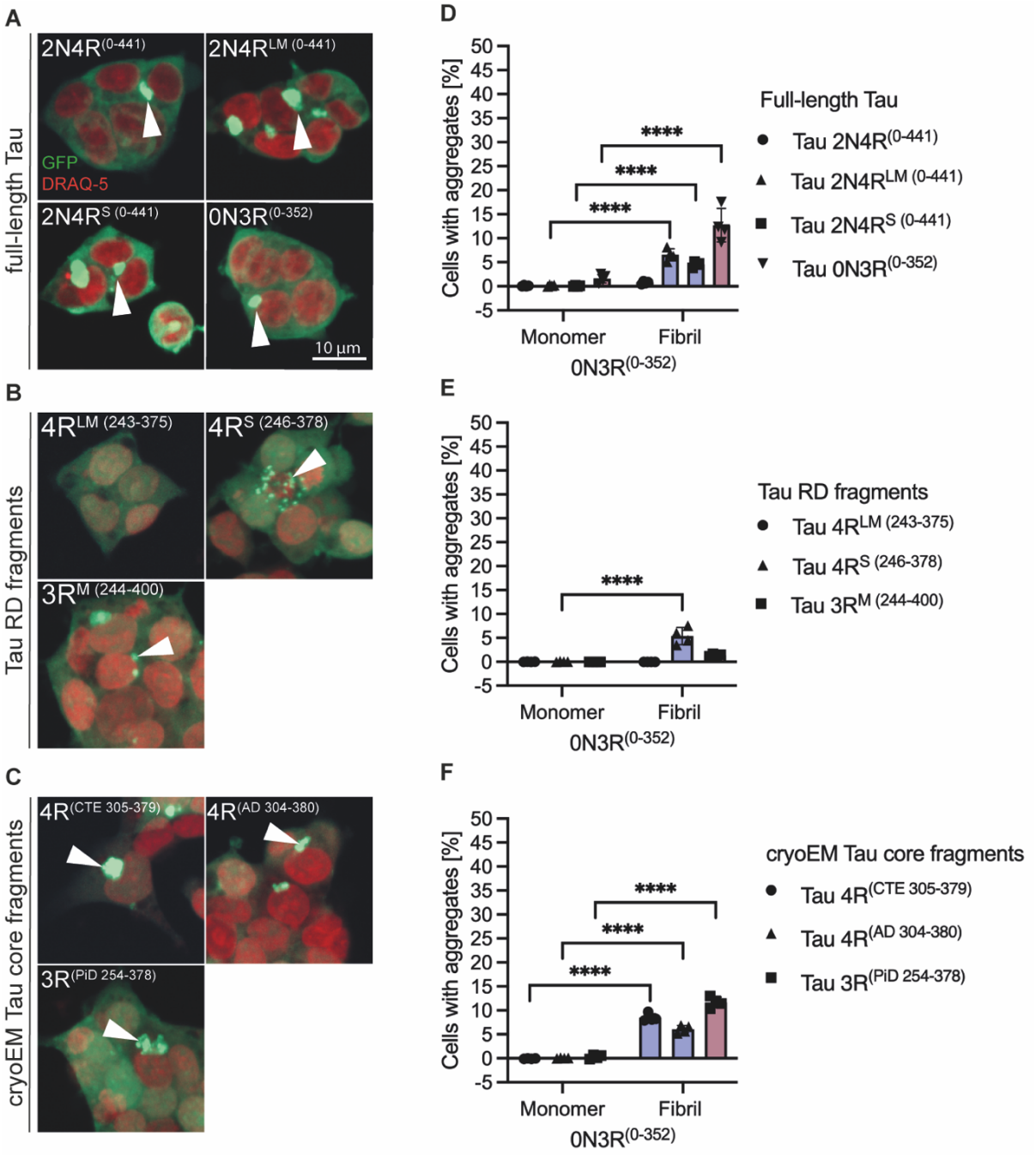

Figure 14 Recombinant 0N3R$^{(0-352)}$ fibrils induce Tau 3R and 4R variant aggregation. (A-C) Representative confocal images of GFP-tagged **(A)** full-length Tau, **(B)** Tau RD fragments, and **(C)** cryoEM Tau core fragments stably expressed in HEK cells. Cells were induced with 1.5 µM recombinant 0N3R$^{(0-352)}$ fibrils and fixed after 48 hours. Nuclei were stained with DRAQ-5. Arrowheads indicate cytosolic aggregates of the corresponding Tau variant. **(D-F)** Tau aggregate quantification. Pink: Cell lines expressing Tau 3R. Blue: Cell expressing Tau 4R. Cells treated with recombinant 0N3R$^{(0-352)}$ monomer served as control. The percentage of cells with aggregated Tau was calculated as the number of aggregate-positive cells per total cells, set to 100 %. Data are presented as mean ± SD (n=4). Two-way ANOVA was used for statistical analysis. The mean was compared to the control (P: **** >0.0001). Three **(D-F)** independent experiments with four technical replicates were carried out with similar results. Scalebar: 10 µm.

Tau 0N3R$^{(0-352)}$ fibril still needs to be resolved. Still, NMR analysis and protease digestion revealed residues similar to the rigid core of Tau fibrils from 3R PiD patients (Chakraborty et al., 2023). Consistent with the published data, full-length Tau, Tau RD fragments, and cryoEM

Tau core fragments showed recombinant Tau 0N3R$^{(0\text{-}352)}$ fibril-induced aggregates independent of the expressed Tau 3R or 4R variant (Figure 14 A-C). Surprisingly, the Tau 4R$^{LM\ (243\text{-}375)}$ RD fragments were the only Tau variant not seeded. Further, quantification showed less than 1 % of cells containing full-length Tau 2N4R$^{(0\text{-}441)}$ aggregates. Cells expressing full-length Tau 2N4R$^{LM\ (0\text{-}441)}$ had 7 %, full-length Tau 2N4R$^{S\ (0\text{-}441)}$ 5 %, and full-length Tau 0N3R$^{(0\text{-}352)}$ 13 % cells with aggregates (Figure 14 D). Tau 4R$^{S\ (246\text{-}378)}$ RD fragments exhibited a seeding efficiency of 5 % when exposed to recombinant Tau 0N3R$^{(0\text{-}352)}$ fibrils (Figure 14 E). Interestingly, recombinant Tau 0N3R$^{(0\text{-}352)}$ fibrils did not seed Tau 4R$^{LM\ (243\text{-}375)}$ RD fragments, and Tau 3R$^{M\ (244\text{-}400)}$ RD fragments showed aggregation in less than 1 % of the cells. In contrast, recombinant Tau 0N3R$^{(0\text{-}352)}$ fibrils seeded all cryoEM Tau core fragments (Figure 14 E). Cells expressing cryoEM Tau 4R$^{(CTE\ 305\text{-}379)}$ showed 8 %, cryoEM Tau 4R$^{(AD\ 304\text{-}380)}$ 6 %, and cryoEM Tau 3R$^{(PiD\ 254\text{-}378)}$ core fragments 12 % cells with aggregates after the exposure to recombinant Tau 0N3R$^{(0\text{-}352)}$ fibrils (Figure 14 F). The highest seeding efficiency was observed in cells expressing full-length Tau 0N3R$^{(0\text{-}352)}$. It may have a similar conformation to the recombinant Tau 0N3R$^{(0\text{-}352)}$ fibrils because the sequence shares identical residues, possibly resulting in a similar amyloid core conformation. In conclusion, we confirmed that in our cell panel, the homo- and heterotypic aggregation of Tau 3R and 4R variants is possible by recombinant Tau 0N3R$^{(0\text{-}352)}$ fibrils. All cell lines except cells that express Tau 4R$^{LM\ (243\text{-}375)}$ RD fragments can be used for recombinant Tau 0N3R$^{(0\text{-}352)}$ seed detection. The seeding barrier between recombinant Tau 0N3R$^{(0\text{-}352)}$ fibrils and Tau 4R$^{LM\ (243\text{-}375)}$ RD fragments expressed in cells remains to be elucidated. As hypothesised, recombinant Tau 0N3R$^{(0\text{-}352)}$ fibrils have homo- and heterotypic seeding capabilities in our cell model, consistent with the literature.

5.6 CryoEM Tau 3R$^{(PiD\ 254\text{-}378)}$ core fragments that have been seeded with PiD brain homogenate induce more selective Tau aggregation than recombinant Tau 0N3R$^{(0\text{-}352)}$ fibrils

In our cell panel, recombinant Tau 0N3R$^{(0\text{-}352)}$ fibrils can induce Tau 3R and 4R variants expressed in cells. Recombinant Tau 0N3R$^{(0\text{-}352)}$ fibrils supposedly resemble the fibril core of Tau fibrils from PiD patients, previously shown by NMR (Chakraborty et al., 2023). Still, it was shown that Tau 3R fibrils obtained from the brain homogenate of PiD patients resulted in a 3R:4R seeding barrier toward Tau 1N4R$^{(0\text{-}412)}$ and seeded only Tau 1N3R$^{(0\text{-}381)}$ (Tarutani et al. 2021). As our cryoEM Tau 3R$^{(PiD\ 254\text{-}378)}$ core fragment represents the residues of the amyloid core of PiD patients, we investigated whether the aggregated cryoEM Tau 3R$^{(PiD\ 254\text{-}378)}$ core fragments have a similar seeding pattern to recombinant Tau 0N3R$^{(0\text{-}352)}$ fibrils, or to Tau 3R fibrils from PiD patients. Therefore, we chose a cell extract that was obtained from HEK cells

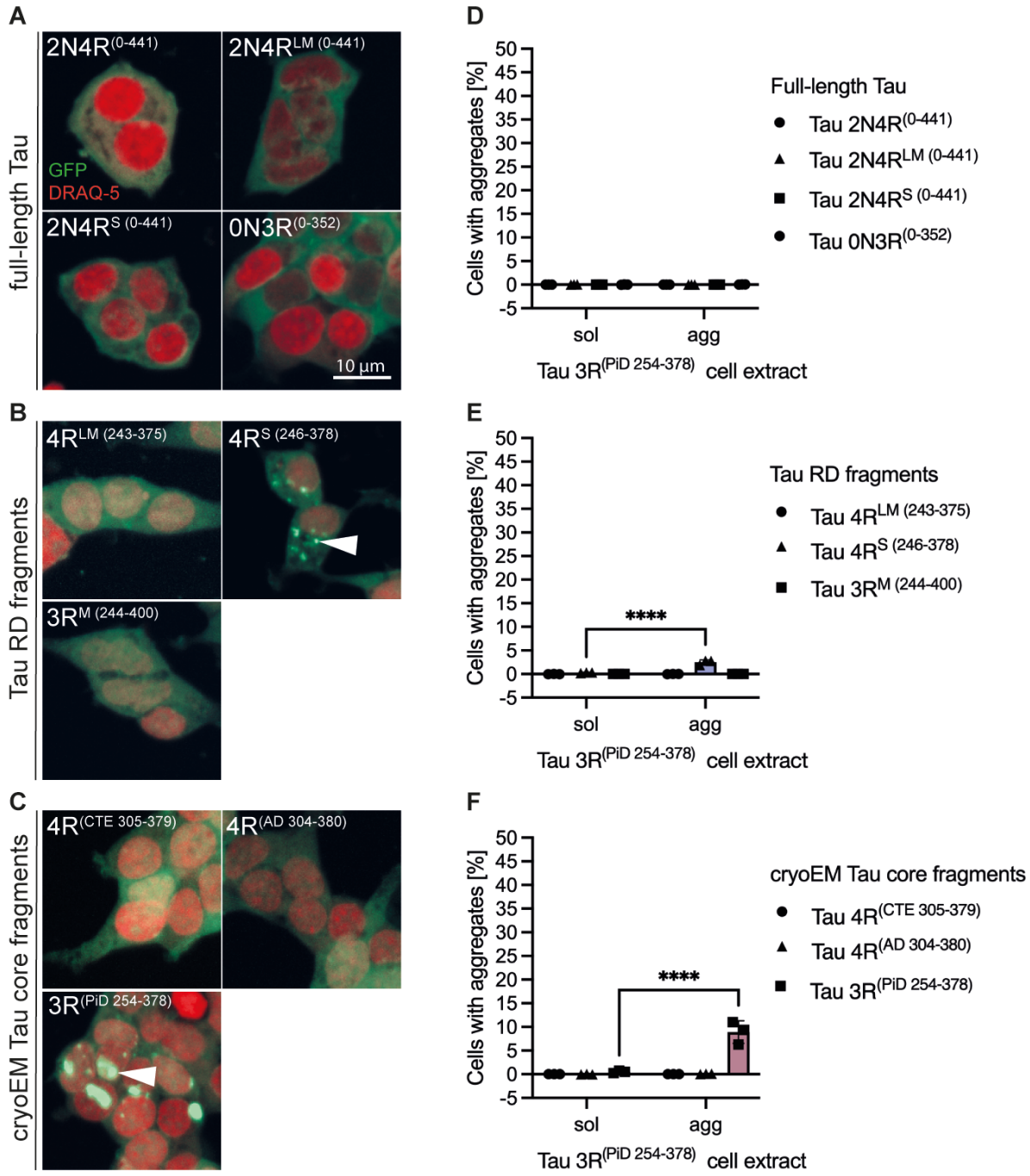

Figure 15 Tau 3R$^{(PiD\ 254-378),\ agg}$ cell extract seeds Tau 4R$^{S\ (246-378)}$ and Tau 3R$^{(PiD\ 254-378)}$ variants. (A-C) Representative confocal images of GFP-tagged **(A)** full-length Tau, **(B)** Tau RD fragments, and **(C)** cryoEM Tau core fragments stably expressed in HEK cells and exposed to cell extract containing 3R PiD aggregates (PiD^{agg}). Nuclei were stained with DRAQ-5. Arrowheads indicate cytosolic aggregates of the corresponding Tau variant. **(D-F)** Tau aggregate quantification. Cells treated with soluble PiD cell extract served as controls. The percentage of cells with aggregated Tau was calculated as the number of aggregate-positive cells per total cells, set to 100 s%. Data are presented as mean ± SD (n=4). Two-way ANOVA was used for statistical analysis. The mean was compared to the control (P: **** >0.0001. Three **(D-F)** independent experiments with three technical replicates were carried out with similar results. Sol: Soluble. Agg: Aggregated.

stably propagating the aggregated cryoEM Tau 3R$^{(PiD\ 254-378)}$ core fragments (Tau 3R$^{(PiD\ 254-378),\ agg}$ cell extract), initially induced with human 3R PiD brain homogenate. The cryoEM Tau 3R$^{(PiD\ 254-378)}$ core fragment differs in length from the recombinant Tau 0N3R$^{(0-352)}$ fibril, as the

N-terminus and the first 10 residues of R1 are removed. In addition, the C-terminus is 26 residues longer. Cell extract from HEK cells expressing soluble cryoEM Tau 3R$^{(PiD\ 254\text{-}378)}$ core fragments was used as a control and did not induce aggregation of the Tau variants in any cell line. In contrast to the recombinant Tau 0N3R$^{(0\text{-}352)}$ fibrils, full-length Tau variants were not seeded by Tau 3R$^{(PiD\ 254\text{-}378),\ agg}$ cell extract (Figure 15 A). Tau 4R$^{S\ (246\text{-}378)}$ RD fragments and the core fragment of the cryoEM Tau 3R$^{(PiD\ 254\text{-}378)}$ were the only variants that developed aggregates when exposed to Tau 3R$^{(PiD\ 254\text{-}378),\ agg}$ cell extract (Figure 15 B-C). Aggregate quantification confirmed that none of the cell lines expressing full-length Tau variants were induced (Figure 15 D). Cells expressing the Tau 4R$^{S\ (246\text{-}378)}$ RD fragments had fewer aggregates (3 %) than cells expressing the cryoEM Tau 3R$^{(PiD\ 254\text{-}378)}$ core fragments (9 %) (Figure 15 E-F). The seeding efficiency of recombinant Tau 0N3R$^{(0\text{-}352)}$ fibrils and Tau 3R$^{(PiD\ 254\text{-}378),\ agg}$ cell extract was similar in cells expressing Tau 4R$^{S\ (246\text{-}378)}$ RD fragments and cryoEM Tau 3R$^{(PiD\ 254\text{-}378)}$ core fragments. CryoEM Tau 3R$^{(PiD\ 254\text{-}378)}$ core fragment aggregates seem to have a specific amyloid core conformation that is compatible only with the sequence of Tau 4R$^{S\ (246\text{-}378)}$ RD fragments and the sequence of cryoEM Tau 3R$^{(PiD\ 254\text{-}378)}$ core fragments expressed in cells. We conclude that the Tau 3R$^{(PiD\ 254\text{-}378),\ agg}$ cell extract contains aggregates with a specific conformation that are most compatible with the sequence of the cryoEM Tau 3R$^{(PiD\ 254\text{-}378)}$ core fragments because the sequence is the same and may allow a similar amyloid core conformation. Consequently, the seeding pattern of the Tau 3R$^{(PiD\ 254\text{-}378),\ agg}$ cell extract is highly selective in that it mainly seeds cryoEM Tau 3R$^{(PiD\ 254\text{-}378)}$ core fragments and a few Tau 4R$^{S\ (246\text{-}378)}$ RD fragments. Hence, its seeding pattern differs from recombinant Tau 0N3R$^{(0\text{-}352)}$ fibrils, which seed Tau 3R and 4R. The seeding pattern of Tau 3R$^{(PiD\ 254\text{-}378),\ agg}$ cell extract is closer to that of Tau 3R fibrils from PiD patients because it mainly seeds the Tau 3R variant. This may be due to the length of the cryoEM Tau 3R$^{(PiD\ 254\text{-}378)}$ core fragment, which may allow only distinct intramolecular interactions to build the amyloid core similar to the Tau fibrils isolated from PiD patients. Further studies are needed to investigate this aspect. These findings argue that aggregated cryoEM Tau 3R$^{(PiD\ 254\text{-}378)}$ core fragments have a distinct seeding pattern that is more selective than that of recombinant 0N3R$^{(0\text{-}352)}$ fibrils and closely resembles that of Tau fibrils obtained from PiD patient brain homogenate. This finding confirms that the cryoEM Tau fragments may adopt intramolecular interactions similar to the Tau amyloid fibrils obtained from patient brains, enabling a specific disease-associated core fold.

5.7 Tau 3R and 4R variants expressed in cells can discriminate between 3R, 4R and 3R/4R Tauopathies

So far, we have demonstrated that within our cell panel, Tau 4R variants are seeded by recombinant Tau 2N4R$^{L\ (0\text{-}441)}$ fibrils and PS19 Tau 1N4R$^{S\ (0\text{-}411)}$ brain homogenate. In contrast, Tau 3R variants are not seeded by Tau 4R fibrils due to a 4R:3R seeding barrier. Interestingly, recombinant 0N3R$^{(0\text{-}352)}$ fibrils seeded Tau 3R and 4R variants. Contrary to that, Tau 3R$^{(PiD\ 254\text{-}378),\ agg}$ cell extract mainly seeded the cryoEM Tau 3R$^{(PiD\ 254\text{-}378)}$ core fragment, suggesting that the cryoEM Tau fragment was able to form intramolecular interactions similar to Tau amyloid fibrils obtained from patient brains, enabling a specific core fold. As the cryoEM structures of the used seeds in this project are unknown, except for Tau aggregates obtained from PS19 1N4R$^{S\ (0\text{-}441)}$ brain homogenate, it is difficult to determine if the observed seeding barriers are physiologically relevant. However, the previous experiments helped to establish the cell lines and understand the general sensitivity and specificity of the used full-length Tau, Tau RD fragments, and cryoEM Tau core fragments towards Tau 3R or 4R seeds. Brain homogenate from Tauopathy patients can be used to obtain Tau seeds with biologically relevant structures. Patient-derived Tau fibrils allow us to investigate if the cell lines are sensitive enough to detect Tau seeds from patient brains and if they can discriminate between Tauopathies. In addition, seeding differences between recombinant and human Tau fibrils and aggregation differences between the Tau RD fragments and the shorter cryoEM Tau core fragments can be uncovered using the cell panel. To the best of our knowledge, no cell panel has yet been established to detect and discriminate between 3R and 4R Tauopathies with cells expressing cryoEM Tau core fragments.

To test if Tau aggregation can be induced in the cell lines and if distinct seeding patterns can be used to discriminate between Tauopathies, we examined 64 brain homogenates of Tauopathy patients. Here, we show representative results from 29 brain samples: Healthy controls (C-C5), 3R PiD (1-7), 4R CBD (7-12), 4R PSP (13-17), and 3R/4R AD (18-24). First, the presence of Tau aggregates in the brains of patients was verified. The samples were diluted to 20 µg of total protein in SDS-supplemented lysis buffer and were used for filter trap assay (FTA) (Figure 16). The brains of healthy control patients (C) did not show a signal, as amorphous aggregates and soluble proteins will unfold and pass through the membrane. Only amyloid aggregates will be captured on the membrane as amyloid resists SDS treatment. All 4R CBD, 4R PSP, 3R PiD, and 3R/4R samples showed signals, though of varying intensity. The highest levels of aggregates were detected in 3R PiD brain homogenate sample 1, 4R CBD brain homogenate samples 9 and 12, 4R PSP brain homogenate samples 15, 17 and 18, and 3R/4R AD brain homogenate sample 22. Low amounts of Tau aggregates were found

in 4R PSP brain homogenate samples 13, 14, and 16 and 3R/4R AD brain homogenate samples 19 and 20. A caveat is that we only detect large Tau amyloid aggregates with the FTA, while we lose the small, potentially toxic and seeding competent Tau species, such as oligomeric Tau (Chang and Kuret, 2008). We conclude that all Tauopathy brains, except the controls, contain amyloidogenic Tau, with varying amounts of total aggregated Tau.

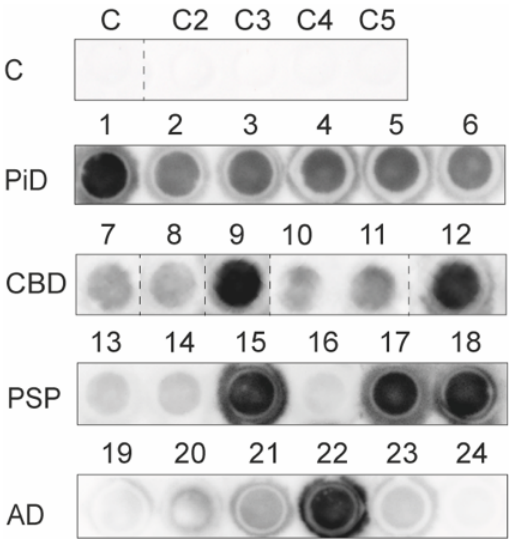

Figure 16 3R PiD, 4R CBD, 4R PSP, and 3R/4R AD patient brain homogenates contain Tau aggregates. Brain homogenates were diluted in SDS-containing lysis buffer to 20 µg total protein and used for FTA. Samples were incubated for 10 minutes on the PVDF membrane. Numbers correspond to individual patient brains: 1-6 PiD, 7-12 CBD, 13-18 PSP, 19-24 AD and C-C5 healthy controls. C: Control. Anti-Tau antibody (MBD) was used to detect Tau.

As the presence of Tau aggregates was confirmed by FTA, the Tauopathy brain homogenates were used to test if the Tau variants expressed in our cell panel could be seeded and if our cell panel could discriminate between Tau 3R and 4R fibrils. Cells expressing Tau $3R^{M\ (244\text{-}400)}$ RD fragments and cryoEM Tau $3R^{(PiD\ 254\text{-}378)}$ core fragments were used as cell lines for Tau 3R variants, and cells expressing Tau $4R^{S\ (246\text{-}378)}$ RD fragments and cryoEM Tau $4R^{(AD\ 304\text{-}380)}$ core fragments were chosen as representative cell lines for Tau 4R variants. These cell lines were selected due to their high sensitivity for patient-derived Tau seeds (Figure 17). The cell lines expressing Tau variants that showed little or no aggregation when exposed to the patient's brain homogenate were excluded. Selected cell lines were exposed to 1.5 µl of brain homogenate from 3R PiD, 4R CBD, 4R PSP, or 3R/4R AD patients *(*Table S1*)*. Notably, the total amount of protein added to the cell was not adjusted to assess whether the cell lines could detect varying amounts of Tau aggregates in the patient's brain homogenates. Representative confocal images showed that 3R PiD brain homogenate seeded the Tau 3R variants and rarely Tau $4R^{(AD\ 304\text{-}380)}$ RD fragments but not cryoEM Tau $4R^{S\ (246\text{-}378)}$ core fragments

(Figure 17 A). 4R CBD and 4R PSP brain homogenate induced Tau $4R^{S\ (246\text{-}378)}$ RD fragments and cryoEM Tau $4R^{(AD\ 304\text{-}380)}$ core fragments but not, or very rarely the Tau 3R variants (Figure 17 B-C). 3R/4R AD brain homogenate seeded all Tau 3R and 4R variants (Figure 17 D). This was expected since AD is a mixed Tauopathy, and Tau 3R and 4R isoforms aggregate when cells expressing Tau variants are exposed to AD brain homogenate (Tarutani et al., 2021; Longhini et al., 2024). The representative confocal images demonstrated that the selected cell lines were sensitive enough to detect Tau seeds in patient brains and that bilateral seeding barriers exist, except for 3R/4R Tauopathies. Automated image analysis was then applied to confirm the specific seeding patterns that could be used to discriminate between 3R, 4R and 3R/4R Tauopathies. Recall that the automated image analysis is based on a fluorescence threshold to detect the GFP-tagged aggregates. Cells expressing soluble Tau variants can have diffuse green dots with a weak GFP intensity that are not considered aggregates but as background and are therefore not counted.

3R PiD brain homogenate was used to determine whether the cells exhibit a specific seeding pattern when exposed to Tau 3R fibrils to discriminate them from Tau fibrils obtained from 4R Tauopathies. Cells expressing Tau $3R^{M\ (244\text{-}400)}$ RD fragments and cryoEM Tau $3R^{(PiD\ 254\text{-}378)}$ core fragments were highly susceptible to Tau seeds from 3R PiD brain homogenate (Figure 17 E). Still, the seeding efficiency highly depends on the amount of Tau 3R seeds within the brain. When induced with 3R PiD brain homogenate sample 1, cells expressing Tau $3R^{M\ (244\text{-}400)}$ RD fragments showed the highest seeding efficiency of 32 % of cells with aggregates. 3R PiD brain homogenate sample 1 also had the strongest signal in the FTA within the 3R PiD brain homogenate samples. 3R PiD brain homogenate samples 2-4 seeded 8-14 % of cells with Tau $3R^{M\ (244\text{-}400)}$ RD fragment aggregates, while 3R PiD brain homogenate samples 5 and 6 induced the weakest Tau $3R^{M\ (244\text{-}400)}$ RD fragment aggregation in the cells (2-4 %). The cells expressing cryoEM Tau $3R^{(PiD\ 254\text{-}378)}$ core fragments showed a similar seeding pattern, with 3R PiD brain homogenate sample 1 being the most effective seeder (26 %) and 3R PiD brain homogenate samples 5 and 6 having a low seeding rate of only 2-5 % (Figure 17 F). In cells that express Tau $4R^{S\ (246\text{-}378)}$ RD fragments, 3R PiD brain homogenate seeding was poor (Figure 17 G). In cells that express cryoEM Tau $4R^{(AD\ 304\text{-}380)}$ core fragments, aggregates were only detected for 3R PiD brain homogenate samples 1 and 2 (3-5 %) (Figure 17 H). One limitation of the assay is the amount of Tau seeds within the patient's brain needed to induce detectable aggregation. 3R PiD brain homogenate sample 6 seeding was poor in all four cell lines, independent of the expressed Tau 3R or 4R variant. Therefore, a clear differentiation is only possible when sufficient Tau seeds are within the patient's brain. We conclude that 3R PiD brain homogenate that contains sufficient Tau 3R seeds favours homotypic seeding in cells expressing Tau $3R^{M\ (244\text{-}400)}$ RD fragments and cryoEM Tau $3R^{(PiD\ 254\text{-}378)}$ core fragments,

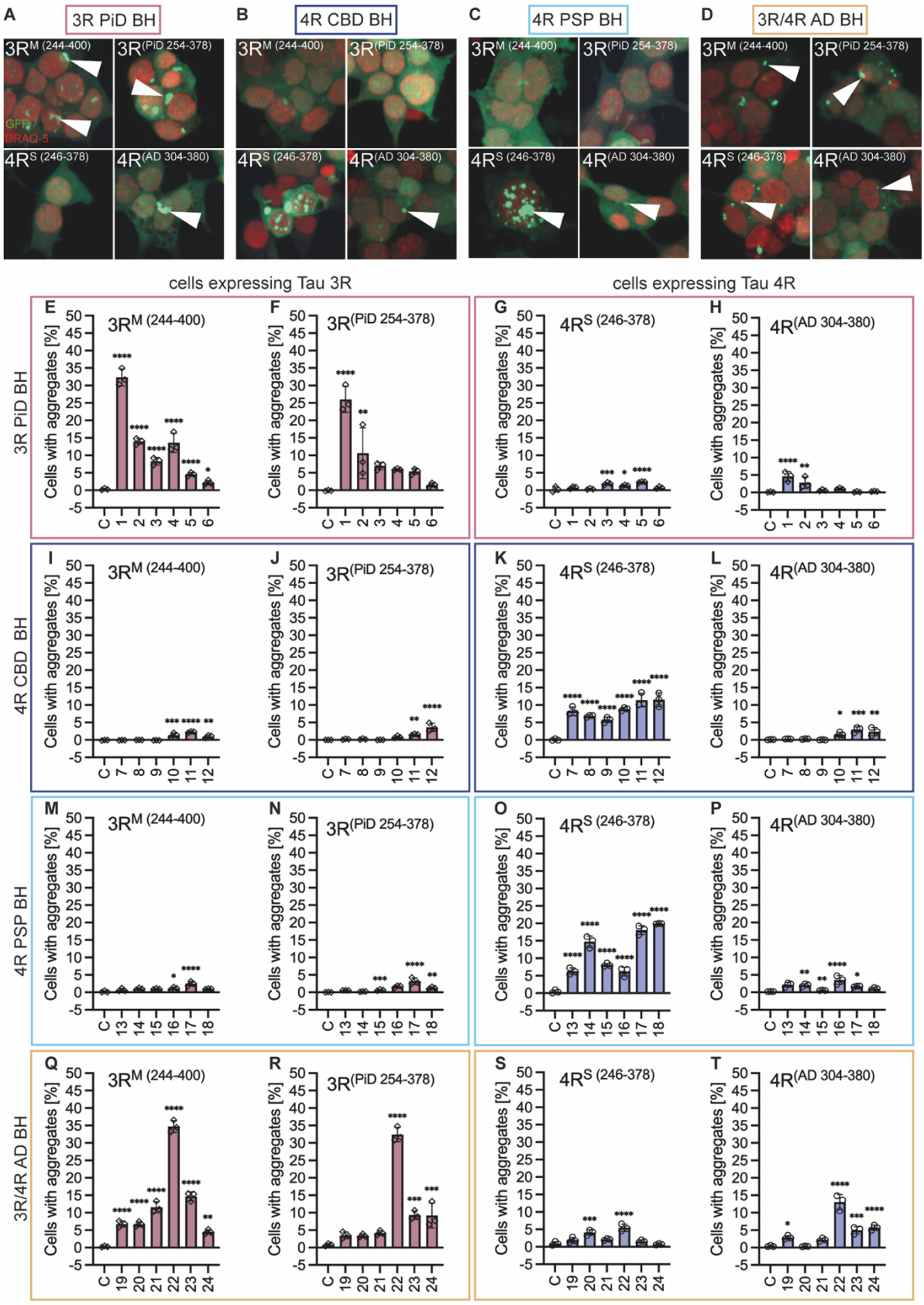
A
3R PiD BH
B
4R CBD BH
C
4R PSP BH
D
3R/4R AD BH
3RM (244-400)
3R(PiD 254-378)
4RS (246-378)
4R(AD 304-380)
GFP
DRAQ-5
cells expressing Tau 3R
cells expressing Tau 4R
3R PiD BH
4R CBD BH
4R PSP BH
3R/4R AD BH
Cells with aggregates [%]
E
F
G
H
I
J
K
L
M
N
O
P
Q
R
S
T

Figure 17 Cell lines expressing Tau 3R$^{M\ (244\text{-}400)}$ RD fragments, cryoEM Tau 3R$^{(PiD\ 254\text{-}378)}$ core fragments, Tau 4R$^{S\ (246\text{-}378)}$ RD fragments, and cryoEM Tau 4R$^{(AD\ 304\text{-}380)}$ core fragments can discriminate between 3R, 4R, and 3R/4R patient brain homogenate. Patient brain homogenate (BH) was added to the soluble Tau-expressing cells. Cells were fixed after 96 hours and imaged with an automated confocal microscope. **(A-D)** Representative images of GFP-tagged HEK Tau 3R$^{M\ (244\text{-}400)}$ RD fragments, cryoEM Tau 3R$^{(PiD\ 254\text{-}378)}$ core fragments, Tau 4R$^{S\ (246\text{-}378)}$ RD fragments, and Tau 4R$^{(AD\ 304\text{-}380)}$ core fragments cells seeded by 3R PiD, 4R CBD, 4R PSP, and 3R/4R AD brain homogenate. **(E-T)** Automated image analysis using fluorescence intensities determined the percentage of cells with aggregated Tau variants. Numbers on the X-axis indicate individual patients: 1-6 PiD, 7-12 CBD, 13-18 PSP, 19-24 AD. C: Control. BH: Brain homogenate. Results are presented as mean ± SD (n=3). One-way ANOVA was used for statistical analysis. Means were compared to the control (P: **** >0.0001). Three **(E-T)** independent experiments were carried out with similar results.

with only weak heterotypic seeding in cells expressing Tau 4R$^{S\ (246\text{-}378)}$ RD fragments and cryoEM Tau 4R$^{(AD\ 304\text{-}380)}$ core fragments. In contrast, recombinant 0N3R$^{(0\text{-}352)}$ fibrils induced robust seeding in cells expressing Tau 3R and 4R, which reveals that the recombinant 0N3R$^{(0\text{-}352)}$ fibril conformation may be different from Tau fibrils obtained from PiD patients. The cells that express the Tau 3R variants showed similar 3R PiD brain homogenate seeding patterns despite the length differences between the Tau 3R$^{M\ (244\text{-}400)}$ RD fragments and the cryoEM Tau 3R$^{(PiD\ 254\text{-}378)}$ core fragments. Thus, the differences in the sequence length by the truncation of 10 residues at the beginning of the core fragment sequences in R1 and 22 residues at the C-terminus do not seem to affect Tau aggregation. This highlights that the cell lines that express Tau 3R variants can be seeded best by Tau 3R aggregates from PiD patient brains, while the cells that express Tau 4R show a 3R:4R seeding barrier towards Tau 3R aggregates with only minimal seeding.

Next, we investigated whether our cell lines had a unique seeding pattern for Tau aggregates obtained from 4R Tauopathy patients to distinguish them from Tau aggregates of 3R patients suffering, for example, from PiD. We used brain homogenate of 4R CBD and 4R PSP patients as Tau 4R seeds. When 4R CBD brain homogenate was used as a seed, the cells expressing Tau 3R variants showed only minimal seeding of 1-4 % (Figure 17 I-J). However, the seeding efficiency increased to 6-12 % of cells with aggregates in cells expressing Tau 4R$^{S\ (246\text{-}378)}$ RD fragments (Figure 17 K). Similar to results obtained with cells expressing Tau 3R variants, 4R CBD brain homogenate samples showed only low to no seeding in cells expressing cryoEM Tau 4R$^{(AD\ 304\text{-}380)}$ core fragments (< 5 %) (Figure 17 L). The seeding pattern of the 4R PSP brain homogenate was comparable to that of the 4R CBD brain homogenate (Figure 17 M-P). Tau 3R variants expressed in cells could not, or only minimally, be seeded (< 3 %) (Figure 17 M-N). Cells expressing Tau 4R$^{S\ (246\text{-}378)}$ RD fragments were best seeded by 4R PSP brain homogenate with 4-20 % of cells with aggregates, whereas cells expressing cryoEM Tau 4R$^{(AD\ 304\text{-}380)}$ core fragments showed only 2-4 % cells with aggregates (Figure 17 O-P). Despite the strong FTA signals of 4R PSP samples 15 and 18 and the same amount of protein added (2.8 µg in 1.5 µl) (Table S1) to the cells, we show that the seeding efficiency varied. In particular, it is not

necessarily correlated to the FTA signal and the total amount of protein added to the cells. This may be because the FTA cannot detect small seeding-competent Tau species. If this unknown fraction of small, seeding-competent Tau species is not correlated to the amount of protein, it can account for the differences. We conclude that 4R CBD and 4R PSP brain homogenate induced minimal Tau 3R aggregate formation due to the 4R:3R seeding barrier, as seen for recombinant Tau $2N4R^{L\ (0\text{-}441)}$ fibrils and PS19 Tau $1N4R^{S\ (0\text{-}412)}$ brain homogenate. 4R CBD and 4R PSP brain homogenates seeded Tau $4R^{S\ (246\text{-}378)}$ RD fragments and only weakly seeded cryoEM Tau $4R^{(AD\ 304\text{-}380)}$ core fragments, suggesting that cryoEM Tau $4R^{(AD\ 304\text{-}380)}$ core fragments may not be compatible with the 4R CBD and 4R PSP fibril core conformation. This allows us to reliably detect Tau aggregates obtained from 4R Tauopathies using the cells expressing Tau $4R^{S\ (246\text{-}378)}$ RD fragments. In contrast, the cells expressing the Tau 3R variants and those expressing cryoEM Tau $4R^{(AD\ 304\text{-}380)}$ core fragments show minimal seeding activity. This confirms the bilateral seeding barrier between Tau 3R and 4R isoforms and highlights that the cryoEM Tau $4R^{(AD\ 304\text{-}380)}$ core fragments are incompatible with the fibril cores of Tau 3R and 4R seeds derived from patients. In addition, we can use the cells expressing Tau $3R^{M\ (244\text{-}400)}$ RD fragments, cryoEM Tau $3R^{(PiD\ 254\text{-}378)}$ core fragments and Tau $4R^{S\ (246\text{-}378)}$ RD fragments to discriminate between 3R and 4R Tauopathies as the seeding patterns are different between Tau 3R and 4R seeds. Only within 4R Tauopathies, like 4R CBD and 4R PSP, discrimination is not feasible with our cell model.

Subsequently, we used 3R/4R AD brain homogenate to determine if we get a third seeding pattern that we could use to distinguish between 3R, 4R and 3R/4R Tauopathies. 3R/4R AD brain homogenate contains Tau 3R and 4R aggregates. Therefore, we expected 3R/4R AD brain homogenate to induce Tau aggregates in all four cell lines. Strikingly, the cells expressing the Tau 3R variants were most sensitive to 3R/4R AD brain homogenate. Cells expressing Tau 3R variants had up to 35 % of cells with aggregates when exposed to 3R/4R AD brain homogenate sample 22 (Figure 17 Q-R). By contrast, only a maximum of 5 % of cells with aggregates were detected in the cells expressing Tau $4R^{S\ (246\text{-}378)}$ RD fragments (Figure 17 S), and 13 % of cells with aggregates in cells expressing cryoEM Tau $4R^{(AD\ 304\text{-}380)}$ core fragments (Figure 17 T). The cryoEM Tau $4R^{(AD\ 304\text{-}380)}$ core fragments expressed by the cells showed minimal to no seeding when exposed to Tau seeds from 3R or 4R Tauopathies. Conversely, it was most compatible with the Tau aggregates obtained from 3R/4R AD patients. 3R/4R AD brain homogenate containing Tau 3R and 4R aggregates showed significantly higher seeding potency in cells expressing Tau 3R than in cells expressing Tau 4R. This could be attributed to increased Tau 3R seeds in the brain homogenate or decreased conformational compatibility between the Tau 4R variants expressed in the cell lines and the 3R/4R AD brain homogenate seeds. The cryoEM Tau

$4R^{(AD\ 304\text{-}380)}$ core fragments were seeded best by the 3R/4R brain homogenate, which may be due to the length of the construct, which potentially allows the adoption of the specific conformation of the AD amyloid core. Hence, it shows the highest seeding activity when Tau 3R/4R seeds from AD patients are used. When exposed to a 3R/4R Tauopathy brain homogenate with sufficiently high Tau seed concentration, we conclude that all four cell lines should exhibit seeding activity, with Tau 3R variants being seeded best, followed by the Tau 4R variants. The seeding pattern differs from Tau aggregates in 3R and 4R Tauopathies, where only the respective Tau 3R or Tau 4R variants show increased numbers of cells with aggregates.

Our results demonstrate for the first time that the combination of the four cell lines, composed of Tau RD fragments and cryoEM Tau core fragments, can be used to discriminate between 3R, 4R, and 3R/4R Tauopathies given that sufficient amounts of seeds are present in the sample for seed induction in our cell panel. Tau aggregates from 3R Tauopathies can be identified by the seeding barrier towards Tau 4R variants, which allows mainly the seeding of Tau 3R variants. In this case, HEK cells expressing Tau $3R^{M\ (244\text{-}400)}$ RD fragments and cryoEM Tau $3R^{(PiD\ 254\text{-}378)}$ core fragments can detect 3R Tauopathies with high numbers of cells with aggregates. In contrast, cells expressing Tau 4R variants will show only a minimal number of cells with aggregates. The truncated R1 and C-terminus of the cryoEM Tau $3R^{(PiD\ 254\text{-}378)}$ core fragments did not affect the aggregation potential compared to the Tau $3R^{M\ (244\text{-}400)}$ RD fragments. Therefore, both Tau 3R variants are suitable for Tau 3R aggregate detection. To identify Tau aggregates from 4R Tauopathies, cells expressing Tau $4R^{S\ (246\text{-}378)}$ RD fragments can be used in contrast to the cells expressing Tau 3R variants. Due to the 4R:3R seeding barrier, more cells with aggregates should be detected in the cells expressing the Tau $4R^{S\ (246\text{-}378)}$ RD fragments when Tau aggregates from 4R Tauopathy patients are added. CryoEM Tau $4R^{(AD\ 304\text{-}380)}$ core fragments expressed in HEK cells showed minimal seeding activity in the presence of Tau 3R or 4R aggregates and were most seeded with 3R/4R AD brain homogenate. This suggests that cryoEM Tau core fragments may be highly selective for their disease-specific seed conformation, as the length of the expressed cryoEM Tau core fragment can potentially adapt only to specific conformations. More cryoEM Tau core fragments must be expressed in cells to confirm this hypothesis. So far, we can only discriminate between 3R, 4R and 3R/4R Tauopathies but not between Tauopathies with the same isoform, like 4R CBD and 4R PSP. Nevertheless, the different seeding patterns between the full-length Tau, Tau RD fragments and the cryoEM Tau core fragments induced with recombinant Tau fibrils, transgenic mouse or patient brain homogenate highlight the importance of using disease-relevant models. The fibril assembly conditions, as well as the length of the Tau variants, could have an impact on conformation-dependent seeding.

6 Discussion

6.1 A semi-automated compound screen identified two Tau aggregation inhibitors

Tauopathies, such as AD, CBD, CTE, and PiD, are characterised by the ordered assembly of Tau into amyloid fibrils. It is proposed that Tau aggregates can spread between cells intercellularly to different brain regions (Braak and Braak, 1991; Novak et al., 2011). Since pathological Tau can be toxic and Tau levels in the brain correlate with clinical symptoms, such as cognitive decline, inhibiting Tau aggregation is a potential therapeutic strategy to prevent or slow disease progression. This study used our previously established semi-automated high-content screen to identify further Tau aggregation inhibitors. Two hits, C22 and C57, were identified in a pool of over 144 compounds.

C22 potently inhibited GFP-tagged Tau $4R^{LM\ (243\text{-}375)}$ aggregation in HEK cells. C22 had an IC_{50} of 1.5 µM when incubated for 48 hours with the cells exposed to Tau $2N4R^{L\ (0\text{-}441),\ agg}$ cell extract. At 17.5 µM of C22, less than 2 % of cells with aggregates were detected. The reduced number of cells with aggregates in the presence of C22 was independent of the used Tau seeds, such as recombinant Tau fibrils or Tau seeds obtained from brain homogenate of transgenic mice or EVs from cells stably propagating Tau aggregates. Only the IC_{50} varied. For cells exposed to PS19 Tau $1N4R^{S\ (0\text{-}412)}$ brain homogenate and C22, the C22 IC_{50} was 7.5 µM. When EVs derived from HEK cells stably propagating Tau GFP^{AD} aggregates were used as seeds, the C22 IC_{50} was 5.5 µM. The total Tau in the PS19 Tau $1N4R^{S\ (0\text{-}412)}$ brain homogenate and EVs is unknown, which may explain the discrepancy in the C22 IC_{50}. Interestingly, the inhibition of Tau aggregation with C22 was only efficient within a specific time window of 7 hours after seed addition. Once Tau aggregation was initiated, the effect of C22 in inhibiting Tau aggregation decreased drastically. Tau aggregation increased, the later C22 was administered to the cells, to the point where it had no effect. This suggests that once a certain amount of Tau seeds has entered the cell and the prion-like replication of Tau aggregates in the cytosol has begun, it is difficult to intervene in the process. C22 is thought to target Tau directly. Further investigation is needed to determine whether it also affects cellular mechanisms involved in Tau aggregation. One possible time point of inhibition could be cell entry. Tau entry into cells has been suggested to be regulated via HSPGs and LRP1 (Rauch et al., 2018; Rauch et al., 2020). Knockdown of LRP1 in cells and *in vivo* prevented Tau endocytosis. The RD and the N-terminus appear to interact with the LRP1 domain. Hence, the target of C22 could be the RD, N-terminus or LRP1 to prevent Tau aggregation in the cytosol by inhibiting the uptake of pathological Tau from the extracellular space. Another

proposed mechanism by which Tau enters the cytosol is through nanoscale lysosomal membrane damage (Rose et al., 2024). How Tau damages the membrane remains to be elucidated. Another possible time point of C22 to intervene in the aggregation process could be the enhanced clearance of soluble Tau and Tau aggregates. C22 inhibited aggregation not only of Tau but also of NM. This shows that the effect of C22 might be independent of the Tau amyloid protein. *In vitro,* C22 reduced the ThT signal when incubated with recombinant Tau $2N4R^{L\,(0\text{-}441)}$ fibrils (Prof. Dr. Zweckstetter, personal communication). This confirms that C22 binds to the amyloid fibril. Whether C22 also has an effect at the cellular level needs further investigation. C57 also showed a promising impact on Tau aggregation when added to the cells before the Tau seeds. The IC_{50} is similar to C57 (1.7 µM) and C22 (1.5 µM). In contrast, once Tau aggregation was initiated, C57 had no impact on Tau aggregation. Whether C22 and C57 share a similar target on the amyloid fibrils and whether they are involved in cellular processes that might inhibit Tau aggregation needs further study. As C22 cannot cross the BBB, derivatives of C57 are being tested, which might be as effective as C22. C57 has not shown overt cytotoxicity and can be tested *in vivo*. Therefore, C57 could be used as a drug to prevent Tau aggregation, which may be best administered at early disease stages. This emphasises the importance of early diagnosis of Tauopathies in line with rapid advances in blood-based biomarkers.

6.2 A cell panel to investigate Tau aggregation and to differentiate between Tauopathies

Several cell models have been established to study Tau uptake, inter- and intracellular propagation, and transmission. Many of these models use Tau 4R isoforms or truncated Tau fragments, transiently or stably expressed by HEK or other cell lines. CryoEM has demonstrated that Tauopathies are associated with different Tau amyloid core folds. Tauopathies present with a range of clinical symptoms, potentially due to the accumulation of Tau aggregates with specific amyloid cores comprising certain polypeptide regions of the Tau 3R and 4R isoforms. However, the precise impact of the diverse Tau amyloid folds on the prion-like propagation of Tau aggregates remains to be elucidated. This project used HEK cells expressing full-length Tau 3R and 4R isoforms, Tau RD fragments, and the recently identified cryoEM Tau core fragments of AD, CBD, CTE and PiD amino-terminally fused to monomeric GFP. We investigated their tendency to aggregate spontaneously and their aggregation upon exposure to Tau 3R and 4R amyloid fibrils from different sources. Further, we studied the possible discrimination between Tauopathies based on specific seeding patterns of Tau fibrils isolated from patients. The novel cell panel is anticipated to be a valuable tool in identifying pharmacological agents that impede the induction of disease-specific Tau aggregation. Further, it can be used to understand the cellular mechanisms underlying Tau aggregation, propagation and transmission. The findings of this study may contribute to developing novel therapeutic strategies for inhibiting or reducing Tau aggregation by compounds.

6.2.1 Spontaneous aggregation of cryoEM Tau core fragments

To study the spontaneous aggregation of full-length Tau, Tau RD fragments, and cryoEM Tau core fragments, they were transiently overexpressed in HEK cells. In its native state, Tau is a highly soluble, intrinsically disordered protein with little tendency to aggregate (Chirita et al., 2005; Mandelkow and Mandelkow, 2012). It is not known what initiates the self-assembly of Tau *in vivo*, but it has been suggested that anionic lipid membranes facilitate the aggregation of Tau (Chirita et al., 2003; Zhao et al., 2004; Kuret et al., 2005). Dysfunctional endolysosomal pathways could increase the levels of Lipofuscin, which has been proposed to capture Tau monomers and induce their conformational change (Ihara et al., 2012; Wischik et al., 2018; Pasquale et al., 2022). Imbalances of the Tau 3R:4R ratio caused by mutations affecting exon 10 can also lead to Tau pathology (Niblock and Gallo, 2012). Among others, PTMs such as phosphorylation could additionally facilitate Tau aggregation (Lindwall and Cole, 1984; Mandelkow et al., 1995; Iqbal et al., 2005; Chang et al., 2011; Takeda et al., 2015; Heinisch

and Brandt, 2016). In this project, we have shown that the full-length Tau 4R and 3R isoforms do not spontaneously aggregate in cells. Whether the Tau variants expressed in our cell panel have PTMs is unknown. The Tau RD fragments also did not self-aggregate when transiently overexpressed by HEK cells as seen by others. The N- and C-terminus are suggested to fold back onto the RD in a "paperclip" loop, preventing spontaneous aggregation of full-length Tau and the Tau RD fragments by shielding the aggregation-prone motifs within the RD (Jeganathan et al., 2006; Wang et al., 2007). In detail, the N-terminal inserts (N1, N2) mask the core aggregation motifs via electrostatic repulsion (Hou et al., 2021). In addition, the residues of the C-terminus have been shown to play an important role in inhibiting Tau aggregation (Abraha et al., 2000). Tau $3R^{(243\text{-}380,\ \Delta R2)}$ and Tau $4R^{(243\text{-}380)}$ only aggregated spontaneously when the S320F mutation, known from FTDP-17, was inserted in R3 (Strang et al., 2018; Chen et al., 2023) or the Tau $4R^{(244\text{-}372,\ \Delta K280)}$ was used (Khlistunova et al., 2006). Strikingly, in our cell model, the transient overexpression of all cryoEM Tau core fragments resulted in the formation of spontaneous aggregates that stained positive with the amyloid dye Amylo Glo. Spontaneous aggregation was the fastest when all R1 and R2 residues were missing, as for the cryoEM $Tau^{(AD\ 306\text{-}378)}$ core fragment. This finding is supported by Carlomagno et al., who showed that AD fibrils corresponding to our $Tau^{(AD\ 306\text{-}378)}$ construct assembled spontaneously when incubated *in vitro* without an inducer but with continuous agitation (Carlomagno et al., 2021). All cryoEM Tau core fragments expressed in our cell panel contain the amyloid motif ^{306}VQIVYK^{311} (PHF6) in R3. Amyloid motifs are directly involved in aggregation (Bergen et al., 2000). PHF6 is incorporated into the fibril core of Tau 3R and 4R as it forms the cross-β-structure (Fitzpatrick et al., 2017). The Tau $4R^{LM\ (243\text{-}375)}$ RD, Tau $4R^{S\ (246\text{-}378)}$ RD fragment, and the cryoEM Tau $4R^{(CBD\ 274\text{-}380)}$ core fragment contain an additional amyloid motif ^{275}VQIINK^{280} (PHF6*) in R2, which is also buried within the fibril core of all Tau 4R variants (Zhang et al., 2020). The PHF6* or PHF6 amyloid motif is located at the beginning of our cryoEM Tau core fragments, except for the cryoEM Tau $3R^{(PiD\ 254\text{-}378)}$ core fragment. The cryoEM $Tau^{(AD\ 306\text{-}378)}$ core fragment, the shortest Tau variant used in our cell panel, directly starts with PHF6. The other cryoEM Tau core fragments have additional N-terminal residues at the beginning of the core sequence. This might explain the high propensity of the cryoEM $Tau^{(AD\ 306\text{-}378)}$ core fragment to spontaneously aggregate as the N- and C-terminus are removed and the amyloid motifs are exposed. Consequently, the protective "paperclip" loop is disrupted, potentially enabling spontaneous aggregation (Wischik et al., 1996; Wang et al., 2007; Wischik et al., 2018). CryoEM Tau $4R^{(AD\ 304\text{-}380)}$, Tau $4R^{(CTE\ 305\text{-}379)}$, and Tau $3R^{(CTE\ 274\text{-}379)}$ core fragments start one or two residues before the PHF6 but differ in one residue at the C-terminus and lack all or most of R2. CryoEM Tau $4R^{(CBD\ 274\text{-}380)}$ core fragments incorporate all of R2, which could influence its higher propensity to spontaneously aggregate because of

both amyloid motifs, PHF6* in R2 and PHF6 in R3. In contrast, the PHF6 in our cryoEM Tau 3R$^{(PiD\ 254-378)}$ core fragments is shielded by R1, which might reduce the number of cells with spontaneous aggregates. This suggests that residues flanking the PHF6* and PHF6, as well as residues at the N- and C-terminus, could affect the spontaneous aggregation of Tau. The mechanism of spontaneous Tau aggregation of the transiently expressed cryoEM Tau fragments and the potential role of PTMs remains to be elucidated. However, the cryoEM Tau core fragments that aggregate spontaneously could be used to rapidly screen for Tau aggregation inhibitors without needing exogenous Tau fibrils.

6.2.2 The proteasome clears cryoEM Tau core fragments prone to spontaneous aggregation

Limited proteolysis of pathogenic proteins and increased protein levels are implicated in neurodegeneration. Proteasomal and autophagic degradation systems regulate the clearance of physiological and pathophysiological forms of Tau (Rubinsztein, 2006). Conversely, proteolytic cleavage can result in the formation of aggregates (Gamblin et al., 2003; Rissman et al., 2004; Wang et al., 2007; Dufty et al., 2007). In our cell model, we showed that the transient expression of Tau led to spontaneous aggregation of the cryoEM Tau core fragments, which were not cleared by the cells. Although previous studies suggested that the UPS and ALP did not interact with P301L mutated Tau 2N4R$^{(0-441)}$ aggregates stably propagated in cells (Guo et al., 2016), autophagic vacuoles and ubiquitinated NFTs can be found in AD patients in the affected brain regions (Cole and Timiras, 1987; Brion et al., 1989; He et al., 1993; Nixon et al., 2005). In our model, the stable expression did not lead to spontaneous aggregation of any Tau variants. This might be because transient transfection results in a high plasmid copy number per cell and, consequently, high protein expression levels (Fus-Kujawa et al., 2021). In contrast, lentiviral transduction usually results in only a few integration events with lower protein expression levels. High protein levels of intracellular Tau can lead to spontaneous aggregation, as described previously (Seidler et al., 2019). Therefore, transient expression might favour spontaneous aggregation of the short cryoEM Tau fragments, whereas stable transfection results in lower protein levels, preventing spontaneous aggregation. Full-length Tau, Tau RD fragments, cryoEM Tau 4R$^{(CTE\ 305-379)}$, cryoEM Tau 4R$^{(AD\ 304-380)}$ and cryoEM Tau 3R$^{(PiD\ 254-378)}$ core fragments could be stably expressed, as confirmed by immunofluorescence and WB. Lentiviral transduction of cryoEM Tau$^{(AD\ 306-378)}$, Tau 4R$^{(CBD\ 274-380)}$ and Tau 3R$^{(CTE\ 274-379)}$ core fragments resulted in low protein levels with weak GFP signals and WB bands. The soluble Tau protein, which is intrinsically disordered, can be degraded directly by the 20S proteasome or ubiquitin-dependent by the 26S proteasome (Liu et al., 2003; Guharoy et al., 2018; Opoku-Nsiah and Gestwicki, 2018). This could be the reason for the low protein levels of the cryoEM Tau$^{(AD\ 306-378)}$, Tau 4R$^{(CBD\ 274-380)}$ and Tau 3R$^{(CTE\ 274-379)}$ core

fragments. To confirm the proteasomal degradation of cryoEM Tau$^{(AD\ 306\text{-}378)}$, Tau 4R$^{(CBD\ 274\text{-}380)}$ and Tau 3R$^{(CTE\ 274\text{-}379)}$ core fragments in the cells, we used the proteasome inhibitor MG132. Previous studies have shown that proteasomal inhibition can increase Tau protein levels in cells by preventing Tau clearance (Della David et al., 2002; Liu et al., 2009). Protein levels of cryoEM Tau$^{(AD\ 306\text{-}378)}$, Tau 4R$^{(CBD\ 274\text{-}380)}$ and Tau 3R$^{(CTE\ 274\text{-}379)}$ core fragments were increased when proteasomal clearance was inhibited with MG132, followed by spontaneous aggregation. To prevent elevated protein levels of the cryoEM Tau$^{(AD\ 306\text{-}378)}$, Tau 4R$^{(CBD\ 274\text{-}380)}$ and Tau 3R$^{(CTE\ 274\text{-}379)}$ core fragments, the cells might upregulate the ubiquitin ligases for enhanced proteasomal degradation to prevent spontaneous Tau aggregation. The proteasome cannot properly degrade Tau aggregates, which contributes to neurodegeneration (Wang et al., 2010; Myeku et al., 2016; Cheng et al., 2018; Boland et al., 2018). The ALP could take over in this case as it clears larger, longer-lived proteins and aggregates (Johansen and Lamark, 2011). The role of the ALP was not investigated in our study. Another possibility could be the natural selection of cells with a weak expression of the cryoEM Tau$^{(AD\ 306\text{-}378)}$, Tau 4R$^{(CBD\ 274\text{-}380)}$ and Tau 3R$^{(CTE\ 274\text{-}379)}$ core fragments during single-cell cloning, possibly favouring cells without detrimental spontaneous Tau aggregation and, therefore, cells with low protein levels of the cryoEM Tau$^{(AD\ 306\text{-}378)}$, Tau 4R$^{(CBD\ 274\text{-}380)}$ and Tau 3R$^{(CTE\ 274\text{-}379)}$ core fragments. The protein levels of the soluble cryoEM Tau core fragments in the cells might be a critical factor that could facilitate Tau aggregation. Stably expressed cryoEM Tau 4R$^{(CTE\ 305\text{-}379)}$, cryoEM Tau 4R$^{(AD\ 304\text{-}380),}$ and cryoEM Tau 3R$^{(PiD\ 254\text{-}378)}$ core fragments did not show spontaneous aggregation over several cell passages. Whether and why the protein level threshold for spontaneous aggregation is lower of the cryoEM Tau 4R$^{(CTE\ 305\text{-}379)}$, cryoEM Tau 4R$^{(AD\ 304\text{-}380)}$ and cryoEM Tau 3R$^{(PiD\ 254\text{-}378)}$ core fragments remains to be elucidated. The degradation of soluble Tau could prevent spontaneous aggregation. In contrast to our data, it has been shown that inhibition of the proteasome blocks the rapid formation of Tau aggregates in HEK cells expressing P301S mutated Tau 0N4R. This suggests that the proteasomal pathway can also promote Tau fibril fragmentation (Cliffe et al., 2019; Dimou et al., 2023). Furthermore, the valosin-containing protein (VCP) was identified to disaggregate Tau aggregates in a ubiquitin- and proteasome-dependent manner in primary mouse neurons, generating seeding-competent Tau species (Saha et al., 2023). This shows that proteasomal degradation can be beneficial in preventing Tau aggregation and detrimental in neurodegeneration, as the proteasome can either clear aggregation-prone Tau monomers or enhance Tau propagation. How cells perceive the increased propensity of Tau to aggregate spontaneously at high protein levels needs to be further investigated. The HEK cells stably expressing the cryoEM Tau core fragments could be used to examine the molecular mechanisms that promote and prevent spontaneous aggregation.

6.2.3 4R:3R seeding barrier between Tau 3R variants and Tau 4R variants that lack parts of R2

To study if Tau 4R seeds could induce aggregation of Tau 4R variants and whether a Tau 4R:3R seeding barrier exists, we used recombinant Tau 2N4R$^{L\ (0\text{-}441)}$ fibrils and PS19 Tau 1N4R$^{S\ (0\text{-}412)}$ brain homogenate as Tau 4R seeds. Although recombinant Tau fibrils have been widely used to investigate the prion-like aggregation of Tau, many of these fibrils have been assembled using heparin. Heparin assists and stabilises the formation of Tau aggregates (Goedert et al., 1996; Kampers et al., 1996; Pérez et al., 1996). Yet, this results in a heterogeneous structure of the fibrils that differs from the structure of amyloid fibrils found in patients (Fichou et al., 2018; Zhang et al., 2019). To address this issue, we used cofactor-free assembled recombinant Tau 2N4R$^{L\ (0\text{-}441)}$ fibrils, which have a rigid core similar to CBD patient fibrils, as shown by NMR (Chakraborty et al., 2021). It remains to be determined if the cryoEM structures confirm the NMR data. The PS19 Tau 1N4R$^{S\ (0\text{-}412)}$ amyloid fibril core was resolved by cryoEM and resembled an intermediate core length of heparin-induced and AD Tau fibrils (Schweighauser et al., 2023). We have shown that with the cofactor-free recombinant Tau 2N4R$^{L\ (0\text{-}441)}$ fibrils and the PS19 Tau 1N4R$^{S\ (0\text{-}412)}$ brain homogenate, solely the induction of mutated full-length Tau 4R variants and Tau 4R RD fragments was possible. This finding is supported by the observation that recombinant Tau 4R$^{(244\text{-}372)}$ can seed recombinant Tau 4R$^{(244\text{-}372)}$ monomers but not recombinant Tau 3R$^{(244\text{-}372,\ \Delta R2)}$ monomers *in vitro* (Dinkel et al., 2011; Yu et al., 2012). Seeds composed of fibrillised Tau 4R peptides that include R2 and R3 also induced only Tau variants in cells expressing full-length Tau 2N4R$^{(0\text{-}441)}$ but not full-length Tau 2N3R variants (Longhini et al., 2024). This suggests different conformations of Tau 4R seeds that contain R2 and Tau 3R monomers that lack R2, resulting in a 4R:3R seeding barrier. Our wildtype Tau 2N4R$^{(0\text{-}441)}$ variant was an exception, which the Tau 4R seeds could not aggregate. This confirmed previous studies showing that recombinant P301L mutated Tau 2N4R$^{(0\text{-}441)}$ fibrils cannot induce wildtype full-length Tau 2N4R$^{(0\text{-}441)}$ (Aoyagi et al., 2007). Conversely, it has been shown that recombinant full-length wildtype Tau 2N4R$^{(0\text{-}441)}$ fibrils can recruit full-length wildtype Tau 2N4R$^{(0\text{-}441)}$ and also Tau 0N3R$^{(0\text{-}352)}$ monomers. Still, recombinant P301L mutated Tau 2N4R$^{(0\text{-}441)}$ fibrils cannot seed wildtype full-length Tau 2N4R$^{(0\text{-}441)}$ or Tau 3R variants (Kumar and Udgaonkar, 2018; Weismiller et al., 2018). Stepwise truncation of the C-terminus of recombinant wildtype Tau 2N4R$^{(0\text{-}441)}$ fibrils eliminated its ability to seed Tau 3R monomers. Deletion of the N-terminus increased the 4R:3R seeding barrier between recombinant full-length wildtype Tau 2N4R$^{(0\text{-}441)}$ fibrils and Tau 3R monomers (Kumar and Udgaonkar, 2018; Weismiller et al., 2018). This suggests a synergistic role in Tau aggregation for N- and C-terminal residues. In our cell panel, the 4R:3R seeding barrier between recombinant mutated Tau 2N4R$^{L\ (0\text{-}441)}$ fibrils or PS19 Tau 1N4R$^{S\ (0\text{-}412)}$ fibrils and Tau

3R isoforms is further supported by the finding that the insertion of P301 mutations, such as P301L and P301S, creates a strong 4R:3R seeding barrier (Kumar and Udgaonkar, 2018; Weismiller et al., 2018). P301 mutations alter the Tau 4R conformation, making surface contact with Tau 3R monomers nearly impossible (Hilary Ann Weismiller, 2019). P301 mutations are frequently found in familial 4R Tauopathies, highlighting their crucial role in forming specific conformers during aggregation (Goedert, 2005). P301L increases the aggregation propensity of Tau by lowering the energetic barriers, allowing cross-β-sheet formation. This facilitates the formation of intermolecular hydrophobic contacts for fibril assembly (Vigers et al., 2023). It has also been shown that Tau 3R seems to be protected against aggregation by an extensive hydrogen bonding network, which is less stable in Tau 4R (Longhini et al., 2024). This instability lowers the energy barrier of Tau 4R, which facilitates its aggregation. Surprisingly, in our cell model, the aggregation of cryoEM Tau $4R^{(CTE\ 305\text{-}379)}$ and Tau $4R^{(AD\ 304\text{-}380)}$ core fragments containing only 1-2 residues of R2 was impossible with recombinant Tau $2N4R^{L\ (0\text{-}441)}$ fibrils and PS19 Tau $1N4R^{S\ (0\text{-}412)}$ brain homogenate. The R2-R4 are buried in the fibril cores of recombinant Tau $2N4R^{L\ (0\text{-}441)}$ fibrils and PS19 Tau $1N4R^{S\ (0\text{-}412)}$ fibrils. In contrast, cryoEM Tau $4R^{(CTE\ 305\text{-}379)}$ and Tau $4R^{(AD\ 304\text{-}380)}$ core fragments lack most of R2 at the beginning of the core fragment, except for 1-2 residues. This may make them structurally incompatible with the fold of the Tau 4R seeds that contain all of R2-R4 in their fibril core. The presence of different core units within the fibril structure, with or without mutations, and the fragment length might lead to different fibril conformations and create 4R:3R seeding barriers, as well as a seeding barrier between Tau 4R seeds that contain all of R2 and Tau 4R variants with a truncated R2. Thus, expressing the cryoEM Tau core and Tau RD fragments in cells can help to determine the essential roles of the N-, C-terminus and the RD in Tau seeding barriers, structural compatibility, aggregation, and propagation.

6.2.4 Conformational differences between recombinant Tau $0N3R^{(0\text{-}352)}$ fibrils and Tau seeds formed by brain homogenate-seeded cryoEM Tau $3R^{(PiD\ 254\text{-}378)}$ core fragments could explain different seeding barriers

The observed 4R:3R cross-seeding barrier was asymmetric in our cell panel, as recombinant Tau $0N3R^{(0\text{-}352)}$ fibrils induced aggregates in all cell lines except in cells expressing Tau $4R^{LM\ (243\text{-}375)}$ RD fragments. This is in line with the finding that recombinant Tau $3R^{(244\text{-}372,\ \Delta R2)}$ fibrils can seed both recombinant Tau $4R^{(244\text{-}372)}$ and Tau $3R^{(244\text{-}372,\ \Delta R2)}$ monomers *in vitro* (Dinkel et al. 2011). The reasons for the asymmetric cross-seeding barrier have not yet been solved. In contrast to the findings that recombinant Tau 3R fibrils can seed recombinant Tau 3R and 4R monomers, it was shown that Tau 3R fibrils from brain homogenate of PiD patients had a 3R:4R seeding barrier (Tarutani et al. 2021). We studied if the cryoEM Tau $3R^{(PiD\ 254\text{-}378)}$ core

fragments expressed in our cell panel can be seeded with Tau 3R fibrils derived from PiD patients. Recombinant Tau 0N3R$^{(0\text{-}352)}$ fibrils contain the same amino acid residues in the rigid core (~260-380, ΔR2) that also form the cryoEM PiD core (254-378, ΔR2) in PiD patients (Chakraborty et al., 2023). We used cell extract from HEK cells expressing cryoEM Tau 3R$^{(PiD\ 254\text{-}378)}$ core fragments stably propagating Tau 3R$^{(PiD\ 254\text{-}378),\ agg}$. Tau 3R$^{(PiD\ 254\text{-}378),\ agg}$ was initially seeded with 3R PiD brain homogenate. The exact structure of the core of fibrils propagated in these cells is unknown. Interestingly, Tau 3R$^{(PiD\ 254\text{-}378),\ agg}$ cell extract induced only aggregates in cell lines expressing Tau 4R$^{S\ (246\text{-}378)}$ RD fragments and cryoEM Tau 3R$^{(PiD\ 254\text{-}378)}$ core fragments, albeit to different degrees. Tau 3R$^{(PiD\ 254\text{-}378),\ agg}$ cell extract seeded best cells expressing cryoEM Tau 3R$^{(PiD\ 254\text{-}378)}$ core fragments and only a few cells expressing Tau 4R$^{S\ (246\text{-}378)}$ RD fragments. The cryoEM Tau 3R$^{(PiD\ 254\text{-}378)}$ core fragment expressed in cells covers the exact residues of the Tau amyloid core found in PiD patients. Therefore, it may only enable selective intramolecular interactions similar to the ones within the cryoEM core fragment of the Tau 3R$^{(PiD\ 254\text{-}378),\ agg}$ in the cell extract. Thus, the Tau 3R$^{(PiD\ 254\text{-}378),\ agg}$ seeding pattern differs from that of recombinant Tau 0N3R$^{(0\text{-}352)}$ fibrils. Even though recombinant Tau 0N3R$^{(0\text{-}352)}$ fibrils and Tau 3R$^{(PiD\ 254\text{-}378),\ agg}$ contain the same residues that form the amyloid core in PiD Tau fibrils, the length of the whole construct and the residues included within the fibril core might result in different intramolecular interactions and thus amyloid folds. Tau 3R$^{(PiD\ 254\text{-}378),\ agg}$ more closely resembles the pattern of Tau 3R fibrils from PiD patients by mainly seeding the Tau 3R variant. Still, we do not know the conformation of the aggregated cryoEM Tau 3R$^{(PiD\ 254\text{-}378)}$ fragments within our cells. Tarutani and colleagues showed that the fibril conformation of Tau 1N3R$^{(0\text{-}381)}$ or 1N4R$^{(0\text{-}412)}$ expressed in cells is similar but not identical to Tau fibrils derived from patients (Tarutani et al., 2023). However, our cryoEM Tau core fragments might allow only specific intramolecular interactions that potentially adopt the original Tau fibril conformation found in patients more closely. Therefore, future experiments will include cryoEM of the aggregated cryoEM Tau core fragments obtained from our cells. We conclude that the length of the Tau seeds and the residues within the fibril core play an important role in seeding barriers. The shorter the Tau variant, the more selective the conformation of the amyloid cores will be, likely because of the decreased possibility of intramolecular interactions. Combining the exact polypeptide sequence of the fibril core region with patient-derived fibrils might enable replication of the specific amyloid core conformation of the Tau fibrils isolated from Tauopathies.

Table 15 Seeding barriers between Tau 3R and 4R variants.

Fibril	Source	Tau variant	*In vitro/ In cellula*	Seeding barrier	Seeding	Reference
Tau 3R$^{(244\text{-}372,\ \Delta R2)}$	Recombinant	Tau 3R$^{(244\text{-}372,\ \Delta R2)}$	*In vitro*	-	Yes	(Dinkel et al. 2011)
		Tau 4R$^{(244\text{-}372)}$	*In vitro*	-	Yes	(Dinkel et al. 2011)
Tau 4R$^{(244\text{-}372)}$	Recombinant	Tau 3R$^{(244\text{-}372,\ \Delta R2)}$	*In vitro*	4R:3R	No	(Dinkel et al. 2011)
		Tau 4R$^{(244\text{-}372)}$	*In vitro*	-	Yes	(Dinkel et al., 2011)
3R PiD brain homogenate (all six Tau isoforms)	PiD patient	Tau 1N3R$^{(0\text{-}381)}$	*In cellula*	-	Yes	(Tarutani et al. 2021)
		Tau 1N4R$^{(0\text{-}412)}$	*In cellula*	3R:4R	No	(Tarutani et al., 2021)
Tau 0N3R$^{(0\text{-}352)}$	Recombinant	Tau 0N3R$^{(0\text{-}352)}$ Tau 3R$^{M\ (244\text{-}400)}$ Tau 3R$^{(PiD\ 254\text{-}378)}$	*In cellula*	-	Yes	Our study
		Tau 2N4R$^{(0\text{-}441)}$ Tau 2N4R$^{LM\ (0\text{-}441)}$ Tau 2N4R$^{S\ (0\text{-}441)}$ Tau 4R$^{S\ (246\text{-}378)}$ Tau 4R$^{(AD\ 304\text{-}380)}$	*In cellula*	-	Yes	Our study
Tau 3R$^{(PiD\ 254\text{-}378),\ agg}$ cell extract	Cell line propagating Tau 3R$^{(PiD\ 254\text{-}378),\ agg}$ after seeding with PiD BH	Tau 4R$^{S\ (246\text{-}378)}$ RD fragments	*In cellula*	-	Minimal seeding	Our study
		cryoEM Tau 3R$^{(PiD\ 254\text{-}378)}$ core fragments	*In cellula*	-	Yes	Our study

6.2.5 3R:4R seeding barrier between Tau 3R fibrils from PiD brain homogenate and Tau 4R variants expressed in cells

Patient brain homogenates can be used to study Tau aggregation and propagation to avoid the uncertainty of the given structure of recombinant Tau fibrils, Tau aggregates induced *in cellula*, and formed in Tau transgenic mice. In this project, cells expressing Tau $3R^{M\ (244\text{-}400)}$ RD fragments, cryoEM Tau $3R^{(PiD\ 254\text{-}378)}$ core fragments, Tau $4R^{S\ (246\text{-}378)}$ RD fragments and cryoEM Tau $4R^{(AD\ 304\text{-}380)}$ core fragments were exposed to brain homogenate from PiD patients with Tau 3R fibrils. Only the cell lines expressing Tau 3R variants showed a high number of cells with aggregates. In contrast, cells expressing Tau 4R variants showed a 3R:4R seeding barrier with only minimal numbers of cells with aggregates. This is consistent with previous studies reporting that PiD brain homogenate can induce mainly Tau 3R and only minimal Tau 4R variants expressed in cells (Nonaka et al., 2010; Woerman et al., 2016; Tarutani et al., 2021). In contrast, recombinant Tau $0N3R^{(0\text{-}352)}$ fibrils could seed Tau 3R and Tau 4R aggregation in the cells. This suggests that although the recombinant fibrils were assembled *in vitro* without cofactors (Chakraborty et al., 2023), the PiD Tau fibril conformation in the brains of the patients might still differ from the core conformation of the recombinant Tau $0N3R^{(0\text{-}352)}$ fibrils. As the cell extract containing cryoEM Tau $3R^{(PiD\ 254\text{-}378),\ agg}$, initially induced with PiD brain homogenate, mainly induced cryoEM Tau $3R^{(PiD\ 254\text{-}378)}$ core fragment aggregates, it more closely resembles the seeding pattern of 3R PiD patient fibrils. This suggests that the initial Tau seed from the PiD patient imprinted its conformation onto cellular cryoEM Tau $3R^{(PiD\ 254\text{-}378)}$, leading to a conformation-dependent seeding pattern. Conformation-dependent Tau seeding was also observed when Tau aggregates were isolated from the PiD patient's brain and introduced into cells expressing Tau $1N3R^{(0\text{-}381)}$ (Tarutani et al., 2021). The Tau $3R^{M\ (244\text{-}400)}$ variant has been used in a real-time quaking-induced conversion (RT-QuIC) seed amplification assay to detect 3R and 3R/4R Tau seeds (Metrick et al., 2020). In our cell assay, the Tau $3R^{M\ (244\text{-}400)}$ variant also faithfully detected 3R PiD and 3R/4R AD seeds, independent of the V337M mutation. Interestingly, seeding of the cryoEM Tau $3R^{(PiD\ 254\text{-}378)}$ core fragment PiD brain homogenate was comparable to the seeding of the Tau $3R^{M\ (244\text{-}400)}$ RD fragments. Independent of the truncated R1 and the shorter C-terminus in Tau $3R^{M\ (244\text{-}400)}$ RD. Therefore, we suggest using the cryoEM Tau $3R^{(PiD\ 254\text{-}378)}$ core fragment instead of the Tau $3R^{M\ (244\text{-}400)}$ RD fragments as it might not make a difference in 3R or 3R/4R Tauopathy fibril-induced aggregation but may play a role in spontaneous aggregation as cryoEM Tau $3R^{(PiD\ 254\text{-}378)}$ core fragments spontaneously aggregate and Tau $3R^{M\ (244\text{-}400)}$ RD fragments do not spontaneously aggregate. The challenge is to determine why *in vitro* assembled recombinant Tau $0N3R^{(0\text{-}352)}$ fibrils do not discriminate between Tau 3R and 4R monomers and what contributes to the

selective seeding of Tau 3R by 3R PiD brain homogenate. This highlights the importance of using physiologically relevant Tau seeds to understand Tau aggregation and propagation.

6.2.6 Seeding with 4R CBD and 4R PSP brain homogenates results in a 4R:3R seeding barrier in our cell model

In line with the finding that 3R PiD brain homogenate preferentially seeded Tau 3R variants expressed in the cells, 4R CBD and 4R PSP brain homogenate induced mainly Tau $4R^{S\ (246\text{-}378)}$ RD fragments and only minimally aggregation of Tau 3R variants in the cell lines. This is in line with a general Tau 4R:3R seeding barrier between Tau 4R seeds and Tau 3R monomers, as described by others (Nonaka et al., 2010; Dinkel et al., 2011; Woerman et al., 2016; Tarutani et al., 2021; Longhini et al., 2024). In our cell models, for the 4R:3R seeding barrier, it does not seem to make a difference if recombinant full-length Tau $2N4R^{L\ (0\text{-}441)}$ fibrils, PS19 Tau $1N4R^{S\ (0\text{-}412)}$ fibrils, or 4R CBD/4R PSP Tauopathy brain homogenates were used to induce seeding. Strikingly, the cryoEM Tau $4R^{(AD\ 304\text{-}380)}$ core fragment was not aggregating when cells were exposed to 4R CBD or 4R PSP brain homogenates. This is in line with our previous results, showing that recombinant full-length Tau $2N4R^{L\ (0\text{-}441)}$ and PS19 Tau $1N4R^{S\ (0\text{-}412)}$ fibrils could also not induce the aggregation of cryoEM Tau $4R^{(AD\ 304\text{-}380)}$ core fragments. $CBD^{(274\text{-}380)}$ and $PSP^{(272\text{-}381)}$ cryoEM fibril cores incorporate all residues of R2, R3 and R4 plus 12 residues of the C-terminus (Zhang et al., 2020; Shi et al., 2021; Mishra, 2023). The R2 of the cryoEM Tau $4R^{(AD\ 304\text{-}380)}$ core fragment is truncated and includes only the last two residues of R2. This might lead to a transmission barrier between Tau 4R fibrils with a more extended amyloid core and the R2 truncated cryoEM Tau $4R^{(AD\ 304\text{-}380)}$ core fragments expressed in cells. The correct fibril conformation may not be adopted due to the mismatch of repeats incorporated into the fibril core. Furthermore, CBD has a four-layered fibril core, and PSP has a three-layered fibril core (Zhang et al., 2020; Shi et al., 2021; Mishra, 2023). In contrast, the AD core is only two-layered (Fitzpatrick et al., 2017). This might enhance the conformational barrier between the cryoEM Tau $4R^{(AD\ 304\text{-}380)}$ core fragment and Tau fibrils derived from CBD and PSP patients. The cryoEM Tau $4R^{(AD\ 304\text{-}380)}$ core fragment might not be able to form the intramolecular interactions which are needed for the specific CBD (106 residues)/PSP (109 residues) fibril core conformation, as fewer residues are included within the AD fibril core (67 residues). The cell panel lacks a cell line that expresses a patient-derived cryoEM Tau 4R core fragment that includes all residues of R2, can be stably expressed by the cells without spontaneous aggregation and can be seeded by Tau fibrils. So far, with the Tau $4R^{S\ (246\text{-}378)}$ RD fragments, we can only discriminate between 3R and 4R Tauopathies, but not within 4R Tauopathies, like CBD and PSP. Thus, it is important to include other cryoEM Tau 4R core fragments. For example, cryoEM Tau 4R $PSP^{(272\text{-}381)}$ or cryoEM Tau 4R Argyrophilic Grain

Disease$^{(273/279-381)}$ core fragments. Including more cell lines that express the extended cryoEM Tau 4R core fragments, it can be investigated whether the cryoEM Tau 4R core fragments are generally prone to spontaneous aggregation and if they can be selectively seeded by the corresponding Tau 4R fibrils isolated from Tauopathy patients.

6.2.7 CryoEM Tau 4R$^{(AD\ 304-380)}$ core fragments are selectively seeded by 3R/4R AD brain homogenate

Besides 3R and 4R Tauopathies, there are mixed 3R/4R Tauopathies, such as AD. AD brain homogenate induced Tau 3R and 4R variants expressed by our cells, as expected, but with a preference for Tau 3R variants. Of all seeds used, the cryoEM Tau 4R$^{(AD\ 304-380)}$ core fragments were seeded best by the 3R/4R AD brain homogenate. This contradicts the finding that AD seeds require Tau 3R and 4R co-expression to induce aggregation (Woerman et al., 2016). Our finding that the expression of either Tau 3R or 4R is sufficient for AD brain homogenate-induced aggregation is supported by studies that demonstrated aggregation of either Tau 1N3R$^{(0-381)}$ or 1N4R$^{(0-412)}$ in cells exposed to AD brain homogenate (Tarutani et al., 2021). Results from other groups also revealed that full-length Tau 3R isoforms have faster aggregation kinetics when exposed to AD brain homogenate than full-length Tau 4R isoforms (Wu et al. 2022; He et al. 2020; Tarutani et al. 2021; Tarutani et al. 2023). The reason for the increased aggregation kinetics of Tau 3R isoforms in the presence of 3R/4R AD seeds from patient brains is unknown. However, it is suggested that R2 may play a critical role, as it is the major structural difference between Tau 3R and 4R isoforms. Recent NMR data revealed that AD fibrils recruit either Tau 3R and 4R monomers alone or Tau 3R and 4R monomers in a 40:60 ratio *in vitro* (Dregni et al., 2022). The single and mixed fibrils were found to have the same structure. A mouse line expressing equal amounts of all six Tau isoforms showed that Tau seeds from human Tauopathy brains retained isoform-specific seeding with 4R:3R and 3R:4R seeding barriers *in vivo* (He et al. 2020). When human AD seeds were injected into mice expressing only Tau 3R or 4R, and the resulting AD-3R or AD-4R seeds were reintroduced into mice expressing all six Tau isoforms, Tau 3R and 4R isoforms aggregated. Therefore, He and colleagues suggest that disease-specific seeding is independent of the isoform but somewhat dependent on seed conformation, supported by the cryoEM data (He et al., 2020). In our study, we showed that 3R PiD, 4R CBD, and 4R PSP seeds could only minimally induce the aggregation of the cryoEM Tau 4R$^{(AD\ 304-380)}$ core fragments, whereas 3R/4R AD seeds induced the most cells with cryoEM Tau 4R$^{(AD\ 304-380)}$ core fragment aggregates. The more extended two-layered 3R PiD, four-layered 4R CBD, and three-layered 4R PSP fibril core folds are stabilised by more intramolecular interactions (Zhang et al., 2020; Shi et al., 2021; Mishra, 2023), which the shorter cryoEM Tau 4R$^{(AD\ 304-380)}$ core fragments might not be able to adapt.

The length of the cryoEM Tau 4R$^{(AD\ 304\text{-}380)}$ core fragments may allow only the adoption of the specific conformation of the one-layered AD amyloid core. This confirms that the seed conformation plays an important role in disease-specific seeding. If this is precisely the case for 3R/4R AD brain homogenate, it remains to be seen, as other 3R/4R Tauopathies, such as brain homogenate of 3R/4R CTE patients, need to be tested in our cell model. We demonstrated that the expression of the exact length of the core regions is essential as the shorter cryoEM Tau$^{(AD\ 306\text{-}378)}$ core fragment was more prone to spontaneous aggregation compared to the more extended cryoEM Tau 4R$^{(AD\ 304\text{-}380)}$ core fragment when transiently expressed. Stable expression of the cryoEM Tau$^{(AD\ 306\text{-}378)}$ core fragment was only possible at weak protein levels as it was cleared by the proteasome to probably prevent spontaneous aggregation. Thus, two more residues at the beginning and the end of the cryoEM Tau 4R$^{(AD\ 304\text{-}380)}$ core fragment made it less prone to spontaneous aggregation, demonstrating the importance of the length of Tau constructs in aggregation. Further, the stable expression of the cryoEM Tau 4R$^{(CTE\ 305\text{-}379)}$ core fragment was possible without spontaneous aggregation in the cells. Still, we could not detect cryoEM Tau 4R$^{(CTE\ 305\text{-}379)}$ core fragment aggregation when exposed to brain homogenate of 3R, 4R or 3R/4R Tauopathy patients (data not shown). It could be that cryoEM Tau 4R$^{(CTE\ 305\text{-}379)}$ core fragments can only be seeded by 3R/4R CTE brain homogenate. As for the cryoEM Tau 4R$^{(AD\ 304\text{-}380)}$, core fragment seeding was mainly possible with 3R/4R AD brain homogenate. Interestingly, there is only one residue difference at the beginning and the end between the cryoEM Tau 4R$^{(CTE\ 305\text{-}379)}$ core fragments and the cryoEM Tau 4R$^{(AD\ 304\text{-}380)}$ core fragment. Compared to the AD$^{(304\text{-}380)}$ core fold, the β-helix region of the CTE$^{(305\text{-}379)}$ core fold is less tightly packed, which leads to differences in intramolecular hydrophobic interactions. The more open CTE fold enables a hydrophobic cavity with an unknown proteinaceous density at the tip of the C-shaped CTE fibril core, which is absent in the AD fibril core. Further, they differ in their protofilament-protofilament interface packing (Falcon et al., 2019). These findings highlight that forming different fibril conformations is possible despite similar protein sequences, like in AD and CTE fibril cores. The different fibril core conformations might explain why the cryoEM Tau 4R$^{(CTE\ 305\text{-}379)}$ core fragment could not be seeded by the 3R/4R AD brain homogenate. This demonstrates that the length of the fibril core, cellular environment, and incorporation of cofactors might play an important role in Tau aggregation. Yet, the forces dictating the disease-specific fold remain to be elucidated. Nevertheless, the cryoEM Tau 4R$^{(AD\ 304\text{-}380)}$ core fragment may provide a unique opportunity to selectively identify 3R/4R AD aggregates, as it may have features that only allow the selective seeding by 3R/4R AD brain homogenate.

6.2.8 Cell panel allows discrimination of some Tauopathies

The unique seeding patterns of Tauopathy patient fibrils described above in our cell lines expressing Tau 3R and 4R variants can be used to discriminate between 3R, 4R, and 3R/4R Tauopathies if sufficient amounts of seeds are present in the sample for seed induction. Strikingly, the FTA signal of the patient's brain samples did not always correlate with the seeding activity in the cell panel. This might be due to the differences in the total protein to which the cells were exposed or the fact that the FTA reflects only the amount of amyloidogenic Tau. Soluble seeding competent Tau intermediates, like monomers or oligomers, pass through the membrane. Therefore, the FTA only reproduces parts of seeding competent Tau. In PS19 mice, seed-competent Tau monomers were detected with associated dimers and trimers and only a few larger species formed before oligomeric or fibrillar Tau (Mirbaha et al., 2022). These soluble Tau monomers induced seeding in the cells expressing Tau. The heat-shock protein 70 (HSP70) disaggregation machinery can disassemble pathological Tau extracted from human AD brain tissue, producing mono- and oligomeric Tau species still seeding competent when added to Tau expressed in cells (Nachman et al., 2020). This confirms that amyloidogenic Tau and soluble monomeric, high, and low molecular Tau fragments that the FTA does not capture can induce Tau aggregation. This might explain the high seeding activity of Tauopathy samples despite low FTA signals. Another factor that could influence the total Tau in a given biological sample is the stage of the patient's disease. Here, we used samples from the hippocampus, pons and the superior frontal gyrus (SFG). For example, for PiD, we only obtained hippocampal samples in which PiD bodies can be found at the earliest stage of Braak III (Lee et al., 2001; Kovacs et al., 2013). As the Braak stages for our PiD samples were only available for samples 3 and 6 (Braak stage III), it is possible that there was less Tau overall in the samples as the hippocampus was only starting to be affected by PiD bodies. Although the disease stage of PiD sample 1 (2.8 µg) is unknown, there is likely more total seeding competent Tau within sample 1 than in sample 3 (2.6 µg), as sample 1 induced above 20 % cells with aggregates more than sample 3 (Table S1). In further experiments, the total amount of Tau should be adjusted, for example, by immunoprecipitation, to compare the amount of seeding competent Tau between different disease stages in each sample.

Based on the previously discovered 3R:4R seeding barrier (Tarutani et al., 2021), 3R Tauopathies can be identified in our model by using the Tau 3R cell lines expressing Tau $3R^{M\ (244\text{-}400)}$ RD fragments and cryoEM Tau $3R^{(PiD\ 254\text{-}378)}$ core fragments in comparison to cells expressing the Tau $4R^{S\ (246\text{-}378)}$ RD fragments. The cells expressing Tau 3R variants will predominantly show cells with aggregates, while cells expressing the Tau 4R variants will have minimal amounts of cells with aggregates. The Tau $3R^{M\ (244\text{-}400)}$ RD fragment was

previously used in an RT-QuIC assay and effectively detected 3R PiD aggregates (Metrick et al., 2020), which we confirm in our cell model. The truncated R1 and C-terminus of the cryoEM Tau 3R$^{(PiD\ 254-378)}$ core fragments did not affect the aggregation potential compared to the longer Tau 3R$^{M\ (244-400)}$ RD fragments. Therefore, both Tau 3R variants are suitable for Tau 3R aggregate detection. Vice versa, the 4R:3R seeding barrier can be used to identify 4R Tauopathies, as mainly cells expressing Tau 4R$^{S\ (246-378)}$ RD fragments will show cells with aggregates. In contrast, the cells expressing Tau 3R variants show only minimal numbers of cells with aggregates. Since Tau 4R$^{S\ (246-378)}$ RD fragments were the only ones that included the residues of the entire four repeats of the RD (R1-R4), we conclude that the entire R2 is essential for Tau 4R seeding. Truncation or the lack of R2 diminished Tau 4R aggregation when exposed to Tau 4R seeds from Tauopathy patients. In line with previous experiments (Tarutani et al., 2021; Longhini et al., 2024), AD brain homogenate seeded Tau 3R and 4R in our cell lines expressing either Tau 3R$^{M\ (244-400)}$ RD fragments, cryoEM Tau 3R$^{(PiD\ 254-378)}$ core fragments, Tau 4R$^{S\ (246-378)}$ RD fragments, or cryoEM Tau 4R$^{(AD\ 304-380)}$ core fragments. Still, AD brain homogenates mainly seeded Tau 3R variants, also shown by others (He et al., 2020; Tarutani et al., 2021; Wu et al., 2022; Tarutani et al., 2023). Interestingly, cells expressing the cryoEM Tau 4R$^{(AD\ 304-380)}$ core fragment were seeded best by the 3R/4R AD brain homogenate. This suggests that cryoEM Tau core fragments may be selectively incorporated into growing fibrils induced by disease-specific conformers, as the length of the expressed cryoEM Tau core fragment might dictate the possible specific conformations the monomer can adopt. More cryoEM Tau core fragments must be expressed in cells, and more Tau fibrils from different Tauopathies must be used for aggregate induction to confirm this hypothesis. The various seeding patterns in cells expressing full-length Tau, Tau RD fragments and the cryoEM Tau core fragments exposed to recombinant Tau fibrils, transgenic mouse or patient brain homogenate highlight the importance of using disease-relevant models. The fibril assembly conditions in vitro and in vivo and the Tau fibril and monomer length could impact conformation-dependent seeding. So far, we cannot discriminate between 4R Tauopathies, like 4R CBD and 4R PSP. Nevertheless, the combination of the four cell lines Tau 3R$^{M\ (244-400)}$ RD fragments, cryoEM Tau 3R$^{(PiD\ 254-378)}$ core fragments, Tau 4R$^{S\ (246-378)}$ RD fragments, or cryoEM Tau 4R$^{(AD\ 304-380)}$ core fragments can be used to discriminate between 3R, 4R and 3R/4R Tauopathies.

6.2.9 Sensitivity and specificity of our cell panel in comparison to other cell and *in vitro* models

Spontaneous aggregation, proteasomal clearance, spontaneous self-assembly, and a seeding barrier between Tau 3R and 4R isoforms represent important features of Tauopathies

that can be further investigated using our cell panel. But what is the difference between our cell panel and existing *in vitro* and cell models? To the best of our knowledge, this is the first cell panel that includes the cryoEM Tau core fragments: Tau$^{(AD\ 306-378)}$, Tau 4R$^{(AD\ 304-380)}$, Tau 4R$^{(CBD\ 274-380)}$, Tau 3R$^{(CTE\ 274-379)}$, Tau 4R$^{(CTE\ 305-379)}$ Tau 3R$^{(PiD\ 254-378)}$. Previous studies have often used the well-established FRET-based Tau seeding assay (Furman and Diamond 2017). This assay is based on the expression of the Tau 4R RD$^{(244-372)}$ harbouring the P301S mutation, tagged with either CFP or YFP. Exposure to exogenous Tau seeds results in a FRET signal, which is detected and quantified by flow cytometry. An advantage of our model is that it is optimised for a semi-automated workflow. This means that instead of using a 96-well format, as in the FRET assay, we use a 384-well format, which reduces the amount of valuable biological Tau seeds required. We also used a shorter protocol for the incubation times. Specifically, we added the Tau seeds 1 hour after plating the cells, compared to the Diamond protocol, where the cells were incubated for 24 hours before exposure to the Tau seeds (Furman and Diamond, 2017). Seed incubation with the cells was comparable to other groups, requiring 24-72 hours when recombinant fibrils and patient brain homogenate were used (Guo and Lee, 2011; Woerman et al., 2016; Furman et al., 2017; Kaufman et al., 2017; Tanaka et al., 2019; Shin et al., 2019; Annadurai et al., 2023). A highlight of our workflow is an automated confocal microscope and an automated image analysis pipeline. This simplifies and shortens the protocol, as the cells do not need to be detached from the plate after seeding but can be directly fixed and scanned. In addition, with the semi-automated workflow, we can monitor how toxic the experiments are for the cells to ensure that only viable cells are selected for the analysis. A further advantage is that we express the exact residues of the amyloid cores associated with different Tauopathies in the cells. Since the disease-specific Tau fibril cores were identified by cryoEM (Goedert et al., 2024), we know that not all residues of R1 (244-274) are present within the fibril core for Tau 3R and not all residues of R2 (275-305) are included within the Tau 4R fibril core. Additionally, the number of residues of the C-terminus varies between Tauopathies. Woerman and colleagues were among the first to express the Tau 3R$^{(243-375,\ \Delta R2)}$ in cells (Woerman et al., 2016). Tau 3R$^{(243-375,\ \Delta R2)}$ includes all residues of R1-R4. In contrast, in the 3R PiD$^{(254-378)}$ fibril core, not all residues of R1 and three additional residues of the C-terminus are included compared to the Woerman construct (Falcon et al., 2018b). The P301S mutated Tau 4R$^{(246-378)}$ and Tau 3R$^{(243-375,\ \Delta R2)}$ include more residues than the cryoEM Tau fragments, which might allow for more intramolecular interactions that potentially lead to amyloid conformations that are not disease-specific. We have shown that the cryoEM Tau fragments can only be selectively seeded by patient-derived Tau fibrils. This argues that the length of the Tau constructs probably affects the fibril conformation and its intramolecular interactions that might enable disease-specific fibril conformations. Therefore, the widely

used P301S mutated Tau 4R$^{(244\text{-}372)}$ and Tau 3R$^{(243\text{-}375,\ \Delta R2)}$ might not be the most suited for studying intracellular Tau spreading and propagation.

The assays used to study Tau aggregation vary in their sensitivity. The Diamond group's ultrasensitive next-generation cells expressing the P301S mutated Tau RD$^{(244\text{-}372)}$ detected Tau aggregates seeded with 153 pg to 1.2 ng total protein of immunoprecipitated 3R/4R AD patient fibrils (Hitt et al., 2021). We did not immunoprecipitate the Tau from our samples. Instead, we used 1.5 µl of 10 % Tauopathy brain homogenate. Due to the FTA assay, we know the total protein (1.4-2.8 µg) (Table S1) but do not know how much total Tau or seeding-competent Tau was added to the cells. According to other studies, about 0.5-1.2 ng normal Tau/µg protein and 0.07-0.49 ng abnormally phosphorylated Tau/µg protein, depending on the brain region, can be detected in patient brain samples (Khatoon et al., 1994; Han et al., 2017). Hence, we would have added approximately 700 pg to 3.36 ng normal Tau and 98 pg to 1.37 ng abnormally phosphorylated Tau protein to the cells, similar to the amount the Diamond lab used. However, we need to immunoprecipitate the Tau in future experiments to validate the sensitivity of our cell panel. So far, we can only estimate the amount of total Tau and seeding competent Tau added to the cells. More reasons for differences in sensitivity could also be based on expression levels, as codon usage optimisation, the promotor, the linker, mutations, and the transfection method that affects the plasmid copy number impact the amount of soluble Tau that can be aggregated (Hitt et al., 2021; Fus-Kujawa et al., 2021). Moreover, whether recombinant Tau fibrils, brain homogenate or immunoprecipitated Tau is used could account for differences in the number of cells with aggregates. However, our cell lines expressing Tau 3R$^{M\ (244\text{-}400)}$ RD fragments and cryoEM Tau 3R$^{(PiD\ 254\text{-}378)}$ core fragments showed 30-35 % cells with aggregates when seeded with 1.5 µl of 10 % Tauopathy brain homogenate. We are the first to use the cryoEM Tau fragments in cells and show that cryoEM Tau 3R$^{(PiD\ 254\text{-}378)}$ core fragments can be predominantly seeded by 3R Tauopathy brain homogenate compared to Tau 4R variants and that the cryoEM Tau 4R$^{(AD\ 304\text{-}380)}$ core fragment is seeded best by 3R/4R AD brain homogenate. This enables an effective detection method for Tau 3R aggregates based on the 3R:4R seeding barrier and confirms the disease-specific seeding of the cryoEM Tau 4R$^{(AD\ 304\text{-}380)}$ core fragment by 3R/4R AD brain homogenate. Future experiments could include validating the sensitivity of the cell panel by using immunoprecipitated Tau from brain homogenate and CSF from patients.

6.3 Limitations of the study

Tau aggregates have been associated with various neurodegenerative diseases known as Tauopathies. Despite extensive research, the mechanism of inter- and intracellular prion-like Tau propagation and transmission remains to be elucidated. Here, we demonstrated that HEK cells expressing Tau $4R^{LM\ (243\text{-}375)}$ RD fragments can be used for a semi-automated high-throughput screen to identify compounds that inhibit Tau aggregation. C22 and C57 were identified as potent Tau aggregation inhibitors. One major challenge is that C22 is too large to pass the blood-brain barrier. While C57 passes the blood-brain barrier and has a comparable IC_{50} to C22. Thus, it would be important to identify the target of C57 and screen for further derivates that pass the blood-brain barrier and are as effective as C22 and C57.

Since cryoEM has shown that Tau can fold into different amyloid conformers associated with different Tauopathies (Fitzpatrick et al., 2017; Falcon et al., 2018b; Falcon et al., 2019; Zhang et al., 2020), we generated HEK cells expressing Tau fragments of the length of the cryoEM Tau cores of fibrils from AD, CBD, CTE and PiD patients. By expressing the exact residues of the amyloid core, we hypothesised that disease-specific Tau aggregates might be formed. One limitation might be that the cryoEM Tau cores of AD, CBD and CTE are prone to spontaneous aggregation. Another is that proteasomal clearance results in weak protein levels when stably expressed in cells, which renders them unsuitable for investigating Tau fibril-induced aggregation. Still, they can be used to study the mechanisms involved in spontaneous aggregation.

One limitation of this study is that we do not know the cryoEM structures of the recombinant Tau $2N4R^{L\ (0\text{-}441)}$ and Tau $0N3R^{(0\text{-}352)}$ fibrils or the cryoEM structures of the fibrils formed by our cryoEM Tau core fragments in cells. It has been shown recently that Tau $1N3R^{(0\text{-}381)}$ or $1N4R^{(0\text{-}412)}$ expressed in cells could be seeded with AD and CBD brain homogenate, but the induced-fibril structure differed from the disease-specific folds identified by cryoEM (Tarutani et al. 2023). In our assay, the truncation of R2 and more residues at the C-terminus in cryoEM Tau $4R^{(AD\ 304\text{-}380)}$ core fragments diminished Tau 4R seeding by Tau 4R brain homogenates. However, it was seeded best by 3R/4R AD brain homogenate. This could be due to the same intramolecular interactions upon aggregation, which enforce a core structure similar to the Tau amyloid core of fibrils derived from AD patients. It remains to be seen whether the cryoEM Tau core fragments adopt the same fibril core conformation as the Tau fibrils isolated from Tauopathy patients.

Further, we can only discriminate between 3R, 4R and 3R/4R Tauopathies but not within Tauopathies that involve the same Tau isoform. So far, the panel misses a cryoEM Tau 4R core fragment to investigate disease-specific 4R fibril-induced aggregation. 4R CBD and 4R

PSP brain homogenate induced a similar seeding pattern in cells expressing the Tau $4R^{S\ (246\text{-}378)}$ RD fragment. Therefore, the Tau $4R^{S\ (246\text{-}378)}$ RD fragments cannot be used to differentiate between these two Tauopathies. CBD and PSP are 4R Tauopathies but differ in the layer number of their core fold and their protofilament number. This conformational difference might be helpful in selectively seeding their corresponding cryoEM Tau core fragments. Future experiments could include the expression of the cryoEM Tau core fragment of PSP in cells to study whether it shows the most cells with aggregates when it is exposed to 4R PSP brain homogenate. Additionally, 3R/4R CTE brain homogenate could validate the selective seeding of 3R/4R Tauopathy brain homogenate in combination with the respective cryoEM Tau core fragment. Thus, it would be of great interest to investigate whether the cryoEM Tau disease folds can be replicated in our cell model to discriminate between and within 3R, 4R and 3R/4R Tauopathies.

Another limitation is the sensitivity of cell based assays. The Marc Diamond ultrasensitive HEK cells expressing the P301S mutated Tau 4R $RD^{(244\text{-}372)}$ detect Tau in the pico- to nanogram range when Tau seeds are immunoprecipitated (Hitt et al., 2021). In contrast, RT-QuIC can detect pico- to femtograms of Tau seeds in the brain(Saijo et al., 2017; Kraus et al., 2019; Saijo et al., 2020; Metrick et al., 2020). Nevertheless, RT-QuIC may not amplify the original Tau fibril fold as seen for α-synuclein (Burger et al., 2021; Lövestam et al., 2021). Replication of the correct fibril fold in the cells is also challenging. Tarutani and colleagues showed that 3R/4R AD and 4R CBD patient brain homogenate template Tau $1N3R^{(0\text{-}381)}$ and $1N4R^{(0\text{-}412)}$ in cells, but the resulting fibril structure differed from the disease-specific folds identified by cryoEM (Tarutani et al., 2023). Our cell model depends on sufficient seeds to induce Tau aggregation to differentiate between 3R, 4R and 3R/4R Tauopathies. So far, we do not know the amount of total Tau added to the cells and, therefore, do not know the assay's sensitivity. We used different amounts of total protein to test the sensitivity of our cell model. We demonstrated that the total amount of protein does not necessarily correlate with the amount of seeding competent Tau. Future experiments could focus on increasing the sensibility by immunoprecipitating the seeding competent Tau to determine if the cell panel assay can detect femto-to nanogramme of Tau.

6.4 Relevance

Tauopathies such as AD are a significant burden to our society. AD affected approximately 55 million people in 2019, rising to 139 million by 2050 (Alzheimer's Association, 2024). Despite extensive research, most Tau-targeting therapies have failed in later-stage clinical trials (Cummings et al, 2024). Definitive clinical diagnosis of AD and other Tauopathies is only possible through post-mortem neuropathological evaluation (Caselli et al., 2017). Tauopathies are clinically heterogeneous diseases characterised by neuronal loss, cognitive decline and, finally, death. The mechanisms of Tau aggregation and propagation remain to be elucidated. In this study, we have generated a cell panel based on full-length Tau, Tau RD fragments, and cryoEM Tau core fragments, which can be used to understand spontaneous amyloid formation, clearance of Tau aggregates and fibril-induced Tau aggregation. We can further use the cell panel to discriminate between Tauopathies. Our cell panel may help define the pathological Tau isoform (3R, 4R, 3R/4R) of the corresponding Tauopathy by testing the seeding ability of patient samples in a cell panel expressing Tau RD fragments and cryoEM Tau core fragments. Testing more brain homogenates from patients with different Tauopathies, such as CTE, will validate the results. CryoEM can be used to determine whether the conformation of the seeds is faithfully reproduced within our cell lines or whether the Tau variant expressed influences the conformation of the induced amyloid. We can also use the cell panel to investigate the cellular mechanisms underlying Tau 3R, 4R, and 3R/4R seed dissemination and propagation. Spontaneous aggregation of the cryoEM Tau core fragments allows the study of cellular mechanisms that favour or prevent Tau aggregation. Further, we have successfully established a semi-automated high-content screen for Tau inhibitors in our lab and identified C22 and C57 as potent Tau aggregation inhibitors. The cryoEM Tau core fragments may help to identify compounds with potential selective inhibitory effects on Tau 3R or 4R aggregation. Spontaneously aggregating Tau variants can be used to rapidly screen for Tau aggregation inhibitors without the need for exogenous Tau fibrils. While we have focused on patient brain homogenate in this work, it would be interesting to test whether our cell panel can detect Tau aggregates from CSF and the blood of Tauopathy patients. This would make it a valuable tool for the pre-mortem discrimination between Tauopathies. Findings from this study might help to develop new therapeutic strategies to inhibit or reduce the aggregation of Tau by compounds.

Acknowledgements

First, I would like to thank my supervisor, Prof. Dr. Ina Vorberg, for allowing me to do my PhD in her laboratory. Thank you for your enthusiastic encouragement, constructive criticism, and reliable guidance during this project. Our endless discussions about the multiple projects helped me to stay on track and pushed my confidence.

In addition, I would like to thank Prof. Dr. Jörg Höhfeld for agreeing to be the second examiner of my dissertation. I would also like to thank Prof. Dr. Albert Haas and Jun-Prof. Dr. Marie-Christine Simon for taking the time to serve on my exam committee.

Furthermore, I would like to thank Prof. Dr. Markus Zweckstetter, Dr. Lisa Ramirez, and Dr. Pijush Chakraborty, who collaborated with us on the high-throughput screen. Thank you for the endless supply of recombinant fibrils and compounds and your feedback.

To all current and former members of the AG Vorberg group who have supported me along the way, a big and heartfelt thank you! I especially want to thank my lab bestie and great friend, Annika W. Our endless discussions, calculations, bus rides, crying, laughter, and evenings on the balcony carried me through highs and lows. It would have not been the same without you! I would also like to thank André and Lydia for always being there to answer questions and for their constant patience and support. Thank you, Nazli Altinisik, for inspiring discussions and your support. In addition, I would like to thank Carla for the best cookies and the joyful mood you brought to the lab. Further, I would like to thank Stephanie for her support from my bachelor's to my PhD and for all the fun nights we spent together with Annika B. Moreover, I would like to thank all the DZNE DRs for our fantastic time at BBQs, game nights, after-work events and parties.

I would also like to thank the LMF and LAT facilities, especially Ireen König, Hans Fried, Philip Denner, Josephine Blersch, Birgit Kurkowsky and Anja Meyer-Berhorn for helping me with my experiments.

Finally, I would like to deeply thank my family, Marion, Gernot and Leonie for their constant loving support and deep faith in me. In addition, I would like to thank my friends Katja, Anna and Amelie. My special thanks go to my partner, Paul, for your continuous reassurance, encouragement, motivation, and unconditional love! Thank you for always being there for me!

References

Abraha, A., N. Ghoshal, T. C. Gamblin, V. Cryns, R. W. Berry, J. Kuret, and L. I. Binder. 2000. C-terminal inhibition of tau assembly in vitro and in Alzheimer's disease. *Journal of cell science* 113 Pt 21:3737–3745. doi:10.1242/jcs.113.21.3737.

Agadjanyan, M. G., K. Zagorski, I. Petrushina, H. Davtyan, K. Kazarian, M. Antonenko, J. Davis, C. Bon, M. Blurton-Jones, D. H. Cribbs, and A. Ghochikyan. 2017. Humanized monoclonal antibody armanezumab specific to N-terminus of pathological tau: characterization and therapeutic potency. *Molecular neurodegeneration* 12(1):33. doi:10.1186/s13024-017-0172-1.

Aguzzi, A., and A. M. Calella. 2009. Prions: protein aggregation and infectious diseases. *Physiological reviews* 89(4):1105–1152. doi:10.1152/physrev.00006.2009.

Albert, M., G. Mairet-Coello, C. Danis, S. Lieger, R. Caillierez, S. Carrier, E. Skrobala, I. Landrieu, A. Michel, M. Schmitt, M. Citron, P. Downey, J.-P. Courade, L. Buée, and M. Colin. 2019. Prevention of tau seeding and propagation by immunotherapy with a central tau epitope antibody. *Brain a journal of neurology* 142(6):1736–1750. doi:10.1093/brain/awz100.

Alquezar, C., S. Arya, and A. W. Kao. 2020. Tau Post-translational Modifications: Dynamic Transformers of Tau Function, Degradation, and Aggregation. *Frontiers in neurology* 11:595532. doi:10.3389/fneur.2020.595532.

Alzheimer, A. 1907. Über eine eigenartige Erkrankung der Hirnrinde 64(146-8).

Alzheimer's Association. 2024. Alzheimer's Association 2024 Alzheimer's Disease Facts and Figures.

Ambadipudi, S., J. Biernat, D. Riedel, E. Mandelkow, and M. Zweckstetter. 2017. Liquid-liquid phase separation of the microtubule-binding repeats of the Alzheimer-related protein Tau. *Nature communications* 8(1):275. doi:10.1038/s41467-017-00480-0.

Annadurai, N., A. Kubickova, I. Frydrych, M. Hajduch, and V. Das. 2023. Differential seeding by exogenous R2 and R3 fibrils influences autophagic degradation of intracellular tau aggregates in Tau K18 P301S cells. 33 pp.

Annadurai, N., J. B. de Sanctis, M. Hajdúch, and V. Das. 2021. Tau secretion and propagation: Perspectives for potential preventive interventions in Alzheimer's disease and other tauopathies. *Experimental neurology* 343:113756. doi:10.1016/j.expneurol.2021.113756.

Anne D. Sperfeld, Michael B. Collatz, Hartmut Baier, Markus Palmbach, Alexander Storch, Johannes Schwarz, Klaus Tatsch, Sven Reske, Marijke Joosse, Peter Heutink, and Albert C. Ludolph. 2001. FTDP-17: An early-onset phenotype with parkinsonism and epileptic seizures caused by a novel mutation.

Antoniou, N., K. Prodromidou, G. Kouroupi, I. Boumpoureka, M. Samiotaki, G. Panayotou, M. Xilouri, I. Kloukina, L. Stefanis, R. Grailhe, E. Taoufik, and R. Matsas. 2022. High content screening and proteomic analysis identify a kinase inhibitor that rescues pathological phenotypes in a patient-derived model of Parkinson's disease. *NPJ Parkinson's disease* 8(1):15. doi:10.1038/s41531-022-00278-y.

Aoyagi, H., M. Hasegawa, and A. Tamaoka. 2007. Fibrillogenic nuclei composed of P301L mutant tau induce elongation of P301L tau but not wild-type tau. *The Journal of biological chemistry* 282(28):20309–20318. doi:10.1074/jbc.M611876200.

Arakhamia, T., C. E. Lee, Y. Carlomagno, D. M. Duong, S. R. Kundinger, K. Wang, D. Williams, M. DeTure, D. W. Dickson, C. N. Cook, N. T. Seyfried, L. Petrucelli, and A. W. P. Fitzpatrick. 2020. Posttranslational Modifications Mediate the Structural Diversity of Tauopathy Strains. *Cell* 180(4):633-644.e12. doi:10.1016/j.cell.2020.01.027.

Arriagada, P. V., J. H. Growdon, E. T. Hedley-Whyte, and B. T. Hyman. 1992. Neurofibrillary tangles but not senile plaques parallel duration and severity of Alzheimer's disease. *Neurology* 42(3 Pt 1):631–639. doi:10.1212/wnl.42.3.631.

Aswathy, P. M., P. S. Jairani, and P. S. Mathuranath. 2010. Genetics of frontotemporal lobar degeneration. *Annals of Indian Academy of Neurology* 13(Suppl 2):S55-62. doi:10.4103/0972-2327.74246.

Bahnassawy, L., N. Nicolaisen, C. Untucht, B. Mielich-Süss, L. Reinhardt, J. S. Ried, M. P. Morawe, D. Geist, A. Finck, E. Käfer, J. Korffmann, M. Townsend, B. Ravikumar, V. Lakics, M. Cik, and P. Reinhardt. 2024. Establishment of a high-content imaging assay for tau aggregation in hiPSC-derived neurons differentiated from two protocols to routinely evaluate compounds and genetic perturbations. *SLAS discovery advancing life sciences R & D* 29(2):100137. doi:10.1016/j.slasd.2023.12.009.

Barteneva, N. S., E. Fasler-Kan, M. Bernimoulin, J. N. H. Stern, E. D. Ponomarev, L. Duckett, and I. A. Vorobjev. 2013. Circulating microparticles: square the circle. *BMC cell biology* 14:23. doi:10.1186/1471-2121-14-23.

Bateman, R. J., P. S. Aisen, B. de Strooper, N. C. Fox, C. A. Lemere, J. M. Ringman, S. Salloway, R. A. Sperling, M. Windisch, and C. Xiong. 2011. Autosomal-dominant Alzheimer's disease: a review and proposal for the prevention of Alzheimer's disease. *Alzheimer's research & therapy* 3(1):1. doi:10.1186/alzrt59.

Beach, T. G., S. E. Monsell, L. E. Phillips, and W. Kukull. 2012. Accuracy of the clinical diagnosis of Alzheimer disease at National Institute on Aging Alzheimer Disease Centers, 2005-2010. *Journal of neuropathology and experimental neurology* 71(4):266–273. doi:10.1097/NEN.0b013e31824b211b.

Bennett, R. E., S. L. DeVos, S. Dujardin, B. Corjuc, R. Gor, J. Gonzalez, A. D. Roe, M. P. Frosch, R. Pitstick, G. A. Carlson, and B. T. Hyman. 2017. Enhanced Tau Aggregation in the Presence of Amyloid β. *The American journal of pathology* 187(7):1601–1612. doi:10.1016/j.ajpath.2017.03.011.

Bergen, M. von, P. Friedhoff, J. Biernat, J. Heberle, E. M. Mandelkow, and E. Mandelkow. 2000. Assembly of tau protein into Alzheimer paired helical filaments depends on a local sequence motif ((306)VQIVYK(311)) forming beta structure. *Proceedings of the National Academy of Sciences of the United States of America* 97(10):5129–5134. doi:10.1073/pnas.97.10.5129.

Berry, R. W., A. Abraha, S. Lagalwar, N. LaPointe, T. C. Gamblin, V. L. Cryns, and L. I. Binder. 2003. Inhibition of tau polymerization by its carboxy-terminal caspase cleavage fragment. *Biochemistry* 42(27):8325–8331. doi:10.1021/bi027348m.

Berryman, J. T., S. E. Radford, and S. A. Harris. 2011. Systematic examination of polymorphism in amyloid fibrils by molecular-dynamics simulation. *Biophysical journal* 100(9):2234–2242. doi:10.1016/j.bpj.2011.02.060.

Biernat, J., N. Gustke, G. Drewes, E. M. Mandelkow, and E. Mandelkow. 1993. Phosphorylation of Ser262 strongly reduces binding of tau to microtubules: distinction between PHF-like immunoreactivity and microtubule binding. *Neuron* 11(1):153–163. doi:10.1016/0896-6273(93)90279-z.

Bigio, E. H., D. F. Brown, and C. L. White. 1999. Progressive supranuclear palsy with dementia: cortical pathology. *Journal of neuropathology and experimental neurology* 58(4):359–364. doi:10.1097/00005072-199904000-00006.

Bok, E., E. Leem, B.-R. Lee, J. M. Lee, C. J. Yoo, E. M. Lee, and J. Kim. 2021. Role of the Lipid Membrane and Membrane Proteins in Tau Pathology. *Frontiers in cell and developmental biology* 9:653815. doi:10.3389/fcell.2021.653815.

Boland, B., W. H. Yu, O. Corti, B. Mollereau, A. Henriques, E. Bezard, G. M. Pastores, D. C. Rubinsztein, R. A. Nixon, M. R. Duchen, G. R. Mallucci, G. Kroemer, B. Levine, E.-L.

Eskelinen, F. Mochel, M. Spedding, C. Louis, O. R. Martin, and M. J. Millan. 2018. Promoting the clearance of neurotoxic proteins in neurodegenerative disorders of ageing. *Nature reviews. Drug discovery* 17(9):660–688. doi:10.1038/nrd.2018.109.

Boutajangout, A., J. Ingadottir, P. Davies, and E. M. Sigurdsson. 2011. Passive immunization targeting pathological phospho-tau protein in a mouse model reduces functional decline and clears tau aggregates from the brain. *Journal of neurochemistry* 118(4):658–667. doi:10.1111/j.1471-4159.2011.07337.x.

Braak, H., and E. Braak. 1991. Neuropathological stageing of Alzheimer-related changes. *Acta neuropathologica* 82(4):239–259. doi:10.1007/BF00308809.

Bramblett, G. T., M. Goedert, R. Jakes, S. E. Merrick, J. Q. Trojanowski, and V. M. Lee. 1993. Abnormal tau phosphorylation at Ser396 in Alzheimer's disease recapitulates development and contributes to reduced microtubule binding. *Neuron* 10(6):1089–1099. doi:10.1016/0896-6273(93)90057-x.

Brion, J. P., J. N. Octave, and A. M. Couck. 1994. Distribution of the phosphorylated microtubule-associated protein tau in developing cortical neurons. *Neuroscience* 63(3):895–909. doi:10.1016/0306-4522(94)90533-9.

Brion, J. P., D. Power, D. Hue, A. M. Couck, B. H. Anderton, and J. Flament-Durand. 1989. Heterogeneity of ubiquitin immunoreactivity in neurofibrillary tangles of Alzheimer's disease. *Neurochemistry international* 14(2):121–128. doi:10.1016/0197-0186(89)90111-3.

Brunello, C. A., M. Merezhko, R.-L. Uronen, and H. J. Huttunen. 2020. Mechanisms of secretion and spreading of pathological tau protein. *Cellular and molecular life sciences CMLS* 77(9):1721–1744. doi:10.1007/s00018-019-03349-1.

Budd Haeberlein, S., P. S. Aisen, F. Barkhof, S. Chalkias, T. Chen, S. Cohen, G. Dent, O. Hansson, K. Harrison, C. von Hehn, T. Iwatsubo, C. Mallinckrodt, C. J. Mummery, K. K. Muralidharan, I. Nestorov, L. Nisenbaum, R. Rajagovindan, L. Skordos, Y. Tian, C. H. van Dyck, B. Vellas, S. Wu, Y. Zhu, and A. Sandrock. 2022. Two Randomized Phase 3 Studies of Aducanumab in Early Alzheimer's Disease. *The journal of prevention of Alzheimer's disease* 9(2):197–210. doi:10.14283/jpad.2022.30.

Bugiani, O., J. R. Murrell, G. Giaccone, M. Hasegawa, G. Ghigo, M. Tabaton, M. Morbin, A. Primavera, F. Carella, C. Solaro, M. Grisoli, M. Savoiardo, M. G. Spillantini, F. Tagliavini, M. Goedert, and B. Ghetti. 1999. Frontotemporal dementia and corticobasal degeneration in a family with a P301S mutation in tau. *Journal of neuropathology and experimental neurology* 58(6):667–677. doi:10.1097/00005072-199906000-00011.

Bulic, B., M. Pickhardt, E.-M. Mandelkow, and E. Mandelkow. 2010. Tau protein and tau aggregation inhibitors. *Neuropharmacology* 59(4-5):276–289. doi:10.1016/j.neuropharm.2010.01.016.

Burger, D., A. Fenyi, L. Bousset, H. Stahlberg, and R. Melki. 2021. Cryo-EM structure of alpha-synuclein fibrils amplified by PMCA from PD and MSA patient brains.

Calafate, S., W. Flavin, P. Verstreken, and D. Moechars. 2016. Loss of Bin1 Promotes the Propagation of Tau Pathology. *Cell reports* 17(4):931–940. doi:10.1016/j.celrep.2016.09.063.

Campello, L., J. Esteve-Rudd, N. Cuenca, and J. Martín-Nieto. 2013. The ubiquitin-proteasome system in retinal health and disease. *Molecular neurobiology* 47(2):790–810. doi:10.1007/s12035-012-8391-5.

Canu, N., L. Dus, C. Barbato, M. T. Ciotti, C. Brancolini, A. M. Rinaldi, M. Novak, A. Cattaneo, A. Bradbury, and P. Calissano. 1998. Tau cleavage and dephosphorylation in cerebellar granule neurons undergoing apoptosis. *The Journal of neuroscience the official journal of the Society for Neuroscience* 18(18):7061–7074. doi:10.1523/JNEUROSCI.18-18-07061.1998.

Cao, J., M. B. Zhong, C. A. Toro, L. Zhang, and D. Cai. 2019. Endo-lysosomal pathway and ubiquitin-proteasome system dysfunction in Alzheimer's disease pathogenesis. *Neuroscience letters* 703:68–78. doi:10.1016/j.neulet.2019.03.016.

Cardarelli, F., L. Digiacomo, C. Marchini, A. Amici, F. Salomone, G. Fiume, A. Rossetta, E. Gratton, D. Pozzi, and G. Caracciolo. 2016. The intracellular trafficking mechanism of Lipofectamine-based transfection reagents and its implication for gene delivery. *Scientific reports* 6:25879. doi:10.1038/srep25879.

Carlomagno, Y., S. Manne, M. DeTure, M. Prudencio, Y.-J. Zhang, R. Hanna Al-Shaikh, J. A. Dunmore, L. M. Daughrity, Y. Song, M. Castanedes-Casey, L. J. Lewis-Tuffin, K. A. Nicholson, Z. K. Wszolek, D. W. Dickson, A. W. P. Fitzpatrick, L. Petrucelli, and C. N. Cook. 2021. The AD tau core spontaneously self-assembles and recruits full-length tau to filaments. *Cell reports* 34(11):108843. doi:10.1016/j.celrep.2021.108843.

Caselli, R. J., T. G. Beach, D. S. Knopman, and N. R. Graff-Radford. 2017. Alzheimer Disease: Scientific Breakthroughs and Translational Challenges. *Mayo Clinic proceedings* 92(6):978–994. doi:10.1016/j.mayocp.2017.02.011.

Castillo-Carranza, D. L., U. Sengupta, M. J. Guerrero-Muñoz, C. A. Lasagna-Reeves, J. E. Gerson, G. Singh, D. M. Estes, A. D. T. Barrett, K. T. Dineley, G. R. Jackson, and R. Kayed. 2014. Passive immunization with Tau oligomer monoclonal antibody reverses tauopathy phenotypes without affecting hyperphosphorylated neurofibrillary tangles. *The Journal of neuroscience the official journal of the Society for Neuroscience* 34(12):4260–4272. doi:10.1523/JNEUROSCI.3192-13.2014.

Chaari, A. 2019. Molecular chaperones biochemistry and role in neurodegenerative diseases. *International journal of biological macromolecules* 131:396–411. doi:10.1016/j.ijbiomac.2019.02.148.

Chai, X., S. Wu, T. K. Murray, R. Kinley, C. V. Cella, H. Sims, N. Buckner, J. Hanmer, P. Davies, M. J. O'Neill, M. L. Hutton, and M. Citron. 2011. Passive immunization with anti-Tau antibodies in two transgenic models: reduction of Tau pathology and delay of disease progression. *The Journal of biological chemistry* 286(39):34457–34467. doi:10.1074/jbc.M111.229633.

Chakraborty, P., G. Rivière, A. Hebestreit, A. I. de Opakua, I. M. Vorberg, L. B. Andreas, and M. Zweckstetter. 2023. Acetylation discriminates disease-specific tau deposition. *Nature communications* 14(1):5919. doi:10.1038/s41467-023-41672-1.

Chakraborty, P., G. Rivière, S. Liu, A. I. de Opakua, R. Dervişoğlu, A. Hebestreit, L. B. Andreas, I. M. Vorberg, and M. Zweckstetter. 2021. Co-factor-free aggregation of tau into seeding-competent RNA-sequestering amyloid fibrils. *Nature communications* 12(1):4231. doi:10.1038/s41467-021-24362-8.

Chang, E., S. Kim, K. N. Schafer, and J. Kuret. 2011. Pseudophosphorylation of tau protein directly modulates its aggregation kinetics. *Biochimica et biophysica acta* 1814(2):388–395. doi:10.1016/j.bbapap.2010.10.005.

Chang, E., and J. Kuret. 2008. Detection and quantification of tau aggregation using a membrane filter assay. *Analytical Biochemistry* 373(2):330–336. doi:10.1016/j.ab.2007.09.015.

Chen, D., S. Bali, R. Singh, A. Wosztyl, V. Mullapudi, J. Vaquer-Alicea, P. Jayan, S. Melhem, H. Seelaar, J. C. van Swieten, M. I. Diamond, and L. A. Joachimiak. 2023. FTD-tau S320F mutation stabilizes local structure and allosterically promotes amyloid motif-dependent aggregation. *Nature communications* 14(1):1625. doi:10.1038/s41467-023-37274-6.

Chen, D., K. W. Drombosky, Z. Hou, L. Sari, O. M. Kashmer, B. D. Ryder, V. A. Perez, D. R. Woodard, M. M. Lin, M. I. Diamond, and L. A. Joachimiak. 2019. Tau local structure shields an amyloid-forming motif and controls aggregation propensity. *Nature communications* 10(1):2493. doi:10.1038/s41467-019-10355-1.

Cheng, C., S. A. Reis, E. T. Adams, D. M. Fass, S. P. Angus, T. J. Stuhlmiller, J. Richardson, H. Olafson, E. T. Wang, D. Patnaik, R. L. Beauchamp, D. A. Feldman, M. C. Silva, M. Sur, G. L. Johnson, V. Ramesh, B. L. Miller, S. Temple, K. S. Kosik, B. C. Dickerson, and S. J. Haggarty. 2021. High-content image-based analysis and proteomic profiling identifies Tau phosphorylation inhibitors in a human iPSC-derived glutamatergic neuronal model of tauopathy. *Scientific reports* 11(1):17029. doi:10.1038/s41598-021-96227-5.

Cheng, J., B. J. North, T. Zhang, X. Dai, K. Tao, J. Guo, and W. Wei. 2018. The emerging roles of protein homeostasis-governing pathways in Alzheimer's disease. *Aging cell* 17(5):e12801. doi:10.1111/acel.12801.

Cheung, Z. H., and N. Y. Ip. 2011. Autophagy deregulation in neurodegenerative diseases - recent advances and future perspectives. *Journal of neurochemistry* 118(3):317–325. doi:10.1111/j.1471-4159.2011.07314.x.

Chirita, C. N., E. E. Congdon, H. Yin, and J. Kuret. 2005. Triggers of full-length tau aggregation: a role for partially folded intermediates. *Biochemistry* 44(15):5862–5872. doi:10.1021/bi0500123.

Chirita, C. N., M. Necula, and J. Kuret. 2003. Anionic micelles and vesicles induce tau fibrillization in vitro. *The Journal of biological chemistry* 278(28):25644–25650. doi:10.1074/jbc.M301663200.

Choi, S. H., Y. H. Kim, M. Hebisch, C. Sliwinski, S. Lee, C. D'Avanzo, H. Chen, B. Hooli, C. Asselin, J. Muffat, J. B. Klee, C. Zhang, B. J. Wainger, M. Peitz, D. M. Kovacs, C. J. Woolf, S. L. Wagner, R. E. Tanzi, and D. Y. Kim. 2014. A three-dimensional human neural cell culture model of Alzheimer's disease. *Nature* 515(7526):274–278. doi:10.1038/nature13800.

Chung, D.-E. C., S. Roemer, L. Petrucelli, and D. W. Dickson. 2021. Cellular and pathological heterogeneity of primary tauopathies. *Molecular neurodegeneration* 16(1):57. doi:10.1186/s13024-021-00476-x.

Ciechanover, A. 2006. Intracellular protein degradation: from a vague idea thru the lysosome and the ubiquitin-proteasome system and onto human diseases and drug targeting. *Experimental biology and medicine (Maywood, N.J.)* 231(7):1197–1211. doi:10.1177/153537020623100705.

Clark, L. N., P. Poorkaj, Z. Wszolek, D. H. Geschwind, Z. S. Nasreddine, B. Miller, D. Li, H. Payami, F. Awert, K. Markopoulou, A. Andreadis, I. D'Souza, V. M. Lee, L. Reed, J. Q. Trojanowski, V. Zhukareva, T. Bird, G. Schellenberg, and K. C. Wilhelmsen. 1998. Pathogenic implications of mutations in the tau gene in pallido-ponto-nigral degeneration and related neurodegenerative disorders linked to chromosome 17. *Proceedings of the National Academy of Sciences of the United States of America* 95(22):13103–13107. doi:10.1073/pnas.95.22.13103.

Clavaguera, F., T. Bolmont, R. A. Crowther, D. Abramowski, S. Frank, A. Probst, G. Fraser, A. K. Stalder, M. Beibel, M. Staufenbiel, M. Jucker, M. Goedert, and M. Tolnay. 2009. Transmission and spreading of tauopathy in transgenic mouse brain. *Nature cell biology* 11(7):909–913. doi:10.1038/ncb1901.

Cleveland, D. W., Hwo, S. Y., and M. W. Kirschner. 1977. Purification of tau, a microtubule-associated protein that induces assembly of microtubules from purified tubulin. *Journal of molecular biology* 116(2):207–225. doi:10.1016/0022-2836(77)90213-3.

Cliffe, R., J. C. Sang, F. Kundel, D. Finley, D. Klenerman, and Y. Ye. 2019. Filamentous Aggregates Are Fragmented by the Proteasome Holoenzyme. *Cell reports* 26(8):2140-2149.e3. doi:10.1016/j.celrep.2019.01.096.

Cocucci, E., and J. Meldolesi. 2015. Ectosomes and exosomes: shedding the confusion between extracellular vesicles. *Trends in cell biology* 25(6):364–372. doi:10.1016/j.tcb.2015.01.004.

Cohen, A. S., and E. Calkins. 1959. Electron microscopic observations on a fibrous component in amyloid of diverse origins. *Nature* 183(4669):1202–1203. doi:10.1038/1831202a0.

Cohen, T. J., J. L. Guo, D. E. Hurtado, L. K. Kwong, I. P. Mills, J. Q. Trojanowski, and V. M. Y. Lee. 2011. The acetylation of tau inhibits its function and promotes pathological tau aggregation. *Nature communications* 2:252. doi:10.1038/ncomms1255.

Cole, G. M., and P. S. Timiras. 1987. Ubiquitin-protein conjugates in Alzheimer's lesions. *Neuroscience letters* 79(1-2):207–212. doi:10.1016/0304-3940(87)90698-7.

Condomitti, G., and J. de Wit. 2018. Heparan Sulfate Proteoglycans as Emerging Players in Synaptic Specificity. *Frontiers in molecular neuroscience* 11:14. doi:10.3389/fnmol.2018.00014.

Congdon, E. E., J. W. Wu, N. Myeku, Y. H. Figueroa, M. Herman, P. S. Marinec, J. E. Gestwicki, C. A. Dickey, W. H. Yu, and K. E. Duff. 2012. Methylthioninium chloride (methylene blue) induces autophagy and attenuates tauopathy in vitro and in vivo. *Autophagy* 8(4):609–622. doi:10.4161/auto.19048.

Courade, J.-P., R. Angers, G. Mairet-Coello, N. Pacico, K. Tyson, D. Lightwood, R. Munro, D. McMillan, R. Griffin, T. Baker, D. Starkie, R. Nan, M. Westwood, M.-L. Mushikiwabo, S. Jung, G. Odede, B. Sweeney, A. Popplewell, G. Burgess, P. Downey, and M. Citron. 2018. Epitope determines efficacy of therapeutic anti-Tau antibodies in a functional assay with human Alzheimer Tau. *Acta neuropathologica* 136(5):729–745. doi:10.1007/s00401-018-1911-2.

Creekmore, B. C., Y.-W. Chang, and E. B. Lee. 2021. The Cryo-EM Effect: Structural Biology of Neurodegenerative Disease Aggregates. *Journal of neuropathology and experimental neurology* 80(6):514–529. doi:10.1093/jnen/nlab039.

Crowe, A., C. Ballatore, E. Hyde, J. Q. Trojanowski, and V. M.-Y. Lee. 2007. High throughput screening for small molecule inhibitors of heparin-induced tau fibril formation. *Biochemical and biophysical research communications* 358(1):1–6. doi:10.1016/j.bbrc.2007.03.056.

Crowe, A., W. Huang, C. Ballatore, R. L. Johnson, A.-M. L. Hogan, R. Huang, J. Wichterman, J. McCoy, D. Huryn, D. S. Auld, A. B. Smith, J. Inglese, J. Q. Trojanowski, C. P. Austin, K. R. Brunden, and V. M.-Y. Lee. 2009. Identification of aminothienopyridazine inhibitors of tau assembly by quantitative high-throughput screening. *Biochemistry* 48(32):7732–7745. doi:10.1021/bi9006435.

Crowther, R. A. 1991. Straight and paired helical filaments in Alzheimer disease have a common structural unit. *Proceedings of the National Academy of Sciences of the United States of America* 88(6):2288–2292. doi:10.1073/pnas.88.6.2288.

Cummings, J., Y. Zhou, G. Lee, K. Zhong, J. Fonseca, and F. Cheng. 2024. Alzheimer's disease drug development pipeline: 2024. *Alzheimer's & dementia (New York, N. Y.)* 10(2):e12465. doi:10.1002/trc2.12465.

Currens, L., N. Harrison, M. Schmidt, H. Amjad, W. Mu, S. W. Scholz, J. Bang, and A. Pantelyat. 2023. A case of familial frontotemporal dementia caused by a progranulin gene mutation. *Clinical parkinsonism & related disorders* 9:100213. doi:10.1016/j.prdoa.2023.100213.

Dai, C., X. Chen, S. F. Kazim, F. Liu, C.-X. Gong, I. Grundke-Iqbal, and K. Iqbal. 2015. Passive immunization targeting the N-terminal projection domain of tau decreases tau pathology and improves cognition in a transgenic mouse model of Alzheimer disease and tauopathies. *Journal of neural transmission (Vienna, Austria 1996)* 122(4):607–617. doi:10.1007/s00702-014-1315-y.

Dalby, B., S. Cates, A. Harris, E. C. Ohki, M. L. Tilkins, P. J. Price, and V. C. Ciccarone. 2004. Advanced transfection with Lipofectamine 2000 reagent: primary neurons, siRNA, and high-throughput applications. *Methods (San Diego, Calif.)* 33(2):95–103. doi:10.1016/j.ymeth.2003.11.023.

Del Conde, I., C. N. Shrimpton, P. Thiagarajan, and J. A. López. 2005. Tissue-factor-bearing microvesicles arise from lipid rafts and fuse with activated platelets to initiate coagulation. *Blood* 106(5):1604–1611. doi:10.1182/blood-2004-03-1095.

DeLeo, A. M., and T. Ikezu. 2018. Extracellular Vesicle Biology in Alzheimer's Disease and Related Tauopathy. *Journal of neuroimmune pharmacology the official journal of the Society on NeuroImmune Pharmacology* 13(3):292–308. doi:10.1007/s11481-017-9768-z.

Della David, C., R. Layfield, L. Serpell, Y. Narain, M. Goedert, and M. G. Spillantini. 2002. Proteasomal degradation of tau protein. *Journal of neurochemistry* 83(1):176–185. doi:10.1046/j.1471-4159.2002.01137.x.

Devi, G., A. Fotiou, D. Jyrinji, B. Tycko, S. DeArmand, E. Rogaeva, Y. Q. Song, H. Medieros, Y. Liang, A. Orlacchio, J. Williamson, P. St George-Hyslop, and R. Mayeux. 2000. Novel presenilin 1 mutations associated with early onset of dementia in a family with both early-onset and late-onset Alzheimer disease. *Archives of neurology* 57(10):1454–1457. doi:10.1001/archneur.57.10.1454.

DeVos, S. L., B. T. Corjuc, D. H. Oakley, C. K. Nobuhara, R. N. Bannon, A. Chase, C. Commins, J. A. Gonzalez, P. M. Dooley, M. P. Frosch, and B. T. Hyman. 2018. Synaptic Tau Seeding Precedes Tau Pathology in Human Alzheimer's Disease Brain. *Frontiers in neuroscience* 12:267. doi:10.3389/fnins.2018.00267.

DeVos, S. L., D. K. Goncharoff, G. Chen, C. S. Kebodeaux, K. Yamada, F. R. Stewart, D. R. Schuler, S. E. Maloney, D. F. Wozniak, F. Rigo, C. F. Bennett, J. R. Cirrito, D. M. Holtzman, and T. M. Miller. 2013. Antisense reduction of tau in adult mice protects against seizures. *The Journal of neuroscience the official journal of the Society for Neuroscience* 33(31):12887–12897. doi:10.1523/JNEUROSCI.2107-13.2013.

DeVos, S. L., R. L. Miller, K. M. Schoch, B. B. Holmes, C. S. Kebodeaux, A. J. Wegener, G. Chen, T. Shen, H. Tran, B. Nichols, T. A. Zanardi, H. B. Kordasiewicz, E. E. Swayze, C. F. Bennett, M. I. Diamond, and T. M. Miller. 2017. Tau reduction prevents neuronal loss and reverses pathological tau deposition and seeding in mice with tauopathy. *Science translational medicine* 9(374). doi:10.1126/scitranslmed.aag0481.

Dickson, D. W., C. Bergeron, S. S. Chin, C. Duyckaerts, D. Horoupian, K. Ikeda, K. Jellinger, P. L. Lantos, C. F. Lippa, S. S. Mirra, M. Tabaton, J. P. Vonsattel, K. Wakabayashi, and I. Litvan. 2002. Office of Rare Diseases neuropathologic criteria for corticobasal degeneration. *Journal of neuropathology and experimental neurology* 61(11):935–946. doi:10.1093/jnen/61.11.935.

Dickson, D. W., R. Rademakers, and M. L. Hutton. 2007. Progressive supranuclear palsy: pathology and genetics. *Brain pathology (Zurich, Switzerland)* 17(1):74–82. doi:10.1111/j.1750-3639.2007.00054.x.

Dikic, I. 2017. Proteasomal and Autophagic Degradation Systems. *Annual review of biochemistry* 86:193–224. doi:10.1146/annurev-biochem-061516-044908.

Dimou, E., T. Katsinelos, G. Meisl, B. J. Tuck, S. Keeling, A. E. Smith, E. Hidari, J. Y. L. Lam, M. Burke, S. Lövestam, R. T. Ranasinghe, W. A. McEwan, and D. Klenerman. 2023. Super-resolution imaging unveils the self-replication of tau aggregates upon seeding. *Cell reports* 42(7):112725. doi:10.1016/j.celrep.2023.112725.

Dinkel, P. D., A. Siddiqua, H. Huynh, M. Shah, and M. Margittai. 2011. Variations in filament conformation dictate seeding barrier between three- and four-repeat tau. *Biochemistry* 50(20):4330–4336. doi:10.1021/bi2004685.

Doherty, G. J., and H. T. McMahon. 2009. Mechanisms of endocytosis. *Annual review of biochemistry* 78:857–902. doi:10.1146/annurev.biochem.78.081307.110540.

Donaldson, J. G. 2019. Macropinosome formation, maturation and membrane recycling: lessons from clathrin-independent endosomal membrane systems. *Philosophical transactions of the Royal Society of London. Series B, Biological sciences* 374(1765):20180148. doi:10.1098/rstb.2018.0148.

Douglas, P. M., and A. Dillin. 2010. Protein homeostasis and aging in neurodegeneration. *The Journal of cell biology* 190(5):719–729. doi:10.1083/jcb.201005144.

Dregni, A. J., P. Duan, H. Xu, L. Changolkar, N. El Mammeri, V. M.-Y. Lee, and M. Hong. 2022. Fluent molecular mixing of Tau isoforms in Alzheimer's disease neurofibrillary tangles. *Nature communications* 13(1):2967. doi:10.1038/s41467-022-30585-0.

Drewes, G., B. Trinczek, S. Illenberger, J. Biernat, G. Schmitt-Ulms, H. E. Meyer, E. M. Mandelkow, and E. Mandelkow. 1995. Microtubule-associated protein/microtubule affinity-regulating kinase (p110mark). A novel protein kinase that regulates tau-microtubule interactions and dynamic instability by phosphorylation at the Alzheimer-specific site serine 262. *The Journal of biological chemistry* 270(13):7679–7688. doi:10.1074/jbc.270.13.7679.

Dufty, B. M., L. R. Warner, S. T. Hou, S. X. Jiang, T. Gomez-Isla, K. M. Leenhouts, J. T. Oxford, M. B. Feany, E. Masliah, and T. T. Rohn. 2007. Calpain-cleavage of alpha-synuclein: connecting proteolytic processing to disease-linked aggregation. *The American journal of pathology* 170(5):1725–1738. doi:10.2353/ajpath.2007.061232.

Dujardin, S., S. Bégard, R. Caillierez, C. Lachaud, L. Delattre, S. Carrier, A. Loyens, M.-C. Galas, L. Bousset, R. Melki, G. Aurégan, P. Hantraye, E. Brouillet, L. Buée, and M. Colin. 2014. Ectosomes: a new mechanism for non-exosomal secretion of tau protein. *PloS one* 9(6):e100760. doi:10.1371/journal.pone.0100760.

Dumanchin, C., A. Camuzat, D. Campion, P. Verpillat, D. Hannequin, B. Dubois, P. Saugier-Veber, C. Martin, C. Penet, F. Charbonnier, Y. Agid, T. Frebourg, and A. Brice. 1998. Segregation of a missense mutation in the microtubule-associated protein tau gene with familial frontotemporal dementia and parkinsonism. *Human molecular genetics* 7(11):1825–1829. doi:10.1093/hmg/7.11.1825.

Eanes, E. D., and G. G. Glenner. 1968. X-ray diffraction studies on amyloid filaments. *The journal of histochemistry and cytochemistry official journal of the Histochemistry Society* 16(11):673–677. doi:10.1177/16.11.673.

Ebru Ercan, Sameh Eid, Christian Weber, Alexandra Kowalski, Maria Bichmann, Annika Behrendt, Frank Matthes, Sybille Krauss, Peter Reinhardt, Simone Fulle, and Dagmar E. Ehrnhoefer. 2017. A validated antibody panel for the characterization of tau post-translational modifications 12. doi:10.1186/s13024-017-0229-1.

Eisenberg, D., and M. Jucker. 2012. The amyloid state of proteins in human diseases. *Cell* 148(6):1188–1203. doi:10.1016/j.cell.2012.02.022.

Eisenberg, D. S., and M. R. Sawaya. 2017. Structural Studies of Amyloid Proteins at the Molecular Level. *Annual review of biochemistry* 86:69–95. doi:10.1146/annurev-biochem-061516-045104.

Evans, L. D., T. Wassmer, G. Fraser, J. Smith, M. Perkinton, A. Billinton, and F. J. Livesey. 2018. Extracellular Monomeric and Aggregated Tau Efficiently Enter Human Neurons through Overlapping but Distinct Pathways. *Cell reports* 22(13):3612–3624. doi:10.1016/j.celrep.2018.03.021.

Falcon, B., J. Noad, H. McMahon, F. Randow, and M. Goedert. 2018a. Galectin-8-mediated selective autophagy protects against seeded tau aggregation. *The Journal of biological chemistry* 293(7):2438–2451. doi:10.1074/jbc.M117.809293.

Falcon, B., W. Zhang, A. G. Murzin, G. Murshudov, H. J. Garringer, R. Vidal, R. A. Crowther, B. Ghetti, S. H. W. Scheres, and M. Goedert. 2018b. Structures of filaments from Pick's disease reveal a novel tau protein fold. *Nature* 561(7721):137–140. doi:10.1038/s41586-018-0454-y.

Falcon, B., W. Zhang, M. Schweighauser, A. G. Murzin, R. Vidal, H. J. Garringer, B. Ghetti, S. H. W. Scheres, and M. Goedert. 2018c. Tau filaments from multiple cases of sporadic and inherited Alzheimer's disease adopt a common fold. *Acta neuropathologica* 136(5):699–708. doi:10.1007/s00401-018-1914-z.

Falcon, B., J. Zivanov, W. Zhang, A. G. Murzin, H. J. Garringer, R. Vidal, R. A. Crowther, K. L. Newell, B. Ghetti, M. Goedert, and S. H. W. Scheres. 2019. Novel tau filament fold in

chronic traumatic encephalopathy encloses hydrophobic molecules. *Nature* 568(7752):420–423. doi:10.1038/s41586-019-1026-5.

Fallini, C., B. Khalil, C. L. Smith, and W. Rossoll. 2020. Traffic jam at the nuclear pore: All roads lead to nucleocytoplasmic transport defects in ALS/FTD. *Neurobiology of disease* 140:104835. doi:10.1016/j.nbd.2020.104835.

Felice, F. G. de, D. Wu, M. P. Lambert, S. J. Fernandez, P. T. Velasco, P. N. Lacor, E. H. Bigio, J. Jerecic, P. J. Acton, P. J. Shughrue, E. Chen-Dodson, G. G. Kinney, and W. L. Klein. 2008. Alzheimer's disease-type neuronal tau hyperphosphorylation induced by A beta oligomers. *Neurobiology of aging* 29(9):1334–1347. doi:10.1016/j.neurobiolaging.2007.02.029.

Ferrari, A., F. Hoerndli, T. Baechi, R. M. Nitsch, and J. Götz. 2003. beta-Amyloid induces paired helical filament-like tau filaments in tissue culture. *The Journal of biological chemistry* 278(41):40162–40168. doi:10.1074/jbc.M308243200.

Fichou, Y., M. Vigers, A. K. Goring, N. A. Eschmann, and S. Han. 2018. Heparin-induced tau filaments are structurally heterogeneous and differ from Alzheimer's disease filaments. *Chemical communications (Cambridge, England)* 54(36):4573–4576. doi:10.1039/c8cc01355a.

Finkelshtein, D., A. Werman, D. Novick, S. Barak, and M. Rubinstein. 2013. LDL receptor and its family members serve as the cellular receptors for vesicular stomatitis virus. *Proceedings of the National Academy of Sciences of the United States of America* 110(18):7306–7311. doi:10.1073/pnas.1214441110.

Fitzpatrick, A. W. P., B. Falcon, S. He, A. G. Murzin, G. Murshudov, H. J. Garringer, R. A. Crowther, B. Ghetti, M. Goedert, and S. H. W. Scheres. 2017. Cryo-EM structures of tau filaments from Alzheimer's disease. *Nature* 547(7662):185–190. doi:10.1038/nature23002.

Flavin, W. P., L. Bousset, Z. C. Green, Y. Chu, S. Skarpathiotis, M. J. Chaney, J. H. Kordower, R. Melki, and E. M. Campbell. 2017. Endocytic vesicle rupture is a conserved mechanism of cellular invasion by amyloid proteins. *Acta neuropathologica* 134(4):629–653. doi:10.1007/s00401-017-1722-x.

Forlenza, O. V., B. S. Diniz, M. Radanovic, F. S. Santos, L. L. Talib, and W. F. Gattaz. 2011. Disease-modifying properties of long-term lithium treatment for amnestic mild cognitive impairment: randomised controlled trial. *The British journal of psychiatry the journal of mental science* 198(5):351–356. doi:10.1192/bjp.bp.110.080044.

Friedhoff, P., A. Schneider, E. M. Mandelkow, and E. Mandelkow. 1998. Rapid assembly of Alzheimer-like paired helical filaments from microtubule-associated protein tau monitored by fluorescence in solution. *Biochemistry* 37(28):10223–10230. doi:10.1021/bi980537d.

Frost, B., R. L. Jacks, and M. I. Diamond. 2009. Propagation of tau misfolding from the outside to the inside of a cell. *The Journal of biological chemistry* 284(19):12845–12852. doi:10.1074/jbc.M808759200.

Furman, J. L., and M. I. Diamond. 2017. FRET and Flow Cytometry Assays to Measure Proteopathic Seeding Activity in Biological Samples. *Methods in molecular biology (Clifton, N.J.)* 1523:349–359. doi:10.1007/978-1-4939-6598-4_23.

Furman, J. L., B. B. Holmes, and M. I. Diamond. 2015. Sensitive Detection of Proteopathic Seeding Activity with FRET Flow Cytometry. *Journal of visualized experiments JoVE*(106):e53205. doi:10.3791/53205.

Furman, J. L., J. Vaquer-Alicea, C. L. White, N. J. Cairns, P. T. Nelson, and M. I. Diamond. 2017. Widespread tau seeding activity at early Braak stages. *Acta neuropathologica* 133(1):91–100. doi:10.1007/s00401-016-1644-z.

Fus-Kujawa, A., P. Prus, K. Bajdak-Rusinek, P. Teper, K. Gawron, A. Kowalczuk, and A. L. Sieron. 2021. An Overview of Methods and Tools for Transfection of Eukaryotic Cells in vitro. *Frontiers in bioengineering and biotechnology* 9:701031. doi:10.3389/fbioe.2021.701031.

Gadhave, K., N. Bolshette, A. Ahire, R. Pardeshi, K. Thakur, C. Trandafir, A. Istrate, S. Ahmed, M. Lahkar, D. F. Muresanu, and M. Balea. 2016. The ubiquitin proteasomal system: a potential target for the management of Alzheimer's disease. *Journal of cellular and molecular medicine* 20(7):1392–1407. doi:10.1111/jcmm.12817.

Gamblin, T. C., F. Chen, A. Zambrano, A. Abraha, S. Lagalwar, A. L. Guillozet, M. Lu, Y. Fu, F. Garcia-Sierra, N. LaPointe, R. Miller, R. W. Berry, L. I. Binder, and V. L. Cryns. 2003. Caspase cleavage of tau: linking amyloid and neurofibrillary tangles in Alzheimer's disease. *Proceedings of the National Academy of Sciences of the United States of America* 100(17):10032–10037. doi:10.1073/pnas.1630428100.

Gerson, J. E., D. L. Castillo-Carranza, and R. Kayed. 2014. Advances in therapeutics for neurodegenerative tauopathies: moving toward the specific targeting of the most toxic tau species. *ACS chemical neuroscience* 5(9):752–769. doi:10.1021/cn500143n.

Gestwicki, J. E., and D. Garza. 2012. Protein quality control in neurodegenerative disease. *Progress in molecular biology and translational science* 107:327–353. doi:10.1016/B978-0-12-385883-2.00003-5.

Ghetti, B., A. L. Oblak, B. F. Boeve, K. A. Johnson, B. C. Dickerson, and M. Goedert. 2015. Invited review: Frontotemporal dementia caused by microtubule-associated protein tau gene (MAPT) mutations: a chameleon for neuropathology and neuroimaging. *Neuropathology and applied neurobiology* 41(1):24–46. doi:10.1111/nan.12213.

Gibbons, G. S., V. M. Y. Lee, and J. Q. Trojanowski. 2019. Mechanisms of Cell-to-Cell Transmission of Pathological Tau: A Review. *JAMA neurology* 76(1):101–108. doi:10.1001/jamaneurol.2018.2505.

Goedert, M. 1993. Tau protein and the neurofibrillary pathology of Alzheimer's disease. *Trends in neurosciences* 16(11):460–465. doi:10.1016/0166-2236(93)90078-z.

Goedert, M. 2005. Tau gene mutations and their effects. *Movement disorders official journal of the Movement Disorder Society* 20 Suppl 12:S45-52. doi:10.1002/mds.20539.

Goedert, M., R. A. Crowther, S. H. W. Scheres, and M. G. Spillantini. 2024. Tau and neurodegeneration. *Cytoskeleton (Hoboken, N.J.)* 81(1):95–102. doi:10.1002/cm.21812.

Goedert, M., and R. Jakes. 1990. Expression of separate isoforms of human tau protein: correlation with the tau pattern in brain and effects on tubulin polymerization. *The EMBO journal* 9(13):4225–4230. doi:10.1002/j.1460-2075.1990.tb07870.x.

Goedert, M., R. Jakes, M. G. Spillantini, M. Hasegawa, M. J. Smith, and R. A. Crowther. 1996. Assembly of microtubule-associated protein tau into Alzheimer-like filaments induced by sulphated glycosaminoglycans. *Nature* 383(6600):550–553. doi:10.1038/383550a0.

Goedert, M., and M. G. Spillantini. 2011. Pathogenesis of the tauopathies. *Journal of molecular neuroscience MN* 45(3):425–431. doi:10.1007/s12031-011-9593-4.

Goedert, M., M. G. Spillantini, R. Jakes, D. Rutherford, and R. A. Crowther. 1989. Multiple isoforms of human microtubule-associated protein tau: sequences and localization in neurofibrillary tangles of Alzheimer's disease. *Neuron* 3(4):519–526. doi:10.1016/0896-6273(89)90210-9.

Gousset, K., E. Schiff, C. Langevin, Z. Marijanovic, A. Caputo, D. T. Browman, N. Chenouard, F. de Chaumont, A. Martino, J. Enninga, J.-C. Olivo-Marin, D. Männel, and C. Zurzolo. 2009. Prions hijack tunnelling nanotubes for intercellular spread. *Nature cell biology* 11(3):328–336. doi:10.1038/ncb1841.

Graham, D. L., A. J. Gray, J. A. Joyce, D. Yu, J. O'Moore, G. A. Carlson, M. S. Shearman, T. L. Dellovade, and H. Hering. 2014. Increased O-GlcNAcylation reduces pathological tau without affecting its normal phosphorylation in a mouse model of tauopathy. *Neuropharmacology* 79:307–313. doi:10.1016/j.neuropharm.2013.11.025.

Guharoy, M., T. Lazar, and P. Tompa. 2018. Disordered Substrates of the 20S Proteasome Link Degradation with Phase Separation. *Proteomics* 18(21-22):e1800276. doi:10.1002/pmic.201800276.

Guillozet-Bongaarts, A. L., M. E. Cahill, V. L. Cryns, M. R. Reynolds, R. W. Berry, and L. I. Binder. 2006. Pseudophosphorylation of tau at serine 422 inhibits caspase cleavage: in vitro evidence and implications for tangle formation in vivo. *Journal of neurochemistry* 97(4):1005–1014. doi:10.1111/j.1471-4159.2006.03784.x.

Guo, J. L., A. Buist, A. Soares, K. Callaerts, S. Calafate, F. Stevenaert, J. P. Daniels, B. E. Zoll, A. Crowe, K. R. Brunden, D. Moechars, and V. M. Y. Lee. 2016. The Dynamics and Turnover of Tau Aggregates in Cultured Cells: INSIGHTS INTO THERAPIES FOR TAUOPATHIES. *The Journal of biological chemistry* 291(25):13175–13193. doi:10.1074/jbc.M115.712083.

Guo, J. L., and V. M.-Y. Lee. 2011. Seeding of normal Tau by pathological Tau conformers drives pathogenesis of Alzheimer-like tangles. *The Journal of biological chemistry* 286(17):15317–15331. doi:10.1074/jbc.M110.209296.

Haase, C., J. T. Stieler, T. Arendt, and M. Holzer. 2004. Pseudophosphorylation of tau protein alters its ability for self-aggregation. *Journal of neurochemistry* 88(6):1509–1520. doi:10.1046/j.1471-4159.2003.02287.x.

Hamano, T., T. F. Gendron, E. Causevic, S.-H. Yen, W.-L. Lin, C. Isidoro, M. DeTure, and L. Ko. 2008. Autophagic-lysosomal perturbation enhances tau aggregation in transfectants with induced wild-type tau expression. *The European journal of neuroscience* 27(5):1119–1130. doi:10.1111/j.1460-9568.2008.06084.x.

Hampel, H., S. J. Teipel, T. Fuchsberger, N. Andreasen, J. Wiltfang, M. Otto, Y. Shen, R. Dodel, Y. Du, M. Farlow, H.-J. Möller, K. Blennow, and K. Buerger. 2004. Value of CSF beta-amyloid1-42 and tau as predictors of Alzheimer's disease in patients with mild cognitive impairment. *Molecular psychiatry* 9(7):705–710. doi:10.1038/sj.mp.4001473.

Han, P., G. Serrano, T. G. Beach, R. J. Caselli, J. Yin, N. Zhuang, and J. Shi. 2017. A Quantitative Analysis of Brain Soluble Tau and the Tau Secretion Factor. *Journal of neuropathology and experimental neurology* 76(1):44–51. doi:10.1093/jnen/nlw105.

Hardy, J. 2006. Alzheimer's disease: the amyloid cascade hypothesis: an update and reappraisal. *Journal of Alzheimer's disease JAD* 9(3 Suppl):151–153. doi:10.3233/jad-2006-9s317.

Hardy, J., and D. Allsop. 1991. Amyloid deposition as the central event in the aetiology of Alzheimer's disease. *Trends in pharmacological sciences* 12(10):383–388. doi:10.1016/0165-6147(91)90609-v.

Hastings, N. B., X. Wang, L. Song, B. D. Butts, D. Grotz, R. Hargreaves, J. Fred Hess, K.-L. K. Hong, C. R.-R. Huang, L. Hyde, M. Laverty, J. Lee, D. Levitan, S. X. Lu, M. Maguire, V. Mahadomrongkul, E. J. McEachern, X. Ouyang, T. W. Rosahl, H. Selnick, M. Stanton, G. Terracina, D. J. Vocadlo, G. Wang, J. L. Duffy, E. M. Parker, and L. Zhang. 2017. Inhibition of O-GlcNAcase leads to elevation of O-GlcNAc tau and reduction of tauopathy and cerebrospinal fluid tau in rTg4510 mice. *Molecular neurodegeneration* 12(1):39. doi:10.1186/s13024-017-0181-0.

Havens, M. A., D. M. Duelli, and M. L. Hastings. 2013. Targeting RNA splicing for disease therapy. *Wiley interdisciplinary reviews. RNA* 4(3):247–266. doi:10.1002/wrna.1158.

He, S., and S. H. W. Scheres. 2017. Helical reconstruction in RELION. *Journal of structural biology* 198(3):163–176. doi:10.1016/j.jsb.2017.02.003.

He, Y., C. Duyckaerts, P. Delaère, F. Piette, and J. J. Hauw. 1993. Alzheimer's lesions labelled by anti-ubiquitin antibodies: comparison with other staining techniques. A study of 15 cases with graded intellectual status in ageing and Alzheimer's disease. *Neuropathology and applied neurobiology* 19(4):364–371. doi:10.1111/j.1365-2990.1993.tb00453.x.

He, Z., J. D. McBride, H. Xu, L. Changolkar, S.-J. Kim, B. Zhang, S. Narasimhan, G. S. Gibbons, J. L. Guo, M. Kozak, G. D. Schellenberg, J. Q. Trojanowski, and V. M.-Y. Lee. 2020. Transmission of tauopathy strains is independent of their isoform composition. *Nature communications* 11(1):7. doi:10.1038/s41467-019-13787-x.

Hebestreit, A. S. 2020. Cell-Based Assays for Testing Inhibitors of Tau Aggregation.

Heinisch, J. J., and R. Brandt. 2016. Signaling pathways and posttranslational modifications of tau in Alzheimer's disease: the humanization of yeast cells. *Microbial cell (Graz, Austria)* 3(4):135–146. doi:10.15698/mic2016.04.489.

Hilary Ann Weismiller. 2019. Mechanistic Insight into Tau Fibril Cross-Seeding Barriers: Structural Order and Disorder(1543). https://digitalcommons.du.edu/etd/1543.

Hitt, B. D., J. Vaquer-Alicea, V. A. Manon, J. D. Beaver, O. M. Kashmer, J. N. Garcia, and M. I. Diamond. 2021. Ultrasensitive tau biosensor cells detect no seeding in Alzheimer's disease CSF. *Acta neuropathologica communications* 9(1):99. doi:10.1186/s40478-021-01185-8.

Hofmann, J. P., P. Denner, C. Nussbaum-Krammer, P.-H. Kuhn, M. H. Suhre, T. Scheibel, S. F. Lichtenthaler, H. M. Schätzl, D. Bano, and I. M. Vorberg. 2013. Cell-to-cell propagation of infectious cytosolic protein aggregates. *Proceedings of the National Academy of Sciences of the United States of America* 110(15):5951–5956. doi:10.1073/pnas.1217321110.

Holmes, B. B., S. L. DeVos, N. Kfoury, M. Li, R. Jacks, K. Yanamandra, M. O. Ouidja, F. M. Brodsky, J. Marasa, D. P. Bagchi, P. T. Kotzbauer, T. M. Miller, D. Papy-Garcia, and M. I. Diamond. 2013. Heparan sulfate proteoglycans mediate internalization and propagation of specific proteopathic seeds. *Proceedings of the National Academy of Sciences of the United States of America* 110(33):E3138-47. doi:10.1073/pnas.1301440110.

Holmes, B. B., and M. I. Diamond. 2017. Cellular Models for the Study of Prions. *Cold Spring Harbor perspectives in medicine* 7(2). doi:10.1101/cshperspect.a024026.

Holmes, B. B., J. L. Furman, T. E. Mahan, T. R. Yamasaki, H. Mirbaha, W. C. Eades, L. Belaygorod, N. J. Cairns, D. M. Holtzman, and M. I. Diamond. 2014. Proteopathic tau seeding predicts tauopathy in vivo. *Proceedings of the National Academy of Sciences of the United States of America* 111(41):E4376-85. doi:10.1073/pnas.1411649111.

Hopp, S. C., Y. Lin, D. Oakley, A. D. Roe, S. L. DeVos, D. Hanlon, and B. T. Hyman. 2018. The role of microglia in processing and spreading of bioactive tau seeds in Alzheimer's disease. *Journal of neuroinflammation* 15(1):269. doi:10.1186/s12974-018-1309-z.

Hosokawa, M., T. Arai, M. Masuda-Suzukake, T. Nonaka, M. Yamashita, H. Akiyama, and M. Hasegawa. 2012. Methylene blue reduced abnormal tau accumulation in P301L tau transgenic mice. *PloS one* 7(12):e52389. doi:10.1371/journal.pone.0052389.

Hou, Z., D. Chen, B. D. Ryder, and L. A. Joachimiak. 2021. Biophysical properties of a tau seed. *Scientific reports* 11(1):13602. doi:10.1038/s41598-021-93093-z.

Hu, Z.-W., L. Vugmeyster, D. F. Au, D. Ostrovsky, Y. Sun, and W. Qiang. 2019. Molecular structure of an N-terminal phosphorylated β-amyloid fibril. *Proceedings of the National Academy of Sciences of the United States of America* 116(23):11253–11258. doi:10.1073/pnas.1818530116.

Hughes, M. P., M. R. Sawaya, D. R. Boyer, L. Goldschmidt, J. A. Rodriguez, D. Cascio, L. Chong, T. Gonen, and D. S. Eisenberg. 2018. Atomic structures of low-complexity protein segments reveal kinked β sheets that assemble networks. *Science (New York, N.Y.)* 359(6376):698–701. doi:10.1126/science.aan6398.

Hutton, M., C. L. Lendon, P. Rizzu, M. Baker, S. Froelich, H. Houlden, S. Pickering-Brown, S. Chakraverty, A. Isaacs, A. Grover, J. Hackett, J. Adamson, S. Lincoln, D. Dickson, P. Davies, R. C. Petersen, M. Stevens, E. de Graaff, E. Wauters, J. van Baren, M. Hillebrand, M. Joosse, J. M. Kwon, P. Nowotny, L. K. Che, J. Norton, J. C. Morris, L. A. Reed, J. Trojanowski, H. Basun, L. Lannfelt, M. Neystat, S. Fahn, F. Dark, T. Tannenberg, P. R.

Dodd, N. Hayward, J. B. Kwok, P. R. Schofield, A. Andreadis, J. Snowden, D. Craufurd, D. Neary, F. Owen, B. A. Oostra, J. Hardy, A. Goate, J. van Swieten, D. Mann, T. Lynch, and P. Heutink. 1998. Association of missense and 5'-splice-site mutations in tau with the inherited dementia FTDP-17. *Nature* 393(6686):702–705. doi:10.1038/31508.

Ihara, Y., M. Morishima-Kawashima, and R. Nixon. 2012. The ubiquitin-proteasome system and the autophagic-lysosomal system in Alzheimer disease. *Cold Spring Harbor perspectives in medicine* 2(8). doi:10.1101/cshperspect.a006361.

Iijima, M., T. Tabira, P. Poorkaj, G. D. Schellenberg, J. Q. Trojanowski, V. M. Lee, M. L. Schmidt, K. Takahashi, T. Nabika, T. Matsumoto, Y. Yamashita, S. Yoshioka, and H. Ishino. 1999. A distinct familial presenile dementia with a novel missense mutation in the tau gene. *Neuroreport* 10(3):497–501. doi:10.1097/00001756-199902250-00010.

Ingham, D. J., K. M. Hillyer, M. J. McGuire, and T. C. Gamblin. 2022. In vitro Tau Aggregation Inducer Molecules Influence the Effects of MAPT Mutations on Aggregation Dynamics. *Biochemistry* 61(13):1243–1259. doi:10.1021/acs.biochem.2c00111.

Iqbal, K., A. d. C. Alonso, S. Chen, M. O. Chohan, E. El-Akkad, C.-X. Gong, S. Khatoon, B. Li, F. Liu, A. Rahman, H. Tanimukai, and I. Grundke-Iqbal. 2005. Tau pathology in Alzheimer disease and other tauopathies. *Biochimica et biophysica acta* 1739(2-3):198–210. doi:10.1016/j.bbadis.2004.09.008.

Iqbal, K., F. Liu, and C.-X. Gong. 2016. Tau and neurodegenerative disease: the story so far. *Nature reviews. Neurology* 12(1):15–27. doi:10.1038/nrneurol.2015.225.

Ittner, A., J. Bertz, L. S. Suh, C. H. Stevens, J. Götz, and L. M. Ittner. 2015. Tau-targeting passive immunization modulates aspects of pathology in tau transgenic mice. *Journal of neurochemistry* 132(1):135–145. doi:10.1111/jnc.12821.

Ittner, L. M., Y. D. Ke, F. Delerue, M. Bi, A. Gladbach, J. van Eersel, H. Wölfing, B. C. Chieng, M. J. Christie, I. A. Napier, A. Eckert, M. Staufenbiel, E. Hardeman, and J. Götz. 2010. Dendritic function of tau mediates amyloid-beta toxicity in Alzheimer's disease mouse models. *Cell* 142(3):387–397. doi:10.1016/j.cell.2010.06.036.

Jeganathan, S., M. von Bergen, H. Brutlach, H.-J. Steinhoff, and E. Mandelkow. 2006. Global hairpin folding of tau in solution. *Biochemistry* 45(7):2283–2293. doi:10.1021/bi0521543.

Jia, L., Q. Qiu, H. Zhang, L. Chu, Y. Du, J. Zhang, C. Zhou, F. Liang, S. Shi, S. Wang, W. Qin, Q. Wang, F. Li, Q. Wang, Y. Li, L. Shen, Y. Wei, and J. Jia. 2019. Concordance between the assessment of Aβ42, T-tau, and P-T181-tau in peripheral blood neuronal-derived exosomes and cerebrospinal fluid. *Alzheimer's & dementia the journal of the Alzheimer's Association* 15(8):1071–1080. doi:10.1016/j.jalz.2019.05.002.

Johansen, T., and T. Lamark. 2011. Selective autophagy mediated by autophagic adapter proteins. *Autophagy* 7(3):279–296. doi:10.4161/auto.7.3.14487.

Joshi, B. S., M. A. de Beer, B. N. G. Giepmans, and I. S. Zuhorn. 2020. Endocytosis of Extracellular Vesicles and Release of Their Cargo from Endosomes. *ACS nano* 14(4):4444–4455. doi:10.1021/acsnano.9b10033.

Kalra, H., G. P. C. Drummen, and S. Mathivanan. 2016. Focus on Extracellular Vesicles: Introducing the Next Small Big Thing. *International journal of molecular sciences* 17(2):170. doi:10.3390/ijms17020170.

Kampers, T., P. Friedhoff, J. Biernat, E. M. Mandelkow, and E. Mandelkow. 1996. RNA stimulates aggregation of microtubule-associated protein tau into Alzheimer-like paired helical filaments. *FEBS letters* 399(3):344–349. doi:10.1016/s0014-5793(96)01386-5.

Katsinelos, T., M. Zeitler, E. Dimou, A. Karakatsani, H.-M. Müller, E. Nachman, J. P. Steringer, C. Ruiz de Almodovar, W. Nickel, and T. R. Jahn. 2018. Unconventional Secretion Mediates the Trans-cellular Spreading of Tau. *Cell reports* 23(7):2039–2055. doi:10.1016/j.celrep.2018.04.056.

Kaufman, S. K., and M. I. Diamond. 2013. Prion-like propagation of protein aggregation and related therapeutic strategies. *Neurotherapeutics the journal of the American Society for Experimental NeuroTherapeutics* 10(3):371–382. doi:10.1007/s13311-013-0196-3.

Kaufman, S. K., D. W. Sanders, T. L. Thomas, A. J. Ruchinskas, J. Vaquer-Alicea, A. M. Sharma, T. M. Miller, and M. I. Diamond. 2016. Tau Prion Strains Dictate Patterns of Cell Pathology, Progression Rate, and Regional Vulnerability In Vivo. *Neuron* 92(4):796–812. doi:10.1016/j.neuron.2016.09.055.

Kaufman, S. K., T. L. Thomas, K. Del Tredici, H. Braak, and M. I. Diamond. 2017. Characterization of tau prion seeding activity and strains from formaldehyde-fixed tissue. *Acta neuropathologica communications* 5(1):41. doi:10.1186/s40478-017-0442-8.

Kenessey, A., and S. H. Yen. 1993. The extent of phosphorylation of fetal tau is comparable to that of PHF-tau from Alzheimer paired helical filaments. *Brain research* 629(1):40–46. doi:10.1016/0006-8993(93)90478-6.

Kfoury, N., B. B. Holmes, H. Jiang, D. M. Holtzman, and M. I. Diamond. 2012. Trans-cellular propagation of Tau aggregation by fibrillar species. *The Journal of biological chemistry* 287(23):19440–19451. doi:10.1074/jbc.M112.346072.

Khatoon, S., I. Grundke-Iqbal, and K. Iqbal. 1994. Levels of normal and abnormally phosphorylated tau in different cellular and regional compartments of Alzheimer disease and control brains. *FEBS letters* 351(1):80–84. doi:10.1016/0014-5793(94)00829-9.

Khlistunova, I., J. Biernat, Y. Wang, M. Pickhardt, M. von Bergen, Z. Gazova, E. Mandelkow, and E.-M. Mandelkow. 2006. Inducible expression of Tau repeat domain in cell models of tauopathy: aggregation is toxic to cells but can be reversed by inhibitor drugs. *The Journal of biological chemistry* 281(2):1205–1214. doi:10.1074/jbc.M507753200.

Khurana, V., I. Elson-Schwab, T. A. Fulga, K. A. Sharp, C. A. Loewen, E. Mulkearns, J. Tyynelä, C. R. Scherzer, and M. B. Feany. 2010. Lysosomal dysfunction promotes cleavage and neurotoxicity of tau in vivo. *PLoS genetics* 6(7):e1001026. doi:10.1371/journal.pgen.1001026.

KIDD, M. 1963. Paired helical filaments in electron microscopy of Alzheimer's disease. *Nature* 197:192–193. doi:10.1038/197192b0.

KIDD, M. 1964. Alzheimer's Disease - An Electron Microscopical Study. *Brain a journal of neurology* 87:307–320. doi:10.1093/brain/87.2.307.

Kim, I. S., S. Jenni, M. L. Stanifer, E. Roth, S. P. J. Whelan, A. M. van Oijen, and S. C. Harrison. 2017. Mechanism of membrane fusion induced by vesicular stomatitis virus G protein. *Proceedings of the National Academy of Sciences of the United States of America* 114(1):E28-E36. doi:10.1073/pnas.1618883114.

Knopman, D. S., H. Amieva, R. C. Petersen, G. Chételat, D. M. Holtzman, B. T. Hyman, R. A. Nixon, and D. T. Jones. 2021. Alzheimer disease. *Nature reviews. Disease primers* 7(1):33. doi:10.1038/s41572-021-00269-y.

Kobayashi, K., M. Hayashi, T. Kidani, H. Nakano, K. Miyazu, H. Ujike, S. Kuroda, and Y. Koshino. 2002. Pick's disease in 2 brothers with S305N mutation: note in supplement to an earlier communication. *Clinical neuropathology* 21(4):191–193.

Kolay, S., A. R. Vega, D. A. Dodd, V. A. Perez, O. M. Kashmer, C. L. White, and M. I. Diamond. 2022. The dual fates of exogenous tau seeds: Lysosomal clearance versus cytoplasmic amplification. *The Journal of biological chemistry* 298(6):102014. doi:10.1016/j.jbc.2022.102014.

Kovacs, G. G. 2017. Tauopathies. *Handbook of clinical neurology* 145:355–368. doi:10.1016/B978-0-12-802395-2.00025-0.

Kovacs, G. G., A. J. M. Rozemuller, J. C. van Swieten, E. Gelpi, K. Majtenyi, S. Al-Sarraj, C. Troakes, I. Bódi, A. King, T. Hortobágyi, M. M. Esiri, O. Ansorge, G. Giaccone, I. Ferrer, T.

Arzberger, N. Bogdanovic, T. Nilsson, I. Leisser, I. Alafuzoff, J. W. Ironside, H. Kretzschmar, and H. Budka. 2013. Neuropathology of the hippocampus in FTLD-Tau with Pick bodies: a study of the BrainNet Europe Consortium. *Neuropathology and applied neurobiology* 39(2):166–178. doi:10.1111/j.1365-2990.2012.01272.x.

Krammer, C., D. Kryndushkin, M. H. Suhre, E. Kremmer, A. Hofmann, A. Pfeifer, T. Scheibel, R. B. Wickner, H. M. Schätzl, and I. Vorberg. 2009. The yeast Sup35NM domain propagates as a prion in mammalian cells. *Proceedings of the National Academy of Sciences of the United States of America* 106(2):462–467. doi:10.1073/pnas.0811571106.

Kraus, A., E. Saijo, M. A. Metrick, K. Newell, C. J. Sigurdson, G. Zanusso, B. Ghetti, and B. Caughey. 2019. Seeding selectivity and ultrasensitive detection of tau aggregate conformers of Alzheimer disease. *Acta neuropathologica* 137(4):585–598. doi:10.1007/s00401-018-1947-3.

Kühlbrandt, W. 2014. Biochemistry. The resolution revolution. *Science (New York, N.Y.)* 343(6178):1443–1444. doi:10.1126/science.1251652.

Kumar, H., and J. B. Udgaonkar. 2018. Mechanistic and Structural Origins of the Asymmetric Barrier to Prion-like Cross-Seeding between Tau-3R and Tau-4R. *Journal of molecular biology* 430(24):5304–5312. doi:10.1016/j.jmb.2018.09.010.

Kundel, F., L. Hong, B. Falcon, W. A. McEwan, T. C. T. Michaels, G. Meisl, N. Esteras, A. Y. Abramov, T. J. P. Knowles, M. Goedert, and D. Klenerman. 2018. Measurement of Tau Filament Fragmentation Provides Insights into Prion-like Spreading. *ACS chemical neuroscience* 9(6):1276–1282. doi:10.1021/acschemneuro.8b00094.

Kuret, J., E. E. Congdon, G. Li, H. Yin, X. Yu, and Q. Zhong. 2005. Evaluating triggers and enhancers of tau fibrillization. *Microscopy research and technique* 67(3-4):141–155. doi:10.1002/jemt.20187.

Lane-Donovan, C., G. T. Philips, and J. Herz. 2014. More than cholesterol transporters: lipoprotein receptors in CNS function and neurodegeneration. *Neuron* 83(4):771–787. doi:10.1016/j.neuron.2014.08.005.

Lasagna-Reeves, C. A., D. L. Castillo-Carranza, U. Sengupta, M. J. Guerrero-Munoz, T. Kiritoshi, V. Neugebauer, G. R. Jackson, and R. Kayed. 2012a. Alzheimer brain-derived tau oligomers propagate pathology from endogenous tau. *Scientific reports* 2:700. doi:10.1038/srep00700.

Lasagna-Reeves, C. A., D. L. Castillo-Carranza, U. Sengupta, J. Sarmiento, J. Troncoso, G. R. Jackson, and R. Kayed. 2012b. Identification of oligomers at early stages of tau aggregation in Alzheimer's disease. *FASEB journal official publication of the Federation of American Societies for Experimental Biology* 26(5):1946–1959. doi:10.1096/fj.11-199851.

Lathuiliere, A., Y. Jo, R. Perbet, C. Donahue, C. Commins, N. Quittot, Z. Fan, R. E. Bennett, and B. T. Hyman. 2023. Specific detection of tau seeding activity in Alzheimer's disease using rationally designed biosensor cells. *Molecular neurodegeneration* 18(1):53. doi:10.1186/s13024-023-00643-2.

Lee, C.-C., A. Nayak, A. Sethuraman, G. Belfort, and G. J. McRae. 2007. A three-stage kinetic model of amyloid fibrillation. *Biophysical journal* 92(10):3448–3458. doi:10.1529/biophysj.106.098608.

Lee, G., N. Cowan, and M. Kirschner. 1988. The primary structure and heterogeneity of tau protein from mouse brain. *Science (New York, N.Y.)* 239(4837):285–288. doi:10.1126/science.3122323.

Lee, M. J., J. H. Lee, and D. C. Rubinsztein. 2013. Tau degradation: the ubiquitin-proteasome system versus the autophagy-lysosome system. *Progress in neurobiology* 105:49–59. doi:10.1016/j.pneurobio.2013.03.001.

Lee, V. M., M. Goedert, and J. Q. Trojanowski. 2001. Neurodegenerative tauopathies. *Annual review of neuroscience* 24:1121–1159. doi:10.1146/annurev.neuro.24.1.1121.

Lemke, E. A. 2016. The Multiple Faces of Disordered Nucleoporins. *Journal of molecular biology* 428(10 Pt A):2011–2024. doi:10.1016/j.jmb.2016.01.002.

Levine, P. M., A. Galesic, A. T. Balana, A.-L. Mahul-Mellier, M. X. Navarro, C. A. de Leon, H. A. Lashuel, and M. R. Pratt. 2019. α-Synuclein O-GlcNAcylation alters aggregation and toxicity, revealing certain residues as potential inhibitors of Parkinson's disease. *Proceedings of the National Academy of Sciences of the United States of America* 116(5):1511–1519. doi:10.1073/pnas.1808845116.

Li, L., B. A. Nguyen, V. Mullapudi, Y. Li, L. Saelices, and L. A. Joachimiak. 2023. Disease-associated patterns of acetylation stabilize tau fibril formation. *Structure (London, England 1993)* 31(9):1025-1037.e4. doi:10.1016/j.str.2023.05.020.

Li, L., X. Zhang, and W. Le. 2010. Autophagy dysfunction in Alzheimer's disease. *Neuro-degenerative diseases* 7(4):265–271. doi:10.1159/000276710.

Li, W., and V. M.-Y. Lee. 2006. Characterization of two VQIXXK motifs for tau fibrillization in vitro. *Biochemistry* 45(51):15692–15701. doi:10.1021/bi061422.

Liberta, F., S. Loerch, M. Rennegarbe, A. Schierhorn, P. Westermark, G. T. Westermark, B. P. C. Hazenberg, N. Grigorieff, M. Fändrich, and M. Schmidt. 2019. Cryo-EM fibril structures from systemic AA amyloidosis reveal the species complementarity of pathological amyloids. *Nature communications* 10(1):1104. doi:10.1038/s41467-019-09033-z.

Lindwall, G., and R. D. Cole. 1984. Phosphorylation affects the ability of tau protein to promote microtubule assembly. *Journal of Biological Chemistry* 259(8):5301–5305. doi:10.1016/S0021-9258(17)42989-9.

Liu, C.-W., M. J. Corboy, G. N. DeMartino, and P. J. Thomas. 2003. Endoproteolytic activity of the proteasome. *Science (New York, N.Y.)* 299(5605):408–411. doi:10.1126/science.1079293.

Liu, F., B. Li, E.-J. Tung, I. Grundke-Iqbal, K. Iqbal, and C.-X. Gong. 2007. Site-specific effects of tau phosphorylation on its microtubule assembly activity and self-aggregation. *The European journal of neuroscience* 26(12):3429–3436. doi:10.1111/j.1460-9568.2007.05955.x.

Liu, S., S.-E. Heumüller, A. Hossinger, S. A. Müller, O. Buravlova, S. F. Lichtenthaler, P. Denner, and I. M. Vorberg. 2023. Reactivated endogenous retroviruses promote protein aggregate spreading. *Nature communications* 14(1):5034. doi:10.1038/s41467-023-40632-z.

Liu, S., A. Hossinger, S. Göbbels, and I. M. Vorberg. 2017. Prions on the run: How extracellular vesicles serve as delivery vehicles for self-templating protein aggregates. *Prion* 11(2):98–112. doi:10.1080/19336896.2017.1306162.

Liu, S., A. Hossinger, S.-E. Heumüller, A. Hornberger, O. Buravlova, K. Konstantoulea, S. A. Müller, L. Paulsen, F. Rousseau, J. Schymkowitz, S. F. Lichtenthaler, M. Neumann, P. Denner, and I. M. Vorberg. 2021. Highly efficient intercellular spreading of protein misfolding mediated by viral ligand-receptor interactions. *Nature communications* 12(1):5739. doi:10.1038/s41467-021-25855-2.

Liu, Y.-H., W. Wei, J. Yin, G.-P. Liu, Q. Wang, F.-Y. Cao, and J.-Z. Wang. 2009. Proteasome inhibition increases tau accumulation independent of phosphorylation. *Neurobiology of aging* 30(12):1949–1961. doi:10.1016/j.neurobiolaging.2008.02.012.

Long, S., C. Benoist, and W. Weidner. 2023. World Alzheimer Report 2023: Reducing dementia risk: never too early, never too late.

Longhini, A. P., A. DuBose, S. Lobo, V. Vijayan, Y. Bai, E. K. Rivera, J. Sala-Jarque, A. Nikitina, D. C. Carrettiero, M. T. Unger, O. R. Sclafani, V. Fu, E. R. Beckett, M. Vigers, L. Buée, I. Landrieu, S. Shell, J. E. Shea, S. Han, and K. S. Kosik. 2024. Precision proteoform design for 4R tau isoform selective templated aggregation. *Proceedings of the National Academy*

of Sciences of the United States of America 121(15):e2320456121. doi:10.1073/pnas.2320456121.

Lossos, A., A. Reches, A. Gal, J. P. Newman, D. Soffer, J. M. Gomori, M. Boher, D. Ekstein, I. Biran, Z. Meiner, O. Abramsky, and H. Rosenmann. 2003. Frontotemporal dementia and parkinsonism with the P301S tau gene mutation in a Jewish family. *Journal of neurology* 250(6):733–740. doi:10.1007/s00415-003-1074-4.

Lövestam, S., M. Schweighauser, T. Matsubara, S. Murayama, T. Tomita, T. Ando, K. Hasegawa, M. Yoshida, A. Tarutani, M. Hasegawa, M. Goedert, and S. H. W. Scheres. 2021. Seeded assembly in vitro does not replicate the structures of α-synuclein filaments from multiple system atrophy. *FEBS open bio* 11(4):999–1013. doi:10.1002/2211-5463.13110.

Lovestone, S., M. Boada, B. Dubois, M. Hüll, J. O. Rinne, H.-J. Huppertz, M. Calero, M. V. Andrés, B. Gómez-Carrillo, T. León, and T. Del Ser. 2015. A phase II trial of tideglusib in Alzheimer's disease. *Journal of Alzheimer's disease JAD* 45(1):75–88. doi:10.3233/JAD-141959.

Lu, J.-X., W. Qiang, W.-M. Yau, C. D. Schwieters, S. C. Meredith, and R. Tycko. 2013. Molecular structure of β-amyloid fibrils in Alzheimer's disease brain tissue. *Cell* 154(6):1257–1268. doi:10.1016/j.cell.2013.08.035.

Lu, M., and K. S. Kosik. 2001. Competition for microtubule-binding with dual expression of tau missense and splice isoforms. *Molecular biology of the cell* 12(1):171–184. doi:10.1091/mbc.12.1.171.

Lyons, S., D. Trépel, T. Lynch, R. Walsh, and S. O'Dowd. 2023. The prevalence and incidence of progressive supranuclear palsy and corticobasal syndrome: a systematic review and meta-analysis. *Journal of neurology* 270(9):4451–4465. doi:10.1007/s00415-023-11791-2.

Mahul-Mellier, A.-L., B. Fauvet, A. Gysbers, I. Dikiy, A. Oueslati, S. Georgeon, A. J. Lamontanara, A. Bisquertt, D. Eliezer, E. Masliah, G. Halliday, O. Hantschel, and H. A. Lashuel. 2014. c-Abl phosphorylates α-synuclein and regulates its degradation: implication for α-synuclein clearance and contribution to the pathogenesis of Parkinson's disease. *Human molecular genetics* 23(11):2858–2879. doi:10.1093/hmg/ddt674.

Mair, W., J. Muntel, K. Tepper, S. Tang, J. Biernat, W. W. Seeley, K. S. Kosik, E. Mandelkow, H. Steen, and J. A. Steen. 2016. FLEXITau: Quantifying Post-translational Modifications of Tau Protein in Vitro and in Human Disease. *Analytical chemistry* 88(7):3704–3714. doi:10.1021/acs.analchem.5b04509.

Malbica, J. O., and K. R. Monson. 1975. New and expedient determination of atenolol in biological samples. *Journal of pharmaceutical sciences* 64(12):1992–1994. doi:10.1002/jps.2600641219.

Mandelkow, E. M., J. Biernat, G. Drewes, N. Gustke, B. Trinczek, and E. Mandelkow. 1995. Tau domains, phosphorylation, and interactions with microtubules. *Neurobiology of aging* 16(3):355-62; discussion 362-3. doi:10.1016/0197-4580(95)00025-a.

Mandelkow, E.-M., and E. Mandelkow. 2012. Biochemistry and cell biology of tau protein in neurofibrillary degeneration. *Cold Spring Harbor perspectives in medicine* 2(7):a006247. doi:10.1101/cshperspect.a006247.

Martin, L., X. Latypova, and F. Terro. 2011. Post-translational modifications of tau protein: implications for Alzheimer's disease. *Neurochemistry international* 58(4):458–471. doi:10.1016/j.neuint.2010.12.023.

Masters, C. L., G. Simms, N. A. Weinman, G. Multhaup, B. L. McDonald, and K. Beyreuther. 1985. Amyloid plaque core protein in Alzheimer disease and Down syndrome. *Proceedings of the National Academy of Sciences of the United States of America* 82(12):4245–4249. doi:10.1073/pnas.82.12.4245.

Matsuo, E. S., R. W. Shin, M. L. Billingsley, A. van deVoorde, M. O'Connor, J. Q. Trojanowski, and V. M. Lee. 1994. Biopsy-derived adult human brain tau is phosphorylated at many of the

same sites as Alzheimer's disease paired helical filament tau. *Neuron* 13(4):989–1002. doi:10.1016/0896-6273(94)90264-x.

McKee, A. C., R. C. Cantu, C. J. Nowinski, E. T. Hedley-Whyte, B. E. Gavett, A. E. Budson, V. E. Santini, H.-S. Lee, C. A. Kubilus, and R. A. Stern. 2009. Chronic traumatic encephalopathy in athletes: progressive tauopathy after repetitive head injury. *Journal of neuropathology and experimental neurology* 68(7):709–735. doi:10.1097/NEN.0b013e3181a9d503.

McKee, A. C., T. D. Stein, P. T. Kiernan, and V. E. Alvarez. 2015. The neuropathology of chronic traumatic encephalopathy. *Brain pathology (Zurich, Switzerland)* 25(3):350–364. doi:10.1111/bpa.12248.

McKee, A. C., R. A. Stern, C. J. Nowinski, T. D. Stein, V. E. Alvarez, D. H. Daneshvar, H.-S. Lee, S. M. Wojtowicz, G. Hall, C. M. Baugh, D. O. Riley, C. A. Kubilus, K. A. Cormier, M. A. Jacobs, B. R. Martin, C. R. Abraham, T. Ikezu, R. R. Reichard, B. L. Wolozin, A. E. Budson, L. E. Goldstein, N. W. Kowall, and R. C. Cantu. 2013. The spectrum of disease in chronic traumatic encephalopathy. *Brain a journal of neurology* 136(Pt 1):43–64. doi:10.1093/brain/aws307.

Medina, M., J. J. Garrido, and F. G. Wandosell. 2011. Modulation of GSK-3 as a Therapeutic Strategy on Tau Pathologies. *Frontiers in molecular neuroscience* 4:24. doi:10.3389/fnmol.2011.00024.

Metrick, M. A., N. d. C. Ferreira, E. Saijo, A. Kraus, K. Newell, G. Zanusso, M. Vendruscolo, B. Ghetti, and B. Caughey. 2020. A single ultrasensitive assay for detection and discrimination of tau aggregates of Alzheimer and Pick diseases. *Acta neuropathologica communications* 8(1):22. doi:10.1186/s40478-020-0887-z.

Mirbaha, H., D. Chen, V. Mullapudi, S. J. Terpack, C. L. White, L. A. Joachimiak, and M. I. Diamond. 2022. Seed-competent tau monomer initiates pathology in a tauopathy mouse model. *The Journal of biological chemistry* 298(8):102163. doi:10.1016/j.jbc.2022.102163.

Mishra, S. 2023. Emerging Trends in Cryo-EM-based Structural Studies of Neuropathological Amyloids. *Journal of molecular biology* 435(24):168361. doi:10.1016/j.jmb.2023.168361.

Moe, J. G., C. Gluchowski, P. K. Krishnamurthy, and E. J. Davidowitz. 2017. [P4–589]: CNS Drug-Like Inhibitors of Tau Oligomerization. *Alzheimer's & Dementia* 13(7S_Part_32). doi:10.1016/j.jalz.2017.07.752.

Moe, J. G., P. K. Krishnamurthy, P. Lopez, G. Papiani, D. Romero, H. Bian, M. E. McDonnel, A. B. Reitz, C. Gluchowski, and E. J. Davidowitz. 2016. P1-084: Small Molecule TAU Oligomerization Inhibitors. *Alzheimer's & Dementia* 12(7S_Part_9). doi:10.1016/j.jalz.2016.06.832.

Montecalvo, A., A. T. Larregina, W. J. Shufesky, D. B. Stolz, M. L. G. Sullivan, J. M. Karlsson, C. J. Baty, G. A. Gibson, G. Erdos, Z. Wang, J. Milosevic, O. A. Tkacheva, S. J. Divito, R. Jordan, J. Lyons-Weiler, S. C. Watkins, and A. E. Morelli. 2012. Mechanism of transfer of functional microRNAs between mouse dendritic cells via exosomes. *Blood* 119(3):756–766. doi:10.1182/blood-2011-02-338004.

Morelli, A. E., A. T. Larregina, W. J. Shufesky, M. L. G. Sullivan, D. B. Stolz, G. D. Papworth, A. F. Zahorchak, A. J. Logar, Z. Wang, S. C. Watkins, L. D. Falo, and A. W. Thomson. 2004. Endocytosis, intracellular sorting, and processing of exosomes by dendritic cells. *Blood* 104(10):3257–3266. doi:10.1182/blood-2004-03-0824.

Morley, J. F., H. R. Brignull, J. J. Weyers, and R. I. Morimoto. 2002. The threshold for polyglutamine-expansion protein aggregation and cellular toxicity is dynamic and influenced by aging in Caenorhabditis elegans. *Proceedings of the National Academy of Sciences of the United States of America* 99(16):10417–10422. doi:10.1073/pnas.152161099.

Morozova, V., L. S. Cohen, A. E.-H. Makki, A. Shur, G. Pilar, A. El Idrissi, and A. D. Alonso. 2019. Normal and Pathological Tau Uptake Mediated by M1/M3 Muscarinic Receptors Promotes

Opposite Neuronal Changes. *Frontiers in cellular neuroscience* 13:403. doi:10.3389/fncel.2019.00403.

Morris, M., G. M. Knudsen, S. Maeda, J. C. Trinidad, A. Ioanoviciu, A. L. Burlingame, and L. Mucke. 2015. Tau post-translational modifications in wild-type and human amyloid precursor protein transgenic mice. *Nature neuroscience* 18(8):1183–1189. doi:10.1038/nn.4067.

Mukrasch, M. D., S. Bibow, J. Korukottu, S. Jeganathan, J. Biernat, C. Griesinger, E. Mandelkow, and M. Zweckstetter. 2009. Structural polymorphism of 441-residue tau at single residue resolution. *PLoS biology* 7(2):e34. doi:10.1371/journal.pbio.1000034.

Mullapudi, V., J. Vaquer-Alicea, V. Bommareddy, A. R. Vega, B. D. Ryder, C. L. White, M. I. Diamond, and L. A. Joachimiak. 2023. Network of hotspot interactions cluster tau amyloid folds. *Nature communications* 14(1):895. doi:10.1038/s41467-023-36572-3.

Murray, M. E., N. R. Graff-Radford, O. A. Ross, R. C. Petersen, R. Duara, and D. W. Dickson. 2011. Neuropathologically defined subtypes of Alzheimer's disease with distinct clinical characteristics: a retrospective study. *The Lancet. Neurology* 10(9):785–796. doi:10.1016/S1474-4422(11)70156-9.

Myeku, N., C. L. Clelland, S. Emrani, N. V. Kukushkin, W. H. Yu, A. L. Goldberg, and K. E. Duff. 2016. Tau-driven 26S proteasome impairment and cognitive dysfunction can be prevented early in disease by activating cAMP-PKA signaling. *Nature medicine* 22(1):46–53. doi:10.1038/nm.4011.

Nachman, E., A. S. Wentink, K. Madiona, L. Bousset, T. Katsinelos, K. Allinson, H. Kampinga, W. A. McEwan, T. R. Jahn, R. Melki, A. Mogk, B. Bukau, and C. Nussbaum-Krammer. 2020. Disassembly of Tau fibrils by the human Hsp70 disaggregation machinery generates small seeding-competent species. *The Journal of biological chemistry* 295(28):9676–9690. doi:10.1074/jbc.RA120.013478.

Nelson, P. T., I. Alafuzoff, E. H. Bigio, C. Bouras, H. Braak, N. J. Cairns, R. J. Castellani, B. J. Crain, P. Davies, K. Del Tredici, C. Duyckaerts, M. P. Frosch, V. Haroutunian, P. R. Hof, C. M. Hulette, B. T. Hyman, T. Iwatsubo, K. A. Jellinger, G. A. Jicha, E. Kövari, W. A. Kukull, J. B. Leverenz, S. Love, I. R. Mackenzie, D. M. Mann, E. Masliah, A. C. McKee, T. J. Montine, J. C. Morris, J. A. Schneider, J. A. Sonnen, D. R. Thal, J. Q. Trojanowski, J. C. Troncoso, T. Wisniewski, R. L. Woltjer, and T. G. Beach. 2012. Correlation of Alzheimer disease neuropathologic changes with cognitive status: a review of the literature. *Journal of neuropathology and experimental neurology* 71(5):362–381. doi:10.1097/NEN.0b013e31825018f7.

Nelson, R., M. R. Sawaya, M. Balbirnie, A. Ø. Madsen, C. Riekel, R. Grothe, and D. Eisenberg. 2005. Structure of the cross-beta spine of amyloid-like fibrils. *Nature* 435(7043):773–778. doi:10.1038/nature03680.

Neumann, M., W. Schulz-Schaeffer, R. A. Crowther, M. J. Smith, M. G. Spillantini, M. Goedert, and H. A. Kretzschmar. 2001. Pick's disease associated with the novel Tau gene mutation K369I. *Annals of neurology* 50(4):503–513. doi:10.1002/ana.1223.

Neve, R. L., P. Harris, K. S. Kosik, D. M. Kurnit, and T. A. Donlon. 1986. Identification of cDNA clones for the human microtubule-associated protein tau and chromosomal localization of the genes for tau and microtubule-associated protein 2. *Brain research* 387(3):271–280. doi:10.1016/0169-328x(86)90033-1.

Niblock, M., and J.-M. Gallo. 2012. Tau alternative splicing in familial and sporadic tauopathies. *Biochemical Society transactions* 40(4):677–680. doi:10.1042/BST20120091.

Nicholls, S. B., S. L. DeVos, C. Commins, C. Nobuhara, R. E. Bennett, D. L. Corjuc, E. Maury, B. Eftekharzadeh, O. Akingbade, Z. Fan, A. D. Roe, S. Takeda, S. Wegmann, and B. T. Hyman. 2017. Characterization of TauC3 antibody and demonstration of its potential to block tau propagation. *PloS one* 12(5):e0177914. doi:10.1371/journal.pone.0177914.

Nixon, R. A., J. Wegiel, A. Kumar, W. H. Yu, C. Peterhoff, A. Cataldo, and A. M. Cuervo. 2005. Extensive involvement of autophagy in Alzheimer disease: an immuno-electron microscopy study. *Journal of neuropathology and experimental neurology* 64(2):113–122. doi:10.1093/jnen/64.2.113.

Nobuhara, C. K., S. L. DeVos, C. Commins, S. Wegmann, B. D. Moore, A. D. Roe, I. Costantino, M. P. Frosch, R. Pitstick, G. A. Carlson, C. Hock, R. M. Nitsch, F. Montrasio, J. Grimm, A. E. Cheung, A. W. Dunah, M. Wittmann, T. Bussiere, P. H. Weinreb, B. T. Hyman, and S. Takeda. 2017. Tau Antibody Targeting Pathological Species Blocks Neuronal Uptake and Interneuron Propagation of Tau in Vitro. *The American journal of pathology* 187(6):1399–1412. doi:10.1016/j.ajpath.2017.01.022.

Nonaka, T., S. T. Watanabe, T. Iwatsubo, and M. Hasegawa. 2010. Seeded aggregation and toxicity of {alpha}-synuclein and tau: cellular models of neurodegenerative diseases. *The Journal of biological chemistry* 285(45):34885–34898. doi:10.1074/jbc.M110.148460.

Novak, P., M. Prcina, and E. Kontsekova. 2011. Tauons and prions: infamous cousins? *Journal of Alzheimer's disease JAD* 26(3):413–430. doi:10.3233/JAD-2011-110194.

Opoku-Nsiah, K. A., and J. E. Gestwicki. 2018. Aim for the core: suitability of the ubiquitin-independent 20S proteasome as a drug target in neurodegeneration. *Translational research the journal of laboratory and clinical medicine* 198:48–57. doi:10.1016/j.trsl.2018.05.002.

Orr, M. E., and S. Oddo. 2013. Autophagic/lysosomal dysfunction in Alzheimer's disease. *Alzheimer's research & therapy* 5(5):53. doi:10.1186/alzrt217.

Ossenkoppele, R., D. R. Schonhaut, M. Schöll, S. N. Lockhart, N. Ayakta, S. L. Baker, J. P. O'Neil, M. Janabi, A. Lazaris, A. Cantwell, J. Vogel, M. Santos, Z. A. Miller, B. M. Bettcher, K. A. Vossel, J. H. Kramer, M. L. Gorno-Tempini, B. L. Miller, W. J. Jagust, and G. D. Rabinovici. 2016. Tau PET patterns mirror clinical and neuroanatomical variability in Alzheimer's disease. *Brain a journal of neurology* 139(Pt 5):1551–1567. doi:10.1093/brain/aww027.

Ow, S.-Y., and D. E. Dustan. 2014. A brief overview of amyloids and Alzheimer's disease. *Protein science a publication of the Protein Society; eISSN: 1469-896X* 23(10). doi:10.1002/pro.2524.

Padrick, S. B., and A. D. Miranker. 2002. Islet amyloid: phase partitioning and secondary nucleation are central to the mechanism of fibrillogenesis. *Biochemistry* 41(14):4694–4703. doi:10.1021/bi0160462.

Parolini, I., C. Federici, C. Raggi, L. Lugini, S. Palleschi, A. de Milito, C. Coscia, E. Iessi, M. Logozzi, A. Molinari, M. Colone, M. Tatti, M. Sargiacomo, and S. Fais. 2009. Microenvironmental pH is a key factor for exosome traffic in tumor cells. *The Journal of biological chemistry* 284(49):34211–34222. doi:10.1074/jbc.M109.041152.

Pasquale, V. de, M. Scarcella, and L. M. Pavone. 2022. Molecular Mechanisms in Lysosomal Storage Diseases: From Pathogenesis to Therapeutic Strategies. *Biomedicines* 10(4). doi:10.3390/biomedicines10040922.

Pedersen, J. T., and E. M. Sigurdsson. 2015. Tau immunotherapy for Alzheimer's disease. *Trends in molecular medicine* 21(6):394–402. doi:10.1016/j.molmed.2015.03.003.

Pei, J. J., T. Tanaka, Y. C. Tung, E. Braak, K. Iqbal, and I. Grundke-Iqbal. 1997. Distribution, levels, and activity of glycogen synthase kinase-3 in the Alzheimer disease brain. *Journal of neuropathology and experimental neurology* 56(1):70–78. doi:10.1097/00005072-199701000-00007.

Pemberton, J. G., T. Tenkova, P. Felgner, J. Zimmerberg, T. Balla, and J. Heuser. 2024. Defining the EM-signature of successful cell-transfection. *bioRxiv the preprint server for biology*. doi:10.1101/2024.03.07.583927.

Pérez, M., J. M. Valpuesta, M. Medina, E. Montejo de Garcini, and J. Avila. 1996. Polymerization of tau into filaments in the presence of heparin: the minimal sequence required for tau-tau interaction. *Journal of neurochemistry* 67(3):1183–1190. doi:10.1046/j.1471-4159.1996.67031183.x.

Petkova, A. T., Y. Ishii, J. J. Balbach, O. N. Antzutkin, R. D. Leapman, F. Delaglio, and R. Tycko. 2002. A structural model for Alzheimer's beta -amyloid fibrils based on experimental constraints from solid state NMR. *Proceedings of the National Academy of Sciences of the United States of America* 99(26):16742–16747. doi:10.1073/pnas.262663499.

Petri, L., P. Ábrányi-Balogh, D. Vagrys, T. Imre, N. Varró, I. Mándity, A. Rácz, L. Wittner, K. Tóth, E. Z. Tóth, T. Juhász, B. Davis, and G. M. Keserű. 2022. A covalent strategy to target intrinsically disordered proteins: Discovery of novel tau aggregation inhibitors. *European journal of medicinal chemistry* 231:114163. doi:10.1016/j.ejmech.2022.114163.

Phipson, B., S. Lee, I. J. Majewski, W. S. Alexander, and G. K. Smyth. 2016. ROBUST HYPERPARAMETER ESTIMATION PROTECTS AGAINST HYPERVARIABLE GENES AND IMPROVES POWER TO DETECT DIFFERENTIAL EXPRESSION. *The annals of applied statistics* 10(2):946–963. doi:10.1214/16-AOAS920.

Pickhardt, M., M. von Bergen, Z. Gazova, A. Hascher, J. Biernat, E.-M. Mandelkow, and E. Mandelkow. 2005a. Screening for inhibitors of tau polymerization. *Current Alzheimer research* 2(2):219–226. doi:10.2174/1567205053585891.

Pickhardt, M., Z. Gazova, M. von Bergen, I. Khlistunova, Y. Wang, A. Hascher, E.-M. Mandelkow, J. Biernat, and E. Mandelkow. 2005b. Anthraquinones inhibit tau aggregation and dissolve Alzheimer's paired helical filaments in vitro and in cells. *The Journal of biological chemistry* 280(5):3628–3635. doi:10.1074/jbc.M410984200.

Piguet, O., G. M. Halliday, W. G. J. Reid, B. Casey, R. Carman, Y. Huang, J. H. Xuereb, J. R. Hodges, and J. J. Kril. 2011. Clinical phenotypes in autopsy-confirmed Pick disease. *Neurology* 76(3):253–259. doi:10.1212/WNL.0b013e318207b1ce.

Pippin, M., and V. Gupta. 2023. Pick Disease. https://www.ncbi.nlm.nih.gov/books/NBK562226/. Accessed 07/18/2024.

Polanco, J. C., G. R. Hand, A. Briner, C. Li, and J. Götz. 2021. Exosomes induce endolysosomal permeabilization as a gateway by which exosomal tau seeds escape into the cytosol. *Acta neuropathologica* 141(2):235–256. doi:10.1007/s00401-020-02254-3.

Poorkaj, P., T. D. Bird, E. Wijsman, E. Nemens, R. M. Garruto, L. Anderson, A. Andreadis, W. C. Wiederholt, M. Raskind, and G. D. Schellenberg. 1998. Tau is a candidate gene for chromosome 17 frontotemporal dementia. *Annals of neurology* 43(6):815–825. doi:10.1002/ana.410430617.

Prusiner, S. B. 2013. Biology and genetics of prions causing neurodegeneration. *Annual review of genetics* 47:601–623. doi:10.1146/annurev-genet-110711-155524.

Puchtler, H., and F. Sweat. 1965. Congo red as a stain for fluorescence microscopy of amyloid. *The journal of histochemistry and cytochemistry official journal of the Histochemistry Society* 13(8):693–694. doi:10.1177/13.8.693.

Rabouille, C. 2017. Pathways of Unconventional Protein Secretion. *Trends in cell biology* 27(3):230–240. doi:10.1016/j.tcb.2016.11.007.

Radamaker, L., Y.-H. Lin, K. Annamalai, S. Huhn, U. Hegenbart, S. O. Schönland, G. Fritz, M. Schmidt, and M. Fändrich. 2019. Cryo-EM structure of a light chain-derived amyloid fibril from a patient with systemic AL amyloidosis. *Nature communications* 10(1):1103. doi:10.1038/s41467-019-09032-0.

Rajendran, L., J. Bali, M. M. Barr, F. A. Court, E.-M. Krämer-Albers, F. Picou, G. Raposo, K. E. van der Vos, G. van Niel, J. Wang, and X. O. Breakefield. 2014. Emerging roles of extracellular

vesicles in the nervous system. *The Journal of neuroscience the official journal of the Society for Neuroscience* 34(46):15482–15489. doi:10.1523/JNEUROSCI.3258-14.2014.

Rambaran, R. N., and L. C. Serpell. 2008. Amyloid fibrils: abnormal protein assembly. *Prion* 2(3):112–117. doi:10.4161/pri.2.3.7488.

Rauch, J. N., J. J. Chen, A. W. Sorum, G. M. Miller, T. Sharf, S. K. See, L. C. Hsieh-Wilson, M. Kampmann, and K. S. Kosik. 2018. Tau Internalization is Regulated by 6-O Sulfation on Heparan Sulfate Proteoglycans (HSPGs). *Scientific reports* 8(1):6382. doi:10.1038/s41598-018-24904-z.

Rauch, J. N., G. Luna, E. Guzman, M. Audouard, C. Challis, Y. E. Sibih, C. Leshuk, I. Hernandez, S. Wegmann, B. T. Hyman, V. Gradinaru, M. Kampmann, and K. S. Kosik. 2020. LRP1 is a master regulator of tau uptake and spread. *Nature* 580(7803):381–385. doi:10.1038/s41586-020-2156-5.

Rippin, I., and H. Eldar-Finkelman. 2021. Mechanisms and Therapeutic Implications of GSK-3 in Treating Neurodegeneration. *Cells* 10(2). doi:10.3390/cells10020262.

Rissman, R. A., W. W. Poon, M. Blurton-Jones, S. Oddo, R. Torp, M. P. Vitek, F. M. LaFerla, T. T. Rohn, and C. W. Cotman. 2004. Caspase-cleavage of tau is an early event in Alzheimer disease tangle pathology. *The Journal of clinical investigation* 114(1):121–130. doi:10.1172/JCI20640.

Roberson, E. D., K. Scearce-Levie, J. J. Palop, F. Yan, I. H. Cheng, T. Wu, H. Gerstein, G.-Q. Yu, and L. Mucke. 2007. Reducing endogenous tau ameliorates amyloid beta-induced deficits in an Alzheimer's disease mouse model. *Science (New York, N.Y.)* 316(5825):750–754. doi:10.1126/science.1141736.

Roberts, M., I. Sevastou, Y. Imaizumi, K. Mistry, S. Talma, M. Dey, J. Gartlon, H. Ochiai, Z. Zhou, S. Akasofu, N. Tokuhara, M. Ogo, M. Aoyama, H. Aoyagi, K. Strand, E. Sajedi, K. L. Agarwala, J. Spidel, E. Albone, K. Horie, J. M. Staddon, and R. de Silva. 2020. Pre-clinical characterisation of E2814, a high-affinity antibody targeting the microtubule-binding repeat domain of tau for passive immunotherapy in Alzheimer's disease. *Acta neuropathologica communications* 8(1):13. doi:10.1186/s40478-020-0884-2.

Rose, K., T. Jepson, S. Shukla, A. Maya-Romero, M. Kampmann, K. Xu, and J. H. Hurley. 2024. Tau fibrils induce nanoscale membrane damage and nucleate cytosolic tau at lysosomes. *Proceedings of the National Academy of Sciences of the United States of America* 121(22):e2315690121. doi:10.1073/pnas.2315690121.

Ross, C. A., and M. A. Poirier. 2004. Protein aggregation and neurodegenerative disease. *Nature medicine* 10 Suppl:S10-7. doi:10.1038/nm1066.

Rubinsztein, D. C. 2006. The roles of intracellular protein-degradation pathways in neurodegeneration. *Nature* 443(7113):780–786. doi:10.1038/nature05291.

Saha, I., P. Yuste-Checa, M. Da Silva Padilha, Q. Guo, R. Körner, H. Holthusen, V. A. Trinkaus, I. Dudanova, R. Fernández-Busnadiego, W. Baumeister, D. W. Sanders, S. Gautam, M. I. Diamond, F. U. Hartl, and M. S. Hipp. 2023. The AAA+ chaperone VCP disaggregates Tau fibrils and generates aggregate seeds in a cellular system. *Nature communications* 14(1):560. doi:10.1038/s41467-023-36058-2.

Saijo, E., B. Ghetti, G. Zanusso, A. Oblak, J. L. Furman, M. I. Diamond, A. Kraus, and B. Caughey. 2017. Ultrasensitive and selective detection of 3-repeat tau seeding activity in Pick disease brain and cerebrospinal fluid. *Acta neuropathologica* 133(5):751–765. doi:10.1007/s00401-017-1692-z.

Saijo, E., M. A. Metrick, S. Koga, P. Parchi, I. Litvan, S. Spina, A. Boxer, J. C. Rojas, D. Galasko, A. Kraus, M. Rossi, K. Newell, G. Zanusso, L. T. Grinberg, W. W. Seeley, B. Ghetti, D. W. Dickson, and B. Caughey. 2020. 4-Repeat tau seeds and templating subtypes as brain and CSF biomarkers of frontotemporal lobar degeneration. *Acta neuropathologica* 139(1):63–77. doi:10.1007/s00401-019-02080-2.

Saman, S., W. Kim, M. Raya, Y. Visnick, S. Miro, S. Saman, B. Jackson, A. C. McKee, V. E. Alvarez, N. C. Y. Lee, and G. F. Hall. 2012. Exosome-associated tau is secreted in tauopathy models and is selectively phosphorylated in cerebrospinal fluid in early Alzheimer disease. *The Journal of biological chemistry* 287(6):3842–3849. doi:10.1074/jbc.M111.277061.

Sanders, D. W., S. K. Kaufman, S. L. DeVos, A. M. Sharma, H. Mirbaha, A. Li, S. J. Barker, A. C. Foley, J. R. Thorpe, L. C. Serpell, T. M. Miller, L. T. Grinberg, W. W. Seeley, and M. I. Diamond. 2014. Distinct tau prion strains propagate in cells and mice and define different tauopathies. *Neuron* 82(6):1271–1288. doi:10.1016/j.neuron.2014.04.047.

Sawaya, M. R., S. Sambashivan, R. Nelson, M. I. Ivanova, S. A. Sievers, M. I. Apostol, M. J. Thompson, M. Balbirnie, J. J. W. Wiltzius, H. T. McFarlane, A. Ø. Madsen, C. Riekel, and D. Eisenberg. 2007. Atomic structures of amyloid cross-beta spines reveal varied steric zippers. *Nature* 447(7143):453–457. doi:10.1038/nature05695.

Scheltens, P., B. de Strooper, M. Kivipelto, H. Holstege, G. Chételat, C. E. Teunissen, J. Cummings, and W. M. van der Flier. 2021. Alzheimer's disease. *Lancet (London, England)* 397(10284):1577–1590. doi:10.1016/S0140-6736(20)32205-4.

Scheres, S. H. W., B. Ryskeldi-Falcon, and M. Goedert. 2023. Molecular pathology of neurodegenerative diseases by cryo-EM of amyloids. *Nature* 621(7980):701–710. doi:10.1038/s41586-023-06437-2.

Schmidt, A., K. Annamalai, M. Schmidt, N. Grigorieff, and M. Fändrich. 2016. Cryo-EM reveals the steric zipper structure of a light chain-derived amyloid fibril. *Proceedings of the National Academy of Sciences of the United States of America* 113(22):6200–6205. doi:10.1073/pnas.1522282113.

Schmued, L., J. Raymick, W. Tolleson, S. Sarkar, Y.-H. Zhang, and A. Bell-Cohn. 2012. Introducing Amylo-Glo, a novel fluorescent amyloid specific histochemical tracer especially suited for multiple labeling and large scale quantification studies. *Journal of neuroscience methods* 209(1):120–126. doi:10.1016/j.jneumeth.2012.05.019.

Schweighauser, M., A. G. Murzin, J. Macdonald, I. Lavenir, R. A. Crowther, S. H. W. Scheres, and M. Goedert. 2023. Cryo-EM structures of tau filaments from the brains of mice transgenic for human mutant P301S Tau. *Acta neuropathologica communications* 11(1):160. doi:10.1186/s40478-023-01658-y.

Seidler, P. M., D. R. Boyer, K. A. Murray, T. P. Yang, M. Bentzel, M. R. Sawaya, G. Rosenberg, D. Cascio, C. K. Williams, K. L. Newell, B. Ghetti, M. A. DeTure, D. W. Dickson, H. V. Vinters, and D. S. Eisenberg. 2019. Structure-based inhibitors halt prion-like seeding by Alzheimer's disease-and tauopathy-derived brain tissue samples. *The Journal of biological chemistry* 294(44):16451–16464. doi:10.1074/jbc.RA119.009688.

Seidler, P. M., D. R. Boyer, J. A. Rodriguez, M. R. Sawaya, D. Cascio, K. Murray, T. Gonen, and D. S. Eisenberg. 2018. Structure-based inhibitors of tau aggregation. *Nature chemistry* 10(2):170–176. doi:10.1038/nchem.2889.

Selkoe, D. J. 1991. The molecular pathology of Alzheimer's disease. *Neuron* 6(4):487–498. doi:10.1016/0896-6273(91)90052-2.

Sengupta, A., J. Kabat, M. Novak, Q. Wu, I. Grundke-Iqbal, and K. Iqbal. 1998. Phosphorylation of tau at both Thr 231 and Ser 262 is required for maximal inhibition of its binding to microtubules. *Archives of biochemistry and biophysics* 357(2):299–309. doi:10.1006/abbi.1998.0813.

Shi, Y., W. Zhang, Y. Yang, A. G. Murzin, B. Falcon, A. Kotecha, M. van Beers, A. Tarutani, F. Kametani, H. J. Garringer, R. Vidal, G. I. Hallinan, T. Lashley, Y. Saito, S. Murayama, M. Yoshida, H. Tanaka, A. Kakita, T. Ikeuchi, A. C. Robinson, D. Mann, G. G. Kovacs, T. Revesz, B. Ghetti, M. Hasegawa, M. Goedert, and S. Scheres. 2021. Progressive supranuclear palsy tau filament.

Shin, W. S., J. Di, Q. Cao, B. Li, P. M. Seidler, K. A. Murray, G. Bitan, and L. Jiang. 2019. Amyloid β-protein oligomers promote the uptake of tau fibril seeds potentiating intracellular tau aggregation. *Alzheimer's research & therapy* 11(1):86. doi:10.1186/s13195-019-0541-9.

Smith, C., editor. 2023. Greenfield's neuropathology. CRC Press, Boca Raton. volumes cm.

Sowinski, S., C. Jolly, O. Berninghausen, M. A. Purbhoo, A. Chauveau, K. Köhler, S. Oddos, P. Eissmann, F. M. Brodsky, C. Hopkins, B. Onfelt, Q. Sattentau, and D. M. Davis. 2008. Membrane nanotubes physically connect T cells over long distances presenting a novel route for HIV-1 transmission. *Nature cell biology* 10(2):211–219. doi:10.1038/ncb1682.

Spillantini, M. G., T. D. Bird, and B. Ghetti. 1998a. Frontotemporal dementia and Parkinsonism linked to chromosome 17: a new group of tauopathies. *Brain pathology (Zurich, Switzerland)* 8(2):387–402. doi:10.1111/j.1750-3639.1998.tb00162.x.

Spillantini, M. G., R. A. Crowther, W. Kamphorst, P. Heutink, and J. C. van Swieten. 1998b. Tau pathology in two Dutch families with mutations in the microtubule-binding region of tau. *The American journal of pathology* 153(5):1359–1363. doi:10.1016/S0002-9440(10)65721-5.

Spitzer, P., L.-M. Mulzer, T. J. Oberstein, L. E. Munoz, P. Lewczuk, J. Kornhuber, M. Herrmann, and J. M. Maler. 2019. Microvesicles from cerebrospinal fluid of patients with Alzheimer's disease display reduced concentrations of tau and APP protein. *Scientific reports* 9(1):7089. doi:10.1038/s41598-019-43607-7.

Strang, K. H., C. L. Croft, Z. A. Sorrentino, P. Chakrabarty, T. E. Golde, and B. I. Giasson. 2018. Distinct differences in prion-like seeding and aggregation between Tau protein variants provide mechanistic insights into tauopathies. *The Journal of biological chemistry* 293(7):2408–2421. doi:10.1074/jbc.M117.815357.

Sumi, S. M., T. D. Bird, D. Nochlin, and M. A. Raskind. 1992. Familial presenile dementia with psychosis associated with cortical neurofibrillary tangles and degeneration of the amygdala. *Neurology* 42(1):120–127. doi:10.1212/wnl.42.1.120.

Sunde, M., L. C. Serpell, M. Bartlam, P. E. Fraser, M. B. Pepys, and C. C. Blake. 1997. Common core structure of amyloid fibrils by synchrotron X-ray diffraction. *Journal of molecular biology* 273(3):729–739. doi:10.1006/jmbi.1997.1348.

Svensson, K. J., H. C. Christianson, A. Wittrup, E. Bourseau-Guilmain, E. Lindqvist, L. M. Svensson, M. Mörgelin, and M. Belting. 2013. Exosome uptake depends on ERK1/2-heat shock protein 27 signaling and lipid Raft-mediated endocytosis negatively regulated by caveolin-1. *The Journal of biological chemistry* 288(24):17713–17724. doi:10.1074/jbc.M112.445403.

Swuec, P., F. Lavatelli, M. Tasaki, C. Paissoni, P. Rognoni, M. Maritan, F. Brambilla, P. Milani, P. Mauri, C. Camilloni, G. Palladini, G. Merlini, S. Ricagno, and M. Bolognesi. 2019. Cryo-EM structure of cardiac amyloid fibrils from an immunoglobulin light chain AL amyloidosis patient. *Nature communications* 10(1):1269. doi:10.1038/s41467-019-09133-w.

Tacik, P., M. DeTure, K. M. Hinkle, W.-L. Lin, M. Sanchez-Contreras, Y. Carlomagno, O. Pedraza, R. Rademakers, O. A. Ross, Z. K. Wszolek, and D. W. Dickson. 2015. A Novel Tau Mutation in Exon 12, p.Q336H, Causes Hereditary Pick Disease. *Journal of neuropathology and experimental neurology* 74(11):1042–1052. doi:10.1097/NEN.0000000000000248.

Tai, H.-C., A. Serrano-Pozo, T. Hashimoto, M. P. Frosch, T. L. Spires-Jones, and B. T. Hyman. 2012. The synaptic accumulation of hyperphosphorylated tau oligomers in Alzheimer disease is associated with dysfunction of the ubiquitin-proteasome system. *The American journal of pathology* 181(4):1426–1435. doi:10.1016/j.ajpath.2012.06.033.

Takeda, S., S. Wegmann, H. Cho, S. L. DeVos, C. Commins, A. D. Roe, S. B. Nicholls, G. A. Carlson, R. Pitstick, C. K. Nobuhara, I. Costantino, M. P. Frosch, D. J. Müller, D. Irimia, and B. T. Hyman. 2015. Neuronal uptake and propagation of a rare phosphorylated high-

molecular-weight tau derived from Alzheimer's disease brain. *Nature communications* 6:8490. doi:10.1038/ncomms9490.

Tanaka, Y., K. Yamada, K. Satake, I. Nishida, M. Heuberger, T. Kuwahara, and T. Iwatsubo. 2019. Seeding Activity-Based Detection Uncovers the Different Release Mechanisms of Seed-Competent Tau Versus Inert Tau via Lysosomal Exocytosis. *Frontiers in neuroscience* 13:1258. doi:10.3389/fnins.2019.01258.

Tardivel, M., S. Bégard, L. Bousset, S. Dujardin, A. Coens, R. Melki, L. Buée, and M. Colin. 2016. Tunneling nanotube (TNT)-mediated neuron-to neuron transfer of pathological Tau protein assemblies. *Acta neuropathologica communications* 4(1):117. doi:10.1186/s40478-016-0386-4.

Tarutani, A., S. Lövestam, X. Zhang, A. Kotecha, A. C. Robinson, D. M. A. Mann, Y. Saito, S. Murayama, T. Tomita, M. Goedert, S. H. W. Scheres, and M. Hasegawa. 2023. Cryo-EM structures of tau filaments from SH-SY5Y cells seeded with brain extracts from cases of Alzheimer's disease and corticobasal degeneration. *FEBS open bio* 13(8):1394–1404. doi:10.1002/2211-5463.13657.

Tarutani, A., H. Miyata, T. Nonaka, K. Hasegawa, M. Yoshida, Y. Saito, S. Murayama, A. C. Robinson, D. M. A. Mann, T. Tomita, and M. Hasegawa. 2021. Human tauopathy-derived tau strains determine the substrates recruited for templated amplification. *Brain a journal of neurology* 144(8):2333–2348. doi:10.1093/brain/awab091.

Taylor, R. C., and A. Dillin. 2011. Aging as an event of proteostasis collapse. *Cold Spring Harbor perspectives in biology* 3(5). doi:10.1101/cshperspect.a004440.

Tian, T., Y.-L. Zhu, F.-H. Hu, Y.-Y. Wang, N.-P. Huang, and Z.-D. Xiao. 2013. Dynamics of exosome internalization and trafficking. *Journal of cellular physiology* 228(7):1487–1495. doi:10.1002/jcp.24304.

Tolosa, E., I. Litvan, G. U. Höglinger, D. Burn, A. Lees, M. V. Andrés, B. Gómez-Carrillo, T. León, and T. Del Ser. 2014. A phase 2 trial of the GSK-3 inhibitor tideglusib in progressive supranuclear palsy. *Movement disorders official journal of the Movement Disorder Society* 29(4):470–478. doi:10.1002/mds.25824.

Törnquist, M., T. C. T. Michaels, K. Sanagavarapu, X. Yang, G. Meisl, S. I. A. Cohen, T. P. J. Knowles, and S. Linse. 2018. Secondary nucleation in amyloid formation. *Chemical communications (Cambridge, England)* 54(63):8667–8684. doi:10.1039/c8cc02204f.

Tuttle, M. D., G. Comellas, A. J. Nieuwkoop, D. J. Covell, D. A. Berthold, K. D. Kloepper, J. M. Courtney, J. K. Kim, A. M. Barclay, A. Kendall, W. Wan, G. Stubbs, C. D. Schwieters, V. M. Y. Lee, J. M. George, and C. M. Rienstra. 2016. Solid-state NMR structure of a pathogenic fibril of full-length human α-synuclein. *Nature structural & molecular biology* 23(5):409–415. doi:10.1038/nsmb.3194.

Uddin, M. S., D. Tewari, G. Sharma, M. T. Kabir, G. E. Barreto, M. N. Bin-Jumah, A. Perveen, M. M. Abdel-Daim, and G. M. Ashraf. 2020. Molecular Mechanisms of ER Stress and UPR in the Pathogenesis of Alzheimer's Disease. *Molecular neurobiology* 57(7):2902–2919. doi:10.1007/s12035-020-01929-y.

Ukmar-Godec, T., S. Hutten, M. P. Grieshop, N. Rezaei-Ghaleh, M.-S. Cima-Omori, J. Biernat, E. Mandelkow, J. Söding, D. Dormann, and M. Zweckstetter. 2019. Lysine/RNA-interactions drive and regulate biomolecular condensation. *Nature communications* 10(1):2909. doi:10.1038/s41467-019-10792-y.

van Dyck, C. H., C. J. Swanson, P. Aisen, R. J. Bateman, C. Chen, M. Gee, M. Kanekiyo, D. Li, L. Reyderman, S. Cohen, L. Froelich, S. Katayama, M. Sabbagh, B. Vellas, D. Watson, S. Dhadda, M. Irizarry, L. D. Kramer, and T. Iwatsubo. 2023. Lecanemab in Early Alzheimer's Disease. *The New England journal of medicine* 388(1):9–21. doi:10.1056/NEJMoa2212948.

Verghese, P. B., J. M. Castellano, and D. M. Holtzman. 2011. Apolipoprotein E in Alzheimer's disease and other neurological disorders. *The Lancet. Neurology* 10(3):241–252. doi:10.1016/S1474-4422(10)70325-2.

Vigers, M. P., S. Lobo, S. Najafi, A. DuBose, K. Tsay, P. Ganguly, A. P. Longhini, Y. Jin, S. K. Buratto, K. S. Kosik, M. S. Shell, J.-E. Shea, and S. Han. 2023. Tau P301L mutation promotes core 4R tauopathy fibril fold through near-surface water structuring and conformational rearrangement. *bioRxiv the preprint server for biology*. doi:10.1101/2023.11.28.568818.

Vogelsberg-Ragaglia, V., J. Bruce, C. Richter-Landsberg, B. Zhang, M. Hong, J. Q. Trojanowski, and V. M. Lee. 2000. Distinct FTDP-17 missense mutations in tau produce tau aggregates and other pathological phenotypes in transfected CHO cells. *Molecular biology of the cell* 11(12):4093–4104. doi:10.1091/mbc.11.12.4093.

Wallace, A. F., L. O. Hedges, A. Fernandez-Martinez, P. Raiteri, J. D. Gale, G. A. Waychunas, S. Whitelam, J. F. Banfield, and J. J. de Yoreo. 2013. Microscopic evidence for liquid-liquid separation in supersaturated CaCO3 solutions. *Science (New York, N.Y.)* 341(6148):885–889. doi:10.1126/science.1230915.

Walls, K. C., R. R. Ager, V. Vasilevko, D. Cheng, R. Medeiros, and F. M. LaFerla. 2014. p-Tau immunotherapy reduces soluble and insoluble tau in aged 3xTg-AD mice. *Neuroscience letters* 575:96–100. doi:10.1016/j.neulet.2014.05.047.

Wang, Y., V. Balaji, S. Kaniyappan, L. Krüger, S. Irsen, K. Tepper, R. Chandupatla, W. Maetzler, A. Schneider, E. Mandelkow, and E.-M. Mandelkow. 2017. The release and trans-synaptic transmission of Tau via exosomes. *Molecular neurodegeneration* 12(1):5. doi:10.1186/s13024-016-0143-y.

Wang, Y., S. Garg, E.-M. Mandelkow, and E. Mandelkow. 2010. Proteolytic processing of tau. *Biochemical Society transactions* 38(4):955–961. doi:10.1042/BST0380955.

Wang, Y., Y. Zhang, W. Hu, S. Xie, C.-X. Gong, K. Iqbal, and F. Liu. 2015. Rapid alteration of protein phosphorylation during postmortem: implication in the study of protein phosphorylation. *Scientific reports* 5:15709. doi:10.1038/srep15709.

Wang, Y. P., J. Biernat, M. Pickhardt, E. Mandelkow, and E.-M. Mandelkow. 2007. Stepwise proteolysis liberates tau fragments that nucleate the Alzheimer-like aggregation of full-length tau in a neuronal cell model. *Proceedings of the National Academy of Sciences of the United States of America* 104(24):10252–10257. doi:10.1073/pnas.0703676104.

Wegmann, S., B. Eftekharzadeh, K. Tepper, K. M. Zoltowska, R. E. Bennett, S. Dujardin, P. R. Laskowski, D. MacKenzie, T. Kamath, C. Commins, C. Vanderburg, A. D. Roe, Z. Fan, A. M. Molliex, A. Hernandez-Vega, D. Muller, A. A. Hyman, E. Mandelkow, J. P. Taylor, and B. T. Hyman. 2018. Tau protein liquid-liquid phase separation can initiate tau aggregation. *The EMBO journal* 37(7). doi:10.15252/embj.201798049.

Weingarten, M. D., A. H. Lockwood, Hwo, S. Y., and M. W. Kirschner. 1975. A protein factor essential for microtubule assembly. *Proceedings of the National Academy of Sciences of the United States of America* 72(5). https://www.pnas.org/content/72/5/1858.short.

Weismiller, H. A., R. Murphy, G. Wei, B. Ma, R. Nussinov, and M. Margittai. 2018. Structural disorder in four-repeat Tau fibrils reveals a new mechanism for barriers to cross-seeding of Tau isoforms. *The Journal of biological chemistry* 293(45):17336–17348. doi:10.1074/jbc.RA118.005316.

Weissmann, C., M. Enari, P.-C. Klöhn, D. Rossi, and E. Flechsig. 2002. Transmission of prions. *Proceedings of the National Academy of Sciences of the United States of America* 99 Suppl 4(Suppl 4):16378–16383. doi:10.1073/pnas.172403799.

Westermark, P., M. D. Benson, J. N. Buxbaum, A. S. Cohen, B. Frangione, S.-I. Ikeda, C. L. Masters, G. Merlini, M. J. Saraiva, and J. D. Sipe. 2005. Amyloid: toward terminology clarification. Report from the Nomenclature Committee of the International Society of

Amyloidosis. *Amyloid the international journal of experimental and clinical investigation the official journal of the International Society of Amyloidosis* 12(1):1–4. doi:10.1080/13506120500032196.

Whittington, R. A., A. Bretteville, M. F. Dickler, and E. Planel. 2013. Anesthesia and tau pathology. *Progress in neuro-psychopharmacology & biological psychiatry* 47:147–155. doi:10.1016/j.pnpbp.2013.03.004.

Wilcock, G. K., and M. M. Esiri. 1982. Plaques, tangles and dementia. A quantitative study. *Journal of the neurological sciences* 56(2-3):343–356. doi:10.1016/0022-510x(82)90155-1.

Wiltzius, J. J. W., M. Landau, R. Nelson, M. R. Sawaya, M. I. Apostol, L. Goldschmidt, A. B. Soriaga, D. Cascio, K. Rajashankar, and D. Eisenberg. 2009. Molecular mechanisms for protein-encoded inheritance. *Nature structural & molecular biology* 16(9):973–978. doi:10.1038/nsmb.1643.

Wischik, C. M., P. C. Edwards, R. Y. Lai, M. Roth, and C. R. Harrington. 1996. Selective inhibition of Alzheimer disease-like tau aggregation by phenothiazines. *Proceedings of the National Academy of Sciences of the United States of America* 93(20):11213–11218. doi:10.1073/pnas.93.20.11213.

Wischik, C. M., M. Novak, P. C. Edwards, A. Klug, W. Tichelaar, and R. A. Crowther. 1988. Structural characterization of the core of the paired helical filament of Alzheimer disease. *Proceedings of the National Academy of Sciences of the United States of America* 85(13):4884–4888. doi:10.1073/pnas.85.13.4884.

Wischik, C. M., B. O. Schelter, D. J. Wischik, J. M. D. Storey, and C. R. Harrington. 2018. Modeling Prion-Like Processing of Tau Protein in Alzheimer's Disease for Pharmaceutical Development. *Journal of Alzheimer's disease JAD* 62(3):1287–1303. doi:10.3233/JAD-170727.

Wittrup, A., A. Ai, X. Liu, P. Hamar, R. Trifonova, K. Charisse, M. Manoharan, T. Kirchhausen, and J. Lieberman. 2015. Visualizing lipid-formulated siRNA release from endosomes and target gene knockdown. *Nature biotechnology* 33(8):870–876. doi:10.1038/nbt.3298.

Woerman, A. L., A. Aoyagi, S. Patel, S. A. Kazmi, I. Lobach, L. T. Grinberg, A. C. McKee, W. W. Seeley, S. H. Olson, and S. B. Prusiner. 2016. Tau prions from Alzheimer's disease and chronic traumatic encephalopathy patients propagate in cultured cells. *Proceedings of the National Academy of Sciences of the United States of America* 113(50):E8187-E8196. doi:10.1073/pnas.1616344113.

Wszolek, Z. K., R. F. Pfeiffer, M. H. Bhatt, R. L. Schelper, M. Cordes, B. J. Snow, R. L. Rodnitzky, E. C. Wolters, F. Arwert, and D. B. Calne. 1992. Rapidly progressive autosomal dominant parkinsonism and dementia with pallido-ponto-nigral degeneration. *Annals of neurology* 32(3):312–320. doi:10.1002/ana.410320303.

Wu, J. W., M. Herman, L. Liu, S. Simoes, C. M. Acker, H. Figueroa, J. I. Steinberg, M. Margittai, R. Kayed, C. Zurzolo, G. Di Paolo, and K. E. Duff. 2013. Small misfolded Tau species are internalized via bulk endocytosis and anterogradely and retrogradely transported in neurons. *The Journal of biological chemistry* 288(3):1856–1870. doi:10.1074/jbc.M112.394528.

Wu, L., Z. Wang, S. Lad, N. Gilyazova, D. T. Dougharty, M. Marcus, F. Henderson, W. K. Ray, S. Siedlak, J. Li, R. F. Helm, X. Zhu, G. S. Bloom, S.-H. J. Wang, W.-Q. Zou, and B. Xu. 2022. Selective Detection of Misfolded Tau From Postmortem Alzheimer's Disease Brains. *Frontiers in aging neuroscience* 14:945875. doi:10.3389/fnagi.2022.945875.

Xu, D., and J. D. Esko. 2014. Demystifying heparan sulfate-protein interactions. *Annual review of biochemistry* 83:129–157. doi:10.1146/annurev-biochem-060713-035314.

Yagishita, S., Y. Itoh, W. Nan, and N. Amano. 1981. Reappraisal of the fine structure of Alzheimer's neurofibrillary tangles. *Acta neuropathologica* 54(3):239–246. doi:10.1007/BF00687747.

Yanamandra, K., H. Jiang, T. E. Mahan, S. E. Maloney, D. F. Wozniak, M. I. Diamond, and D. M. Holtzman. 2015. Anti-tau antibody reduces insoluble tau and decreases brain atrophy. *Annals of clinical and translational neurology* 2(3):278–288. doi:10.1002/acn3.176.

Yanamandra, K., N. Kfoury, H. Jiang, T. E. Mahan, S. Ma, S. E. Maloney, D. F. Wozniak, M. I. Diamond, and D. M. Holtzman. 2013. Anti-tau antibodies that block tau aggregate seeding in vitro markedly decrease pathology and improve cognition in vivo. *Neuron* 80(2):402–414. doi:10.1016/j.neuron.2013.07.046.

Yoshiyama, Y., M. Higuchi, B. Zhang, S.-M. Huang, N. Iwata, T. C. Saido, J. Maeda, T. Suhara, J. Q. Trojanowski, and V. M.-Y. Lee. 2007. Synapse loss and microglial activation precede tangles in a P301S tauopathy mouse model. *Neuron* 53(3):337–351. doi:10.1016/j.neuron.2007.01.010.

Yu, X., Y. Luo, P. Dinkel, J. Zheng, G. Wei, M. Margittai, R. Nussinov, and B. Ma. 2012. Cross-seeding and conformational selection between three- and four-repeat human Tau proteins. *The Journal of biological chemistry* 287(18):14950–14959. doi:10.1074/jbc.M112.340794.

Yu, Y., X. Run, Z. Liang, Y. Li, F. Liu, Y. Liu, K. Iqbal, I. Grundke-Iqbal, and C.-X. Gong. 2009. Developmental regulation of tau phosphorylation, tau kinases, and tau phosphatases. *Journal of neurochemistry* 108(6):1480–1494. doi:10.1111/j.1471-4159.2009.05882.x.

Yuzwa, S. A., X. Shan, M. S. Macauley, T. Clark, Y. Skorobogatko, K. Vosseller, and D. J. Vocadlo. 2012. Increasing O-GlcNAc slows neurodegeneration and stabilizes tau against aggregation. *Nature chemical biology* 8(4):393–399. doi:10.1038/nchembio.797.

Zhang, W., B. Falcon, A. G. Murzin, J. Fan, R. A. Crowther, M. Goedert, and S. H. Scheres. 2019. Heparin-induced tau filaments are polymorphic and differ from those in Alzheimer's and Pick's diseases. *eLife* 8. doi:10.7554/eLife.43584.

Zhang, W., A. Tarutani, K. L. Newell, A. G. Murzin, T. Matsubara, B. Falcon, R. Vidal, H. J. Garringer, Y. Shi, T. Ikeuchi, S. Murayama, B. Ghetti, M. Hasegawa, M. Goedert, and S. H. W. Scheres. 2020. Novel tau filament fold in corticobasal degeneration. *Nature* 580(7802):283–287. doi:10.1038/s41586-020-2043-0.

Zhao, H., E. K. J. Tuominen, and P. K. J. Kinnunen. 2004. Formation of amyloid fibers triggered by phosphatidylserine-containing membranes. *Biochemistry* 43(32):10302–10307. doi:10.1021/bi049002c.

Zhao, K., Y.-J. Lim, Z. Liu, H. Long, Y. Sun, J.-J. Hu, C. Zhao, Y. Tao, X. Zhang, D. Li, Y.-M. Li, and C. Liu. 2020. Parkinson's disease-related phosphorylation at Tyr39 rearranges α-synuclein amyloid fibril structure revealed by cryo-EM. *Proceedings of the National Academy of Sciences of the United States of America* 117(33):20305–20315. doi:10.1073/pnas.1922741117.

Zhu, X.-C., J.-T. Yu, T. Jiang, and L. Tan. 2013. Autophagy modulation for Alzheimer's disease therapy. *Molecular neurobiology* 48(3):702–714. doi:10.1007/s12035-013-8457-z.

Appendix

Supplementary table 1 Total protein in 1.5 µl of 10 % Tauopathy brain homogenate used in screen and percentage of cells with aggregates induced in cell panel.

Patient BH No.	Total protein [µg] in 1.5 µl	[%] cells with aggregates			
		Tau $3R^{M\ (244-400)}$	Tau $3R^{(PiD\ 254-378)}$	Tau $4R^{S\ (246-378)}$	Tau $4R^{(AD\ 304-380)}$
C	1.6	0.0-0.3	0.0-0.8	0.0-0.9	0.1-0.4
1 PiD	2.8	32.3	26.0	0.8	4.6
2 PiD	2.1	14.0	10.6	0.4	2.8
3 PiD	2.6	8.3	7.0	1.9	0.6
4 PiD	2.0	13.6	6.0	1.3	1.1
5 PiD	2.5	4.6	5.3	2.4	0.2
6 PiD	1.6	2.2	1.5	0.7	0.3
7 CBD	2.1	0.0	0.2	8.3	0.3
8 CBD	2.4	0.0	0.2	6.9	0.3
9 CBD	2.6	0.0	0.0	5.8	0.0
10 CBD	1.7	1.4	0.8	8.9	1.5
11 CBD	2.0	2.3	1.6	11.4	3.0
12 CBD	2.2	1.0	3.6	11.5	2.4
13 PSP	2.2	0.7	0.6	6.2	2.2
14 PSP	2.0	1.0	0.2	14.7	2.1
15 PSP	2.8	1.0	0.7	8.1	0.6
16 PSP	2.0	1.1	1.7	6.1	3.5
17 PSP	3.0	2.5	3.2	18.1	1.7
18 PSP	2.8	1.0	1.3	20.0	1.1
19 AD	1.4	6.8	3.5	1.9	2.9
20 AD	2.1	6.7	3.4	4.1	0.3
21 AD	1.8	11.6	4.2	2.1.	2.3
22 AD	2.0	34.7	32.4	5.5	13.0
23 AD	1.8	14.7	9.3	1.5	5.0
24 AD	2.1	4.5	9.2	0.7	5.7